C.E. SACLAY
DSM

SERVICE DE PHYSIQUE

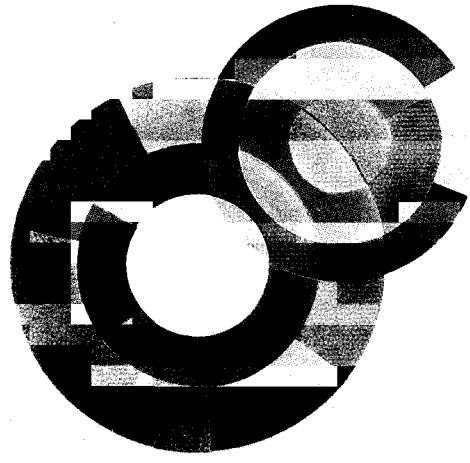

DAPNIA-SPhN-96-14 05/1996

Conceptual Design Report of a Compton Polarimeter for Cebaf Hall A

G. Bardin, C. Cavata, D. Neyret, B. Frois, J.P. Jorda, J.M. Legoff, S. Platchkov, L. Steinmetz, M. Juillard, M. Authier, P. Mangeot, P. Rebourgeard, N. Colombel, P. Girardot, J. Martino, J.C. Sellier, C. Veyssiere, J. Berthot, P.Y. Bertin, V. Breton, H. Fonvieille, Y. Roblin, J.P. Chen

DAPNIA

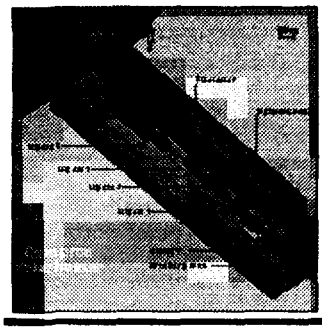

Conceptual Design Report of a Compton Polarimeter for Cebaf Hall A

DAPNIA/SPhN

G. Bardin, C. Cavata, D. Neyret, B. Frois, J. P. Jorda, J. M. Legoff, S. Platchkov, L. Steinmetz

DAPNIA/SEA

M. Juillard

DAPNIA/SED

M. Authier, P. Mangeot, P. Rebourgeard

DAPNIA/SGPI

N. Colombel, P. Girardot

DAPNIA/SIG

J. Martino, J. C. Sellier, C. Veyssiere

IN2P3/LPC

J. Berthot, P. Y. Bertin, V. Breton, H. Fonvieille, Y. Roblin

CEBAF

J.P. Chen

May 9, 1996

ABSTRACT

This report describes the design of the Compton polarimeter for the Cebaf electron beam in End Station A. The method of Compton polarimetry is first introduced. It is shown that at CEBAF beam intensities, the use of standard visible LASER light gives too low counting rates. An amplification scheme of the LASER beam based on a high finesse optical cavity is proposed. Expected luminosities with and without such a cavity are given. The polarimeter setup, including a 4 dipole magnet chicane, a photon and an electron detector, is detailed. The various sources of systematic error on the electron beam polarization measurement are discussed.

Contents

List of Figures

List of Tables

1 Introduction

1.1 Physic Motivations

The Physic program at CEBAF Hall A includes many experiments using $4\,GeV$ (or more) polarized electron beam:

- Study of Parity Violation in electron elastic scattering from proton and ^{4}He [1]
- Measurement of electric form factor of the proton by recoil polarization [2]
- Investigation of the $N \rightarrow \Delta$ transition via polarization observable [3]
- Measurement of the neutron spin structure function at low Q^2 [4]
- ... [5]

Some of these experiments will need beam polarization measurement and monitoring with an accuracy as low as $\Delta P_e/P_e \leq 4\%$ [1],[3],[4] with beam currents ranging from 1 to $100\mu A$.

At Cebaf energies, the simplest way to measure the polarization is through Möller scattering. Unfortunately, Möller Polarimetry is a destructive method, so that measuring the polarization prevents from running an experiment in End Station A. Furthermore, this technique can only be used at low intensity, and experiments requiring high intensity have to assume that beam polarization is intensity independent. That's why, although Compton Polarimetry is more complicated, it is a very attractive technique, since non destructive and that can be used at high current.

1.2 Principle of electron Polarization measurement by Compton Scattering

The longitudinal polarization of the electron beam P_e with respect to the z axis (See Fig. 1) is defined by

$$P_e = \frac{N_e^+ - N_e^-}{N_e^+ + N_e^-}, \tag{1}$$

where $N_e^{\pm}$ is the number of electrons with their spin $s_z^e = \pm\frac{1}{2}$. For a total number of electron N_e, one has the following relations

$$N_e^{\pm} = \frac{N_e}{2}(1 \pm P_e)\,. \tag{2}$$

In a Compton Polarimeter, the longitudinal polarization P_e of the electron beam is extracted from the measurement of the experimental asymmetry A_{exp} in the scattering of a circularly polarized (giving a polarization P_γ) photon beam (from a LASER) on the electron Beam (see Fig. 2) :

$$A_{exp} = \frac{n^+ - n^-}{n^+ + n^-}, \tag{3}$$

where n^+ (resp. n^-) is the number of Compton scattering events before (resp. after) a reversal of the laser polarization ($P_\gamma \rightarrow -P_\gamma$). This experimental asymmetry A_{exp} is related to the known theoretical asymmetry A_l for Compton scattering for electron and photon with spin parallel $\sigma_{\Rightarrow}^{\rightarrow}$ and anti-parallel $\sigma_{\Rightarrow}^{\leftarrow}$,

$$A_l = \frac{\sigma_{\Rightarrow}^{\rightarrow} - \sigma_{\Rightarrow}^{\leftarrow}}{\sigma_{\Rightarrow}^{\rightarrow} + \sigma_{\Rightarrow}^{\leftarrow}}, \tag{4}$$

through the relation

$$A_{exp} = \frac{n^+ - n^-}{n^+ + n^-} = P_e P_\gamma A_l. \tag{5}$$

Indeed if one computes the number of Compton scattering events $n^\pm$, one needs to know what is the mean cross-section $< \sigma >$ for an electron beam with polarization P_e and a photon beam with polarization P_γ.
Identically to the electron case, we define $N_\gamma^\pm$ the number of photon with their spin $s_z^\gamma = \pm 1$ related to the total number of photons N_γ through the relations

$$N_\gamma^\pm = \frac{N_\gamma}{2}(1 \pm P_\gamma). \tag{6}$$

We note that

$$N_e N_\gamma = N_e^+ N_\gamma^+ + N_e^+ N_\gamma^- + N_e^- N_\gamma^+ + N_e^- N_\gamma^-.$$

The mean cross-section is thus (See Fig. 1)

$$< \sigma >= \frac{1}{N_\gamma N_e}\left[\left(N_\gamma^+ N_e^+ + N_\gamma^- N_e^-\right)\sigma_{\Rightarrow}^{\rightarrow} + \left(N_\gamma^- N_e^+ + N_\gamma^+ N_e^-\right)\sigma_{\Rightarrow}^{\leftarrow}\right].$$

Introducing the unpolarized cross-section

$$\sigma_0 = \frac{\sigma_{\Rightarrow}^{\rightarrow} + \sigma_{\Rightarrow}^{\leftarrow}}{2}, \tag{7}$$

yields to

$$\sigma_{\Rightarrow}^{\rightarrow} = \sigma_0(1 + A_l) \qquad , \qquad \sigma_{\Rightarrow}^{\leftarrow} = \sigma_0(1 - A_l). \tag{8}$$

Using Eq. (2),(6),(8), one gets for the cross-section

$$< \sigma >= \sigma_0[1 + P_e P_\gamma A_l], \tag{9}$$

and thus for the counting rate before and after the laser polarization reversal ($P_\gamma \rightarrow -P_\gamma$)

$$n^\pm = \mathcal{L}^\pm T^\pm \quad < \sigma > \; = \mathcal{L}^\pm T^\pm \;\; \sigma_0 \;\; [1 \pm P_e P_\gamma A_l], \tag{10}$$

where $\mathcal{L}^\pm T^\pm$ is the integrated luminosity before and after the Laser polarization reversal. Normalizing these numbers to the same integrated luminosity, we obtain the previous relation (Eq. 5)

$$A_{exp} = \frac{n^+ - n^-}{n^+ + n^-} = P_e P_\gamma A_l. \tag{11}$$

A_{exp} and P_γ are measured quantities and A_l is calculated in the framework of the standard model [6] (see Eq. 24), so that the only unknown quantity is the electron beam longitudinal polarization P_e. This method is a well established technique [7] and is currently used at several high energy machines [8], [9]. Cebaf will be one of the first low energy accelerator to use a Compton polarimeter.

In fact we plan to perform a differential measurement. In order to explicitly show the energy dependence and the detection efficiency, these counting rates can be expressed as:

$$\frac{dn^\pm}{d\rho} = \mathcal{L}^\pm T^\pm \;\; \frac{d\sigma_0}{d\rho} \;\; \epsilon(\rho) \;\; (1 \pm P_e P_\gamma A_l(\rho)). \tag{12}$$

In these equations,

- ρ is the scattered photon energy (normalized to the maximum scattered photon energy)
- $d\sigma_0/d\rho$ is the unpolarized Compton scattering cross section (See section 2.2)
- $\epsilon(\rho)$ is the acceptance of the polarimeter

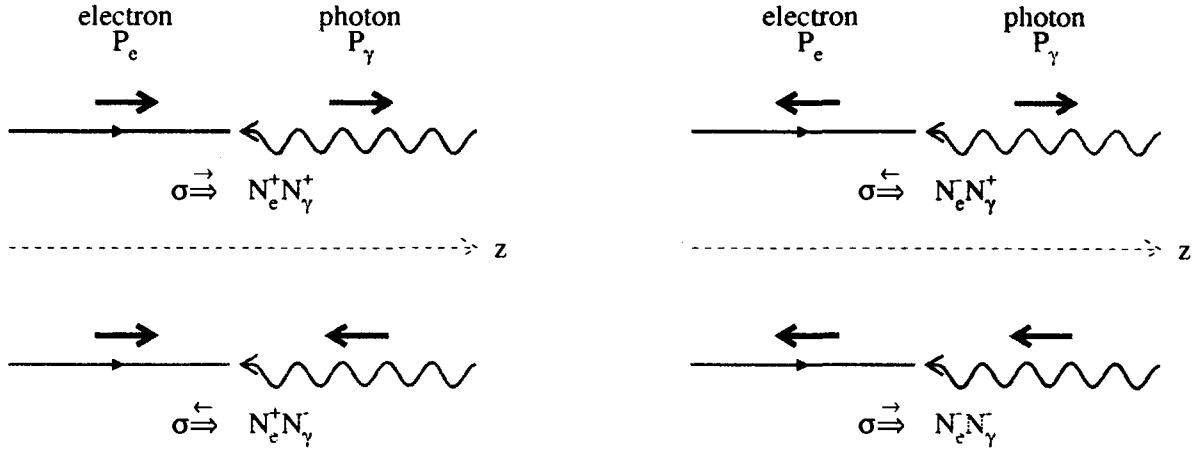

Figure 1: ***The four possible helicity configurations.*** *Electron and Photon Polarizations are defined with respect to the z axis.*

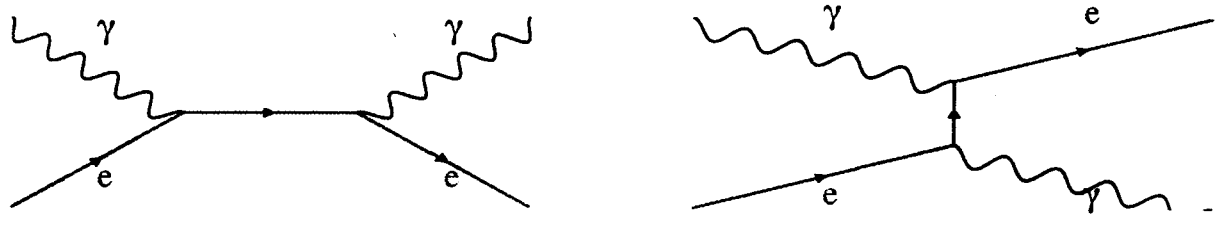

Figure 2: ***Feynman Diagrams for Compton Scattering.***

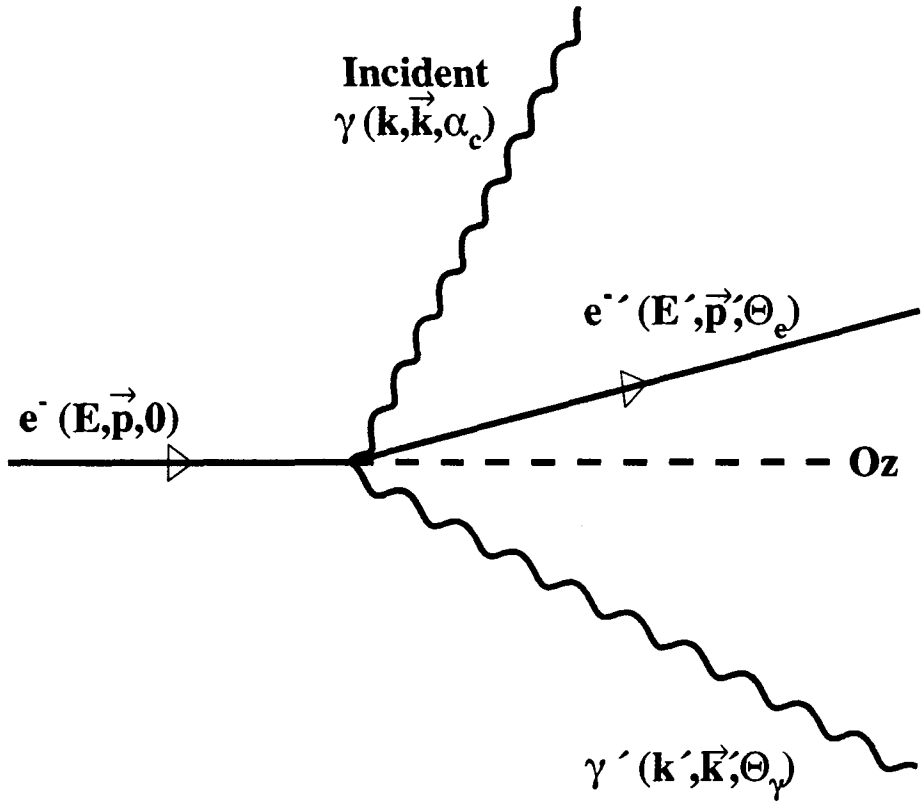

Figure 3: ***Compton Scattering***

2 Compton Scattering

In this section we first recall the kinematic of the Compton scattering, since this will strongly influence our setup. After a brief summary of the dynamic (polarized and unpolarized cross section, longitudinal asymmetry), the statistical accuracy on the polarization measurement will be derived as a function of the luminosity.

2.1 Kinematic of Compton scattering $e\,\gamma \rightarrow e\,\gamma$

We note (Fig. 3)

- Incident electron e with energy E and momentum $\vec{p} = (0, 0, p)$ along (Oz) axis,
- Incident photon γ with energy k , incident angle α_c with respect to (Oz) and momentum $\vec{k} = (0, -k\sin\alpha_c, -k\cos\alpha_c)$,
- Scattered electron e' with energy E', scattering angle θ_e with respect to (Oz) and momentum $\vec{p'} = (p'\sin\theta_e\sin\phi, p'\sin\theta_e\cos\phi, p'\cos\theta_e)$,
- Scattered photon γ' with energy k', scattering angle θ_γ with respect to (Oz) and momentum $\vec{k'} = (k'\sin\theta_\gamma\sin\phi, k'\sin\theta_\gamma\cos\phi, k'\cos\theta_\gamma)$.

In this 2-body kinematic where the initial state is known, only one parameter (with the non relevant angle ϕ between the incident and scattered planes) is necessary to determine the whole kinematic.

The scattered photon energy k' is related to the scattered photon angle θ_γ by :

$$k' = k\frac{E + p\cos\alpha_c}{E + k - p\cos\theta_\gamma + k\cos(\alpha_c - \theta_\gamma)}. \tag{13}$$

For photon incident angle $\alpha_c = 0$, this equation can be simplified, using $\gamma = E/m$, leading to

$$\frac{k'}{k} \simeq \frac{4a\gamma^2}{1 + a\theta_\gamma^2\gamma^2}, \tag{14}$$

where

$$a = \frac{1}{1 + \frac{4k\gamma}{m}} = \frac{1}{1 + \frac{4kE}{m^2}}. \tag{15}$$

The maximum scattered photon energy k'_{max}, corresponding to the minimum scattered electron energy E'_{min}, is reached for $\theta_\gamma = 0.$,

$$k'_{max} = 4ak\gamma^2 = 4ak\frac{E^2}{m^2}, \tag{16}$$

$$E'_{min} = E - k'_{max} + k = E - 4ak\frac{E^2}{m^2} + k \simeq E - 4ak\frac{E^2}{m^2}, \tag{17}$$

while the minimum scattered photon energy k'_{min}, corresponding to the maximum scattered electron energy E'_{max}, is for $\theta_\gamma = \pi$,

$$k'_{min} = k, \tag{18}$$

$$E'_{max} = E - k'_{min} + k = E. \tag{19}$$

The photon scattering angle at which $k' = k'_{max}/2$ is

$$\theta_{\gamma 1/2} = \frac{m}{E\sqrt{a}} = \frac{1}{\gamma\sqrt{a}}. \tag{20}$$

The scattered electron momentum p' is related to the scattered electron angle θ_e by a second order equation:

$$p'^2(C^2 - B^2) - 2ABp' + m^2C^2 - A^2 = 0,$$

$$p' = \frac{AB \pm C\sqrt{(A^2 - m^2(C^2 - B^2))}}{C^2 - B^2},$$

where

$$\begin{aligned} A &= m^2 + Ek + kp\cos\alpha_c, \\ B &= p\cos\theta_e - k\cos(\theta_e - \alpha_c), \\ C &= E + k. \end{aligned}$$

The maximum electron angle is obtained for $A^2 = m^2(C^2 - B^2)$. For small photon incident angle and energy, one gets :

$$\theta_e^{max} \simeq 2\frac{k}{m}. \tag{21}$$

Laser : α_c = 20.0 mrad k = 1.165 eV λ = 1064.2 nm								
$E(GeV)$	1.	2.	3.	4.	5.	6.	7.	8.
a	0.982	0.966	0.949	0.933	0.918	0.903	0.889	0.875
$k'_{max}(MeV)$	18.	69.	152.	266.	410.	580.	777.	999.
$E'_{min}(GeV)$	0.982	1.931	2.848	3.734	4.590	5.420	6.223	7.001
$\theta_{\gamma 1/2}(\mu rad)$	515.5	260.0	174.8	132.2	106.7	89.6	77.4	68.3
$\theta_e^{max}(\mu rad)$	4.56	4.56	4.56	4.56	4.56	4.56	4.56	4.56

Laser : α_c = 20.0 mrad k = 2.330 eV λ = 532.1 nm								
$E(GeV)$	1.	2.	3.	4.	5.	6.	7.	8.
a	0.966	0.933	0.903	0.875	0.849	0.824	0.800	0.778
$k'_{max}(MeV)$	34.	133.	290.	500.	757.	1058.	1399.	1777.
$E'_{min}(GeV)$	0.966	1.867	2.710	3.500	4.243	4.942	5.601	6.223
$\theta_{\gamma 1/2}(\mu rad)$	520.0	264.5	179.2	136.6	110.9	93.8	81.6	72.4
$\theta_e^{max}(\mu rad)$	9.12	9.12	9.12	9.12	9.12	9.12	9.12	9.12

Laser : α_c = 20.0 mrad k = 5.000 eV λ = 248.0 nm								
$E(GeV)$	1.	2.	3.	4.	5.	6.	7.	8.
a	0.929	0.867	0.813	0.765	0.723	0.685	0.651	0.620
$k'_{max}(MeV)$	71.	266.	560.	938.	1384.	1889.	2443.	3039.
$E'_{min}(GeV)$	0.929	1.734	2.440	3.062	3.616	4.111	4.557	4.961
$\theta_{\gamma 1/2}(\mu rad)$	530.2	274.4	188.9	146.0	120.2	102.9	90.5	81.1
$\theta_e^{max}(\mu rad)$	19.57	19.57	19.57	19.57	19.57	19.57	19.57	19.57

Table 1: ***Kinematic Parameters.*** *For different electron beam energies E and for LASER energies of $k = 1.16\ eV$ (up, IR NdYAG), $k = 2.33\ eV$ (middle, Green Argon) and $k = 5.0\ eV$ (down, UV KrF).*

These kinematic parameters are listed in table (1) for a LASER with energy $k = 1.16\ eV$ (resp. $k = 2.33\ eV$, $k = 5.0\ eV$) or wavelength $\lambda = 1064\ nm$ (resp. $\lambda = 532\ nm$, $\lambda = 248\ nm$). The relationships between the energies (k' or E') and the angles (θ_γ or θ_e) of the scattered γ or e^- are shown on figure (4).

One can see (Fig. 4) that **scattered electrons and photons (with $k'/k'_{max} > 0.1$) have a very small opening angle.** This means that to allow scattered photon or electron detection one needs to separate the scattered electron, the scattered photon and the incident electron. This will be done using a **MAGNETIC CHICANE** that will deflect and separate the scattered and incident electron and let room for the photon detector.

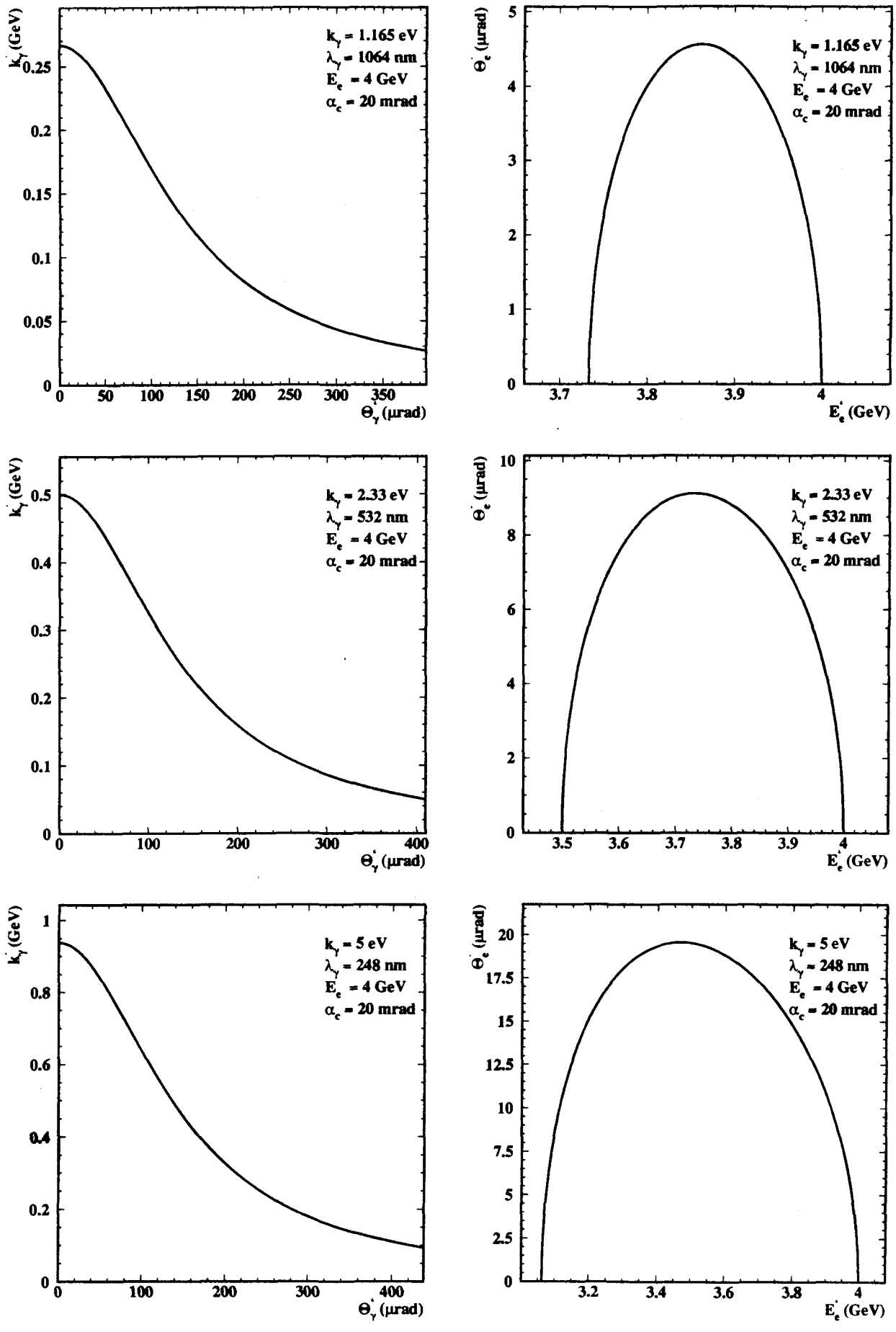

Figure 4: ***Kinematic of the Compton scattering.*** *Scattered γ energy k'_γ as a function of scattered γ angle θ_γ (left). Scattered e^- energy E'_e as a function of scattered e^- angle θ_e (right). For an electron beam energy of 4 GeV and a laser of 1064 nm , 532 nm , and 248 nm , with a crossing angle α_c=20 mrad.*

2.2 Compton Scattering Cross Section and Asymmetry

If the crossing angle α_c is equal to 0., **the differential unpolarized cross section** is [10],[11] (Fig. 5)

$$\frac{d\sigma}{d\rho} = 2\pi r_0^2 a \left[\frac{\rho^2(1-a)^2}{1-\rho(1-a)} + 1 + \left(\frac{1-\rho(1+a)}{1-\rho(1-a)} \right)^2 \right], \tag{22}$$

where

- the classical electron radius r_0 is given by $r_0 = \alpha_c \hbar c/mc^2 = 2.817\ 10^{-13}\ cm$,
- $\rho = k'/k'_{max}$ is the scattered γ energy normalized to the maximal energy (Eq. 16),
- a a kinematic parameter given by Eq. 15 : $a = 1/(1 + \frac{4kE}{m^2})$.

For **the total cross section**, we get after integration of the previous equation (Eq. 22)

$$\sigma = \pi\ {r_0}^2 a \frac{(-1 - 14\ a + 16\ a^2 - 2\ a^3 + a^4 + 2\ \ln(a) - 12\ \ln(a)a - 6\ \ln(a)a^2)}{(-1+a)^3}, \tag{23}$$

which only depends of a i.e. of kE (Eq. 15). The total cross section varies smoothly with kE as shown on figure (6) (see also Tab. 2).

The longitudinal differential asymmetry (Fig. 5, 1) is given by

$$A_l = \frac{\sigma^{\rightarrow}_{\Rightarrow} - \sigma^{\leftarrow}_{\Rightarrow}}{\sigma^{\rightarrow}_{\Rightarrow} + \sigma^{\leftarrow}_{\Rightarrow}} = \frac{2\pi r_0^2 a}{\frac{d\sigma}{d\rho}} (1 - \rho(1+a)) \left[1 - \frac{1}{(1-\rho(1-a))^2} \right],$$

$$A_l = \frac{1}{\left[\frac{\rho^2(1-a)^2}{1-\rho(1-a)} + 1 + \left(\frac{1-\rho(1+a)}{1-\rho(1-a)} \right)^2 \right]} (1 - \rho(1+a)) \left[1 - \frac{1}{(1-\rho(1-a))^2} \right]. \tag{24}$$

The longitudinal asymmetry is maximum for $\rho = 1$, i.e $k' = k'_{max}$ (high energy scattered photon) or $E' = E'_{min}$ (low energy scattered electron) :

$$A_l^{max} = \frac{(1-a)(1+a)}{(1+a^2)}, \tag{25}$$

and is thus almost proportional to $4Ek$ (Tab. 2 and Fig. 6).

We note that the asymmetry A_l (Fig. 5) is negative at low scattered photon energy, positive at higher energy and vanishes for $\rho_0 = 1/(1+a)$, i.e for

$$k'_0 = \frac{2k\gamma^2}{1 + 2\frac{k\gamma}{m}}. \tag{26}$$

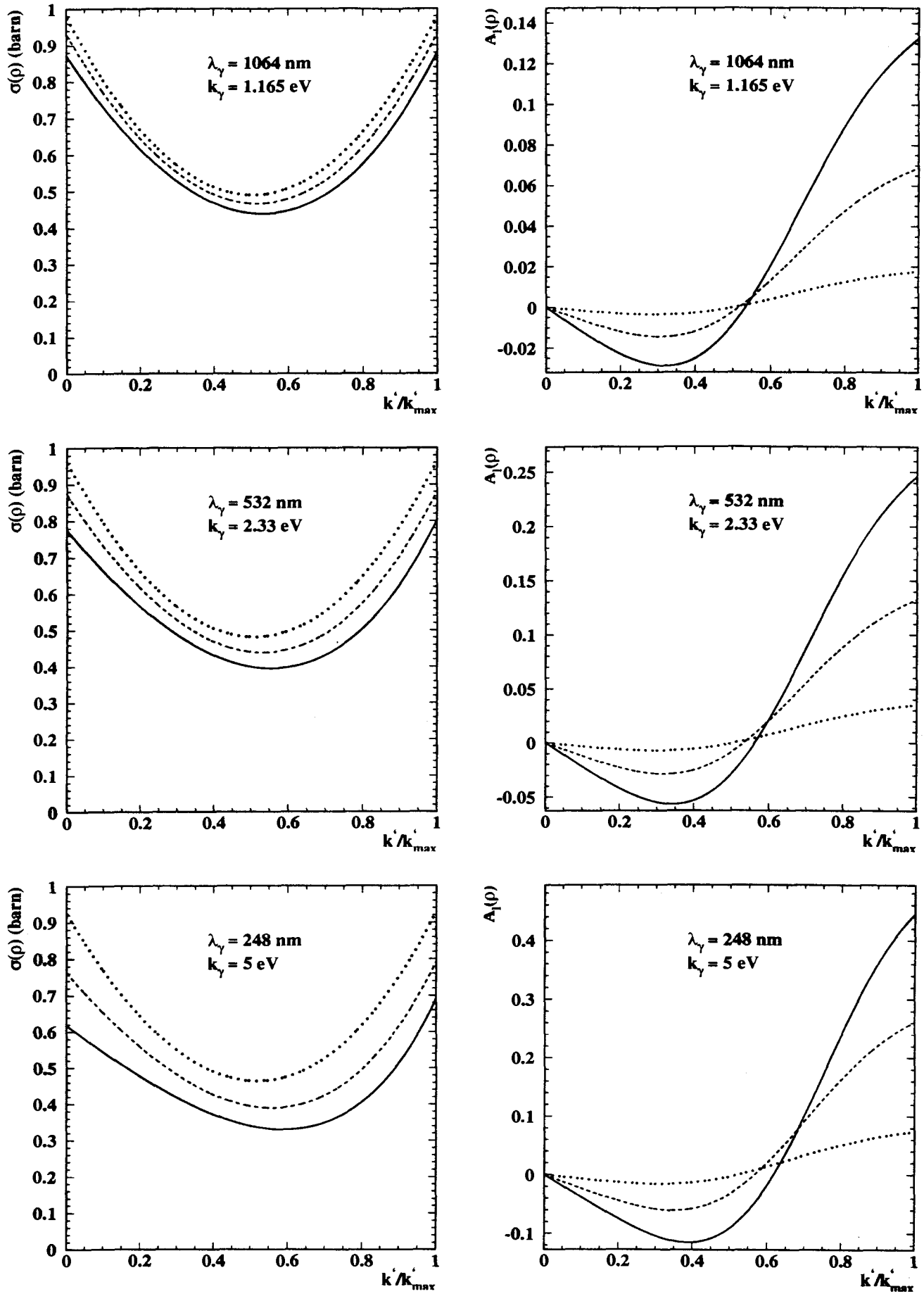

Figure 5: ***Compton unpolarized cross section and longitudinal asymmetry as a function of the scattered photon energy*** k'_γ. *For an electron beam energy of* 8 *GeV (solid line),* 4 *GeV (dashed line) and* 1 *GeV (dotted line) and a* 1064 *nm (Up),* 532 *nm (Middle) and a* 248 *nm (Down) laser, with a crossing angle angle* $\alpha_c = 0$.

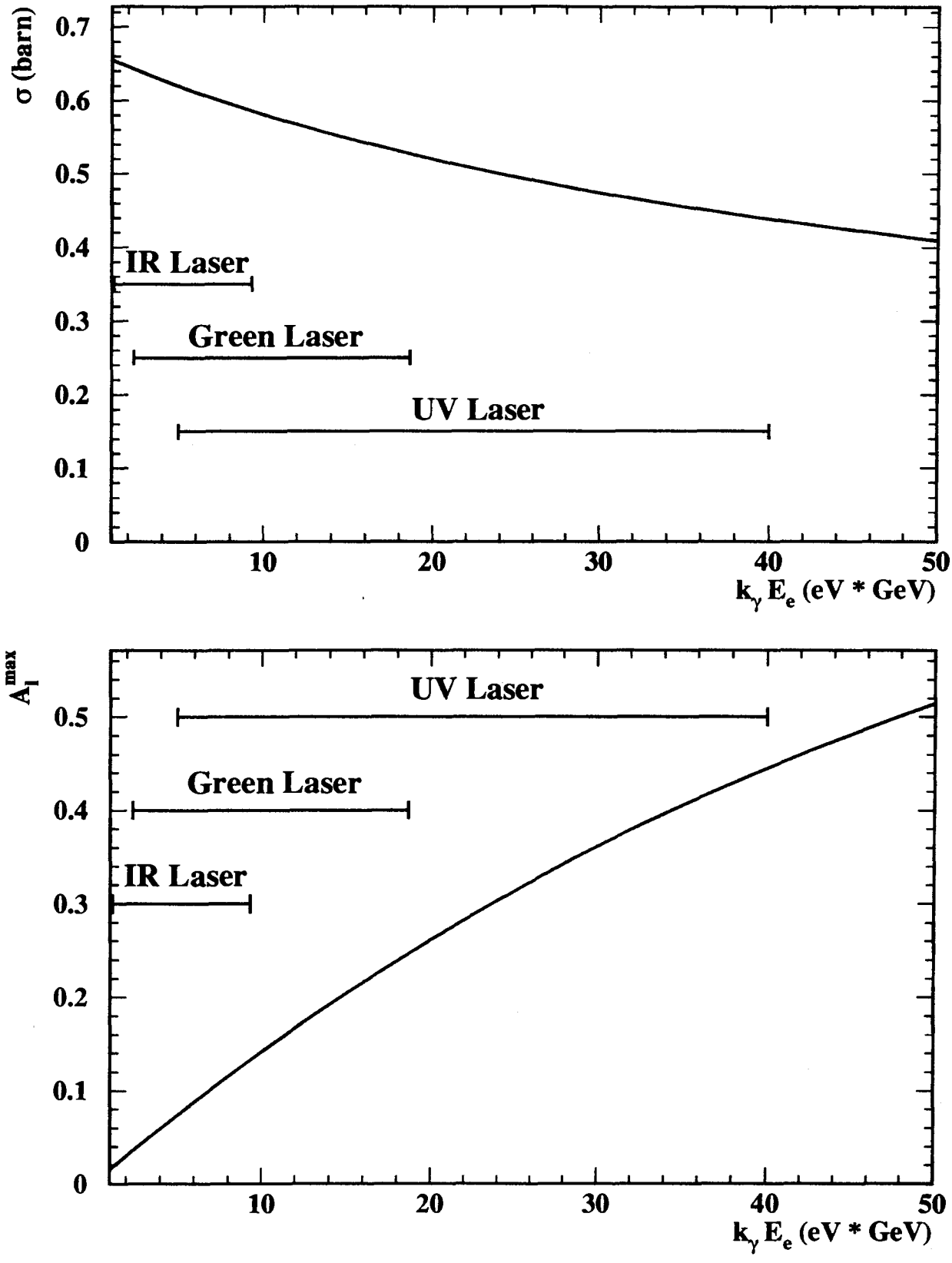

Figure 6: ***Compton total unpolarized cross section and maximum longitudinal asymmetry as a function of*** $k_\gamma E_e$ ***(Laser energy * electron beam energy).*** *Kinematic range for* E_e *varying from* 1 *GeV to* 8 *GeV and for IR,Green and UV Lasers.*

2.3 Consideration on the experimental measurement of the electron polarization

The longitudinal polarization P_e of the electron beam is extracted from the asymmetry between 2 measurements of Compton scattering with parallel (+) or anti parallel (-) polarization of the electron and Laser beams. Each measurement, performed with a luminosity $\mathcal{L}_+$ ($\mathcal{L}_-$) during a time T_+ (T_-), will be later normalized to the same integrated luminosity. According to possible experimental performances of our setup, we consider now 3 possibilities.

- **Differential Polarization Measurement**
  Event by event, the scattered photon or electron energy can be determined. So the numbers of Compton scattering events n^i_+ and n^i_- are measured as a function of the scattered γ or e energy in N_b bins. From the asymmetry of these numbers, a measurement of the polarization P^i_e is performed for each energy bin. The weighted mean of P^i_e gives the electron polarization.

- **Integrated Polarization Measurement**
  Without energy measurement for the scattered particles, only the numbers of compton scattering events integrated over the energy range N_+ and N_- can be measured. From the asymmetry of these numbers, the electron polarization is deduced if we know the detection efficiency and the energy threshold for the scattered particles detection.

- **Energy Polarization weighted Measurement**
  If we can only measure the energy integrated over the energy range , the polarization will be deduced from the asymmetry between the integrated energies E_+ and E_-. In this case, we have also to know the detection efficiency and the energy threshold. Furthermore the error also depends on these 2 parameters.

For the 2 measurements with parallel (anti parallel) polarization of the electron and Laser beams, we assume now in the next sections, where we will examine for these 3 methods their efficiency to reach a given statistical accuracy, the same integrated luminosity $\mathcal{L}_+T_+ = \mathcal{L}_-T_- = \mathcal{L}\ T/2$ (where $\mathcal{L}$ is the mean luminosity and T is the total time of the measurements) and the same differential efficiency $\epsilon_+(\rho) = \epsilon_-(\rho) = \epsilon(\rho)$. The release of these assumptions will be studied in section 11.

2.3.1 Differential Polarization Measurement

The numbers of compton scattering events as a function of the scattered photon energy for each of the N_b energy bins are

$$n^i_+ = \mathcal{L}_+\ T_+ \int_{\rho_i}^{\rho_{i+1}} d\rho\ \epsilon_+(\rho)\ \frac{d\sigma}{d\rho}(\rho)\ (1 + P_e P_\gamma A_l(\rho)), \tag{27}$$

$$n^i_- = \mathcal{L}_-\ T_- \int_{\rho_i}^{\rho_{i+1}} d\rho\ \epsilon_-(\rho)\ \frac{d\sigma}{d\rho}(\rho)\ (1 - P_e P_\gamma A_l(\rho)), \tag{28}$$

where $\frac{d\sigma}{d\rho}(\rho)$ is the unpolarized differential Compton cross section (Eq. 22) and $A_l(\rho)$ the differential asymmetry (Eq. 24).

The experimental asymmetry for each bin is related to the electron polarization by

$$A^i_{exp} = \frac{n^i_+ - n^i_-}{n^i_+ + n^i_-} = P_e P_\gamma \frac{\int d\rho\epsilon\ \frac{d\sigma}{d\rho}\ A_l}{\int d\rho\epsilon\ \frac{d\sigma}{d\rho}} = P_e P_\gamma\ < A_l >_i\ \simeq\ P_e P_\gamma\ A^i_l, \tag{29}$$

where A^i_l is the longitudinal polarization at the center of the bin.

The electron polarization measured for each bin P_e^i given by

$$P_e^i = \frac{A_{exp}^i}{P_\gamma < A_l >_i} \simeq \frac{A_{exp}^i}{P_\gamma \ A_l^i} \tag{30}$$

is then almost independent of the detection efficiency and have an absolute error dP_e^i given by

$$\frac{dP_e^{i\,2}}{P_e^{i\,2}} = \frac{dA_{exp}^{i\ 2}}{A_{exp}^{i\ 2}} = 4\frac{n_+^i n_-^i}{n_t^{i\,3}} \frac{1}{(P_e P_\gamma A_l^i)^2} = \frac{1-(P_e P_\gamma A_l^i)^2}{2n_t^i} \frac{1}{(P_e P_\gamma A_l^i)^2},$$

$$dP_e^{i\,2} = \frac{1-(P_e P_\gamma A_l^i)^2}{2n_t^i} \frac{1}{(P_\gamma A_l^i)^2} = \frac{1}{\mathcal{L}T P_\gamma^2} \frac{1-(P_e P_\gamma A_l^i)^2}{\sigma^i A_l^{i\,2}},$$

where n_t^i is the total number of events for the bin i

$$n_t^i = n_+^i + n_-^i = \mathcal{L}T \int_{\rho_i}^{\rho_{i+1}} d\rho \ \epsilon \ \frac{d\sigma}{d\rho}(\rho) = \mathcal{L}T \ \sigma^i.$$

The final electron polarization, obtained as the weighted mean of these polarization measurements,

$$P_e = \frac{\sum_{i=1}^{N_b} \frac{P_e^i}{dP_e^{i\,2}}}{\sum_{i=1}^{N_b} \frac{1}{dP_e^{i\,2}}}, \tag{31}$$

is also almost independent of the detection efficiency and does not depend on the detection threshold.

The error achieved with a total number of events N_t for an energy threshold ρ_{min}

$$N_t = \sum_{i=1}^{N_b} n_t^i = \mathcal{L}T \int_{\rho_{min}}^{1} d\rho \ \epsilon \ \frac{d\sigma}{d\rho}(\rho) = \mathcal{L}T \ \sigma_t \qquad with \qquad \sigma_t = \int_{\rho_{min}}^{1} d\rho \ \epsilon \ \frac{d\sigma}{d\rho}(\rho) \tag{32}$$

is given by

$$\frac{1}{dP_e^{\ 2}} = \sum_{i=1}^{N_b} \frac{1}{dP_e^{i\,2}} = \mathcal{L}T \ P_\gamma^2 \ \sum_{i=1}^{N_b} \frac{\sigma^i A_l^{i\,2}}{1-(P_e P_\gamma A_l^i)^2} = \mathcal{L}T \ P_\gamma^2 \int_{\rho_{min}}^{1} \frac{\epsilon \ \sigma A_l^{\ 2}}{1-(P_e P_\gamma A_l)^2},$$

$$\left(\frac{dP_e}{P_e}\right)^{-2} = \mathcal{L}T \ P_e^2 P_\gamma^2 \ \sigma_t < \frac{A_l^2}{1-P_e^2 P_\gamma^2 A_l^2} > \simeq \mathcal{L}T \ P_e^2 P_\gamma^2 \ \sigma_t < A_l^2 >, \tag{33}$$

where the mean value $< A_l^2 >$ stands for

$$< A_l^2 > = \frac{\int_{\rho_{min}}^{1} d\rho \ \epsilon(\rho) \ \frac{d\sigma}{d\rho}(\rho) \ A_l(\rho)^2}{\int_{\rho_{min}}^{1} d\rho \ \epsilon(\rho) \ \frac{d\sigma}{d\rho}(\rho)}. \tag{34}$$

The needed time t_D to achieve an accuracy $\Delta P_e/P_e$ is then

$$t_D^{-1} = \mathcal{L} \left(\frac{\Delta P_e}{P_e}\right)^2 P_e^2 P_\gamma^2 \ \sigma_t < \frac{A_l^2}{1-P_e^2 P_\gamma^2 A_l^2} > \simeq \mathcal{L} \left(\frac{\Delta P_e}{P_e}\right)^2 P_e^2 P_\gamma^2 \ \sigma_t < A_l^2 > \tag{35}$$

and corresponds to a total number of events

$$N_t^D = \mathcal{L} t_D \sigma_t \simeq \frac{1}{\left(\frac{\Delta P_e}{P_e}\right)^2 P_e^2 P_\gamma^2 < A_l^2 >}. \tag{36}$$

We note that the needed time t_D as well as the square of the error are proportional to the inverse of $< A_l^2 >$.

2.3.2 Integrated Polarization Measurement

The numbers of compton scattering events integrated over the energy range N_+ and N_- are

$$N_+ = \mathcal{L}_+ \; T_+ \int_{\rho_{min}}^{1} d\rho \; \epsilon_+(\rho) \; \frac{d\sigma}{d\rho}(\rho) \; (1 + P_e P_\gamma A_l(\rho)), \tag{37}$$

$$N_- = \mathcal{L}_- \; T_- \int_{\rho_{min}}^{1} d\rho \; \epsilon_-(\rho) \; \frac{d\sigma}{d\rho}(\rho) \; (1 - P_e P_\gamma A_l(\rho)). \tag{38}$$

The experimental integrated asymmetry is related to the electron polarization by

$$A_{exp} = \frac{N_+ - N_-}{N_+ + N_-} = P_e P_\gamma \; \frac{\int \epsilon \; \sigma A_l}{\int \epsilon \; \sigma} = P_e P_\gamma \; < A_l > \tag{39}$$

where the mean value $< A_l >$ stands for

$$< A_l > = \frac{\int_{\rho_{min}}^{1} d\rho \; \epsilon(\rho) \; \frac{d\sigma}{d\rho}(\rho) \; A_l(\rho)}{\int_{\rho_{min}}^{1} d\rho \; \epsilon(\rho) \; \frac{d\sigma}{d\rho}(\rho)}. \tag{40}$$

Thus the measured electron polarization

$$P_e = \frac{A_{exp}}{P_\gamma \; < A_l >} \tag{41}$$

is proportional to the inverse of the mean longitudinal asymmetry and so depends on the detection efficiency and on the detection threshold ρ_{min}.

The absolute and relative errors on the experimental integrated asymmetry are

$$dA_{exp}{}^2 = 4\frac{N_+ N_-}{N_t{}^3} = \frac{1}{\mathcal{L}T} \; \frac{1}{\sigma_t} \left(1 - \left(P_e P_\gamma \frac{\int \epsilon \sigma A_l}{\sigma_t}\right)^2\right) = \frac{1}{\mathcal{L}T} \; \frac{1}{\sigma_t} \left(1 - (P_e P_\gamma < A_l >)^2\right),$$

$$\left(\frac{dA_{exp}}{A_{exp}}\right)^{-2} = \left(\frac{dP_e}{P_e}\right)^{-2} = \mathcal{L}T \; P_e^2 P_\gamma^2 \; \sigma_t \; \frac{< A_l >^2}{1 - P_e^2 P_\gamma^2 < A_l >^2}, \tag{42}$$

where σ_t and N_t are given by equation (32).

The needed time t_I to achieve an accuracy $\Delta P_e / P_e$ is then

$$t_I^{-1} = \mathcal{L} \left(\frac{\Delta P_e}{P_e}\right)^2 P_e^2 P_\gamma^2 \; \sigma_t \; \frac{< A_l >^2}{1 - P_e^2 P_\gamma^2 < A_l >^2} \simeq \mathcal{L} \left(\frac{\Delta P_e}{P_e}\right)^2 P_e^2 P_\gamma^2 \; \sigma_t < A_l >^2, \tag{43}$$

corresponding to a total number of events

$$N_t^I = \mathcal{L} t_I \sigma_t \simeq \frac{1}{\left(\frac{\Delta P_e}{P_e}\right)^2 \; P_e^2 P_\gamma^2 \; < A_l >^2}. \tag{44}$$

We note that the needed time t_I as well as the square of the error are proportional to the inverse of $< A_l >^2$. We have seen (Fig. 5) that the asymmetry A_l is negative at low scattered photon energy and positive at higher energy. So in an integrated asymmetry measurement, it will be helpful to impose an hardware threshold to cut the lower energy part of that spectrum and increase the mean longitudinal asymmetry.

For a 100% efficiency $\epsilon(\rho)$ of the detection and a threshold ρ_{min}=0, the mean longitudinal (weighted by the cross section) asymmetry is :

$$< A_l > = \frac{\int_0^1 d\rho \ A_l \frac{d\sigma}{d\rho}}{\int_0^1 d\rho \ \frac{d\sigma}{d\rho}} = \frac{\int d\rho \ 2\pi r_0^2 \ (1-\rho(1+a)) \ \left[1 - \frac{1}{(1-\rho(1-a))^2}\right]}{\int \frac{d\sigma}{d\rho}}.$$

$$< A_l > = -\frac{(-5+7\,a-3\,a^2+a^3-2\,\ln(a)-2\,\ln(a)a) \ (-1+a)}{(-1-14\,a+16\,a^2-2\,a^3+a^4+2\,\ln(a)-12\,\ln(a)a-6\,\ln(a)a^2)}. \quad (45)$$

2.3.3 Energy weighted Polarization Measurement

The integrated energy E_+ and E_- over the energy range and over the time t are given by :

$$E_+ = \mathcal{L}_+ T_+ \int_{\rho_{min}}^1 d\rho \ E \ \epsilon_+(\rho) \ \frac{d\sigma}{d\rho}(\rho) \ (1 + P_e P_\gamma A_l(\rho)), \quad (46)$$

$$E_- = \mathcal{L}_- T_- \int_{\rho_{min}}^1 d\rho \ E \ \epsilon_-(\rho) \ \frac{d\sigma}{d\rho}(\rho) \ (1 - P_e P_\gamma A_l(\rho)), \quad (47)$$

with a statistical error $dE_\pm$ due to the fluctuation of the unmeasured number of events $\frac{dN_\pm}{d\rho}$

$$\frac{dN_\pm}{d\rho} = \mathcal{L}_\pm T_\pm \epsilon_\pm \frac{d\sigma}{d\rho}(1 \pm P_e P_\gamma A_l)$$

$$dE_\pm^2 = \mathcal{L}\frac{T}{2} \int_{\rho_{min}}^1 d\rho \ E^2 \ \epsilon_\pm(\rho) \ \frac{d\sigma}{d\rho}(\rho) \ (1 \pm P_e P_\gamma A_l(\rho)). \quad (48)$$

The experimental integrated energy asymmetry is related to the electron polarization by

$$A_{exp} = \frac{E_+ - E_-}{E_+ + E_-} = P_e P_\gamma \frac{\int \epsilon\sigma E A_l}{\int \epsilon\sigma E} = P_e P_\gamma \frac{< E A_l >}{< E >}. \quad (49)$$

Thus the measured electron polarization

$$P_e = \frac{A_{exp}}{P_\gamma \frac{<EA_l>}{<E>}} \quad (50)$$

is proportional to the inverse of the mean longitudinal asymmetry (weighted by the energy) and so depends on the detection efficiency and on the detection threshold ρ_{min}.

The absolute and relative errors on the experimental integrated asymmetry are

$$dA_{exp}{}^2 = 4 \ \frac{E_+^2 \ dE_-^2 + E_-^2 \ dE_+^2}{(E_+ + E_-)^4}$$

$$= \frac{1}{\mathcal{L}T} \frac{(\int \epsilon\sigma E^2)(\int \epsilon\sigma E)^2 + P_e^2 P_\gamma^2 \left[(\int \epsilon\sigma E^2)(\int \epsilon\sigma E A_l)^2 - 2 \ (\int \epsilon\sigma E)(\int \epsilon\sigma E A_l)(\int \epsilon\sigma E^2 A_l) \right]}{(\int \epsilon\sigma E)^4},$$

$$\left(\frac{dA_{exp}}{A_{exp}}\right)^{-2} = \left(\frac{dP_e}{P_e}\right)^{-2} = \mathcal{L}T P_e^2 P_\gamma^2 \sigma_t \frac{< E A_l >^2}{< E^2 >} \frac{1}{1 + P_e^2 P_\gamma^2 \left(\frac{<EA_l>^2}{<E>^2} - 2\frac{<EA_l><E^2A_l>}{<E><E^2>}\right)}, \quad (51)$$

where σ_t is given by equation (32) and the mean value $\frac{<EA_l>^2}{<E^2>}$ by

$$\frac{< EA_l >^2}{< E^2 >} = \frac{\left(\int_{\rho_{min}}^1 d\rho\ \epsilon(\rho)\ \frac{d\sigma}{d\rho}(\rho)\ EA_l(\rho)\right)^2}{\int_{\rho_{min}}^1 d\rho\ \epsilon(\rho)\ \frac{d\sigma}{d\rho}(\rho)\ E^2}. \tag{52}$$

These errors will have to be estimated since we don't measure the number of scattered events.

The needed time t_E to achieve an accuracy $\Delta P_e/P_e$ is then

$$t_E^{-1} = \mathcal{L}\ \left(\frac{\Delta P_e}{P_e}\right)^2\ P_e^2 P_\gamma^2\ \sigma_t\ \frac{< EA_l >^2}{< E^2 >}\ \frac{1}{1 + P_e^2 P_\gamma^2 \left(\frac{<EA_l>^2}{<E>^2} - 2\frac{<EA_l><E^2A_l>}{<E><E^2>}\right)}$$

$$\simeq \mathcal{L}\ \left(\frac{\Delta P_e}{P_e}\right)^2\ P_e^2 P_\gamma^2\ \sigma_t\ \frac{< EA_l >^2}{< E^2 >}, \tag{53}$$

corresponding to a total number of events

$$N_t^E = \mathcal{L} t_E \sigma_t \simeq \frac{1}{\left(\frac{\Delta P_e}{P_e}\right)^2\ P_e^2 P_\gamma^2\ \frac{<EA_l>^2}{<E^2>}}. \tag{54}$$

2.3.4 Conclusions

The needed time or the total number of events to achieve an accuracy $\Delta P_e/P_e$ is given by

$$t_{meth} = \frac{1}{\mathcal{L}\ \left(\frac{\Delta P_e}{P_e}\right)^2\ P_e^2 P_\gamma^2}\ \frac{1}{A_{meth}^2}\ \frac{1}{\sigma_t}, \tag{55}$$

where, according to the method (differential, integrated, energy weighted), A_{meth}^2 stands for (See Eq. 34,40 and 52)

$$< A^2 > \ :\ < A_l >^2 \ :\ \frac{< EA_l >^2}{< E^2 >}$$

with the relation

$$< A_l >^2 \ < \ \frac{< EA_l >^2}{< E^2 >} \ < \ < A^2 >.$$

The integrated unpolarized cross section (Eq. 32) is shown on figure (7).

The needed time for an accuracy $\Delta P_e/P_e = 1\%$, a luminosity $\mathcal{L} = 1\ \mu barn^{-1}s^{-1} = 10^6 barn^{-1}s^{-1}$, a detection efficiency $\epsilon = 100\%$, an electron polarization $P_e = 50\%$ and a Laser polarization $P_\gamma = 100\%$ is plotted on figure (7) for the 3 methods as a function of the energy threshold. We see the advantage for the integrated and energy weighted methods to put a hardware threshold $\rho_{min} \simeq 0.65$. Above this threshold, the 3 methods are equivalent and close ($\simeq 10\%$) to the optimum obtained in the differential method with an energy threshold =0. We recall that for the energy weighted method, the error on the electron polarization will have to be estimated.

Nevertheless, for the integrated and energy weighted methods, the measured polarization (Eq. 41 and 50) depends on the detection efficiency and on the energy threshold. We have plotted (Fig. 7) the variation of the measured asymmetry ($\simeq < A_l >$ or $< EA_l > / < E >$) with the energy threshold for these 2 methods (as well as $\sqrt{< A_l^2 >}$). Around $\rho_{min} \simeq 0.65$ a variation of 1 % on ρ gives a 1 % variation on the measured asymmetry and then on the electron polarization.

Finally, table (2) gives more complete results for some available lasers and for electron beam energies in the CEBAF range. We can see that to perform a 1 % measurement in 1 hour (at 4 GeV with $P_e = 50\%$), we need a luminosity of order of 2.10^3 to $2.10^4\ barn^{-1}s^{-1}$ according to the laser energy.

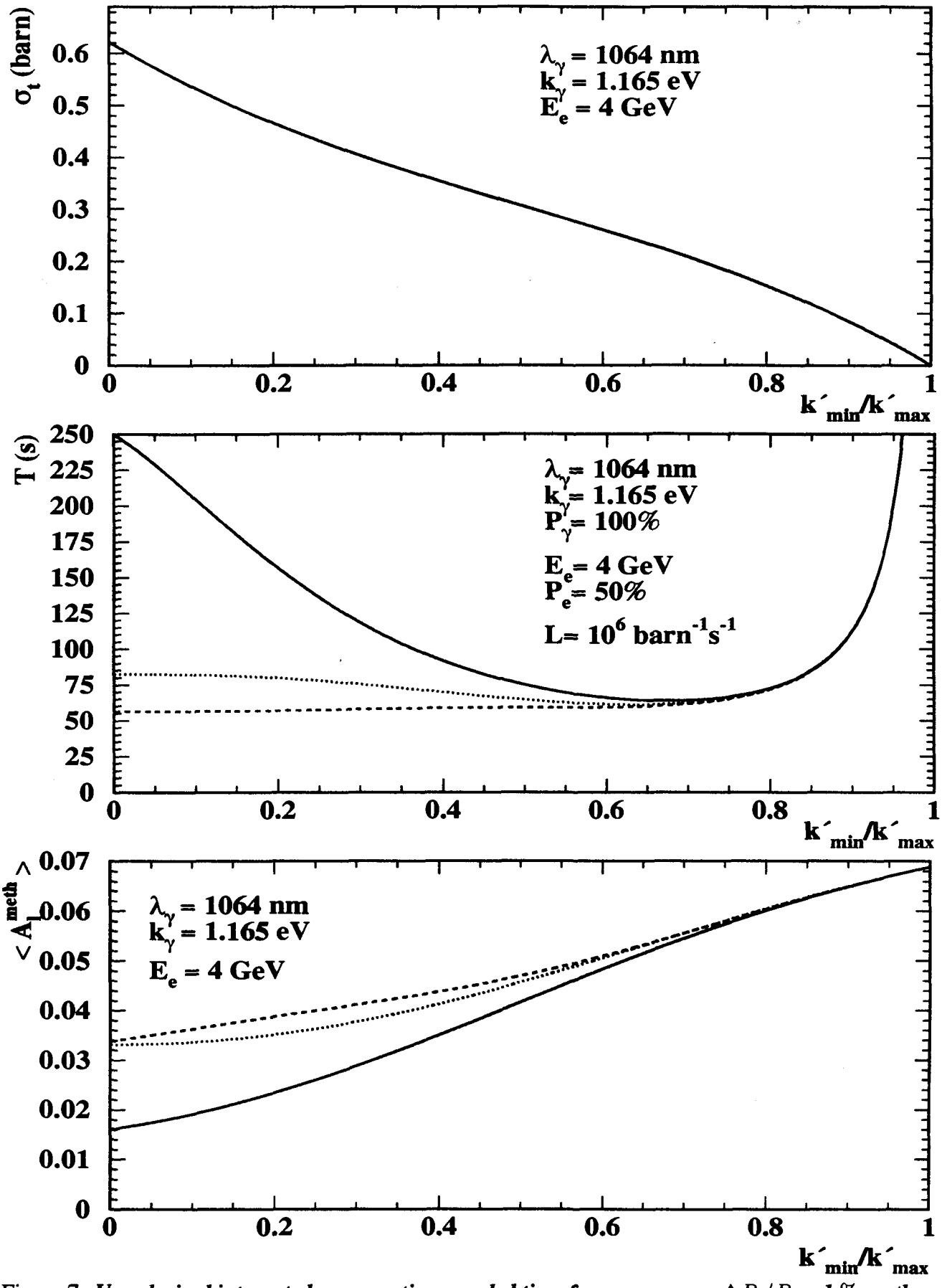

Figure 7: ***Unpolarized integrated cross section, needed time for an accuracy*** $\Delta P_e/P_e = 1\ \%$ ***on the electron polarization, mean asymmetry*** A_l^{meth} ***as a function of energy threshold.*** *For the 3 methods: integrated method (solid line* $A_l^{meth} =< A_l >$*), differential method (dashed line* $A_l^{meth} =< A_l^2 >^{0.5}$*) and energy weighted (dotted line* $A_l^{meth} = < EA_l > / < E >$*). For a laser of 1064 nm and for an electron beam energy of 4 GeV. The needed time is for a luminosity* $\mathcal{L} = 1\ \mu barn^{-1}s^{-1}$*, beam polarizations* $P_e = 50\%$ *and* $P_\gamma = 100\%$.

Laser : k = 1.165 eV λ = 1064.2 nm

E (GeV)	a	σ (barn)	k_{max} (MeV)	k_0 (MeV)	A_l^{max} (%)	$< A_l >$ (%)	$\sqrt{< A_l^2 >}$ (%)	$< A_l >_e$ (%)	t_I (s)	t_D (s)	t_E (s)
1.00	0.982	0.654	17.5	8.8	1.77	0.43	0.88	0.88	3243.	790.	1118.
2.00	0.966	0.643	68.9	35.1	3.51	0.85	1.74	1.72	870.	207.	295.
3.00	0.949	0.632	152.4	78.2	5.21	1.24	2.57	2.53	415.	96.	139.
4.00	0.933	0.622	266.5	137.8	6.88	1.60	3.38	3.31	250.	56.	82.
5.00	0.918	0.612	409.6	213.5	8.53	1.95	4.16	4.06	171.	38.	56.
6.00	0.903	0.603	580.3	304.9	10.14	2.28	4.93	4.78	127.	27.	41.
7.00	0.889	0.594	777.3	411.5	11.72	2.59	5.67	5.48	100.	21.	32.
8.00	0.875	0.585	999.4	533.0	13.27	2.89	6.39	6.14	82.	17.	25.

Laser : k = 2.330 eV λ = 532.1 nm

E (GeV)	a	σ (barn)	k_{max} (MeV)	k_0 (MeV)	A_l^{max} (%)	$< A_l >$ (%)	$\sqrt{< A_l^2 >}$ (%)	$< A_l >_e$ (%)	t_I (s)	t_D (s)	t_E (s)
1.00	0.966	0.643	34.5	17.5	3.51	0.85	1.74	1.72	870.	207.	295.
2.00	0.933	0.622	133.2	68.9	6.88	1.60	3.38	3.31	250.	56.	82.
3.00	0.903	0.603	290.1	152.4	10.14	2.28	4.93	4.78	127.	27.	41.
4.00	0.875	0.585	499.7	266.5	13.27	2.89	6.39	6.14	82.	17.	25.
5.00	0.849	0.569	757.1	409.6	16.27	3.43	7.78	7.40	60.	12.	18.
6.00	0.824	0.554	1058.2	580.3	19.16	3.91	9.09	8.55	47.	9.	14.
7.00	0.800	0.540	1399.2	777.3	21.94	4.33	10.33	9.61	40.	7.	11.
8.00	0.778	0.527	1776.8	999.4	24.60	4.70	11.51	10.58	34.	6.	10.

Laser : k = 5.000 eV λ = 248.0 nm

E (GeV)	a	σ (barn)	k_{max} (MeV)	k_0 (MeV)	A_l^{max} (%)	$< A_l >$ (%)	$\sqrt{< A_l^2 >}$ (%)	$< A_l >_e$ (%)	t_I (s)	t_D (s)	t_E (s)
1.00	0.929	0.619	71.1	36.9	7.37	1.71	3.61	3.53	221.	50.	73.
2.00	0.867	0.580	265.7	142.3	14.16	3.05	6.81	6.52	74.	15.	23.
3.00	0.813	0.548	560.5	309.1	20.39	4.10	9.64	9.03	44.	8.	13.
4.00	0.765	0.520	938.0	531.3	26.11	4.89	12.16	11.11	32.	5.	9.
5.00	0.723	0.495	1384.5	803.5	31.33	5.49	14.40	12.84	27.	4.	7.
6.00	0.685	0.474	1889.0	1121.0	36.11	5.91	16.39	14.25	24.	3.	6.
7.00	0.651	0.455	2443.0	1479.7	40.47	6.19	18.17	15.39	23.	3.	5.
8.00	0.620	0.438	3039.3	1876.1	44.46	6.36	19.76	16.31	23.	2.	5.

Table 2: ***Cross section, kinematic parameters, maximal asymmetry, mean asymmetries*** ($< A_l >$, $< A_l^2 >^{0.5}$, $< EA_l > / < E >$) ***and needed time to obtain an accuracy*** $\Delta P_e/P_e = 1\%$ ***on the electron polarization.*** *For a luminosity* $\mathcal{L} = 1.\ \mu barn^{-1}s^{-1}$, *an electron polarization* $P_e = 50\%$, *a Laser polarization* $P_\gamma = 100\%$ *and with an energy threshold* $\rho_{min} = 0$. *For different electron beam energies* E *and for a LASER of* $k = 1.16\ eV$ *(up, IR NdYAG),* $k = 2.33\ eV$ *(middle, Green Argon) and* $k = 5.0\ eV$ *(down, UV KrF)*

3 Expected Luminosity , Choice of the Laser , Expected Counting Rates

The needed time (Eq. 35,43,53) as well as the total number of events (Eq. 36,44,54) to achieve an accuracy $\Delta P_e/Pe$ on the electron polarization depends, for a given incident e^- energy, on

- the unpolarized Compton cross section , i.e. the energy of the Laser;
- the mean longitudinal asymmetry , i.e. the energy of the Laser;
- the luminosity , i.e. the shapes of the electron and Laser beams and of the crossing angle α_c of the 2 beams.

In the previous section, we have studied the cross section and asymmetry evolution with the beam parameters. We will now look at the luminosity for the interaction of the 2 beams with a crossing angle α_c in order to choose the Laser (see appendix B for more details on the extraction of the luminosity).

For standard continuous Laser (IR, NdYAG, $\lambda = 1064\ nm$, $k = 1.16\ eV$ or Green, Argon, $\lambda = 532\ nm$, $k = 2.33\ eV$), the available power is poor ($\simeq 1\ W$ for Argon and for NdYAG), but they are widely used system, cheap (200 kF) and very reliable. This low power makes the time needed for a 1 % measurement of the electron polarization high, even with a crossing angle α_c=0. To decrease this time, one can use

- a high Power Laser emitting at higher energy (to get an higher asymmetry) such as a pulsed Excimer 80 W (UV, KrF, $\lambda = 248\ nm$, $k = 5\ eV$) with an intensity $I_\gamma = 10^{20}\ \gamma/s$. This kind of Lasers are known to be very expensive (at least 150 k\$ $\simeq$ 800 kF), difficult to run and not reliable. One would then need to install the Laser in an accessible room (outside beam region) and setup a transport for the Laser light.
- a standard continuous Laser coupled with an amplification optical cavity. So one can avoid the Laser beam transportation problem. This elegant solution was presented for γ beam by B. Norum et al. [12]. The Laser is trapped in a cavity made of 2 highly reflective mirrors. To protect the cavity mirrors against the electron beam, a small crossing angle $\alpha_c \simeq 20\ mrad$ is necessary in this case.

A comparison of these 2 solutions will show that similar results can be expected leading to the choice of the safer second one.

3.1 General beam shape

The beam density in the beam frame (x, y, z where z is along the beam axis) is taken as the product of two normalized gaussians in x and y with a normalisation factor N_0

$$\rho(x,y,z) = N_0 \left(\frac{1}{\sqrt{2\pi}\sigma_x(z)}\ exp\left(-\frac{x^2}{2{\sigma_x}^2(z)}\right)\right)\left(\frac{1}{\sqrt{2\pi}\sigma_y(z)}\ exp\left(-\frac{y^2}{2{\sigma_y}^2(z)}\right)\right) \quad (56)$$

where $\sigma_x(z)$ and $\sigma_y(z)$ are the x and y beam sizes at z.

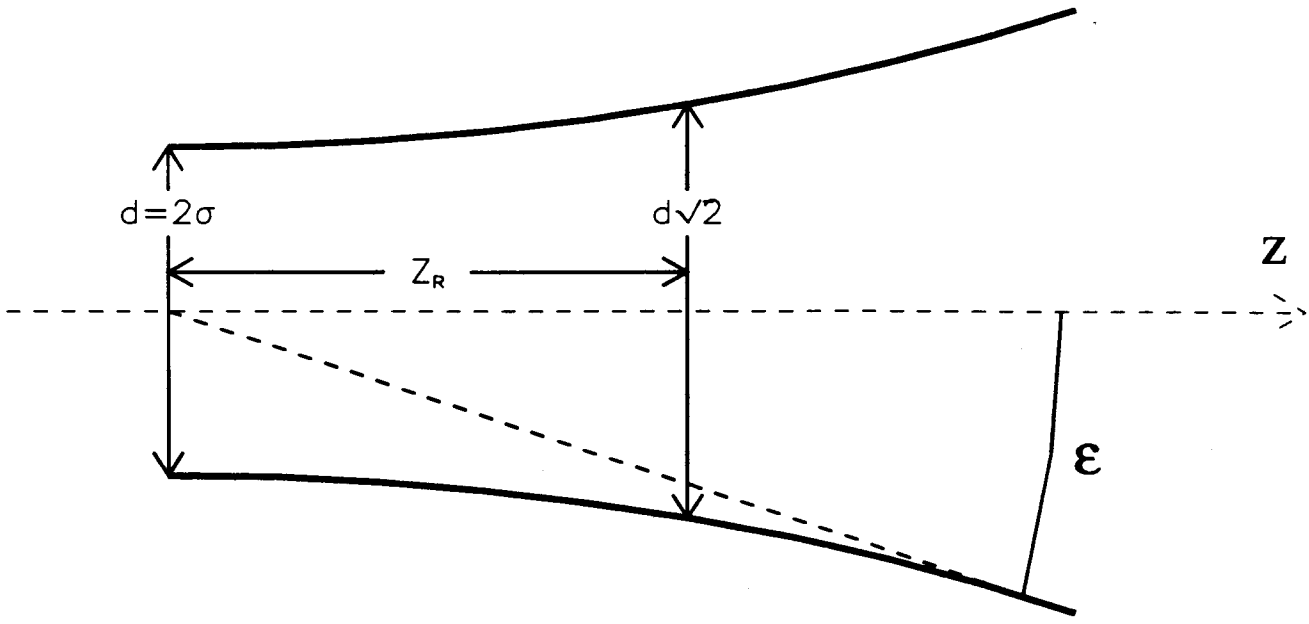

Figure 8: ***Beam shape.*** *Waist d, angular divergence ϵ and Rayleigh range Z_R .*

The evolution along z of these beam extensions is characterized (Fig. 8) by the waist beam size and the angular divergence ϵ (parametrized by the Rayleigh range Z)

$$\sigma_{x,y}{}^2(z) = \sigma_{x,y}{}^2(0) \quad \left(1. + \frac{z^2}{Z_{x,y}{}^2}\right). \tag{57}$$

So that the waist size and the asymptotic angular divergence are

$$\begin{aligned} d(0) &= 2\sigma(0), \\ tan(\epsilon) &= \sigma(0)/Z. \end{aligned} \tag{58}$$

The normalization factor N_0 for the Laser beam (power P_L and wavelength λ) is deduced from :

$$\frac{dN_\gamma}{dt} = \frac{P_L}{h\,\nu} = \frac{N_{0\gamma} \int\int\int \rho_\gamma\, dz\, dx\, dy}{dt} = \frac{N_{0\gamma} \int dz}{dt} = \frac{N_{0\gamma}\, c\, dt}{dt} = N_{0\gamma}\, c,$$

so we have :

$$N_{0\gamma} = \frac{P_L}{h\,\nu\,c} = \frac{P_L\,\lambda}{h\,c^2}. \tag{59}$$

The normalization factor N_0 for the electron beam (intensity I_e) is deduced from :

$$\frac{dN_e}{dt} = \frac{I_e}{e} = \frac{N_{0e} \int\int\int \rho_e\, dz\, dx\, dy}{dt} = \frac{N_{0e} \int dz}{dt} = \frac{N_{0e}\, c\, dt}{dt} = N_{0e}\, c,$$

so we have:

$$N_{0e} = \frac{I_e}{e\,c}. \tag{60}$$

We will assume now that

- the electron and Laser beam are focussed on the same point taken as the origin of the reference system,
- the electron and Laser beam are symmetric in x and y i.e.

$$\sigma_x(z) = \sigma_y(z) = \sigma\sqrt{\left(1. + \frac{z^2}{Z^2}\right)}.$$

3.2 Luminosity and interaction length

The total luminosity for the interaction of the Laser and the electron beams is

$$\mathcal{L} = \int\int\int v_{rel}\ \rho_e\ \rho_\gamma\ dz\ dx\ dy \tag{61}$$

where v_{rel}, the relative velocity of the two beams, is $v_{rel} = c(1 + cos(\alpha_c))$ with α_c crossing angle and ρ_e, ρ_γ are the electron and Laser beam's densities (see appendix B).

3.2.1 Luminosity for zero crossing angle

In the case of zero crossing angle, we have the following characteristics :

1. **Differential luminosity** given by

$$\frac{d\mathcal{L}_0}{dz} = \int\int v_{rel}\ \rho_e\ \rho_\gamma\ dx\ dy = \frac{I_e}{e}\ \frac{P_L\ \lambda}{h\,c^2}\ \frac{1}{\pi}\ \frac{1}{\left(\sigma_e^2 + \sigma_\gamma^2\right) + z^2\left(\left(\frac{\sigma_\gamma}{Z_\gamma}\right)^2 + \left(\frac{\sigma_e}{Z_e}\right)^2\right)},$$

$$\frac{d\mathcal{L}_0}{dz} = \frac{I_e}{e}\ \frac{P_L\ \lambda}{h\,c^2}\ \frac{1}{\pi}\ \frac{1}{\left(\sigma_e^2 + \sigma_\gamma^2\right) + z^2\left(\epsilon_\gamma{}^2 + \epsilon_e{}^2\right)}. \tag{62}$$

   The differential luminosity depends on 4 parameters $(\sigma_e, \epsilon_e, \sigma_\gamma, \epsilon_\gamma)$. For constant beam emittance $\mathcal{E} = \sigma\epsilon$, the width of this distribution (related to the interaction length which will be defined later) decreases when increasing the angular divergences.

2. **Total luminosity** given by

$$\mathcal{L}_0 = \int\int\int v_{rel}\ \rho_e\ \rho_\gamma\ dz\ dx\ dz = \frac{I_e}{e}\ \frac{P_L\ \lambda}{h\,c^2}\ \frac{1}{\sqrt{\left(\frac{\sigma_e^2}{Z_e}\right)^2 + \left(\frac{\sigma_\gamma^2}{Z_\gamma}\right)^2 + \left(\frac{\sigma_e^2}{Z_e}\right)\left(\frac{\sigma_\gamma^2}{Z_\gamma}\right)\left(\frac{Z_\gamma}{Z_e} + \frac{Z_e}{Z_\gamma}\right)}},$$

$$\mathcal{L}_0 = \frac{I_e}{e}\ \frac{P_L\ \lambda}{h\,c^2}\ \frac{1}{\sqrt{\left(\sigma_e\epsilon_e\right)^2 + \left(\sigma_\gamma\epsilon_\gamma\right)^2 + \left(\sigma_e\epsilon_e\right)\left(\sigma_\gamma\epsilon_\gamma\right)\left(\frac{Z_\gamma}{Z_e} + \frac{Z_e}{Z_\gamma}\right)}}. \tag{63}$$

   The total luminosity depends only on 3 parameters : the emittance of the beams ($\mathcal{E}_e = \sigma_e\epsilon_e$, $\mathcal{E}_\gamma = \sigma_\gamma\epsilon_\gamma$) and the beam shape matching (Z_e/Z_γ).

3. **Interaction length**
   Another interesting feature is the interaction length defined as the length containing a fraction κ of the total luminosity $\mathcal{L}_0$ and given by

$$\int_{-L/2}^{L/2} \frac{d\mathcal{L}_0}{dz} dz = \kappa\ \mathcal{L}_0,$$

$$L_0^{int}(\kappa) = 2\ tan\left(\frac{\kappa\pi}{2}\right)\sqrt{\frac{\sigma_e^2 + \sigma_\gamma^2}{\epsilon_e^2 + \epsilon_\gamma^2}}. \tag{64}$$

   As already mentioned for the differential luminosity, the interaction length decreases when increasing the angular divergences and depends on 4 parameters.

4. **Beam optimal matching**
The maximum of luminosity $\mathcal{L}_0^{max}$ is reached for $Z_e = Z_\gamma$, i.e. by matching the electron and Laser beam shapes.

$$\mathcal{L}_0^{max} = \frac{I_e}{e}\,\frac{P_L\,\lambda}{h\,c^2}\,\frac{1}{(\sigma_e\epsilon_e + \sigma_\gamma\epsilon_\gamma)} \qquad with \qquad Z_e = Z_\gamma. \tag{65}$$

Thus, **the maximal luminosity for zero crossing angle is only limited by the emittance of the Laser and electron beams.** In this case the interaction length, which depends only on 2 parameters related either to the electron beam (σ_e , ϵ_e) or to the Laser beam (σ_γ , ϵ_γ), is fixed by the relations

$$L_0^{int}(\kappa) = 2\,tan\left(\frac{\kappa\pi}{2}\right)\,\frac{\sigma_e}{\epsilon_e} = 2\,tan\left(\frac{\kappa\pi}{2}\right)\,\frac{\sigma_\gamma}{\epsilon_\gamma} = 2\,tan\left(\frac{\kappa\pi}{2}\right)\,Z_e = 2\,tan\left(\frac{\kappa\pi}{2}\right)\,Z_\gamma. \tag{66}$$

3.2.2 Luminosity for non zero crossing angle

When the angular divergences of the electron and Laser beams are small wrt the crossing angle α_c, the differential, total luminosity and interaction length can be approximated by

- **Differential luminosity, Interaction length**

$$\frac{d\mathcal{L}}{dz} \simeq c\;(1. + cos(\alpha_c))\;\frac{N_{0e}N_{0\gamma}}{2\pi}\;\frac{1}{\sigma_e^2 + \sigma_\gamma^2}\;exp\left(-\frac{2z^2 sin^2(\alpha_c/2)}{\sigma_e^2 + \sigma_\gamma^2}\right). \tag{67}$$

The differential luminosity distribution is gaussian, so the interaction length for $\kappa = 0.68$ corresponding to $\pm 1\sigma$ is

$$L_{\alpha_c}^{int} \simeq 2\frac{\sqrt{\sigma_e^2 + \sigma_\gamma^2}}{sin(\alpha_c)}. \tag{68}$$

Thus the interaction length is reduced by smaller beam spot sizes or by bigger crossing angle.

- **Total luminosity**

$$\mathcal{L} \simeq c\;(1. + cos(\alpha_c))\;\frac{N_{0e}N_{0\gamma}}{\sqrt{2\pi}}\;\frac{1}{\sqrt{\sigma_e^2 + \sigma_\gamma^2}}\;\frac{1}{sin(\alpha_c)},$$

$$\mathcal{L} \simeq \frac{(1. + cos(\alpha_c))}{\sqrt{2\pi}}\;\frac{I_e}{e}\;\frac{P_L\,\lambda}{h\,c^2}\;\frac{1}{\sqrt{\sigma_e^2 + \sigma_\gamma^2}}\;\frac{1}{sin(\alpha_c)}. \tag{69}$$

The total luminosity is reduced by bigger beam spot sizes or by bigger crossing angle. **Thus a high luminosity for non zero crossing angle depends on the ability to obtain small beam spot sizes and small crossing angle.**

3.3 Choice of the Laser

3.3.1 Standard Laser , zero crossing angle

The maximal luminosity in this case is given by equation (65):

$$\mathcal{L}_0^{max} = \frac{I_e}{e}\,\frac{P_L\,\lambda}{h\,c^2}\,\frac{1}{(\sigma_e\epsilon_e + \sigma_\gamma\epsilon_\gamma)} \qquad with \qquad Z_e = Z_\gamma.$$

The emittance of the electron beam of CEBAF is negligible ($\simeq 10^{-9}\ m\ rad$) in comparison with the Laser emittance which is limited to $\lambda/4/\pi$ for a perfect Laser. Thus in this case the maximal emittance is independent of the Laser wavelength and is given by

$$\begin{aligned}\mathcal{L}_0^{max} = 4\,\pi\,\frac{I_e}{e}\,\frac{P_L}{h\,c^2} &= 131.7\ \ 10^{24} cm^{-2}s^{-1} \quad (I_e(\mu A)\ P_L(W)) \\ &= 131.7\ \ barn^{-1}s^{-1} \quad (I_e(\mu A)\ P_L(W))\,. \end{aligned} \tag{70}$$

For an electron intensity of 100 μA and a Laser power of 1 W, we obtain a luminosity $\mathcal{L} = 1.3\ 10^{28}\ cm^{-2}s^{-1}$. In the best case (Argon Laser of power 0.5 W with emittance $\lambda/4/\pi$, differential method without energy threshold), the time needed for a 1% measurement of the electron polarization at 4 GeV (Tab. 2 and 3) is greater than 43 mn. For a IR NdYAG Laser of 0.5 W, this time increases to 144 mn (Tab. 4).

However, commercial Lasers have greater emittance (at least a factor 1.5) than the limit we have assumed and the Polarimeter is also expected to be used at lower current, especially for experiments using polarized target. For I_e=100 nA, a 1 % measurement becomes difficult (at least 30 days).

Moreover, the interaction length for the maximal luminosity is big and one has to expect a loss of luminosity due to the limited experimental interaction length or due to the non optimal matching of the 2 beams. This point will be discussed more precisely in the next section about the high power Laser solution.

In conclusion, a standard Laser is not a viable solution for the e^- beam energy and intensity range to be covered at CEBAF. We have to increase the luminosity. This can be done by using either a high Power Laser or a standard Laser coupled with an amplification cavity. We will now study these 2 possible solutions.

$\lambda = 532.1nm \quad I_e = 100.00\mu A \quad P_L = 0.50W \quad \alpha_c = 0.0\ mrad$

$\mathcal{E}_\gamma = \lambda/4/\pi$ = 0.4234E-07 m rad , σ_e = 140.0 μm

σ_γ μm	911.	49.	87.	144.	220.	325.	470.	674.	961.	1371.
$\mathcal{L}$ $barn^{-1}s^{-1}$	6433.	2158.	3482.	4713.	5555.	6040.	6292.	6406.	6432.	6383.
L^{int} cm	7211.	62.	125.	250.	500.	1000.	2000.	4000.	8000.	16000.
$Time$ mn	43.	129.	80.	59.	50.	46.	44.	43.	43.	44.

$\mathcal{E}_\gamma = \lambda/4/\pi$ = 0.4234E-07 m rad , σ_e = 52.1 μm

σ_γ μm	339.	77.	115.	166.	238.	339.	484.	694.	1005.	1490.
$\mathcal{L}$ $barn^{-1}s^{-1}$	6433.	5455.	5985.	6265.	6395.	6433.	6395.	6265.	5985.	5455.
L^{int} cm	1000.	62.	125.	250.	500.	1000.	2000.	4000.	8000.	16000.
$Time$ mn	43.	51.	46.	44.	43.	43.	43.	44.	46.	51.

$\mathcal{E}_\gamma = 2\ \lambda/4/\pi$ = 0.8469E-07 m rad , σ_e = 140.0 μm

σ_γ μm	1288.	87.	144.	220.	325.	470.	672.	956.	1358.	1929.
$\mathcal{L}$ $barn^{-1}s^{-1}$	3254.	1741.	2357.	2779.	3023.	3153.	3218.	3247.	3254.	3241.
L^{int} cm	7211.	63.	125.	250.	500.	1000.	2000.	4000.	8000.	16000.
$Time$ mn	85.	160.	118.	100.	92.	88.	86.	86.	85.	86.

$\mathcal{E}_\gamma = 2\ \lambda/4/\pi$ = 0.8469E-07 m rad , σ_e = 52.1 μm

σ_γ μm	480.	114.	166.	237.	338.	480.	682.	970.	1389.	2011.
$\mathcal{L}$ $barn^{-1}s^{-1}$	3254.	2995.	3139.	3211.	3245.	3254.	3245.	3211.	3139.	2995.
L^{int} cm	1000.	62.	125.	250.	500.	1000.	2000.	4000.	8000.	16000.
$Time$ mn	85.	93.	89.	87.	86.	85.	86.	87.	89.	93.

Table 3: ***Luminosity, interaction length and needed time for a 1 % measurement of the electron polarization with Green Argon continuous Laser*** *($k = 2.33\ eV$)* ***and for various Laser beam sizes.*** *Luminosities are given for an electron beam of intensity 100 μA and emittance 10^{-9} $m\ rad$ and for a Laser beam of power 0.5 W and emittance $\lambda/4/\pi$ or $2\lambda/4/\pi$. Interaction length is for κ=0.683. Needed time are given at 4 GeV using differential method with a zero energy threshold and assuming an electron polarization of 50 %. Each table corresponds to a given Laser emittance and electron beam spot size (nominal Cebaf value or size giving an interaction length of 10 m). The second column gives then results for an optimal beam matching while the next ones are for some values of the Laser beam spot size (corresponding to interaction length around 10 m).*

$\lambda = 1064.2nm \quad I_e = 100.00\mu A \quad P_L = 0.50W \quad \alpha_c = 0.0\ mrad$

$\mathcal{E}_\gamma = \lambda/4/\pi$ = 0.8469E-07 m rad , σ_e = 140.0 μm

σ_γ μm	1288.	87.	144.	220.	325.	470.	672.	956.	1358.	1929.
$\mathcal{L}$ $barn^{-1}s^{-1}$	6508.	3482.	4714.	5558.	6046.	6306.	6436.	6495.	6508.	6483.
L^{int} cm	7211.	63.	125.	250.	500.	1000.	2000.	4000.	8000.	16000.
$Time$ mn	144.	270.	199.	169.	155.	149.	146.	145.	144.	145.

$\mathcal{E}_\gamma = \lambda/4/\pi$ = 0.8469E-07 m rad , σ_e = 52.1 μm

σ_γ μm	480.	114.	166.	237.	338.	480.	682.	970.	1389.	2011.
$\mathcal{L}$ $barn^{-1}s^{-1}$	6508.	5991.	6277.	6423.	6489.	6508.	6489.	6423.	6277.	5991.
L^{int} cm	1000.	62.	125.	250.	500.	1000.	2000.	4000.	8000.	16000.
$Time$ mn	144.	157.	150.	146.	145.	144.	145.	146.	150.	157.

$\mathcal{E}_\gamma = 2\,\lambda/4/\pi$ = 0.1694E-06 m rad , σ_e = 140.0 μm

σ_γ μm	1822.	144.	220.	325.	470.	671.	955.	1355.	1920.	2721.
$\mathcal{L}$ $barn^{-1}s^{-1}$	3273.	2357.	2779.	3024.	3155.	3222.	3255.	3270.	3273.	3267.
L^{int} cm	7211.	62.	125.	250.	500.	1000.	2000.	4000.	8000.	16000.
$Time$ mn	287.	399.	338.	311.	298.	292.	289.	287.	287.	288.

$\mathcal{E}_\gamma = 2\,\lambda/4/\pi$ = 0.1694E-06 m rad , σ_e = 52.1 μm

σ_γ μm	679.	166.	237.	337.	479.	679.	962.	1365.	1942.	2779.
$\mathcal{L}$ $barn^{-1}s^{-1}$	3273.	3140.	3215.	3252.	3268.	3273.	3268.	3252.	3215.	3140.
L^{int} cm	1000.	62.	125.	250.	500.	1000.	2000.	4000.	8000.	16000.
$Time$ mn	287.	299.	292.	289.	288.	287.	288.	289.	292.	299.

Table 4: ***Luminosity, interaction length and needed time for a 1 % measurement of the electron polarization with IR NdYAG continuous Laser*** *($k = 1.16\ eV$)* ***and for various Laser beam sizes.*** *Luminosities are given for an electron beam of intensity 100 μA and emittance 10^{-9} $m\ rad$ and for a Laser beam of power 0.5 W and emittance $\lambda/4/\pi$ or $2\lambda/4/\pi$. Interaction length is for κ=0.683. Needed time are given at 4 GeV using differential method with a zero energy threshold and assuming an electron polarization of 50 %. Each table corresponds to a given Laser emittance and electron beam spot size (nominal Cebaf value or size giving an interaction length of 10 m). The second column gives then results for an optimal beam matching while the next ones are for some values of the Laser beam spot size (corresponding to interaction length around 10 m).*

3.3.2 High power UV Laser , zero crossing angle

The maximal luminosity in this case is still given by equation (65) :

$$\mathcal{L}_0^{max} = \frac{I_e}{e}\,\frac{P_L\,\lambda}{h\,c^2}\,\frac{1}{(\sigma_e\epsilon_e + \sigma_\gamma\epsilon_\gamma)} \qquad with \qquad Z_e = Z_\gamma\ .$$

For a low electron intensity of 100 nA and a Laser power of 80 W, we have a luminosity of $\mathcal{L} = 1.10^{27}\ cm^{-2}s^{-1}$ assuming a perfect Laser of emittance $\lambda/4/\pi$. For the differential method without energy threshold, the time needed for a 1% measurement of the electron polarization at 4 GeV (Tab. 2 and 5) is reasonable ($\simeq$ 86 mn) even at this low electron beam current. This time can be considered as a minimal time.

If commercial Lasers have emittance not too far from the limit $\lambda/4/\pi$, this Laser can be a good solution. However , this perfect emittance seems more difficult to reach with an UV Laser than with a Argon or NdYAG Laser due to the smaller wavelength. Furthermore this Laser requires a high power UV beam transport system.

An other very difficult point is the matching between the electron and Laser beams in order to reach the maximal luminosity. We recall here that the interaction length for the maximal luminosity depends only on the shape of one beam (electron or Laser) while the shape of the other beam must be adapted to fulfill the condition $Z_e = Z_\gamma$.
As seen in table (5), for an electron beam with a spot size of 140. μm which is the expected nominal CEBAF spot size at the Compton interaction point and with an emittance of $10^{-9}\ m\ rad$, the interaction length for a perfect Laser and for the maximal luminosity is huge ($\simeq$ 72 m). By decreasing the Laser beam spot i.e. by increasing its angular divergence , we can reduce this interaction length to a more realistic geometrical length ($\simeq$ 10 m), but then the beam matching is not optimal , the luminosity decreases according to equation (63) and the needed time increases to 98 mn (always at 100 nA). To have an idea on the effect of the Laser emittance, we note that if the UV Laser had a worst emittance of $2\lambda/4/\pi$, then the time to get 1% error on P_e with an interaction length of 10 m would increase to 179 mn.
To decrease the interaction length in the beam optimal matching conditions, we have to decrease the electron beam spot size. For a given emittance, the interaction length varies as $L_0^{int} \simeq \sigma_e^2$. If we would have a focalisation of the electron beam to have an electron spot size of 52.1 μm, the interaction length for the maximal luminosity becomes 10 m. The needed time in this case is the minimal one (86 mn) for a Laser with a perfect emittance and becomes 167 mn for a Laser with an emittance 2 times greater.

Such an interaction length assumes the alignment of the 2 beams on a length of 10 m i.e. a zero crossing angle within 20 μrad. On the other hand, it is not obvious that a zero crossing angle can be easily achieved. Some optical elements must be in the electron beam, so we have to study synchrotron radiation damage, protection against accidental electron beam damage. If a small crossing angle is necessary, the needed time will be increased.

$\lambda = 248.0nm \quad I_e = 0.10\mu A \quad P_L = 80.00W \quad \alpha_c = 0.0\ mrad$										
$\mathcal{E}_\gamma = \lambda/4/\pi$ = 0.1973E-07 m rad , σ_e = 140.0 μm										
σ_γ μm	622.	24.	46.	83.	137.	212.	314.	456.	657.	947.
$\mathcal{L}$ $barn^{-1}s^{-1}$	1003.	175.	326.	535.	736.	876.	956.	994.	1003.	986.
L^{int} cm	7211.	62.	125.	250.	500.	1000.	2000.	4000.	8000.	16000.
$Time$ mn	86.	489.	263.	160.	117.	98.	90.	86.	86.	87.
$\mathcal{E}_\gamma = \lambda/4/\pi$ = 0.1973E-07 m rad , σ_e = 52.1 μm										
σ_γ μm	232.	48.	74.	110.	161.	232.	334.	486.	723.	1128.
$\mathcal{L}$ $barn^{-1}s^{-1}$	1003.	709.	860.	947.	990.	1003.	990.	947.	860.	709.
L^{int} cm	1000.	62.	125.	250.	500.	1000.	2000.	4000.	8000.	16000.
$Time$ mn	86.	121.	100.	91.	87.	86.	87.	91.	100.	121.

$\mathcal{E}_\gamma = 2\ \lambda/4/\pi$ = 0.3947E-07 m rad , σ_e = 140.0 μm										
σ_γ μm	880.	46.	83.	137.	212.	313.	454.	650.	928.	1325.
$\mathcal{L}$ $barn^{-1}s^{-1}$	514.	163.	267.	368.	439.	480.	502.	511.	514.	509.
L^{int} cm	7211.	63.	125.	250.	500.	1000.	2000.	4000.	8000.	16000.
$Time$ mn	167.	526.	321.	233.	195.	179.	171.	168.	167.	168.
$\mathcal{E}_\gamma = 2\ \lambda/4/\pi$ = 0.3947E-07 m rad , σ_e = 52.1 μm										
σ_γ μm	328.	74.	110.	160.	229.	328.	468.	671.	974.	1448.
$\mathcal{L}$ $barn^{-1}s^{-1}$	514.	431.	476.	499.	511.	514.	511.	499.	476.	431.
L^{int} cm	1000.	63.	125.	250.	500.	1000.	2000.	4000.	8000.	16000.
$Time$ mn	167.	199.	180.	172.	168.	167.	168.	172.	180.	199.

Table 5: ***Luminosity, interaction length and needed time for a 1 % measurement of the electron polarization with UV KrF high power pulsed Laser*** *($k = 5.0\ eV$)* ***and for various Laser beam sizes.*** *Luminosities are given for an electron beam of intensity 100 nA and emittance 10^{-9} $m\ rad$ and for a Laser beam of power 80 W and emittance $\lambda/4/\pi$ or $2\lambda/4/\pi$. Interaction length is for κ=0.683. Needed time are given at 4 GeV using differential method with a zero energy threshold and assuming an electron polarization of 50 %. Each table corresponds to a given Laser emittance and electron beam spot size (nominal Cebaf value or size giving an interaction length of 10 m). The second column gives then results for an optimal beam matching while the next ones are for some values of the Laser beam spot size (corresponding to interaction length around 10 m).*

3.3.3 Standard Laser with optical cavity , non zero crossing angle

A Fabry-Perrot optical cavity can be used to trap the Laser beam. As explained in section 8.1 and appendix G, this is actually an optical resonator made of 2 highly reflective curved mirrors. The cavity provides an amplification factor G on the luminosity. Some experiments on gravitational waves are using currently optical cavity coupled with NdYAG Laser and values of the cavity gain G greater than 10000 have been obtained [13],[14],[15]. However, to protect the cavity mirrors against the electron beam, a small crossing angle $\alpha_c \simeq 20\ mrad$ is necessary.

- **Dependence of the maximal expected luminosity as a function of the crossing angle.** An approximation for the luminosity in the case of non zero crossing angle of the 2 beams is given by equation (69) :

$$\mathcal{L} = \frac{(1. + cos(\alpha_c))}{\sqrt{2\pi}} \frac{I_e}{e} \frac{P_L\,\lambda}{h\,c^2} \frac{1}{\sqrt{\sigma_e^2 + \sigma_\gamma^2}} \frac{1}{sin(\alpha_c)} .$$

If we can neglect the Laser spot size ($\sigma_\gamma << \sigma_e$), we obtain the maximal luminosity at non zero crossing angle for a cavity of gain G

$$\mathcal{L}_\alpha^{max} \simeq \frac{2}{\sqrt{2\pi}} \frac{I_e}{e} \frac{P_L G}{h\,c^2} \frac{\lambda}{\sigma_e} \frac{1}{sin(\alpha_c)} ,$$

$$\mathcal{L}_\alpha^{max} \simeq 8.36 \quad 10^{24} cm^{-2} s^{-1} \quad \left(\frac{\lambda}{\sigma_e} \frac{I_e(\mu A)\ P_L(W)\ G}{\alpha_c(rad)} \right) , \tag{71}$$

to be compared with the case at zero crossing angle for a perfect Laser (Eq. 70)

$$\mathcal{L}_0^{max} = 131.7 \quad 10^{24} cm^{-2} s^{-1} \quad (I_e(\mu A)\ P_L(W)) .$$

Thus in order to have greater luminosity at a crossing angle $\alpha_c = 20\ mrad$ than at $\alpha_c = 0.\ mrad$, we must have a cavity gain G

$$G > \frac{131.7}{8.36} \alpha_c(rad) \frac{\sigma_e}{\lambda} = 0.315 \frac{\sigma_e}{\lambda} . \tag{72}$$

For the nominal spot size of the CEBAF electron beam ($\sigma_e = 140\ \mu m$), this gives a needed gain $G = 41$ ($resp. G = 83$, $G = 178$) for a Laser wavelength of 1064 nm (resp. 532 nm, 248 nm). With a cavity gain $G = 10000$, a 1 % measurement of the electron polarization at I_e = 100 nA and 4 GeV requires 590 mn for a 0.5 W NdYAG Laser and 357 mn for a 0.5 W Argon Laser. These times hold for the differential method with a zero energy threshold and an electron polarization of 50 %. So a 1 % measurement appears feasible at low beam current with a standard continuous Laser. At I_e = 100 μA, these needed times are less than 1 mn. The interaction length (Eq. 68) for negligible Laser spot size,

$$L_{\alpha_c}^{int} \simeq 2\frac{\sqrt{\sigma_e^2 + \sigma_\gamma^2}}{sin(\alpha_c)} \simeq 2\frac{\sigma_e}{sin(\alpha_c)} ,$$

is small (1.4 cm) in these conditions (electron spot size $\sigma_e = 140\ \mu m$ and $\alpha_c = 20\ mrad$).

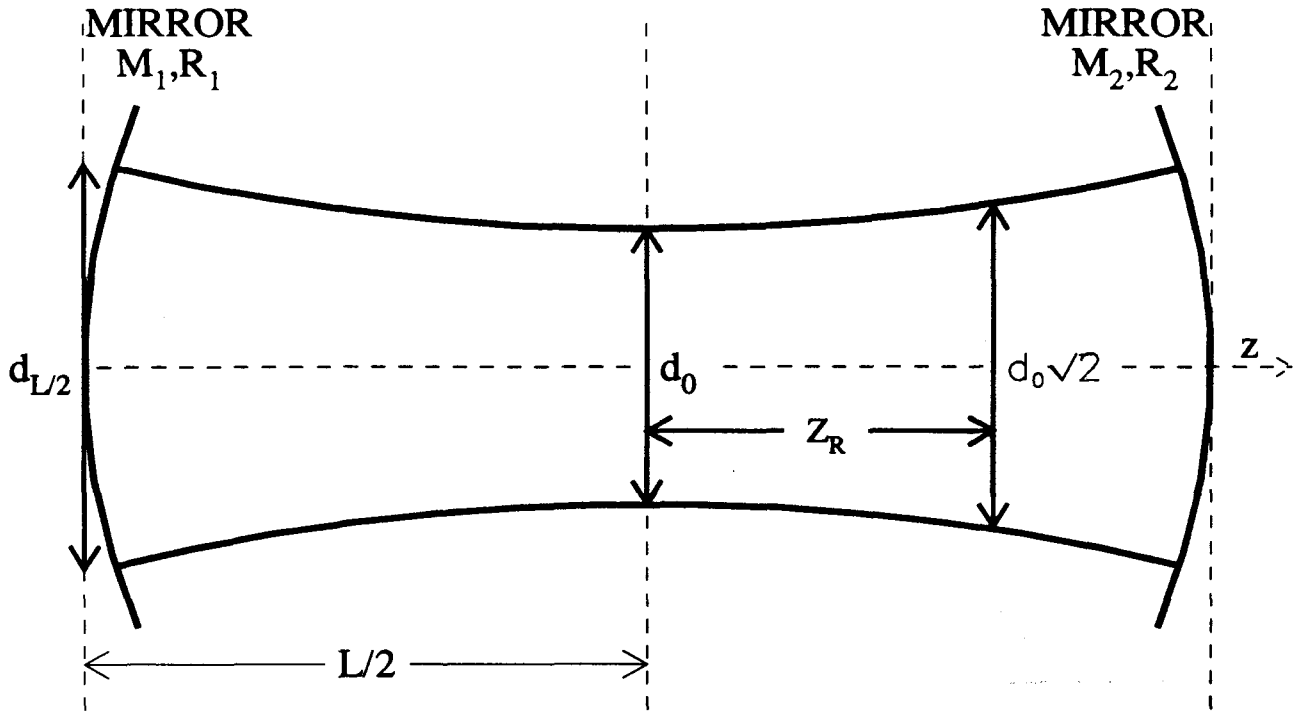

Figure 9: ***Beam shape inside a symmetric resonator.*** *Spot sizes at waist d_0 and at mirrors positions $d_{L/2}$ and Rayleigh range Z_R .*

- **Laser Beam shape inside a symmetric cavity.**
  In the previous estimations, we have neglected the Laser and electron beam shape dependence. More precisely, we have assumed that the angular divergences of the electron and Laser beams were small compared to the crossing angle. We have also neglected the Laser spot size ($\sigma_\gamma << \sigma_e$). The angular divergence of the electron beam is very small ($< 100\ \mu rad$). Here, we will look at the effects of the spot size and of the angular divergence of the Laser beam.

  The general Gaussian shape assumed (Eq. 56, 57 and Fig. 8) depends for beams symmetric in x and y on 2 parameters for instance the size at the waist d_0 and the Rayleigh range Z_R (or the angular divergence ϵ).
  If the Laser beam is trapped inside a cavity consisting of 2 curved mirrors M_1 and M_2 set up facing each other (Fig. 9), these parameters are fixed by the cavity geometry : the length L and the radii of the mirrors R_1 and R_2. The beam shape parameters can be expressed in terms of the resonator g_i parameters (see section 8 and appendix G) defined as

$$g_i = 1 - \frac{L}{R_i}. \tag{73}$$

$\lambda = 1064.2nm \quad L = 1.0m$									
g	-0.999	-0.990	-0.980	-0.970	-0.960	-0.950	-0.940	-0.930	-0.920
$\sigma_\gamma(0)$ μm	30.8	54.8	65.2	72.3	77.8	82.3	86.3	89.8	93.0
$\sigma_\gamma(L/2)$ μm	1376.	775.	652.	590.	550.	521.	498.	480.	465.
Z_R mm	11.2	35.4	50.3	61.7	71.4	80.1	87.9	95.2	102.1
ϵ $mrad$	2.752	1.546	1.298	1.172	1.089	1.028	0.981	0.943	0.911

$\lambda = 532.1nm \quad L = 1.0m$									
g	-0.999	-0.990	-0.980	-0.970	-0.960	-0.950	-0.940	-0.930	-0.920
$\sigma_\gamma(0)$ μm	21.8	38.7	46.1	51.1	55.0	58.2	61.0	63.5	65.7
$\sigma_\gamma(L/2)$ μm	973.	548.	461.	417.	389.	368.	352.	339.	329.
Z_R mm	11.2	35.4	50.3	61.7	71.4	80.1	87.9	95.2	102.1
ϵ $mrad$	1.946	1.093	0.918	0.828	0.770	0.727	0.694	0.667	0.644

Table 6: ***Beam shape parameters.*** *For a symmetric resonator of length $L = 1m$ as a function of the resonator g parameter for beams of wavelength $\lambda = 1064\ nm$ and $\lambda = 532\ nm$.*

For a symmetric resonator ($R_1 = R_2 = R$ i.e. $g_1 = g_2 = g$), we have for the spot sizes at waist d_0, the spot size at mirrors positions $d_{L/2}$, the Rayleigh range Z_R and the angular divergence ϵ :

$$d_0^2 = \frac{L}{2}\frac{\lambda}{\pi}\sqrt{\frac{1+g}{1-g}} = \frac{\lambda}{\pi} Z_R\,, \qquad d_{L/2}^2 = L\frac{\lambda}{\pi}\sqrt{\frac{1}{1-g^2}} \tag{74}$$

$$Z_R = \frac{L}{2}\sqrt{\frac{1+g}{1-g}}\,, \qquad tan(\epsilon)^2 = \frac{1}{2L}\frac{\lambda}{\pi}\sqrt{\frac{1-g}{1+g}}\,. \tag{75}$$

We are interested by small spot size at waist in order to maximize the luminosity (Eq. 69). As seen from equation (74), this corresponds to value of the resonator g parameter close to -1. This value is a limit to have a stable resonator ($-1 \leq g \leq 1$). Table (6) gives the beam shape parameters for various values of g in the range [-1.,-0.92] and for a cavity of length L=1m. Laser beam spot size less than 100 μm can be obtained in this range of g. The angular divergence are closed to 1 $mrad$ to be compared to the crossing angle $\alpha_c = 20\ mrad$. So small corrections ($< 10\%$) to the luminosity must be expected.

The spot size on the mirrors for g=-0.95 is close to 0.5 mm. So we can use mirrors of diameter 7 mm. With a safety distance from the electron beam of 6.5 mm, this gives the considered crossing angle $\alpha_c = 20\ mrad$.

- **Luminosity and Needed time.**
  Table (7) gives the luminosity and the time needed for a 1 % measurement of the electron polarization for various values of g in the range [-1.,-0.92]. These numbers confirm the first estimation where the Laser beam spot size had been neglected. So the conclusion on the feasibility of a 1 % measurement of the electron polarization at I_e=100 nA remains valid.

$\lambda = 1064.2nm \quad I_e = 0.10\mu A \quad P_L = 0.50W \quad G = 10000. \quad \alpha_c = 20.0mrad$

σ_e = 140.0 μm

g	-0.999	-0.990	-0.980	-0.970	-0.960	-0.950	-0.940	-0.930	-0.920
σ_γ μm	30.8	54.8	65.2	72.3	77.8	82.3	86.3	89.8	93.0
$\mathcal{L}$ $barn^{-1}s^{-1}$	1552.	1480.	1441.	1412.	1389.	1370.	1353.	1338.	1324.
L^{int} cm	1.43	1.50	1.54	1.58	1.60	1.62	1.64	1.66	1.68
$Time$ mn	605.	635.	652.	665.	676.	686.	695.	702.	710.

σ_e = 52.1 μm

g	-0.999	-0.990	-0.980	-0.970	-0.960	-0.950	-0.940	-0.930	-0.920
σ_γ μm	30.8	54.8	65.2	72.3	77.8	82.3	86.3	89.8	93.0
$\mathcal{L}$ $barn^{-1}s^{-1}$	3675.	2942.	2664.	2497.	2376.	2283.	2207.	2143.	2087.
L^{int} cm	0.61	0.76	0.84	0.89	0.94	0.97	1.01	1.04	1.07
$Time$ mn	256.	319.	353.	376.	395.	412.	426.	439.	450.

$\lambda = 532.1nm \quad I_e = 0.10\mu A \quad P_L = 0.50W \quad G = 10000. \quad \alpha_c = 20.0mrad$

σ_e = 140.0 μm

g	-0.999	-0.990	-0.980	-0.970	-0.960	-0.950	-0.940	-0.930	-0.920
σ_γ μm	21.8	38.7	46.1	51.1	55.0	58.2	61.0	63.5	65.7
$\mathcal{L}$ $barn^{-1}s^{-1}$	785.	766.	755.	746.	740.	734.	728.	724.	719.
L^{int} cm	1.42	1.45	1.47	1.49	1.50	1.52	1.53	1.54	1.55
$Time$ mn	354.	363.	368.	372.	376.	379.	381.	384.	386.

σ_e = 52.1 μm

g	-0.999	-0.990	-0.980	-0.970	-0.960	-0.950	-0.940	-0.930	-0.920
σ_γ μm	21.8	38.7	46.1	51.1	55.0	58.2	61.0	63.5	65.7
$\mathcal{L}$ $barn^{-1}s^{-1}$	1969.	1713.	1598.	1524.	1468.	1423.	1386.	1354.	1326.
L^{int} cm	0.56	0.65	0.70	0.73	0.76	0.78	0.80	0.82	0.84
$Time$ mn	141.	162.	174.	182.	189.	195.	200.	205.	210.

Table 7: ***Luminosity, interaction length and needed time for a 1 % measurement of the electron polarization with standard continuous Laser*** $k = 1.16\ eV$ ***(IR NdYAG) and*** $k = 2.33\ eV$ ***(Green Argon).*** *Luminosities are given for an electron beam of intensity 100 nA, for a Laser beam of power 0.5 W trapped in a cavity of gain G =10000. Interaction length is for* κ*=0.683. Needed time are given at 4 GeV using differential method with a zero energy threshold and assuming an electron polarization of 50 %. Each table corresponds to a given electron beam spot size. The columns give results for some values of the resonator g parameter.*

3.3.4 Conclusions on the choice of the laser

- **Standard Laser coupled with an optical cavity: Green Argon vs NdYAG**
  Green Argon Laser and IR NdYAG Laser have the same power. For an Argon Laser, the measured asymmetry is higher by a factor 1.9 and the dynamics of the outgoing particles by a factor 2. Thus we may expect lower systematic errors and lower needed time.
  However absorption and scattering on the mirrors increase with incident energy and the cavity gain will be reduced for the Argon Laser. For instance experimental measurements on high reflective $\lambda/4$ multi layer dielectric mirrors, constructed by J.M Makowsky for the VIRGO experiment show a loss of gain of 26 % between 633 nm and 1064 nm. But the main advantage of the commercial solid NdYAG Laser is to allow a slow frequency modulation by a thermal system and a fast one by a piezo. The feedback mechanism between the cavity and the Laser becomes easier to be realized (see section 8 and appendix G).
  Finally, the NdYAG Laser seems the safer solution. Such systems (Laser of 0.5 W coupled with a cavity of length 1 m with a resonator parameter g=-0.95) exists and give currently a gain of 10000.

- **NdYAG Laser coupled with an optical cavity vs high power UV Laser**
  If we compare the needed time for these 2 solutions (Tab. 7 and 5), we found at I_e = 100 nA and σ_e = 100 μm

  - 98 mn for a **UV Laser** of power $P_L = 80\ W$ and for a perfect emittance. This time corresponds to an interaction length ($\kappa = 0.68$) of 10 m.
    If the geometric interaction length is limited to this value, the real time will be 98/.68 = 144 mn. This time may be consider as the minimal time for this method. It needs a perfect alignment of the 2 beams and a perfect emittance for a high power Laser. Commercial Lasers have an emittance far from the perfect emittance (for instance 8*.9 $mm\ mrad$ for the LUMONICS 80 W pulsed excimer KrF Laser i.e. 300 times the perfect emittance) so more realistic time seems to be greater than **100000** mn.
  - 686 mn for a **IR Laser** of power $P_L = 0.5\ W$ with a cavity of gain G=10000 and a resonator g parameter g=-0.95.
    This time may be consider as the maximal time for this method. Lasers of 0.7 W are now available. We can hope to build a cavity with a resonator g parameter closer to -1, to increase the cavity length to 1.5 m which allow to decrease the crossing angle or to obtain higher cavity gain. Time of the order of **300** mn does not seem out of reach.

  We can consider that the needed time for the 2 solutions are close only if UV Lasers can have an emittance close to the perfect limit. Furthermore a smaller electron beam spot size is more efficient for the second solution than for the UV solution. For a zero crossing angle (UV solution), the luminosity is limited by the Laser emittance and the smaller spot size is only used to reduce the interaction length.
  Concerning the systematic errors, the measured asymmetry for an UV Laser is higher by a factor 3.6. Thus we may expect lower systematic errors due to higher asymmetry. However these Lasers are pulsed with very high peak intensity so we have to perform only integrated measurement where the systematic errors are greater than in an "event by event" measurement.
  The dynamics of the outgoing particles is higher by a factor 4 for the UV Laser, allowing better resolution in the electron and photon detector. The interaction length of 10 m will reduce this advantage for the electron detector the only one where the differential method is possible in case

of high rates. For the photon detector, the better resolution is not used since we had to perform the energy weighted method.

- **Conclusion.**
  The NdYAG Laser seems the safer solution since such systems (Laser of 0.5 W coupled with a cavity of length 1 m with a resonator parameter g=-0.95) exists or are under development in several experiments.
  The Argon Laser could be used if systematic errors had to be reduced or if the dynamics of the outgoing particle had to be increased (energy resolution, background and energy threshold in the photon detector, energy threshold in the electron detector). The main problem will be then the feedback mechanism between the Laser and the cavity.
  The high power UV Laser does not give better results than the NdYAG even with an emittance close to the perfect limit. Moreover commercial Laser are far from this limit (by at least a factor 100) and presents some major inconvenients (reliability, safety, difficulty to run, beam transport).

3.4 Expected Counting Rates

In this section, we give the counting rate, needed time and number of events for the proposed setup of the Compton Polarimeter (standard IR NdYAG Laser with optical cavity). We give also the results for a green Laser since tunable frequency doubled NdYAG Laser are available with lower power.

The electron beam of intensity $I_e = 100 \mu A$ and polarization $P_e = 50\ \%$ crosses the Laser beam with a crossing angle $\alpha_c = 20\ mrad$ and a spot size $\sigma_e = 140\ \mu m$.

The Laser beam of power $P_L = 0.5\ W$ and polarization $P_\gamma = 100\ \%$ is trapped inside an optical cavity of length $L = 1\ m$ having a resonator g parameter g = -0.95. The Laser spot size is $\sigma_\gamma = 82\ \mu m$. The cavity gain G increases the luminosity $\mathcal{L}$ by a factor $G = 10000$.

The differential counting rate, depending on the luminosity $\mathcal{L}$ and on the differential unpolarized cross section $d\sigma/d\rho$ (Eq. 22 and Fig. 5) is given by

$$\frac{dN}{d\rho\ dt} = \mathcal{L}\ \frac{d\sigma}{d\rho}\ , \tag{76}$$

where $\rho = k'/k'_{max}$ is the scattered γ energy normalized to the maximal energy.

For a zero energy threshold, we obtain the **total counting rate**

$$\frac{dN}{dt} = \mathcal{L}\ \sigma\ , \tag{77}$$

where σ is the total unpolarized cross section (Eq. 23 and Fig. 6).

We recall the approximated formula for **the luminosity** $\mathcal{L}$ used up to now (Eq. 69) to see the variation with the experimental parameters. In this equation, the angular divergences of the Laser and electron beams have been neglected. In the results presented here, the luminosity $\mathcal{L}$ has been exactly integrated .

$$\mathcal{L} \simeq \frac{2}{\sqrt{2\pi}}\ \frac{I_e}{e}\ \frac{P_L\, G}{h\, c^2}\ \frac{\lambda}{\sqrt{\sigma_e^2 + \sigma_\gamma^2}}\ \frac{1}{sin(\alpha_c)}\ ,$$

where the variation of the Laser beam size σ_γ with the cavity parameters is

$$\sigma_\gamma^2 = \frac{L}{2}\ \frac{\lambda}{4\pi}\ \sqrt{\frac{1\ +\ g}{1\ -\ g}}\ .$$

The needed time for a 1 % measurement of the electron polarization has the general form

$$t_{meth} = \frac{1}{\mathcal{L}\ \left(\frac{\Delta P_e}{P_e}\right)^2\ P_e^2 P_\gamma^2}\ \frac{1}{A^2_{meth}}\ \frac{1}{\sigma}\ , \tag{78}$$

where, according to the method (differential,integrated,energy weighted), the mean longitudinal asymmetry A^2_{meth} stands for

$$< A_l^2 > \ :\ < A_l >^2\ :\ \frac{< E A_l >^2}{< E^2 >}\ .$$

The number of events needed for a 1 % measurement of the electron polarization is obtained from

$$N = \mathcal{L}\ t_{meth}\ \sigma\ . \tag{79}$$

$\lambda = 1064.2nm$ $P_L = 0.5W$ $G = 10000.$ $g = -0.950$ $\sigma_\gamma = 82.3\mu m$ $P_\gamma = 100.0\%$								
$I_e = 100.00\mu A$ $\sigma_e = 140.0\mu m$ $P_e = 50.0\%$ $\alpha_c = 20.0mrad$								
E GeV	1.0	2.0	3.0	4.0	5.0	6.0	7.0	8.0
$\mathcal{L}$ $\mu barn^{-1}s^{-1}$	1.372	1.372	1.372	1.372	1.372	1.372	1.372	1.372
σ $barn$	0.654	0.643	0.632	0.622	0.612	0.603	0.594	0.585
$rate$ Khz	896.5	881.3	866.8	852.9	839.5	826.7	814.4	802.6
$\sqrt{< A_l^2 >}$ %	0.880	1.736	2.567	3.376	4.163	4.928	5.671	6.394
$Time$ s	576.2	150.6	70.0	41.1	27.5	19.9	15.2	12.2
$Events$ 10^6	516.6	132.8	60.7	35.1	23.1	16.4	12.4	9.8

$\lambda = 532.1nm$ $P_L = 0.5W$ $G = 10000.$ $g = -0.950$ $\sigma_\gamma = 58.2\mu m$ $P_\gamma = 100.0\%$								
$I_e = 100.00\mu A$ $\sigma_e = 140.0\mu m$ $P_e = 50.0\%$ $\alpha_c = 20.0mrad$								
E GeV	1.0	2.0	3.0	4.0	5.0	6.0	7.0	8.0
$\mathcal{L}$ $\mu barn^{-1}s^{-1}$	0.734	0.734	0.734	0.734	0.734	0.734	0.734	0.734
σ $barn$	0.643	0.622	0.603	0.585	0.569	0.554	0.540	0.527
$rate$ Khz	471.7	456.5	442.5	429.6	417.7	406.6	396.3	386.7
$\sqrt{< A_l^2 >}$ %	1.736	3.376	4.928	6.394	7.781	9.092	10.333	11.506
$Time$ s	281.5	76.8	37.2	22.7	15.7	11.8	9.4	7.7
$Events$ 10^6	132.8	35.1	16.4	9.8	6.6	4.8	3.7	3.0

Table 8: ***Luminosity, total cross section, counting rate, mean asymmetry, needed time and number of events for a 1 % measurement of the electron polarization with standard continuous Laser*** $k = 1.16$ eV ***(IR) and*** $k = 2.33$ eV ***(Green) coupled with an optical cavity.*** *Luminosities and counting rate are given for an electron beam of intensity 100* μA *and of beam spot size* 140 μm *and for a Laser beam of power 0.5 W and of beam spot size* 82 μm. *The gain of the cavity is G=10000. Needed time and number of events are given for the differential method with a zero energy threshold and for electron and photon polarizations of 50 % and 100 %.*

We present in table (8) the expected counting rate and needed time for a 1 % measurement of the electron polarization as a function of the Laser and electron beam energies. These numbers hold **for the differential method with a zero energy threshold.** Counting rates are typically 850 kHz at the maximum electron beam intensity for a IR Laser. Needed time varies from 12 s at 8 GeV to 517 s at 1 GeV.

With a non zero energy threshold, the counting rates are reduced in the ratio σ_t/σ where σ_t is the differential unpolarized cross section integrated from the energy threshold to the maximum energy (Fig. 7). Table (9) gives values of this ratio for various energy threshold.
The number of events needed increase with the energy threshold like the square of the mean longitudinal asymmetry (Fig. 7). Table (10) gives the variation of the mean longitudinal asymmetry for various energy threshold.
The variation of the needed time with energy threshold depends on the 2 previous variations (cross section and mean longitudinal asymmetry).

We plan to measure both the scattered photon or electron energy to increase the figure of merit of our polarimeter (2 differential measurements with complementary detectors). The next sections will be devoted to the presentation of the experimental setup : magnetic chicane, electron and photon detector, optical cavity.

$\lambda = 1064.2nm \quad \alpha_c = 20.0mrad$

E GeV	1.0	2.0	3.0	4.0	5.0	6.0	7.0	8.0
σ *barn*	0.654	0.643	0.632	0.622	0.612	0.603	0.594	0.585
σ_t/σ ρ_{min} =0.00	1.000	1.000	1.000	1.000	1.000	1.000	1.000	1.000
σ_t/σ ρ_{min} =0.10	0.864	0.864	0.863	0.863	0.863	0.863	0.863	0.863
σ_t/σ ρ_{min} =0.20	0.751	0.751	0.750	0.750	0.749	0.749	0.749	0.748
σ_t/σ ρ_{min} =0.30	0.657	0.656	0.655	0.654	0.653	0.652	0.652	0.651
σ_t/σ ρ_{min} =0.40	0.575	0.573	0.572	0.571	0.569	0.568	0.567	0.566
σ_t/σ ρ_{min} =0.50	0.498	0.497	0.495	0.494	0.493	0.491	0.490	0.489
σ_t/σ ρ_{min} =0.60	0.422	0.421	0.420	0.418	0.417	0.416	0.415	0.414
σ_t/σ ρ_{min} =0.70	0.341	0.340	0.339	0.338	0.337	0.336	0.335	0.334
σ_t/σ ρ_{min} =0.80	0.247	0.247	0.246	0.246	0.245	0.245	0.244	0.244
σ_t/σ ρ_{min} =0.90	0.136	0.136	0.135	0.135	0.135	0.135	0.135	0.135

$\lambda = 532.1nm \quad \alpha_c = 20.0mrad$

E GeV	1.0	2.0	3.0	4.0	5.0	6.0	7.0	8.0
σ *barn*	0.643	0.622	0.603	0.585	0.569	0.554	0.540	0.527
σ_t/σ ρ_{min} =0.00	1.000	1.000	1.000	1.000	1.000	1.000	1.000	1.000
σ_t/σ ρ_{min} =0.10	0.864	0.863	0.863	0.863	0.863	0.863	0.863	0.864
σ_t/σ ρ_{min} =0.20	0.751	0.750	0.749	0.748	0.748	0.748	0.747	0.747
σ_t/σ ρ_{min} =0.30	0.656	0.654	0.652	0.651	0.650	0.649	0.648	0.648
σ_t/σ ρ_{min} =0.40	0.573	0.571	0.568	0.566	0.565	0.563	0.562	0.561
σ_t/σ ρ_{min} =0.50	0.497	0.494	0.491	0.489	0.487	0.486	0.484	0.483
σ_t/σ ρ_{min} =0.60	0.421	0.418	0.416	0.414	0.412	0.410	0.409	0.408
σ_t/σ ρ_{min} =0.70	0.340	0.338	0.336	0.334	0.333	0.331	0.330	0.329
σ_t/σ ρ_{min} =0.80	0.247	0.246	0.245	0.244	0.243	0.242	0.242	0.241
σ_t/σ ρ_{min} =0.90	0.136	0.135	0.135	0.135	0.135	0.135	0.134	0.134

Table 9: ***Variation of the integrated cross section with the energy threshold*** $\rho_{min} = k'_{min}/k'_{max}$. σ *is the total unpolarized cross section while* σ_t *is the differential unpolarized cross section integrated from the energy threshold to the maximum energy.*

$\lambda = 1064.2nm \quad \alpha_c = 20.0mrad$

E GeV	1.0	2.0	3.0	4.0	5.0	6.0	7.0	8.0
$< A_l >= \sqrt{< A_l^2 >}$ %	0.880	1.736	2.567	3.376	4.163	4.928	5.671	6.394
$< A_l >_t / < A_l >$ ρ_{min} =0.00	1.000	1.000	1.000	1.000	1.000	1.000	1.000	1.000
$< A_l >_t / < A_l >$ ρ_{min} =0.10	1.075	1.075	1.075	1.075	1.075	1.075	1.075	1.075
$< A_l >_t / < A_l >$ ρ_{min} =0.20	1.148	1.148	1.148	1.149	1.149	1.149	1.150	1.150
$< A_l >_t / < A_l >$ ρ_{min} =0.30	1.218	1.219	1.220	1.220	1.221	1.221	1.222	1.222
$< A_l >_t / < A_l >$ ρ_{min} =0.40	1.294	1.295	1.296	1.297	1.298	1.298	1.299	1.299
$< A_l >_t / < A_l >$ ρ_{min} =0.50	1.387	1.388	1.390	1.390	1.391	1.392	1.393	1.393
$< A_l >_t / < A_l >$ ρ_{min} =0.60	1.503	1.505	1.507	1.508	1.510	1.511	1.512	1.513
$< A_l >_t / < A_l >$ ρ_{min} =0.70	1.636	1.639	1.643	1.646	1.649	1.652	1.654	1.657
$< A_l >_t / < A_l >$ ρ_{min} =0.80	1.772	1.778	1.784	1.789	1.794	1.799	1.804	1.808
$< A_l >_t / < A_l >$ ρ_{min} =0.90	1.899	1.907	1.915	1.923	1.930	1.938	1.945	1.951

$\lambda = 532.1nm \quad \alpha_c = 20.0mrad$

E GeV	1.0	2.0	3.0	4.0	5.0	6.0	7.0	8.0
$< A_l >= \sqrt{< A_l^2 >}$ %	1.736	3.376	4.928	6.394	7.781	9.092	10.333	11.506
$< A_l >_t / < A_l >$ ρ_{min} =0.00	1.000	1.000	1.000	1.000	1.000	1.000	1.000	1.000
$< A_l >_t / < A_l >$ ρ_{min} =0.10	1.075	1.075	1.075	1.075	1.075	1.075	1.075	1.075
$< A_l >_t / < A_l >$ ρ_{min} =0.20	1.148	1.149	1.149	1.150	1.150	1.150	1.150	1.150
$< A_l >_t / < A_l >$ ρ_{min} =0.30	1.219	1.220	1.221	1.222	1.223	1.224	1.224	1.224
$< A_l >_t / < A_l >$ ρ_{min} =0.40	1.295	1.297	1.298	1.299	1.300	1.301	1.301	1.301
$< A_l >_t / < A_l >$ ρ_{min} =0.50	1.388	1.390	1.392	1.393	1.394	1.395	1.395	1.395
$< A_l >_t / < A_l >$ ρ_{min} =0.60	1.505	1.508	1.511	1.513	1.515	1.516	1.517	1.517
$< A_l >_t / < A_l >$ ρ_{min} =0.70	1.639	1.646	1.652	1.657	1.661	1.664	1.667	1.669
$< A_l >_t / < A_l >$ ρ_{min} =0.80	1.778	1.789	1.799	1.808	1.817	1.824	1.831	1.837
$< A_l >_t / < A_l >$ ρ_{min} =0.90	1.907	1.923	1.938	1.951	1.964	1.977	1.988	1.999

Table 10: ***Variation of the mean asymmetry with the energy threshold*** $\rho_{min} = k'_{min} / k'_{max}$. $< A_l >$ *is the mean asymmetry for a zero energy threshold (* $< A_l^2 >^{0.5}$ *for the differential method) while* $< A_l >_t$ *is the mean asymmetry from the energy threshold to the maximum energy.*

4 The Proposed Experimental Setup

The Compton polarimeter will be installed in the region 2 of the tunnel of Hall A (-41 m to -25.5 m from the Hall A target) i.e. on a total length of 15.5 m for the optical cavity and the magnetic chicane (necessary to perform a non destructive measurement). The four major elements of the setup are

- **A magnetic chicane** ($\int Bdl = 0$) made of 4 identical dipoles (Section 5).
  The deviation is in the vertical plane (perpendicular to the arc bending plane) where the beam spot size is expected to be smaller (in the arc bending plane, the spot size is increased by the energy dispersion and the energy loss by synchrotron radiation). For symmetry reasons, the four dipoles have the same magnetic field and thus the distance between the dipoles 1 and 2 and the distance between the dipoles 3 and 4 must be equal. The distance between the dipoles 2 and 3 has to be minimal to increase the transverse deviation.

- **A Laser and an optical cavity acting as a photon beam amplificator** (Section 8).
  The optical cavity will be installed between the dipoles 2 and 3. The crossing of the electron and Laser beams can be tuned by varying the magnetic fields of the dipoles or with the help of the beam corrector before dipole 1.
  The 2 mirrors, distant of 1 m, lie on an optical table of size 1.5 m. The angle between the electron beam axis and the mirrors axis will be $\alpha_c = 20mrad$. This angle is fixed by the mirror radius ($\simeq 4\ mm$) and a safety gap ($\simeq 6\ mm$) to set the mirror out of the electron beam. The mirrors are in the horizontal plane (perpendicular to the dipole 2 bending plane) in order to reduce the synchrotron radiation. This also allows to run an experiment in a dispersive mode of the beam transport without loss of luminosity at the Compton IP.

- **A gamma detector** located between the dipoles 3 and 4 (Section 6).
  It will be set near the dipole 4 to have a transverse deviation sufficient to put the gamma detector out of the electron beam. The distance from the dipole 4 is fixed by a safety gap ($\simeq 30\ cm$) to keep the detector out of the magnetic field of the dipole.

- **An electron detector** located between the dipoles 3 and 4 (Section 7).
  This location, rather than after dipole 4, will reduce the synchrotron radiation. To have the maximal dispersion and so the minimal resolution, it will be set near the dipole 4. The distance from the dipole 4 is fixed by the vertical size of the detector and by the vacuum pipe (Fig. 10).

Two beam position monitors between the dipoles 2 and 3 and one beam position monitor between the dipoles 3 and 4 will be used to control the electron beam position in the magnetic chicane. The two beam position monitors between the dipoles 2 and 3 have to be installed before and after the cavity and will be used to control the focusing of the electron beam, to give the beam parameters at the interaction point and to control the distances between the beam and the mirrors. The beam position monitor between the dipoles 3 and 4 will be used to give the distance between the electron detector and the electron beam.

The layout of the magnetic chicane is shown on figure (10) while the positioning of the critical elements of the Compton polarimeter is given in table (11). A general layout of the setup is shown on figures (11) and (12).

A comparison with a solution where the optical cavity would be before the first dipole of the magnetic chicane is done in the appendix F. This solution presents some major disadvantages but can be

SET UP	ELEMENT	Z(m)	Length(m)	X(cm)	Y(cm)
MAGNETIC CHICANE		-33.2	15.1	0.	0.
	Beam Corrector	-41.66	0.2	0.	0.
	Valve	-41.05	0.1	0.	0.
	Dipole 1	-40.25	1.	0.	0.
	Dipole 2	-34.85	1.	0.	-30.40
	Dipole 3	-31.55	1.	0.	-30.40
	Dipole 4	-26.15	1.	0.	0.
OPTICAL CAVITY		-33.2	2.	0.	-30.40
	BPM	-34.05	0.2	0.	-30.40
	Mirror 1	-33.7		-1.	-30.40
	Mirror 2	-32.7		1.	-30.40
	BPM	-32.35	0.2	0.	-30.40
γ DETECTOR		-27.10	0.6	0.	-30.40
	Thick absorber	-27.375	0.05	0.	-30.40
	Thin absorber	-27.35125	0.0025	0.	-30.40
	Crystal	-27.205	0.23	0.	-30.40
e^- DETECTOR		-27.45	0.20	0.	[-6.82;-3.82]
	BPM	-27.65	0.2	0.	-8.44

Table 11: ***Compton polarimeter positioning wrt Hall A target center.***

an acceptable alternative if some points not yet studied (general beam line optics) makes the chosen solution less attractive.

A resolution on the scattered Compton γ energy k of about $\sigma(k)/k_{max} \leq 10\%$ is a common requirement for the 2 detectors. We can use then an energy threshold and so improve the statistical precision on the electron polarization measurement (section 2.3). As we have to know the resolution of the detector and to perform a good calibration (appendix E), the use of 2 detectors not sensitive to the same parameters will be a powerful tool for an on-line monitoring. Furthermore we will see later that **the 2 detectors are complementary** :

- The **electron detector** gives an intrinsic good resolution $\sigma(k)/k_{max} \leq 3.0\%$ for all incident energies E and it is not too sensitive to the synchrotron radiation. But it has to be set out of the beam so it can not detect high energy scattered electrons and so low energy Compton γ. This detector can be used efficiently only for $E \geq 3\ GeV$. The resolution depends mainly on the beam size and on the dispersion resolution while the calibration depends on the knowledge of the beam position and of the resolution.

- The **gamma detector** can be used at low incident energy. But the synchrotron rate for $E \geq 6GeV$ is high and it is not sure that this problem can be solved for these energies. The resolution for low energy γ can be high and in this case has to be precisely measured as well as the calibration.

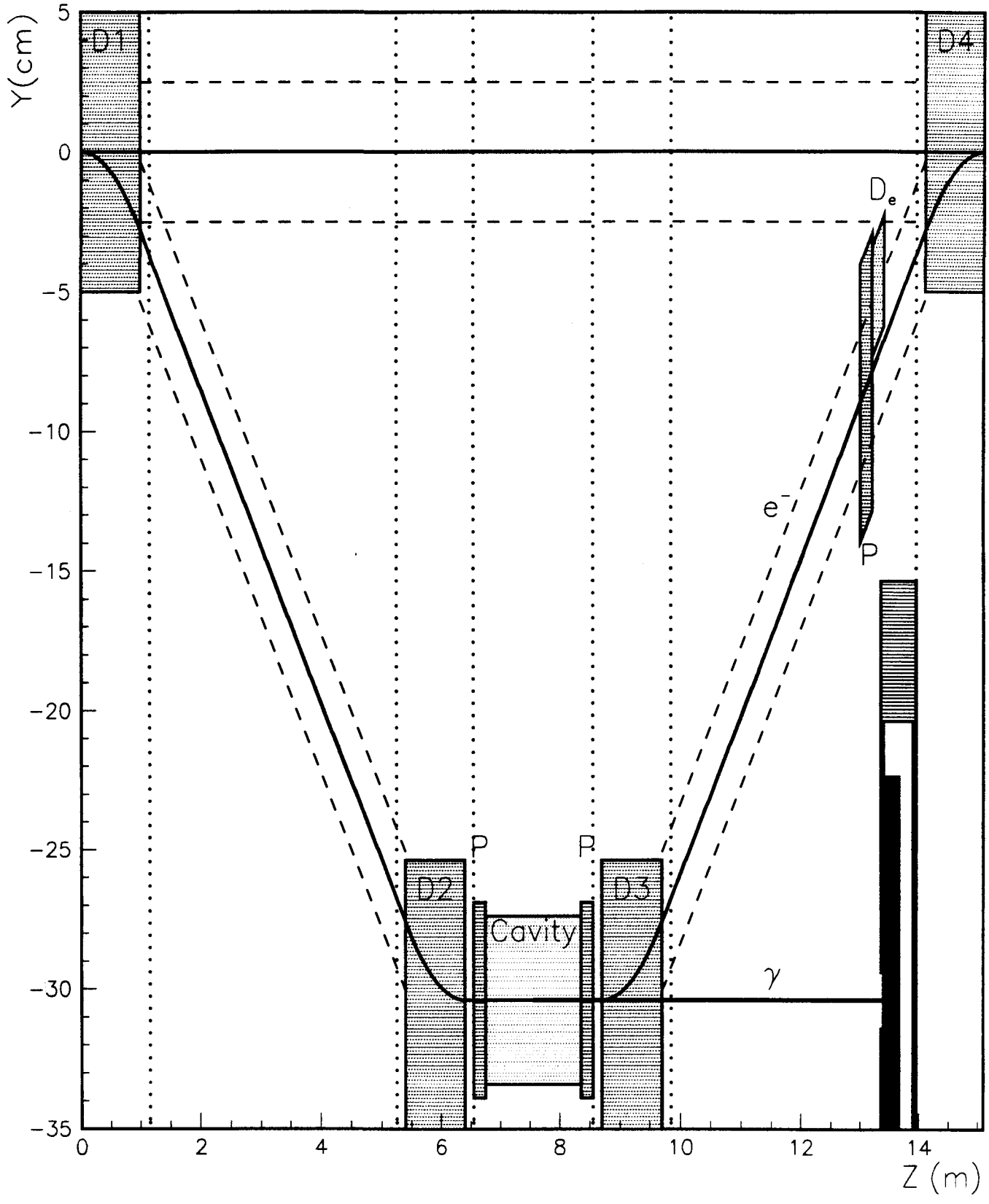

Figure 10: ***Proposed setup (Side View).*** *From Left to right: dipoles D1 and D2 (1 m); Optical cavity fed by the LASER with its 2 associated beam position monitors P (2 m); dipole D3 (1 m); electron and γ detectors; dipole D4 (1 m). The gap between Dipole 1 and 2 or dipole 3 and 4 is 4.4 m. The gap between Dipole 2 and 3 is 2.3 m. Solid lines are the nominal e^- beam trajectory with dipoles ON or OFF. Dashed lines are a beam pipe of 5cm diameter.*

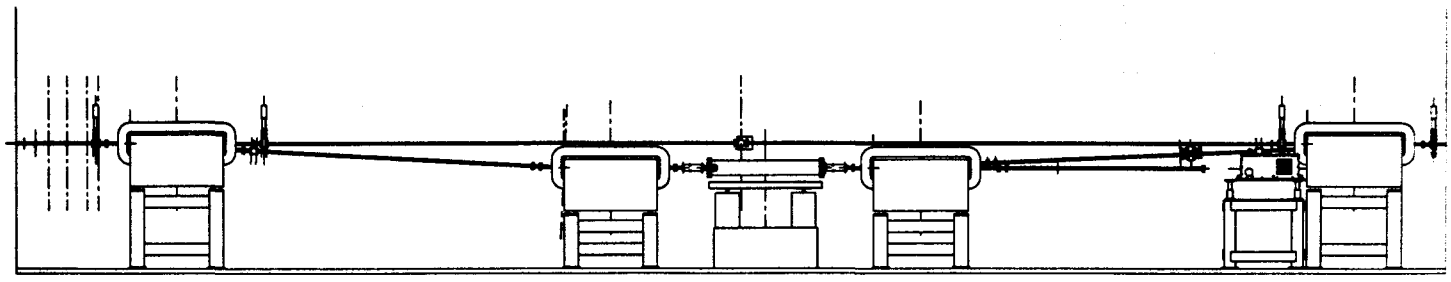

Figure 11: ***Proposed setup (Side View).***

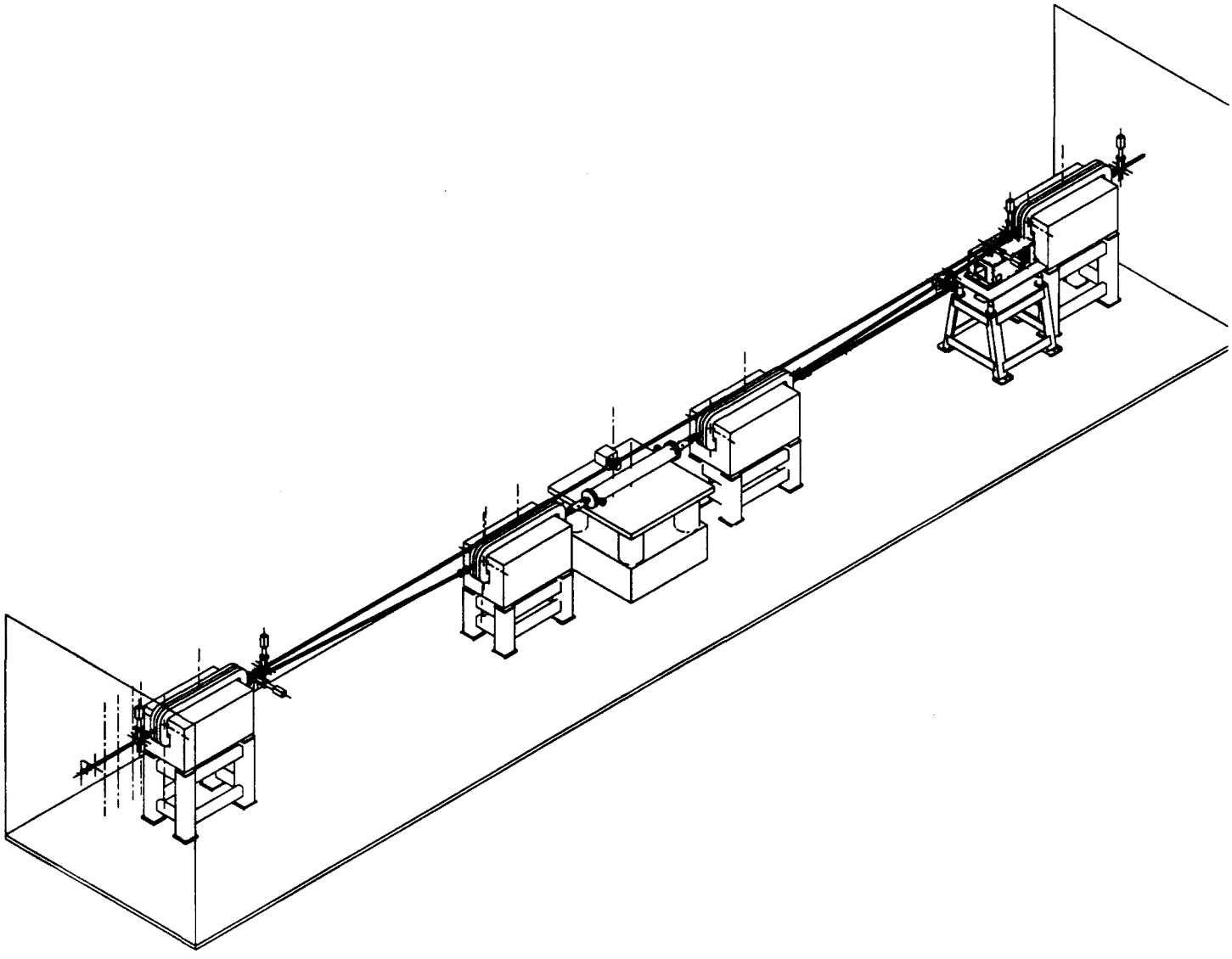

Figure 12: ***Proposed setup***

5 Magnetic Chicane

To allow for scattered photon and electron detection, a magnetic chicane consisting of 4 dipole magnets with magnetic length L_i running with a magnetic field B_i will be used.

5.1 Beam translation

We note (Fig. 13)

- L_i : magnet length of dipole i ,
- R_i : Bending radius for dipole i : $R_i(m) = p(GeV)/0.3/B_i(T)$,
- θ_i : bending angle for dipole i : $sin\theta_i = L_i/R_i$,
- h_i : horizontal deviation for dipole i : $h_i = R_i\,(1 - \cos\theta_i)$,
- D_{ij} : drift between dipole i and dipole j ,
- H_{ij} : horizontal deviation between dipole i and dipole j : $H_{ij} = D_{ij}\,\tan\theta_i$,
- d_{max} : maximal horizontal deviation ,
- d_{tot} : total horizontal deviation .

For beam optics reasons, we want a chicane as symmetrical as possible and at least with the same first 2 dipoles D1 and D2 (i.e. $L_1 = L_2$) and with the same last 2 dipoles D3 and D4 (i.e. $L_3 = L_4$) running with the same magnetic fields i.e. $B_1 = -B_2$ and $-B_3 = B_4$ (Fig. 13). In this case, we have the following relations :

$$R_1 = -R_2\,, \qquad R_4 = -R_3\,, \tag{80}$$

$$\sin\theta_1 = -\sin\theta_2 = \frac{L_1}{R_1}\,, \qquad \sin\theta_4 = -\sin\theta_3 = \frac{L_4}{R_4}\,, \tag{81}$$

$$h_1 = h_2 = R_1\,(1 - \cos\theta_1)\,, \qquad h_3 = h_4 = R_3\,(1 - \cos\theta_3)\,, \tag{82}$$

$$H_{12} = D_{12}\,\tan\theta_1\,, \qquad H_{34} = D_{34}\,\tan\theta_3\,. \tag{83}$$

$$d_{max} = h_1 + H_{12} + h_2 = 2R_1(1 - \cos\theta_1) + D_{12}\tan\theta_1 \;\simeq\; R_1\theta_1^2 + D_{12}\theta_1\,. \tag{84}$$

So that:

$$d_{max} \;\simeq\; 0.3\frac{B_1}{p}\;L_1\;(L_1 + D_{12})\,. \tag{85}$$

The setup that we propose in the tunnel of the Hall A consists of 4 identical magnets, with a magnetic length $L_i = 1\ m$. The total available length for the magnetic chicane is $15.1\ m$ ($15.5\ m$ of the Compton polarimeter region minus $0.4m$ for the external coils of dipoles1 and 4). We keep a distance of $2.3\ m$ between dipoles 2 and 3 for the optical cavity (i.e. $D_{23} = 2.3\ m$). So the remaining drift length are $D_{12} = D_{34} = 4.4\ m$. The magnet fields scale with incident energy up to 8 GeV where the saturation field of $1.5\ T$ is reached. This gives bending angles $\theta_i = 3.222$ deg $= 0.056\ rad$, bending radii $R_i = 17.79\ m$, and transverse deviations $h_i = 2.81\ cm$ and $H_{12} = 24.77\ cm$. The maximal deviation is then $d_{max} = 30.40\ cm$ (Tab. 12).

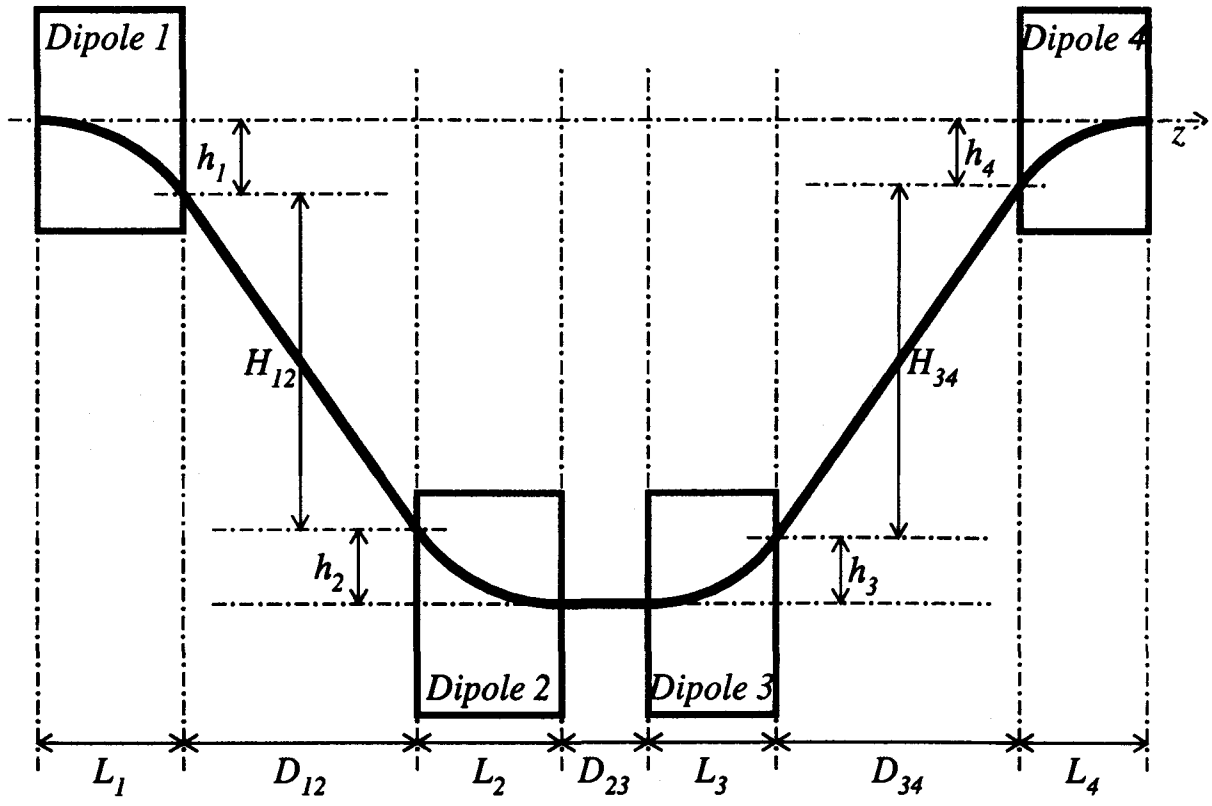

Figure 13: ***Chicane geometry.*** *h_i is the deviation in each dipole with magnetic length L_i and H_{ij} is the deviation between dipole i and j separated by a distance D_{ij}.*

$L_1 = L_2$=1.00 m	$L_3 = L_4$=1.00 m	D_{12}=4.40 m	D_{23}=2.30 m	D_{34}=4.40 m

E	GeV	1.0	2.0	3.0	4.0	5.0	6.0	7.0	8.0
$B_2 = B_1$	Tesla	0.19	0.37	0.56	0.75	0.94	1.12	1.31	1.50
$R_1 = R_2$	m	17.79	17.79	17.79	17.79	17.79	17.79	17.79	17.79
$\theta_2 = \theta_1$	mrad	56.24	56.24	56.24	56.24	56.24	56.24	56.24	56.24
$h_1 = h_2$	cm	2.81	2.81	2.81	2.81	2.81	2.81	2.81	2.81
$B_3 = B_4$	Tesla	0.19	0.37	0.56	0.75	0.94	1.12	1.31	1.50
$R_3 = R_4$	m	17.79	17.79	17.79	17.79	17.79	17.79	17.79	17.79
$\theta_3 = \theta_4$	mrad	56.24	56.24	56.24	56.24	56.24	56.24	56.24	56.24
$h_3 = h_4$	cm	2.81	2.81	2.81	2.81	2.81	2.81	2.81	2.81
H_{12}	cm	24.77	24.77	24.77	24.77	24.77	24.77	24.77	24.77
H_{34}	cm	24.77	24.77	24.77	24.77	24.77	24.77	24.77	24.77
d_{max}	cm	30.40	30.40	30.40	30.40	30.40	30.40	30.40	30.40
d_{tot}	cm	0.00	0.00	0.00	0.00	0.00	0.00	0.00	0.00
θ_{tot}	mrad	0.00	0.00	0.00	0.00	0.00	0.00	0.00	0.00

Table 12: ***Deviations in the magnetic chicane.*** *For different beam energies and magnetic field. h_i is the deviation in each dipole, H_{ij} is the deviation between dipole i and dipole j separated by a distance D_{ij}. d_{max} is the maximal deviation. d_{tot} is the total deviation.*

5.2 Magnet Specifications and associated requirements

The magnet and associated power supply specifications are given in appendix H.

5.2.1 Positioning

The deviation is in the vertical plane (perpendicular to the arc bending plane) where the beam spot size is expected to be smaller (in the arc bending plane, the spot size is increased by the energy dispersion and the energy loss by synchrotron radiation).

5.2.2 Magnetic Measurement

The 4 dipoles must have a total $\int Bdl = 0$ to perform a non destructive measurement. We plan to measure the $\int Bdl$ using the "moving wire" technique [16]. Dipole 1 will be used as reference, and dipole 2, dipole 3 and dipole 4 will have tunable magnetic length. Each pair of dipole (1,2), (2,3) and (3,4) will have their $\int Bdl$ measured and the magnetic length will be adjusted so that $\int Bdl = 0$. The four magnets will be fed in serie.

5.2.3 Power supply stability

The first requirement on the stability of the power supply of the dipoles is given by the required resolution on the electron detector. This effect is discussed in section 7.3 and leads to a required power supply stability of $\simeq 4\ 10^{-4}$.

The second requirement comes from the general beam line stability. As the 4 dipoles will be fed in serie and have a total $\int Bdl = 0$, this stability will be not affected by the power supply instability.

5.3 Beam line tuning

The detailed study of the beam line including the magnetic chicane will be done in close collaboration with the CEBAF machine team. The points to be kept in mind for the optimization of the beam line are the following.

- The beam spot size at the Compton interacting point must have $\sigma \leq 100\ \mu m$ to match the laser beam size. This acts on the luminosity.
- We have not added any quadrupoles for the focusing on the Compton interacting point. If it is necessary, the set of quadrupoles must be before the first dipole or after the last one (if possible) to keep the distance between the dipoles 2 and 3 minimum. Otherwise the bremsstrahlung rate in the electron and gamma detectors and the synchrotron rate in the cavity mirrors and in the gamma detector would be increased.
- For the tuning of the Laser and electron beams crossing between dipoles 2 and 3, we plan to use the vertical beam corrector before dipole 1. The 2 meters needed for the optical cavity includes the 2 associated beam position monitors.
- The beam position monitor before the electron detector is used to measure the distance between the electron beam and the edge of the electron detector. It has to be as close as possible of this detector. A beam position monitor integrated to the electron detector would be the best solution allowing an accurate positioning of the electron beam and the edge of the electron detectors.

5.4 Beam control and monitoring

- **Beam crossing control.**
  The expected Laser size is 2 cm (20 $mrad$ $*$ 1 m) in the horizontal plane and $\simeq$ 100 μm in the vertical one. As already mentioned, the crossing of the electron and Laser beam can be tuned in the vertical plane by acting on the vertical beam corrector before dipole 1. In the horizontal plane, we can use the horizontal beam corrector before dipole 1 to center the electron beam on the center of the cavity. The horizontal angle must be close to 0 to keep a safety gap of $\simeq$ 6 mm between the beam and the cavity mirrors.
  The 2 beam position monitors before and after the cavity are used to control this horizontal safety gap within 1 mm and the vertical beam crossing within a fraction of the beam spot size.

- **Beam line stability after the optical cavity.**
  One of the systematic effects in a measurement using the longitudinal electron polarization given by the Compton polarimeter will be the change of polarization between the Compton interacting point (where the polarization is measured) and the target interacting point. The magnetic elements in this region (at least dipoles 3 and 4 of the chicane) will change the direction of polarization and then the longitudinal polarization. This effect will be discussed in section 11.4 and depends on the $\int Bdl$ of these magnetic elements (or equivalently of the residual bending angle θ_m) and of the ratio between transverse and longitudinal polarization. For a zero ratio, a bending angle $\theta_m \leq 5\ mrad$ ensures a relative systematic effect on the polarization of ≤ 1 % up to 8 GeV. For a very high ratio close to 1, this upper limit becomes $\theta_m \leq 0.5\ mrad$. **Therefore we have to ensure a zero bending angle of all magnetic elements between the Compton and target interacting points within 0.5 mrad.**
  The 2 beam position monitors before and after the cavity will give the beam direction at the Compton interacting point. **Others beam position monitors after the last magnetic element before the target are required to give the beam direction at the target interacting point.**

- **Beam intensity and position stability.**
  The electron polarization is deduced from the experimental asymmetry of the number of Compton events with opposite Laser polarization. So we are not concerned by absolute measurement of the beam intensity and position but only by their stability. In section 11.1.1, we will study the systematic effects induced by the stability of the luminosity (not correlated with the Laser polarization reversals). The conclusions depend strongly (as $f^{\frac{3}{2}}$) on the frequency f of the Laser polarization reversal that we can achieve. Assuming a reversal frequency of $f = 10\ Hz$, the maximum relative variation of the luminosity per unit of time is $dA_{\mathcal{L}}/dt = 2.5\ 10^{-2}\ /s$. Extracting from the expression of the luminosity (Eq. 69) the terms depending on the electron beam

$$\mathcal{L} \propto \frac{I_e}{\sqrt{\sigma_e^2 + \sigma_\gamma^2}}, \tag{86}$$

  we obtain

$$dA_{\mathcal{L}} = \frac{d\mathcal{L}}{\mathcal{L}} = \frac{dI_e}{I_e} \oplus \frac{d\sigma_e}{\sigma_e} \frac{1}{1+\frac{\sigma_\gamma^2}{\sigma_e^2}} = A_{I_e} \oplus A_{\sigma_e} \frac{1}{1+\frac{\sigma_\gamma^2}{\sigma_e^2}}. \tag{87}$$

  Thus the relative stability of the beam intensity and beam spot size must be $\frac{dA_{I_e}}{dt} \leq 2.5\ 10^{-2}\ /s$ **and** $\frac{dA_{\sigma_e}}{dt} \leq 5.\ 10^{-2}\ /s$.
  For a reversal frequency of $f = 1\ Hz$, these upper limits are divided by a factor $10^{3/2} \simeq 30$.

E	GeV	1.0	2.0	3.0	4.0	5.0	6.0	7.0	8.0
Power	$10^{-15}W$	0.029	0.456	2.310	7.300	17.822	36.955	68.464	116.797
N_γ		4.615	9.231	13.846	18.462	23.077	27.693	32.308	36.923
$< \epsilon >$	KeV	0.039	0.308	1.041	2.468	4.820	8.329	13.226	19.743
dE	KeV	0.178	2.848	14.416	45.562	111.235	230.656	427.319	728.987
σ(dE)	KeV	0.172	1.927	7.995	21.955	47.828	90.556	155.810	248.251

Table 13: ***Characteristics of the synchrotron radiation in the magnetic chicane.*** *Radiated power P, mean number of radiated photons N_γ, mean energy of the radiated photons $< \epsilon >$, energy lost by the incident electron dE and dispersion of the energy lost $\sigma(dE)$.*

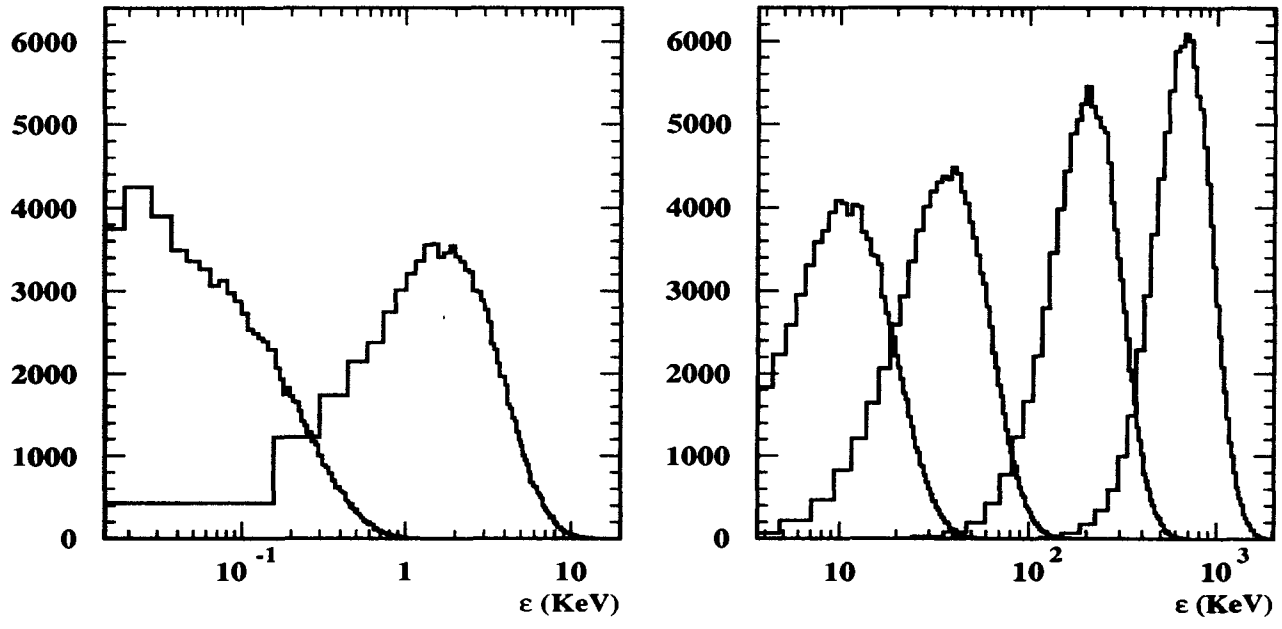

Figure 14: ***Distribution of the synchrotron photon energy (KeV).*** *For $1, 2, 3, 4, 6, 8$ GeV from left to right*

5.5 Energy loss by synchrotron radiation

Due to synchrotron radiation, the electron beam will loose energy in the magnetic chicane (See section C.1) and its dispersion will be increased. For instance, at 4 GeV (resp. 8 GeV) and 0.75 T (resp. 1.5 T), the total energy lost by synchrotron radiation in the chicane will be $dE = 46\ KeV \pm 22\ KeV$ (resp. $729\ KeV \pm 248\ KeV$).

Table (13) gives the characteristics of the synchrotron radiation for an electron of energy E traveling through 4 dipoles (length=1 m , magnetic field B). Figure (14) shows the energy distribution of the radiated photons for different incident energies.

$L_1 = L_2$=1.00 m	D_{12}=4.40 m	$D_\gamma = 5.80m$

$\lambda = 1064.2nm$

E	GeV	1.0	2.0	3.0	4.0	5.0	6.0	7.0	8.0
B_1	Tesla	0.187	0.375	0.562	0.750	0.937	1.125	1.312	1.500
k_{max}	MeV	17.5	68.9	152.4	266.5	409.6	580.3	777.3	999.4
k_0	MeV	8.8	35.1	78.2	137.8	213.5	304.9	411.5	533.0
ρ_0	k_0/k_{max}	0.504	0.509	0.513	0.517	0.521	0.525	0.529	0.533
r_c^0 mm	$\rho_{min} = \rho_0$	2.964	1.482	0.988	0.741	0.593	0.494	0.423	0.370
r_c mm	ρ_{min} =0.10	8.970	4.524	3.042	2.301	1.856	1.559	1.347	1.188
r_c mm	ρ_{min} =0.20	5.980	3.016	2.028	1.534	1.237	1.039	0.898	0.792
r_c mm	ρ_{min} =0.30	4.567	2.304	1.549	1.172	0.945	0.794	0.686	0.605
r_c mm	ρ_{min} =0.40	3.662	1.847	1.242	0.939	0.758	0.637	0.550	0.485
r_c mm	ρ_{min} =0.50	2.990	1.508	1.014	0.767	0.619	0.520	0.449	0.396

Table 14: ***Photon detector collimator size*** r_c ***(see text) as a function of the threshold energy.***

6 Scattered photon Calorimeter

6.1 Set up

The photon detector will be located between dipoles 3 and 4 of the magnetic chicane near dipole 4 where the available transverse deviation of the beam is sufficient. A layout of the photon detector setup is displayed on figure (15).

The energy k'_γ of the Compton scattered photons decreases quickly when the photon scattering angle θ_γ increases (Fig. 4). Then the high energy Compton photons (i.e. with $\rho_{min} = k'_\gamma/k'_{max} \geq 0.1$) are emitted with small angles $\theta_\gamma \leq 2\ mrad$ which gives a size for the Compton photons of $r_c \leq 1\ cm$ for a detector located at a distance $D_\gamma \simeq 5.80\ m$ from the interacting point. This size, given in table (14) for various incident energy and energy threshold is well below the transverse size needed to contain the electromagnetic shower which is of the order of 3 or 4 Moliere radius i.e. $\geq 10\ cm$ for most commonly used fully active calorimeter (Tab. 15).

A thick collimator, with a hole of radius $r_\gamma = r_c + 2mm$ for Compton photons, will be used to protect the detector against synchrotron and low energy bremsstrahlung radiations. Indeed, the photon detector will be irradiated by a high flux of synchrotron photons emitted along a piece $\Delta\Theta$ of the electron trajectory in the dipoles 2 and 3 of the magnetic chicane (See Fig. 15). The thick collimator reduce these synchrotron photons to an acceptable level (section 6.3).

Nevertheless the rate of synchrotron photons in front of the hole of the collimator corresponding to the angle $\Delta\theta$ of the figure (15) is high. A thin absorber of radius r_γ is used to decrease this background.

We will first list the specifications of the γ detector leading to a fully active calorimeter. Then we will look at the synchrotron rate since it is the main problem of the γ detector. This will fix the thickness of the thin absorber. Finally we will study the bremsstrahlung background.

	NaI(Tl)	BGO	BAF_2	CsI(Tl)	CsI	$PbWO_4$	CeF_3
Density (g/cm^3)	3.67	7.13	4.89	4.53	4.53	8.28	6.16
Radiation Length (cm)	2.59	1.12	2.05	1.85	1.85	0.85	1.68
Molière radius (cm)	4.5	2.4	3.4	3.8	3.8	2.19	2.63
Decay time (ns)							
Fast	250	300	0.7	1000	10 , 36	2.2 , 10	9
Slow			600		1000	39	32

Table 15: ***Properties of some inorganic scintillators***

6.2 Photon detector specifications

The **main requirements** for the photon detector are :

- a high signal rate that we plan to reach (850 kHz for a cavity with $G = 10000$).
- a high rate of synchrotron radiation (section 6.3) which can limit the use of this detector for incident electron energy $E \geq 6\ GeV$.
- the transverse size available, fixed by the magnetic chicane.
- the resolution on the energy measurement $\sigma(k)/k_{max} \leq 10\%$ and which has to be known to 5% (Appendix E.2.3).
- the energy calibration which has to be measured with a precision of 0.5% for the threshold and 1% for the slope (Appendix E.2.3).

The choice of the material and the size of the photon detector is still under study. We need a **fully active electromagnetic calorimeter with fast decay time and high radiation hardness**. Among available scintillators (Tab. 15), $PbWO_4$ [17] seems a good candidate apart may be the low light yield.

- The decay time allows to collect 85 % of the charge in 25 ns and makes $PbWO_4$ suitable for high rate experiment.
- Tests of irradiation with gammas and neutrons show that the induced absorption length is small wrt crystal length for exposure up to 2 Mrad [18] [19]. This crystal can be used in high radiation environment.
- Its short radiation length and small Moliere radius lead to a compact design.
- Tests performed at γ energies in the range [0.5 : 2] GeV [20] gives a light yield which seems sufficient for fulfill our resolution requirement. But we have to extend the tests of this crystal at γ energies in the range [10 : 1000] MeV before a definitive decision. Part of these tests are dedicated to optimize the light collection (Appendix I) . Also are planned tests on CeF_3 which can be an alternative solution.
- The temperature dependence of scintillation light yield is high -2 % per ^oC and requires a temperature stabilisation and monitoring system for a precise calibration.

As there is no magnetic field, the **photodetector** will be a photomultiplicator. The **dynamics** of the scattered γ for a given incident energy is weak $\simeq$ 1 : 20 due to the energy threshold ($\rho = 0.1$) defined by the collimator size. The **positioning** has to be made to 1 mm level.

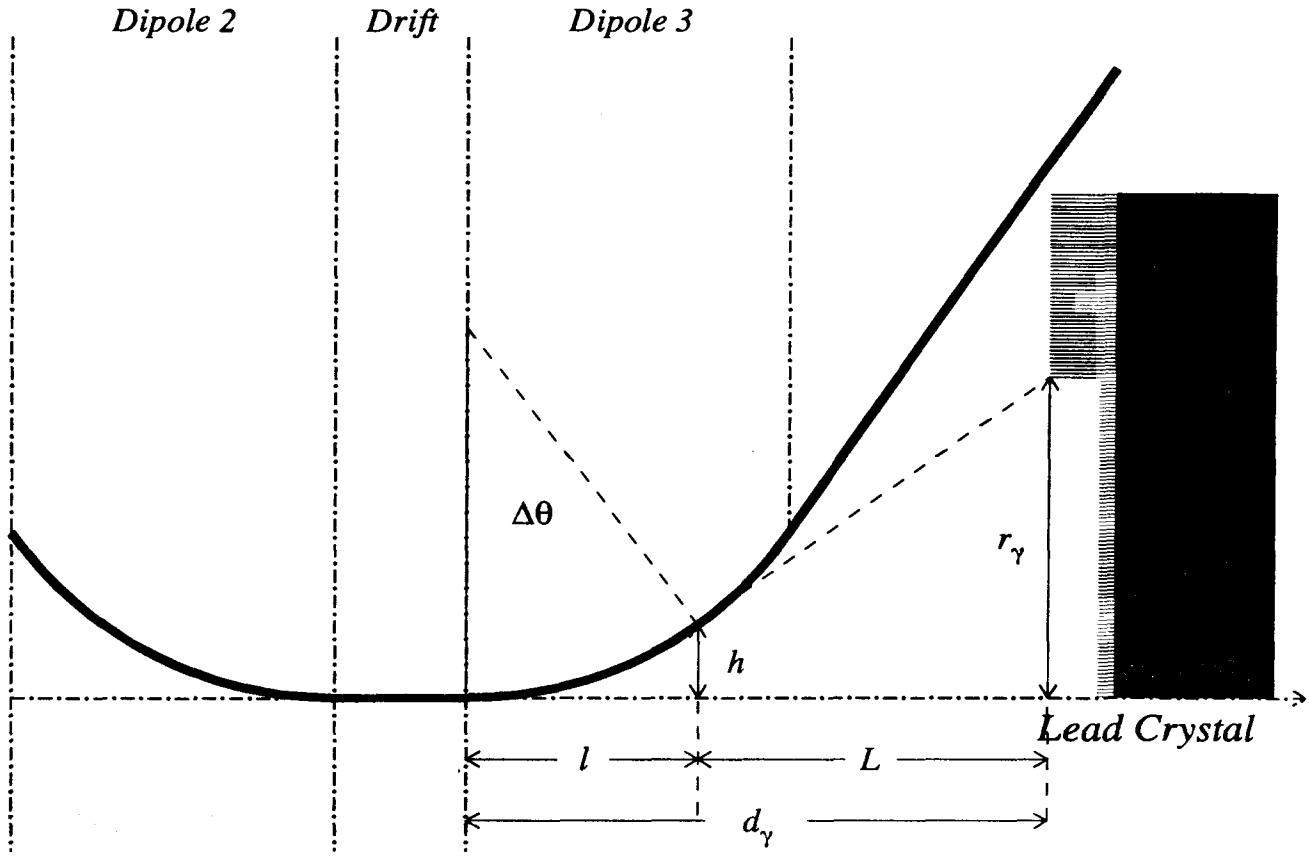

Figure 15: ***Useful angle*** $\Delta\theta$ ***of the electron trajectory for the synchrotron radiation*** *seen by the photon detector of radius* r_γ *at a distance* d_γ *from entrance of Dipole D3.*

6.3 Synchrotron Background for the photon detector

The radiation to be considered here are the synchrotron photons emitted by the exit of dipole 2 and by the entrance of dipole 3 of the magnetic chicane ($B = 0.75\ T$ at 4 GeV and $L = 1\ m$).

The photon detector sees a piece $\Delta\theta$ of the e^- trajectory in the dipoles of the magnetic chicane under an angle ψ (angle between the bending plane and the observation point). So the synchrotron radiation is given by equation (212) of appendix C. As the dimension of the gamma detector in the plane perpendicular to the bending plane is large, the detector integrates over a large number of $\psi\gamma$. So we can use the spectral power density given by equation (217) of appendix C.

If d_γ is the distance between the exit (entrance) of dipole 2 (3) and the upstream side of the γ detector with radius r_γ, then we have (Fig. 15)

$$h = R(1 - \cos\Delta\theta) \quad ; \quad l = R\sin\Delta\theta\ ,$$

where $\Delta\theta$ is the angle of the electron trajectory of synchrotron radiation seen by the a photon detector

$$\tan(\Delta\theta) = \frac{r_\gamma - h}{L} = \frac{r_\gamma - R(1 - \cos\Delta\theta)}{d_\gamma - R\sin\Delta\theta}\ .$$

At first order

$$\Delta\theta \simeq \frac{r_\gamma}{d_\gamma}\ . \tag{88}$$

E	B	r_γ	$\Delta\theta$	P	dn/dt	$<\epsilon>$	$\psi\gamma$	E/100ns
GeV	T	cm	mrad	W	s^{-1}	KeV		GeV/100ns
1.	0.19	1.097	3.94	0.312E-03	0.504E+14	0.386E-01	0.400E+01	0.195E+00
2.	0.37	0.652	2.34	0.297E-02	0.600E+14	0.308E+00	0.476E+01	0.185E+01
3.	0.56	0.504	1.81	0.116E-01	0.696E+14	0.104E+01	0.552E+01	0.724E+01
4.	0.75	0.430	1.54	0.313E-01	0.791E+14	0.247E+01	0.628E+01	0.195E+02
5.	0.94	0.386	1.38	0.685E-01	0.887E+14	0.482E+01	0.704E+01	0.427E+02
6.	1.12	0.356	1.28	0.131E+00	0.982E+14	0.833E+01	0.780E+01	0.818E+02
7.	1.31	0.335	1.20	0.228E+00	0.108E+15	0.132E+02	0.855E+01	0.142E+03
8.	1.50	0.319	1.14	0.371E+00	0.117E+15	0.197E+02	0.931E+01	0.232E+03

Table 16: ***Synchrotron radiation without absorber.*** *For various beam energies and magnetic field at 100 μA. The power and rate seen by the γ detector located at $d_\gamma = 695$ cm from Dipole D2 exit and $d_\gamma = 465$ cm from Dipole D3 entrance are given for a collimator radius r_γ i.e. for $\Delta\theta$. The column $\psi\gamma$ indicates the angular range seen by the detector.*

E	B	r_γ	$\Delta\theta$	P	dn/dt	$<\epsilon>$	$\psi\gamma$	E/100ns
GeV	T	cm	mrad	W	s^{-1}	KeV		GeV/100ns
1.	0.19	1.097	3.94	0.271-131	0.130-116	0.130E+02	0.400E+01	0.169-128
2.	0.37	0.652	2.34	0.242E-32	0.284E-18	0.532E+02	0.476E+01	0.151E-29
3.	0.56	0.504	1.81	0.106E-13	0.878E+00	0.752E+02	0.552E+01	0.660E-11
4.	0.75	0.430	1.54	0.682E-08	0.521E+06	0.818E+02	0.628E+01	0.426E-05
5.	0.94	0.386	1.38	0.107E-05	0.736E+08	0.909E+02	0.704E+01	0.669E-03
6.	1.12	0.356	1.28	0.400E-04	0.153E+10	0.163E+03	0.780E+01	0.250E-01
7.	1.31	0.335	1.20	0.791E-03	0.211E+11	0.234E+03	0.855E+01	0.494E+00
8.	1.50	0.319	1.14	0.636E-02	0.141E+12	0.281E+03	0.931E+01	0.397E+01

Table 17: ***Synchrotron radiation with a 2.5 mm lead absorber.*** *For various beam energies and magnetic field at 100μA. The power and rate seen by the γ detector located at $d_\gamma = 695$ cm from Dipole D2 exit and $d_\gamma = 465$ cm from Dipole D3 entrance are given for a collimator radius r_γ i.e. for $\Delta\theta$. The column $\psi\gamma$ indicates the angular range seen by the detector.*

E	B	r_γ	$\Delta\theta$	P	dn/dt	$<\epsilon>$	$\psi\gamma$	E/100ns
GeV	T	cm	mrad	W	s^{-1}	KeV		GeV/100ns
1.	0.19	1.097	3.94	0.359-211	0.546-197	0.410E+02	0.400E+01	0.224-208
2.	0.37	0.652	2.34	0.197E-47	0.152E-33	0.807E+02	0.476E+01	0.123E-44
3.	0.56	0.504	1.81	0.552E-22	0.402E-08	0.858E+02	0.552E+01	0.345E-19
4.	0.75	0.430	1.54	0.178E-15	0.101E-01	0.110E+03	0.628E+01	0.111E-12
5.	0.94	0.386	1.38	0.725E-10	0.173E+04	0.261E+03	0.704E+01	0.452E-07
6.	1.12	0.356	1.28	0.172E-06	0.341E+07	0.314E+03	0.780E+01	0.107E-03
7.	1.31	0.335	1.20	0.177E-04	0.306E+09	0.361E+03	0.855E+01	0.110E-01
8.	1.50	0.319	1.14	0.354E-03	0.539E+10	0.410E+03	0.931E+01	0.221E+00

Table 18: ***Synchrotron radiation with a 1 cm lead absorber.*** *For various beam energies and magnetic field at 100μA. The power and rate seen by the γ detector located at $d_\gamma = 695$ cm from Dipole D2 exit and $d_\gamma = 465$ cm from Dipole D3 entrance are given for a collimator radius r_γ i.e. for $\Delta\theta$. The column $\psi\gamma$ indicates the angular range seen by the detector.*

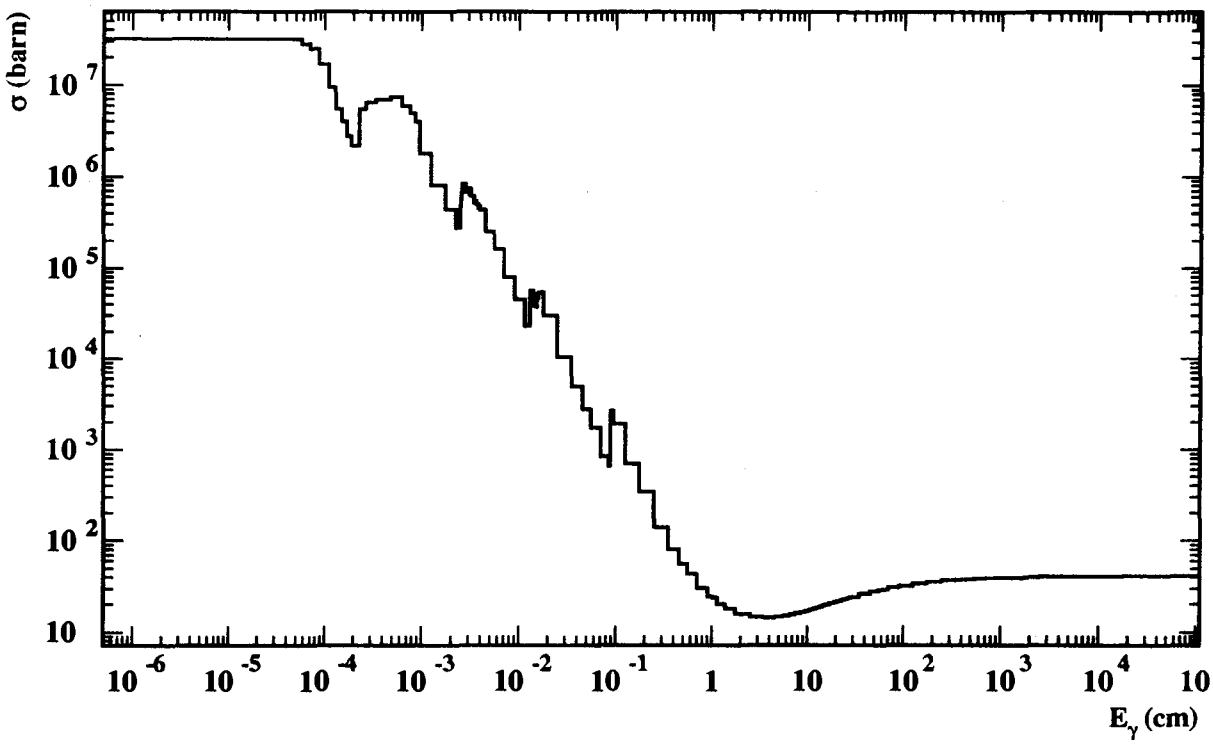

Figure 16: ***Photon total cross section absorption in lead versus photon energy.***

As a collimator we will use a 1 cm thick lead foil with a hole of r_γ at the entrance of the photon detector. The hole radius vary with incident energy to match the Compton angular distribution and is given in table (14). In front of this hole, the thin absorber will be a $2.5\ mm$ lead foil. Absorption cross section for lead is shown on figure (16).

Values of the number $\frac{dn}{dt}$ and mean energy $< \epsilon >$ of synchrotron photon corresponding to the power P_γ are listed in tables (16),(17) and (18) for a hole radius r_γ corresponding to the useful angle $\Delta\theta$ for the 2 dipoles.

At 4 GeV, the 1 cm thick lead collimator will absorb almost all the synchrotron radiation (Tab. 16 and 18). One expects that 0.01 synchrotron photon per second with a mean energy of 0.1 MeV will pass through the collimator.
In front of the $1\ cm$ hole, the $2.5\ mm$ lead foil will give a rate of 0.52 MHz of synchrotron photons with a mean energy of 82 KeV (Tab. 17). For a gate of $\tau = 100\ ns$, this gives 0.052 synchrotron photon with energy close to 80 KeV. Compared with the Compton photons range: $0 \leq k' \leq 500\ MeV$, this background is negligible. This 2.5 mm absorber gives an attenuation of 77 % for 100 MeV photons.

At 6 GeV, the 1 cm thick lead collimator will gives 3.4 MHz of synchrotron photons with a mean energy of 0.31 MeV, i.e a deposited energy of 107 KeV for a gate of $\tau = 100\ ns$.
The 2.5 mm absorber would result in a 1.5 GHz synchrotron rate with 0.16 MeV photon energy. For a $\tau = 100\ ns$ gate, the photon detector will see 153 synchrotron photons with a total energy of 25 MeV. This should be compared with the range for Compton photons: $0 \leq k' \leq 500\ MeV$. It thus may be necessary for the 6 GeV runs to use a thicker absorber, but then the attenuation for 200 MeV photon increases (35 % for 1cm of lead).

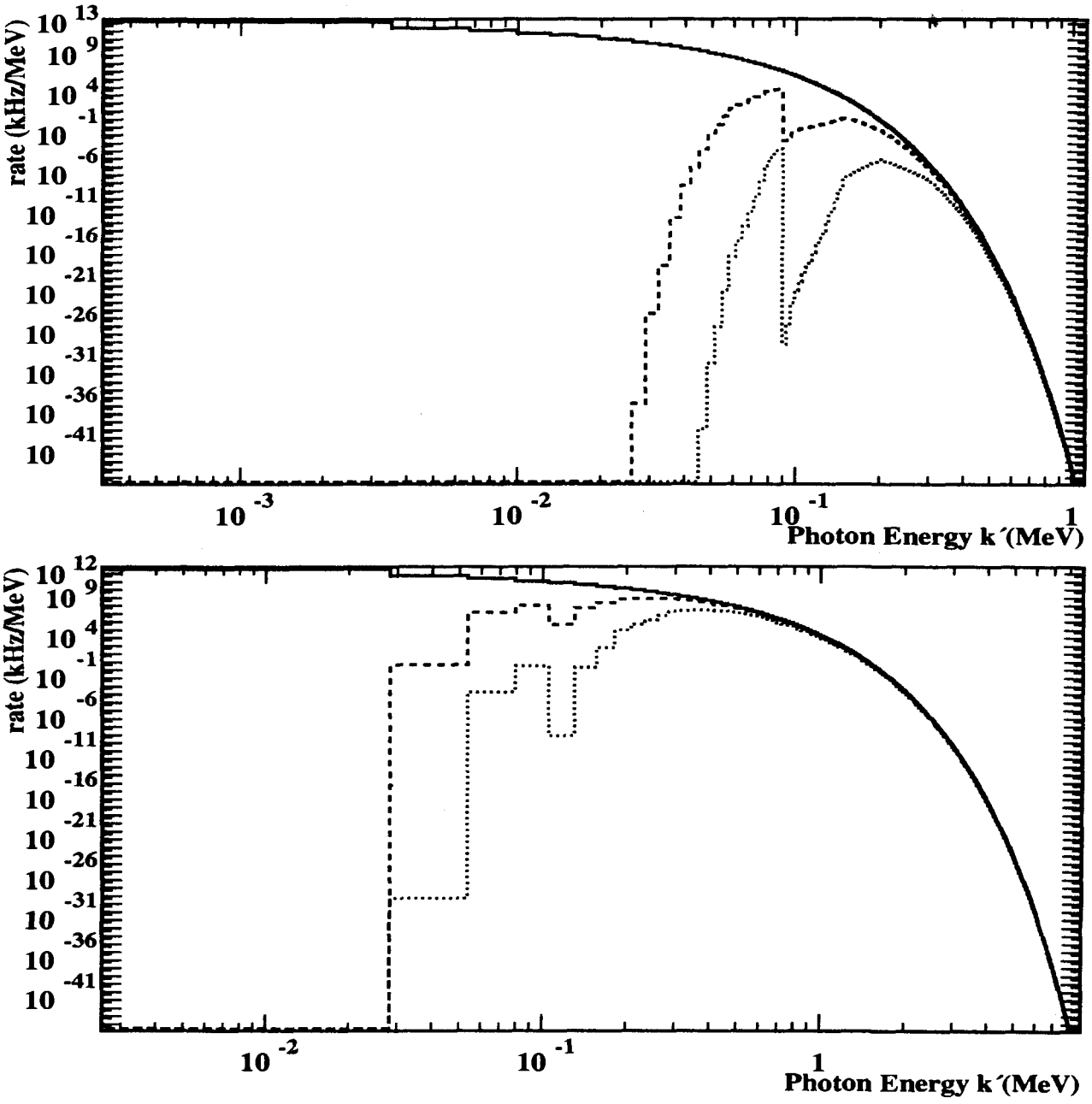

Figure 17: ***Synchrotron rate in the photon detector.*** *For* $100\mu A$ *at 4 GeV (up) and 8 GeV (down) with an lead absorber of thickness 0 mm (solid line), 2.5 mm (dashed line) and 10 mm (dotted line).*

At 8 GeV, the 1 cm thick lead collimator will gives 5.4 GHz of synchrotron photons with a mean energy of 0.41 MeV, i.e 539 photons for a gate of $\tau = 100\ ns$ (Total energy 221 MeV). We have to increase the thickness of the collimator.
The 2.5 mm absorber would result in a 141 GHz synchrotron rate with 0.28 MeV photon energy. For a $\tau = 100\ ns$ gate, the photon detector will see 14100 synchrotron photons with a total energy of 3.97 GeV while the range for Compton photons is only: $0 \leq k' \leq 1\ GeV$. It thus may be also necessary for the 8 GeV runs to use a 1 cm absorber.

Figure (17) gives the synchrotron rate at 4 and 8 GeV for a lead absorber thickness of 0, 2.5 and $10\ mm$.

6.4 Bremsstrahlung for the photon detector

The bremsstrahlung seen by the photon detector is generated between the dipole 2 and 3 of the magnetic chicane. The useful length for bremsstrahlung is then of order $L \simeq 2.5\ m$. In this region, we expect a vacuum of $P = 10^{-8}\ Torr$.

Bremsstrahlung photons are emitted with angles $\theta \simeq 1/\gamma = m/E$ similar to Compton photons (Appendix D.2). Then these photons are fully seen by the photon detector.

The thin absorber will cut the low energy ($k' < 0.5\ MeV$) part of the spectrum. For computing the bremsstrahlung rate, we have used the Tsai cross section (Appendix D.1) with a conservative threshold of $k'_c = 0.1\ MeV$.

Tables (19),(20),(21) and (22) give the full integrated rate and the rate integrated on the Compton range as well as the mean energy deposited in a 100 ns gate. The rates are given for various thickness of the thin absorber $t_{abs} = 0.$, 2.5 and 10 mm. Table (19) is for a laser wavelength $\lambda = 1064\ nm$ (this gives the Compton range) and for a residual vacuum with a mean Z of $Z = 1$ and a STP density $\rho_0 = 0.09\ g/l$. Table (20) is for the same laser wavelength but for a residual vacuum with a mean Z of $Z = 6$ and a STP density $\rho_0 = 1.08\ g/l$. Tables (21) and (22) are for a laser wavelength $\lambda = 532\ nm$.

For a NdYAG Laser ($\lambda = 1064\ nm$), in the worst case ($E = 8\ GeV$,$Z = 6$), the full integrated rate is .52 kHz and the rate integrated on the Compton range is .45 kHz. These rates vary slowly (less than a factor 2) with the incident energy E. This has to be compared with the Compton rate of order 850 kHz (Tab. 8 for a $G = 10000$ cavity). The energy in a 100 ns gate varies from 0.1 KeV for $E = 1\ GeV$ to 4.9 KeV for $E = 8\ GeV$ and had to be compared with the mean Compton energy 9 MeV for $E = 1\ GeV$ to 1 GeV for $E = 8\ GeV$ (Tab. 1).

On figure (18), the expected Compton differential rate is compared with the bremsstrahlung rate at 4 GeV and 8 GeV. A vacuum of $10^{-8}\ Torr$ would result in a weak bremsstrahlung contamination. One sees that a higher threshold on photon energy would reduce this background. The variation of the full integrated rate with the energy threshold is shown on figure (19) to be compared with the variation of the Compton rate (Fig. 5 and Tab. 9).

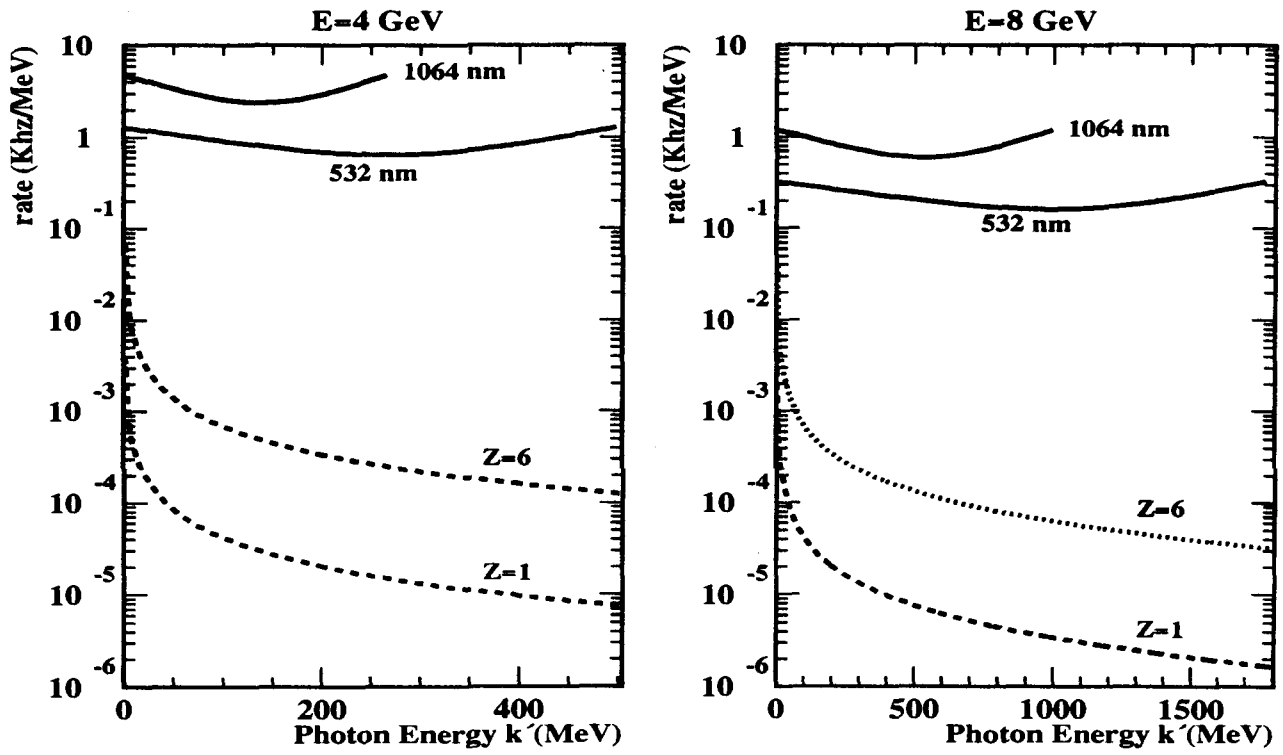

Figure 18: ***Differential Compton rate (solid line) and bremsstrahlung rate (dashed line).*** *At* $4\ GeV$ *(Left) and* $8\ GeV$ *(right) and* $100\mu A$. *Bremsstrahlung rate is for* $2.5\ m$ *vacuum at* $10^{-8}\ Torr$. *Compton rate is for a Laser of power* $P = 0.5\ W$ *with a cavity of* $1\ m$ *length and* $g = -0.95$ *and with a gain of* $G = 10000$.

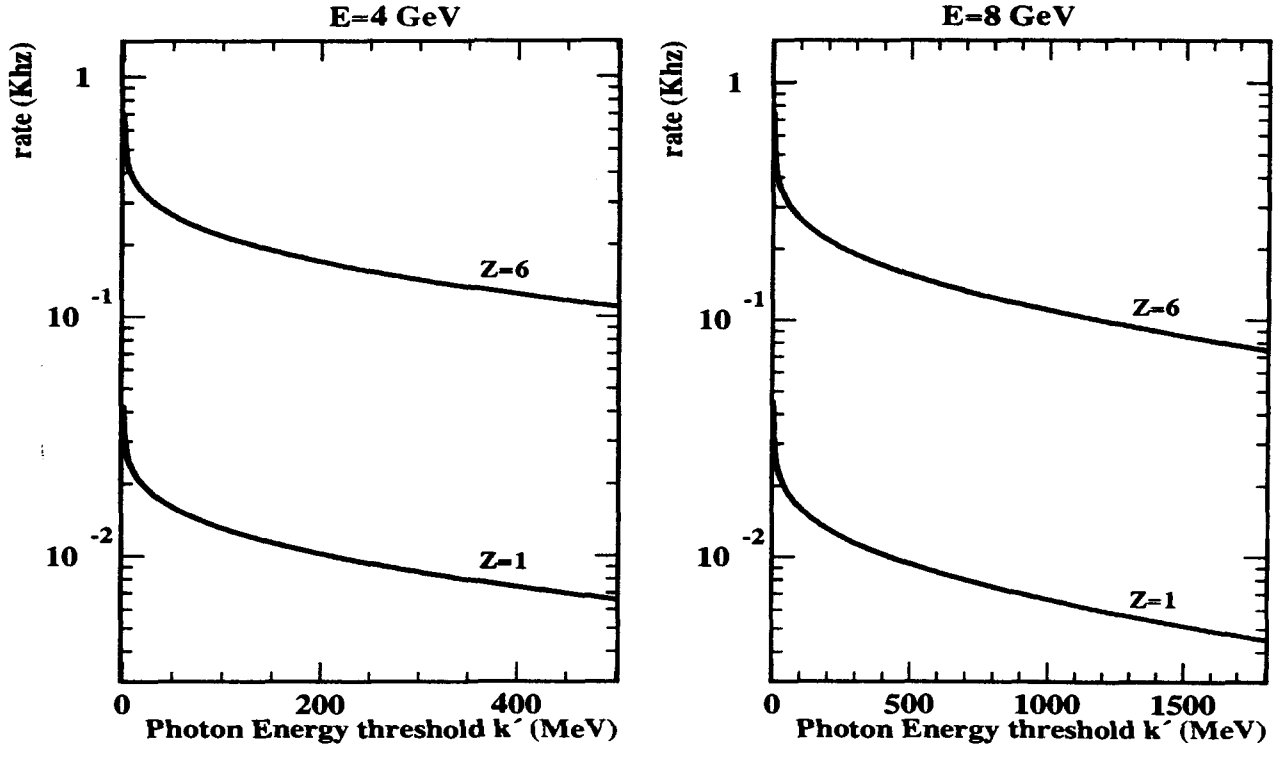

Figure 19: ***Integrated bremsstrahlung rate versus threshold.*** *At* $4\ GeV$ *and* $8\ GeV$ *and at* $100\mu A$ *for* $2.5\ m$ *vacuum at* $10^{-8}\ Torr$.

λ = 1064.2 nm	Z = 1	t_{abs} = 0.00 cm	threshold = 0.100 MeV		
E(GeV)	$k_{max}(GeV)$	$(\frac{dn}{dt})^{tot}$(Khz)	dE^{tot}_{100ns}(KeV)	$(\frac{dn}{dt})^{range}$(Khz)	dE^{range}_{100ns}(KeV)
1.	0.018	0.363E-01	0.297E+00	0.221E-01	0.740E-02
2.	0.069	0.394E-01	0.609E+00	0.278E-01	0.290E-01
3.	0.152	0.413E-01	0.924E+00	0.312E-01	0.637E-01
4.	0.266	0.425E-01	0.124E+01	0.335E-01	0.110E+00
5.	0.410	0.435E-01	0.156E+01	0.353E-01	0.169E+00
6.	0.580	0.443E-01	0.187E+01	0.367E-01	0.237E+00
7.	0.777	0.450E-01	0.219E+01	0.379E-01	0.316E+00
8.	0.999	0.455E-01	0.251E+01	0.389E-01	0.403E+00

λ = 1064.2 nm	Z = 1	t_{abs} = 0.25 cm	threshold = 0.100 MeV		
E(GeV)	$k_{max}(GeV)$	$(\frac{dn}{dt})^{tot}$(Khz)	dE^{tot}_{100ns}(KeV)	$(\frac{dn}{dt})^{range}$(Khz)	dE^{range}_{100ns}(KeV)
1.	0.018	0.263E-01	0.221E+00	0.142E-01	0.630E-02
2.	0.069	0.286E-01	0.447E+00	0.189E-01	0.237E-01
3.	0.152	0.293E-01	0.673E+00	0.217E-01	0.503E-01
4.	0.266	0.308E-01	0.899E+00	0.243E-01	0.854E-01
5.	0.410	0.306E-01	0.113E+01	0.251E-01	0.128E+00
6.	0.580	0.314E-01	0.135E+01	0.255E-01	0.178E+00
7.	0.777	0.323E-01	0.158E+01	0.269E-01	0.235E+00
8.	0.999	0.329E-01	0.181E+01	0.282E-01	0.299E+00

λ = 1064.2 nm	Z = 1	t_{abs} = 1.00 cm	threshold = 0.100 MeV		
E(GeV)	$k_{max}(GeV)$	$(\frac{dn}{dt})^{tot}$(Khz)	dE^{tot}_{100ns}(KeV)	$(\frac{dn}{dt})^{range}$(Khz)	dE^{range}_{100ns}(KeV)
1.	0.018	0.139E-01	0.922E-01	0.815E-02	0.407E-02
2.	0.069	0.148E-01	0.177E+00	0.104E-01	0.132E-01
3.	0.152	0.150E-01	0.261E+00	0.127E-01	0.252E-01
4.	0.266	0.157E-01	0.344E+00	0.133E-01	0.399E-01
5.	0.410	0.162E-01	0.427E+00	0.134E-01	0.570E-01
6.	0.580	0.158E-01	0.510E+00	0.143E-01	0.766E-01
7.	0.777	0.161E-01	0.593E+00	0.141E-01	0.985E-01
8.	0.999	0.165E-01	0.676E+00	0.147E-01	0.123E+00

Table 19: ***Bremsstrahlung radiation for a*** $1064\ nm$ ***Laser.*** *For various beam energies E and thickness absorber t_{abs} at 100 μA for a $2.5\ m$ residual vacuum of $10^{-8}\ Torr$ (mean Z=1). The rate dn/dt and the deposited energy in a $100\ ns$ gate dE_{100ns} are given for the total energy range and for the Compton energy range. The threshold for the bremsstrahlung photons is also mentioned.*

λ = 1064.2 nm	Z = 6	t_{abs} = 0.00 cm	threshold = 0.100 MeV		
E(GeV)	$k_{max}(GeV)$	$(\frac{dn}{dt})^{tot}$(Khz)	dE^{tot}_{100ns}(KeV)	$(\frac{dn}{dt})^{range}$(Khz)	dE^{range}_{100ns}(KeV)
1.	0.018	0.603E+00	0.509E+01	0.363E+00	0.122E+00
2.	0.069	0.652E+00	0.103E+02	0.458E+00	0.477E+00
3.	0.152	0.681E+00	0.156E+02	0.513E+00	0.105E+01
4.	0.266	0.702E+00	0.208E+02	0.552E+00	0.182E+01
5.	0.410	0.718E+00	0.260E+02	0.581E+00	0.277E+01
6.	0.580	0.731E+00	0.313E+02	0.604E+00	0.390E+01
7.	0.777	0.742E+00	0.365E+02	0.624E+00	0.519E+01
8.	0.999	0.751E+00	0.418E+02	0.641E+00	0.663E+01

λ = 1064.2 nm	Z = 6	t_{abs} = 0.25 cm	threshold = 0.100 MeV		
E(GeV)	$k_{max}(GeV)$	$(\frac{dn}{dt})^{tot}$(Khz)	dE^{tot}_{100ns}(KeV)	$(\frac{dn}{dt})^{range}$(Khz)	dE^{range}_{100ns}(KeV)
1.	0.018	0.417E+00	0.379E+01	0.233E+00	0.104E+00
2.	0.069	0.454E+00	0.756E+01	0.310E+00	0.390E+00
3.	0.152	0.475E+00	0.113E+02	0.353E+00	0.828E+00
4.	0.266	0.490E+00	0.151E+02	0.381E+00	0.140E+01
5.	0.410	0.502E+00	0.188E+02	0.403E+00	0.211E+01
6.	0.580	0.511E+00	0.226E+02	0.420E+00	0.293E+01
7.	0.777	0.519E+00	0.263E+02	0.435E+00	0.387E+01
8.	0.999	0.525E+00	0.301E+02	0.446E+00	0.491E+01

λ = 1064.2 nm	Z = 6	t_{abs} = 1.00 cm	threshold = 0.100 MeV		
E(GeV)	$k_{max}(GeV)$	$(\frac{dn}{dt})^{tot}$(Khz)	dE^{tot}_{100ns}(KeV)	$(\frac{dn}{dt})^{range}$(Khz)	dE^{range}_{100ns}(KeV)
1.	0.018	0.219E+00	0.157E+01	0.132E+00	0.669E-01
2.	0.069	0.233E+00	0.299E+01	0.174E+00	0.217E+00
3.	0.152	0.242E+00	0.438E+01	0.194E+00	0.415E+00
4.	0.266	0.247E+00	0.576E+01	0.205E+00	0.656E+00
5.	0.410	0.252E+00	0.714E+01	0.214E+00	0.938E+00
6.	0.580	0.255E+00	0.851E+01	0.221E+00	0.126E+01
7.	0.777	0.258E+00	0.988E+01	0.227E+00	0.162E+01
8.	0.999	0.260E+00	0.112E+02	0.231E+00	0.202E+01

Table 20: ***Bremsstrahlung radiation for a*** $1064\ nm$ ***Laser.*** *For various beam energies* E *and thickness absorber* t_{abs} *at 100* μA *for a* $2.5\ m$ *residual vacuum of* $10^{-8}\ Torr$ *(mean Z=6). The rate* dn/dt *and the deposited energy in a* $100\ ns$ *gate* dE_{100ns} *are given for the total energy range and for the Compton energy range. The threshold for the bremsstrahlung photons is also mentioned.*

λ = 532.1 nm	Z = 1	t_{abs} = 0.00 cm	threshold = 0.100 MeV		
E(GeV)	$k_{max}(GeV)$	$(\frac{dn}{dt})^{tot}$(Khz)	dE^{tot}_{100ns}(KeV)	$(\frac{dn}{dt})^{range}$(Khz)	dE^{range}_{100ns}(KeV)
1.	0.034	0.363E-01	0.297E+00	0.249E-01	0.145E-01
2.	0.133	0.394E-01	0.609E+00	0.305E-01	0.552E-01
3.	0.290	0.413E-01	0.924E+00	0.337E-01	0.118E+00
4.	0.500	0.425E-01	0.124E+01	0.360E-01	0.201E+00
5.	0.757	0.435E-01	0.156E+01	0.376E-01	0.301E+00
6.	1.058	0.443E-01	0.187E+01	0.389E-01	0.417E+00
7.	1.399	0.450E-01	0.219E+01	0.400E-01	0.545E+00
8.	1.777	0.455E-01	0.251E+01	0.410E-01	0.686E+00

λ = 532.1 nm	Z = 1	t_{abs} = 0.25 cm	threshold = 0.100 MeV		
E(GeV)	$k_{max}(GeV)$	$(\frac{dn}{dt})^{tot}$(Khz)	dE^{tot}_{100ns}(KeV)	$(\frac{dn}{dt})^{range}$(Khz)	dE^{range}_{100ns}(KeV)
1.	0.034	0.263E-01	0.221E+00	0.165E-01	0.121E-01
2.	0.133	0.286E-01	0.447E+00	0.221E-01	0.439E-01
3.	0.290	0.293E-01	0.673E+00	0.234E-01	0.913E-01
4.	0.500	0.308E-01	0.899E+00	0.260E-01	0.152E+00
5.	0.757	0.306E-01	0.113E+01	0.267E-01	0.225E+00
6.	1.058	0.314E-01	0.135E+01	0.283E-01	0.308E+00
7.	1.399	0.323E-01	0.158E+01	0.283E-01	0.401E+00
8.	1.777	0.329E-01	0.181E+01	0.296E-01	0.502E+00

λ = 532.1 nm	Z = 1	t_{abs} = 1.00 cm	threshold = 0.100 MeV		
E(GeV)	$k_{max}(GeV)$	$(\frac{dn}{dt})^{tot}$(Khz)	dE^{tot}_{100ns}(KeV)	$(\frac{dn}{dt})^{range}$(Khz)	dE^{range}_{100ns}(KeV)
1.	0.034	0.139E-01	0.922E-01	0.924E-02	0.736E-02
2.	0.133	0.148E-01	0.177E+00	0.124E-01	0.224E-01
3.	0.290	0.150E-01	0.261E+00	0.135E-01	0.423E-01
4.	0.500	0.157E-01	0.344E+00	0.139E-01	0.664E-01
5.	0.757	0.162E-01	0.427E+00	0.140E-01	0.945E-01
6.	1.058	0.158E-01	0.510E+00	0.149E-01	0.126E+00
7.	1.399	0.161E-01	0.593E+00	0.145E-01	0.161E+00
8.	1.777	0.165E-01	0.676E+00	0.151E-01	0.199E+00

Table 21: ***Bremsstrahlung radiation for a*** $532\ nm$ ***Laser.*** *For various beam energies* E *and thickness absorber* t_{abs} *at* 100μ *A for a* $2.5\ m$ *residual vacuum of* $10^{-8}\ Torr$ *(mean Z=1). The rate* dn/dt *and the deposited energy in a* $100\ ns$ *gate* dE_{100ns} *are given for the total energy range and for the Compton energy range. The threshold for the bremsstrahlung photons is also mentioned.*

λ = 532.1 nm	Z = 6	t_{abs} = 0.00 cm	threshold = 0.100 MeV		
E(GeV)	$k_{max}(GeV)$	$(\frac{dn}{dt})^{tot}$(Khz)	dE^{tot}_{100ns}(KeV)	$(\frac{dn}{dt})^{range}$(Khz)	dE^{range}_{100ns}(KeV)
1.	0.034	0.603E+00	0.509E+01	0.410E+00	0.238E+00
2.	0.133	0.652E+00	0.103E+02	0.503E+00	0.908E+00
3.	0.290	0.681E+00	0.156E+02	0.556E+00	0.195E+01
4.	0.500	0.702E+00	0.208E+02	0.592E+00	0.332E+01
5.	0.757	0.718E+00	0.260E+02	0.620E+00	0.496E+01
6.	1.058	0.731E+00	0.313E+02	0.642E+00	0.686E+01
7.	1.399	0.742E+00	0.365E+02	0.660E+00	0.897E+01
8.	1.777	0.751E+00	0.418E+02	0.676E+00	0.113E+02

λ = 532.1 nm	Z = 6	t_{abs} = 0.25 cm	threshold = 0.100 MeV		
E(GeV)	$k_{max}(GeV)$	$(\frac{dn}{dt})^{tot}$(Khz)	dE^{tot}_{100ns}(KeV)	$(\frac{dn}{dt})^{range}$(Khz)	dE^{range}_{100ns}(KeV)
1.	0.034	0.417E+00	0.379E+01	0.271E+00	0.200E+00
2.	0.133	0.454E+00	0.756E+01	0.344E+00	0.723E+00
3.	0.290	0.475E+00	0.113E+02	0.384E+00	0.150E+01
4.	0.500	0.490E+00	0.151E+02	0.411E+00	0.251E+01
5.	0.757	0.502E+00	0.188E+02	0.431E+00	0.370E+01
6.	1.058	0.511E+00	0.226E+02	0.447E+00	0.508E+01
7.	1.399	0.519E+00	0.263E+02	0.460E+00	0.660E+01
8.	1.777	0.525E+00	0.301E+02	0.472E+00	0.827E+01

λ = 532.1 nm	Z = 6	t_{abs} = 1.00 cm	threshold = 0.100 MeV		
E(GeV)	$k_{max}(GeV)$	$(\frac{dn}{dt})^{tot}$(Khz)	dE^{tot}_{100ns}(KeV)	$(\frac{dn}{dt})^{range}$(Khz)	dE^{range}_{100ns}(KeV)
1.	0.034	0.219E+00	0.157E+01	0.154E+00	0.121E+00
2.	0.133	0.233E+00	0.299E+01	0.189E+00	0.368E+00
3.	0.290	0.242E+00	0.438E+01	0.207E+00	0.696E+00
4.	0.500	0.247E+00	0.576E+01	0.217E+00	0.109E+01
5.	0.757	0.252E+00	0.714E+01	0.226E+00	0.156E+01
6.	1.058	0.255E+00	0.851E+01	0.231E+00	0.208E+01
7.	1.399	0.258E+00	0.988E+01	0.237E+00	0.265E+01
8.	1.777	0.260E+00	0.112E+02	0.241E+00	0.327E+01

Table 22: ***Bremsstrahlung radiation for a*** $532\ nm$ ***Laser.*** *For various beam energies E and thickness absorber t_{abs} at 100μ A for a $2.5\ m$ residual vacuum of $10^{-8}\ Torr$ (mean Z=1). The rate dn/dt and the deposited energy in a $100\ ns$ gate dE_{100ns} are given for the total energy range and for the Compton energy range. The threshold for the bremsstrahlung photons is also mentioned.*

7 Scattered electron detector

In a second step, in order to reduce the systematic error on the polarization measurement, we aim to also determine the momentum of the scattered electron by measuring its deviation through the third dipole magnet. This will be helpful at high energy, where the synchrotron rate seen by the photon detector is very important.

7.1 Principle of the measurement

To reduce radiation damage from synchrotron radiation (Section 7.4), the detector will be located between dipole 3 and dipole 4. The final position (80 cm before dipole 4) is a compromise between the maximum dispersion and the space left for the vacuum pipe to be used when the magnetic chicane is not used.

Let L_3 be the length of dipole 3 and l_e the distance between the end of that dipole and the electron detector (Fig. 20). For an electron with momentum p, **the transverse deviation d at the electron detector location** is

$$d = R(1 - \cos\theta) + l_e \tan\theta \,, \tag{89}$$

using

$$\theta = \sin^{-1}\left(\frac{0.3B(T)L_3(m)}{p(GeV)}\right) \quad ; \quad R(m) = \frac{p(GeV)}{0.3B(T)} \,. \tag{90}$$

Electron trajectories for incident energy E and for minimum Compton energy E_{min} corresponding to the maximum Compton γ energy k_{max} are shown on figures (20) and (21) together with the location of the proposed electron detector.

The electron detector must be kept out of the beam. **A minimum safety gap** $d_g = 5\ mm$ seems possible (done at the ALS : linear accelerator of Saclay). The corresponding energy E_{gap} will be the maximal measured energy and **fix the energy threshold on the scattered Compton** γ.

To reduce the dependence of the electron energy measurement with the knowledge of the Dipole 3 Field map, it may be important to be able **to measure the k_0' point**, i.e. to measure scattered electron energy E_0 corresponding to a zero asymmetry.

All these parameters (energies E, E_0, E_{min} and E_{gap} and the corresponding deviations d, d_0, d_{min} and d_{gap}) are given in table (23).

To measure the gap between the electron beam and the electron detector, **a beam position monitor is necessary**. It has to be closest of the electron detector.
Transverse deviations after dipole 4 are also given in table (23). The deviations d_4 and d_4^{min} stand for beam and minimum Compton energy.

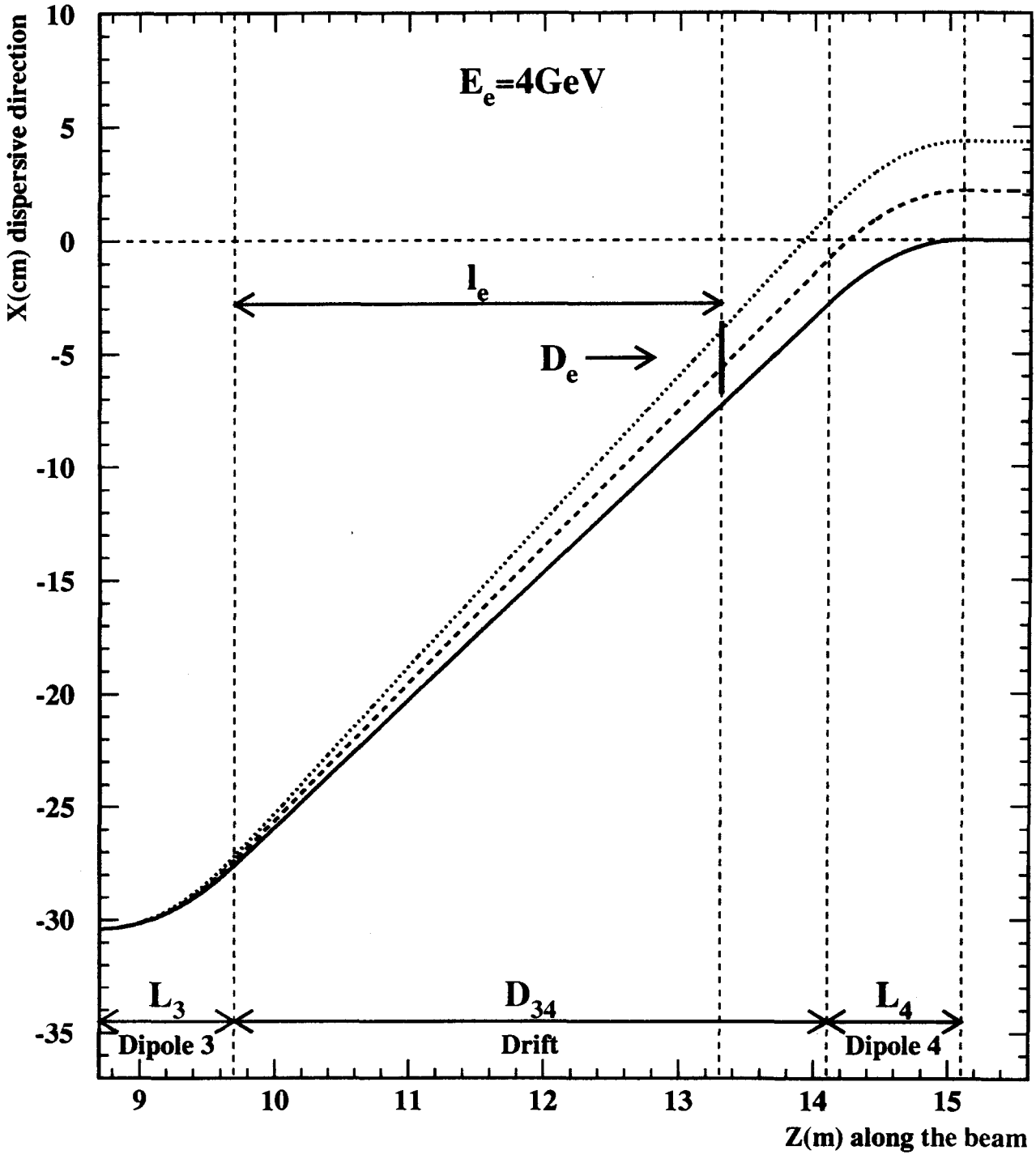

Figure 20: ***Scattered electron envelope at*** $E_e = 4\ GeV$. *Trajectory for Beam energy (solid line) and minimum scattered electron energy at* $k_\gamma = 1.16\ eV$ *(dotted line) and* $k_\gamma = 2.33\ eV$ *(dashed line). Transverse deviation (cm) versus coordinate(m) along the beam axis starting at Dipole 3 entrance.*

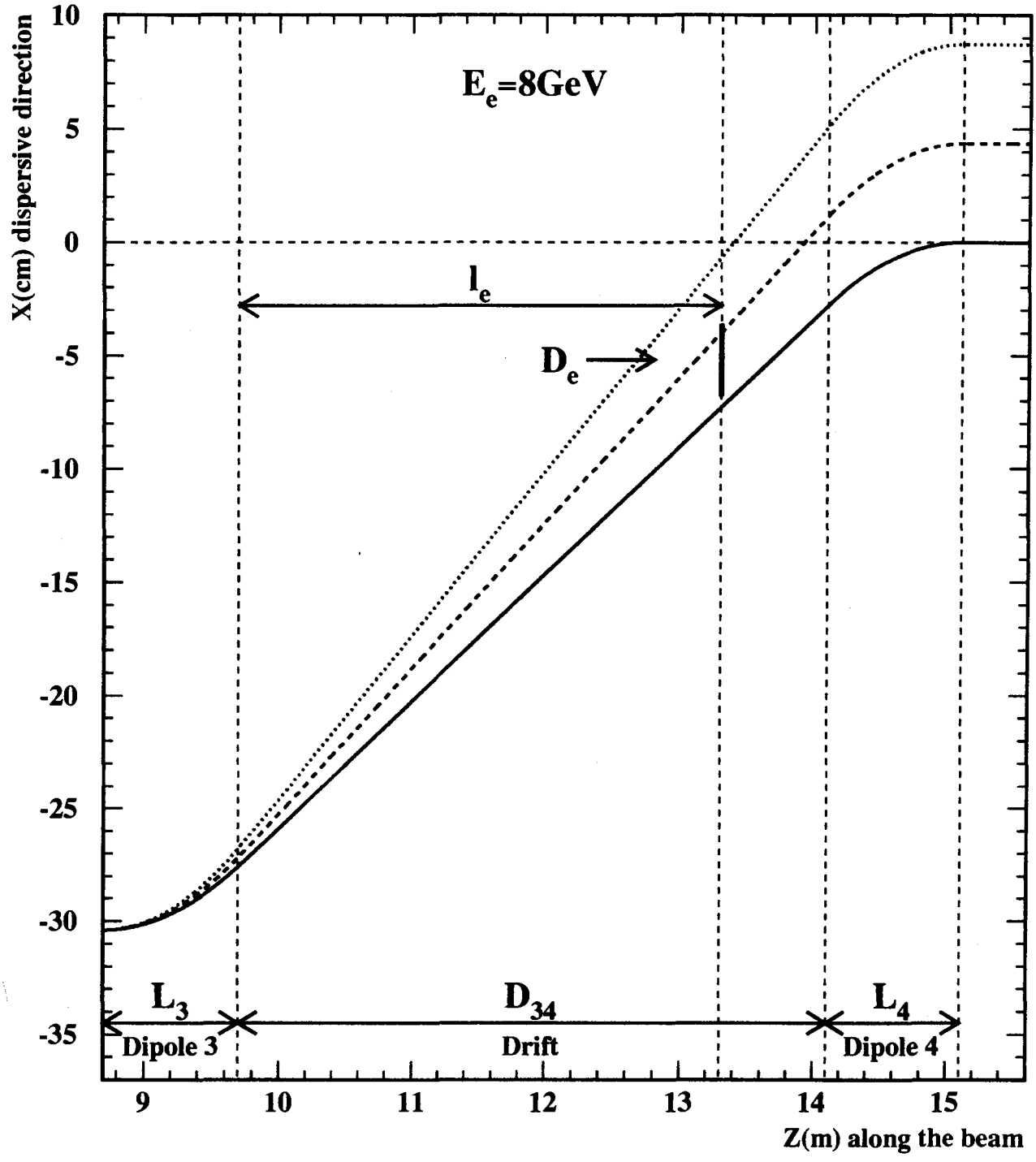

Figure 21: ***Scattered electron envelope at*** $E_e = 8\ GeV$. *Trajectory for Beam energy (solid line) and minimum scattered electron energy at* $k_\gamma = 1.16\ eV$ *(dotted line) and* $k_\gamma = 2.33\ eV$ *(dashed line). Transverse deviation (cm) versus coordinate(m) along the beam axis starting at Dipole 3 entrance.*

$L_3 = L_4$=1.00 m	D_{34}=4.40 m
$l_e = 3.60m$	$Gap\ d_g = 5.0mm$

$\lambda = 1064.2nm$

E	GeV	1.0	2.0	3.0	4.0	5.0	6.0	7.0	8.0
B	Tesla	0.187	0.375	0.562	0.750	0.937	1.125	1.312	1.500
E_0	GeV	0.991	1.965	2.922	3.862	4.786	5.695	6.589	7.467
E_{min}	GeV	0.982	1.931	2.848	3.734	4.590	5.420	6.223	7.001
E_{gap}	GeV	0.979	1.958	2.937	3.915	4.894	5.873	6.852	7.831
d	cm	-7.317	-7.317	-7.317	-7.317	-7.317	-7.317	-7.317	-7.317
d_0	cm	-7.110	-6.904	-6.697	-6.490	-6.284	-6.077	-5.871	-5.664
d_{min}	cm	-6.904	-6.490	-6.077	-5.664	-5.250	-4.837	-4.423	-4.010
d_{gap}	cm	-6.817	-6.817	-6.817	-6.817	-6.817	-6.817	-6.817	-6.817
$d_{min} - d_{gap}$	cm	-0.087	0.326	0.740	1.153	1.566	1.980	2.393	2.807
$d_0 - d_{gap}$	cm	-0.293	-0.087	0.120	0.326	0.533	0.740	0.946	1.153
d_4	cm	0.000	0.000	0.000	0.000	0.000	0.000	0.000	0.000
d_4^{min}	cm	0.544	1.088	1.632	2.177	2.721	3.265	3.810	4.355

$\lambda = 532.1nm$

E	GeV	1.0	2.0	3.0	4.0	5.0	6.0	7.0	8.0
B	Tesla	0.187	0.375	0.562	0.750	0.937	1.125	1.312	1.500
E_0	GeV	0.982	1.931	2.848	3.734	4.590	5.420	6.223	7.001
E_{min}	GeV	0.966	1.867	2.710	3.500	4.243	4.942	5.601	6.223
E_{gap}	GeV	0.979	1.958	2.937	3.915	4.894	5.873	6.852	7.831
d	cm	-7.317	-7.317	-7.317	-7.317	-7.317	-7.317	-7.317	-7.317
d_0	cm	-6.904	-6.490	-6.077	-5.664	-5.250	-4.837	-4.423	-4.010
d_{min}	cm	-6.490	-5.664	-4.837	-4.010	-3.182	-2.355	-1.527	-0.698
d_{gap}	cm	-6.817	-6.817	-6.817	-6.817	-6.817	-6.817	-6.817	-6.817
$d_{min} - d_{gap}$	cm	0.326	1.153	1.980	2.807	3.634	4.462	5.290	6.119
$d_0 - d_{gap}$	cm	-0.087	0.326	0.740	1.153	1.566	1.980	2.393	2.807
d_4	cm	0.000	0.000	0.000	0.000	0.000	0.000	0.000	0.000
d_4^{min}	cm	1.088	2.177	3.265	4.355	5.444	6.534	7.625	8.716

Table 23: ***Transverse deviations at electron detector location.*** *For different beam energies E and Laser wavelengths λ. The transverse deviations for the incident energy E and for the minimum scattered energy E_{min} are given by d and d_{min}. The deviation d_0 stands for the scattered energy E_0 where the longitudinal asymmetry vanishes. The deviation $d_{gap} = d + d_g$ is the beam deviation with a security gap d_g and corresponds to a scattered energy E_{gap}. The useful size of the detector is given by $d_{min} - d_{gap}$. The E_0 point can be measured if $d_0 - d_{gap}$ is positive. After the dipole 4, the transverse deviations for the incident energy E and for the minimum scattered energy E_{min} are given by d_4 and d_4^{min}.*

$L_3 = L_4$=1.00 m	D_{34}=4.40 m

$\lambda = 1064.2nm$	$l_e = 3.60m$	$Gap\ d_g = 5.0mm$

E	GeV	1.0	2.0	3.0	4.0	5.0	6.0	7.0	8.0
k_{max}	MeV	17.5	68.9	152.4	266.5	409.6	580.3	777.3	999.4
B	Tesla	0.187	0.375	0.562	0.750	0.937	1.125	1.312	1.500
Useful size	cm	-0.087	0.326	0.740	1.153	1.566	1.980	2.393	2.807
$< D >$	mm/%	2.408	2.450	2.492	2.535	2.577	2.620	2.662	2.705
$< D >$	mm/MeV	0.241	0.122	0.083	0.063	0.052	0.044	0.038	0.034
$\delta k/k$	%/mm	23.692	11.845	7.896	5.921	4.737	3.947	3.383	2.960
$\partial d/(\partial B/B)$	$\mu/10^{-3}$	235.7	239.9	244.1	248.4	252.7	257.1	261.5	265.9

$\lambda = 532.1nm$	$l_e = 3.60m$	$Gap\ d_g = 5.0mm$

E	GeV	1.0	2.0	3.0	4.0	5.0	6.0	7.0	8.0
k_{max}	MeV	34.5	133.2	290.1	499.7	757.1	1058.2	1399.2	1776.8
B	Tesla	0.187	0.375	0.562	0.750	0.937	1.125	1.312	1.500
Useful size	cm	0.326	1.153	1.980	2.807	3.634	4.462	5.290	6.119
$< D >$	mm/%	2.450	2.535	2.620	2.705	2.790	2.875	2.960	3.045
$< D >$	mm/MeV	0.245	0.127	0.087	0.068	0.056	0.048	0.042	0.038
$\delta k/k$	%/mm	11.845	5.921	3.947	2.960	2.367	1.972	1.690	1.479
$\partial d/(\partial B/B)$	$\mu/10^{-3}$	239.9	248.4	257.1	265.9	274.9	284.0	293.3	302.7

Table 24: ***Magnetic dispersion at electron detector location and energy resolution on the scattered Compton photon.*** *The mean dispersion $< D >$ is given from d_{min} to d_{gap}.*

7.2 Proposed detector

The detector will consist of **3 planes of silicon strips** (See Figure 22) in order to have a high efficiency with a good rejection of accidental coincidences and non directional background.

The useful size of the electron detector $d_{min} - d_{gap}$ is given in table (24). This size is maximal for $E = 8\ GeV$. Its value is 2.81 cm for the NdYAG Laser ($\lambda = 1064\ nm$) and 6.12 cm for the Argon Laser ($\lambda = 532\ nm$). So a detector of 128 channels with a pitch of 250 μm (size 3.2 cm) can be used with the NdYAG Laser and a detector of 256 channels (size 6.4 cm) with the Argon Laser. These sizes are large enough to allow for a reduction of the safety gap d_g if possible.
For a NdYAG Laser, the detector can be used only for electron incident energy above 1 GeV and cover only the upper part of the energy range at 2 GeV.

The k_0' point can be measured if $d_0 - d_{gap}$ is positive (Tab. 23). This is always the case with the Argon Laser except at 1 GeV. For the NdYAG Laser, it is true only for $E \geq 3\ GeV$. Below this value, we can try to reduce the safety gap or to increase the magnetic field (but this implies a bigger range of deviations to be covered).

For the beam pipe, the maximum size $d_4^{min} - d_4$ is reached after dipole 4 and for $E = 8\ GeV$. Its value is 8.72 cm for the Argon Laser and 4.36 cm for the NdYAG Laser (Tab. 23). Scrapers may be inserted in the beam pipe after the e^- detector if required.

Two thin scintillators will be added for triggering the silicon detectors.

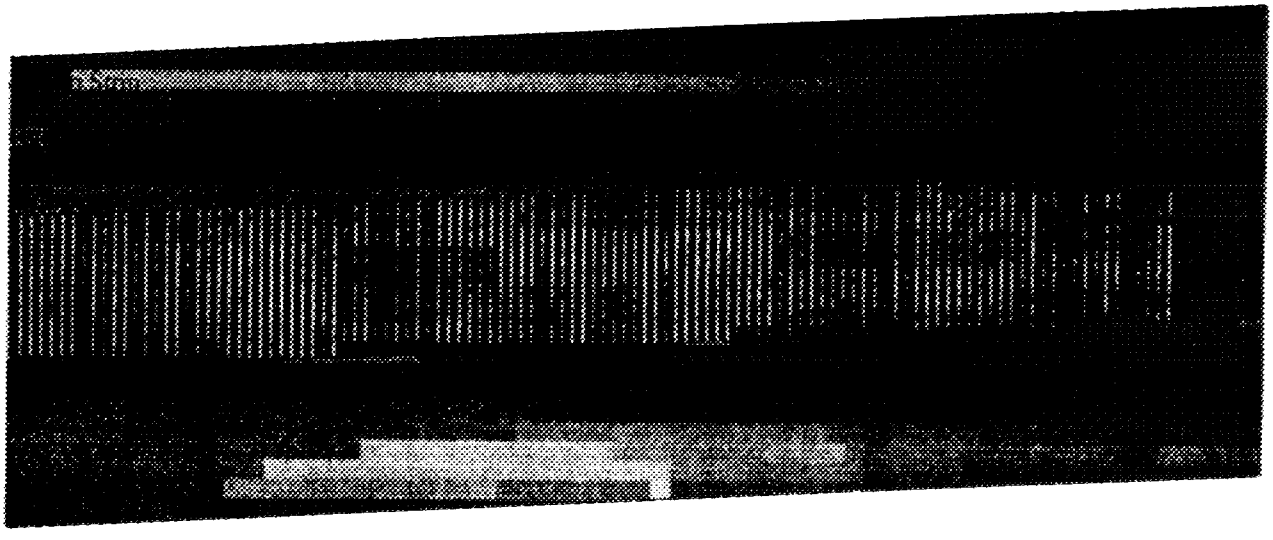

Figure 22: ***Scattered electron detector plane.*** *The size in the dispersive direction is* 3.2 cm. *The strip width is* 200 μm *and the pitch is* 250 μm. *The wafer thickness is* 200 μm.

7.3 Energy resolution and calibration specifications

The effects of the smearing due to the non perfect resolution have to be corrected and the errors on the different parameters governing this resolution (beams interaction size and resolution on the magnetic dispersion) are translated into systematic errors. A bad calibration (which depends on the safety gap measurement and on the magnetic dispersion estimation) would give an error on the theoretical Compton asymmetry and so a systematic error on the polarization measurement. A detailed analysis of these effects is done in appendix E.3 for the NdYAG Laser and determines some of the major requirements for the electron detector and the magnetic chicane to keep the systematic effect on the beam polarization P_e measurement under the 1% requirement.

The resolution on the scattered γ energy k, given by equation (256)

$$\frac{\sigma(k)}{k} = \sigma(\Delta x)\frac{(p_0 - k)^2}{\alpha\, p_0\, k} \bigoplus \sigma(\alpha)\frac{(p_0 - k)}{\alpha\, p_0},$$

is fixed by the transverse size $\sigma(\Delta x)$ of the interaction between the Laser beam and the electron beam. This size, close to $\sigma(\Delta x) = 100\ \mu m$, gives a resolution for the maximal Compton energy k_{max} ranging from 1.2 % at incident energy p_0=2 GeV to 0.3% at 8 GeV (line $\delta k/k$ of Tab. 24). As shown in appendix E.3.3, **the transverse size $\sigma(\Delta x)$ of the interaction between the Laser beam and the electron beam has to be known with a 50 μm precision**. Detailed studies of the electron and Laser beam optics should give such a precision.

The second term of the equation comes from the resolution $\sigma(\alpha)$ on the dispersion α. To have a similar contribution to the one from the beam size, we need :

$$\frac{\sigma(\alpha)}{\alpha} \simeq \frac{\sigma(\Delta x)}{\alpha}\frac{p_0 - k}{k} \simeq \frac{\sigma(\Delta x)}{\alpha}\frac{p_0 - k}{.0175\, p_0^2} \simeq \frac{\sigma(\Delta x)}{\alpha\, .0175\, p_0(GeV)}. \tag{91}$$

With a dispersion of $\alpha \simeq 2.3\ mm/\%$ (Tab. 24), this gives $\sigma(\alpha)/\alpha \simeq 3\ 10^{-3}$ necessary at $E_e = 8\ GeV$. It depends first on the **design of the dipole** and will be further affected by the power supply stability. To have an idea of the sensitivity of the deflection with the power supply stability, we compute

$$\frac{\partial d}{\partial B} = \frac{R}{B}\left[-1 + \cos\theta + \sin\theta\tan\theta + \frac{L_3 l_e}{R^2}\frac{1}{\cos^3\theta}\right]. \tag{92}$$

This corresponds for the k_0 point to $\partial d/\frac{\partial B}{B} = 248\ \mu m/10^{-3}$ (resp. $\partial d/\frac{\partial B}{B} = 266\ \mu m/10^{-3}$) at 4 GeV (resp. at 8 GeV). So a **power supply stability of** 4 10^{-4} will give a contribution corresponding to a resolution on the beam size of less than 107 μm. The resolution is also affected by the Compton scattering angle and the beam angular divergence but these effects are small.
As shown in appendix E.3.3, **the resolution $\sigma(\alpha)$ on the dispersion α has to be known at a 100% level.**

The more stringent problem comes from the necessary good accuracy required for the energy calibration of the detector. Appendix E.3.3 shows that the dispersion had to be known with a 0.5 % accuracy. The dispersion can be deduced from field map measurement or measured to this level. But we have to measure and control the safety gap (i.e. the energy threshold) within 50 μm. So **we need beam position monitors with this accuracy precisely positioned wrt the electron detector**. The calibration can be monitored on line by the gamma detector and also by the measurement of the k_0 point and of the k_{max} edge. The complementarity of the 2 detectors as well as the possibility to measure the k_0 point will reduce the systematic effect.

A **strip width of 250** μm have been chosen to match the expected resolution of 200 μm and gives an energy width on the scattered Compton photon (line $\delta k/k$ of Tab. 24) ranging from 3.0 % for $E_e = 2\ GeV$ to 0.7 % for $E_e = 8\ GeV$. Thus this width allow an energy bining better than the 10 % requirement even at 2 GeV.
The **maximal Compton rate for a strip** can be deduced from the total Compton rate (Tab. 27), the energy threshold (Tab. 51) and the bin energy width (Tab. 50). It will be less than 30 kHz at 2 GeV and decreases up to 6 kHz at 8 GeV.

E	GeV	1.0	2.0	3.0	4.0	5.0	6.0	7.0	8.0
B	Tesla	0.19	0.37	0.56	0.75	0.94	1.12	1.31	1.50
Power X_c =-2.0cm	nW	137.45	168.85	175.90	178.47	179.67	180.33	180.72	180.96
$\theta\gamma$		6.05	11.53	17.13	22.75	28.39	34.03	39.67	45.30
Power X_c =-2.1cm	nW	84.34	97.99	100.89	101.93	102.42	102.68	102.83	102.92
$\theta\gamma$		6.95	13.45	20.05	26.67	33.30	39.92	46.53	53.13

Table 25: ***Synchrotron power in the electron detector.*** *For a beam of* $100\ \mu A$ *and an electron detector of size* $3\ cm * 3\ cm$ *located at a distance from downstream of Dipole 3 of* $3.6\ m$. *The detector center is at* $-2.0\ cm$ *or* $-2.1cm$ *wrt the beam axis.* $\theta\gamma$ *is the mean polar angle weighted by the power.*

7.4 Synchrotron radiation for the electron detector

The results on synchrotron radiation seen by the photon detector were obtained using a partial angular dependence: the angle between the bending plane and the observation point. The angle with respect to the electron trajectory was included in the integration along the electron path, assuming all the radiation was emitted tangential to this path. Because the electron detector will be located in a place where no direct synchrotron is observed, to compute the synchrotron radiation seen by the electron detector, one needs to use the full angular dependence of the synchrotron radiation (Eq. 210 in appendix C) for a piece $\Delta\theta$ of the end of the dipole 3 of the magnetic chicane. We assume that the synchrotron photons coming from the dipole 1 (directly viewed by the electron detector) and from the other dipoles are not seen by the electron detector. We give here this full angular dependence (Eq. 210 of appendix C.2)

$$\frac{\partial^2 P}{\partial\phi\partial cos\theta} = P_0 \frac{3}{8\pi} \frac{1}{\gamma^4} \frac{1}{(1-\beta\cos\theta)^3} \left[1 - \frac{\sin^2\theta\cos^2\phi}{\gamma^2(1-\beta\cos\theta)^2}\right],$$

$$\frac{\partial^2 P}{\partial\phi\partial cos\theta} = P_0 \frac{3\gamma^2}{\pi} \left[\frac{(1+2\gamma^2\theta^2(1-2cos^2\phi)+\gamma^4\theta^4)}{(1+\gamma^2\theta^2)^5}\right],$$

where (Eq. 206)

$$P_0 = \frac{2r_0 cm_e c^2}{3} \frac{\beta^4\gamma^4}{R^2} \frac{R\Delta\theta}{\beta c} \frac{I_e}{e}.$$

We integrate the full angular dependence over the electron path and over the polar coordinates of the electron detector.

The synchrotron power seen by the electron detector, located $3.6\ m$ downstream the end of dipole 3, and $5\ or\ 6\ mm$ away from the beam axis, is given in table (25). This power of order $180\ nW$ is almost independent of the beam energy but varies quickly with the polar angle θ. This could be related to the fact that the electron detector sees large synchrotron radiation angles $\theta\gamma > 10.9$ at $4\ GeV$. For large synchrotron radiation angles, the power increases with energy as $P \simeq 1/\rho$ but the fraction seen by the detector decreases as $F \simeq 1./\theta^4$. The power seen by the detector is then $P \simeq 1./\theta^4/\rho$. This power is located near the beam due to the factor $1./\theta^4$ (Fig. 23).

For large synchrotron radiation angles, only low energy synchrotron photons are important ($\epsilon \leq \epsilon_c$ where the critical energy ϵ_c (Eq. 208 and 209) can be found in Tab. 13). As a consequence, we might hope that a thin absorber (beam pipe wall of $500\ \mu m$) would attenuate this power by a factor at least 10^3 (resp. 20 and 10) at 4 GeV (resp. at 6 and 8 GeV).

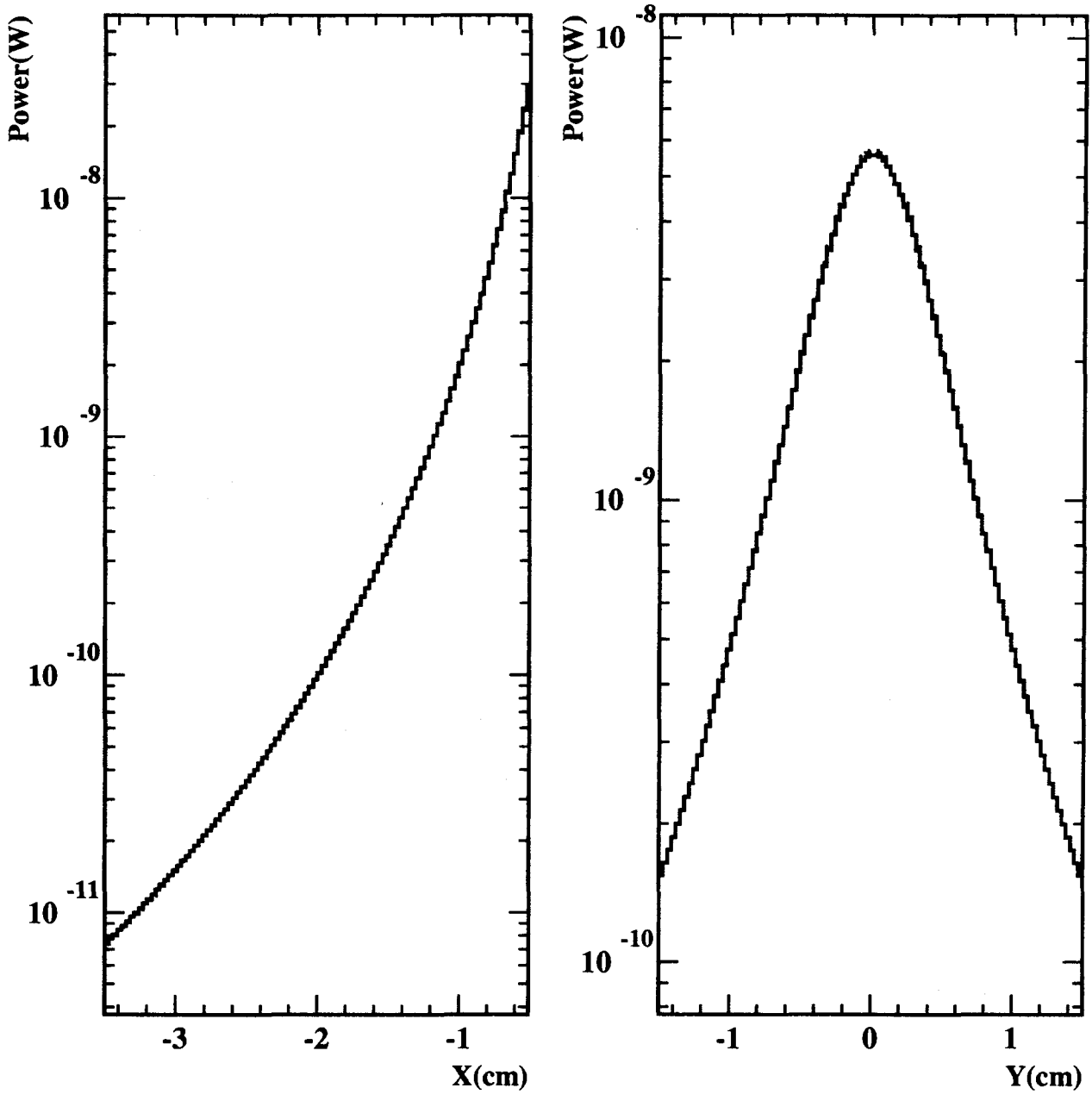

Figure 23: ***Synchrotron power versus position on the electron detector.*** *At 4 GeV (solid line) and 8 GeV (dashed line). X is the dispersive direction*

E	GeV	1.0	2.0	3.0	4.0	5.0	6.0	7.0	8.0
p_{min}	GeV	0.869	1.737	2.606	3.475	4.344	5.212	6.081	6.950
p_{max}	GeV	0.979	1.958	2.937	3.915	4.894	5.873	6.852	7.831
rate Z= 1.	Khz	0.007	0.007	0.007	0.007	0.007	0.007	0.007	0.007
rate Z= 6.	Khz	0.123	0.122	0.122	0.122	0.122	0.122	0.122	0.122

Table 26: ***Bremsstrahlung rate in the electron detector.*** *For various beam energies E at 100 μA for a 2.5 m residual vacuum of 10^{-8} $Torr$ with mean Z =1 and 6 . The rate dn/dt (kHz) is given for the energy range ($[p_{min},p_{max}]$) covered by the electron detector of size 3 cm with a safety gap of 5 mm wrt beam.*

$\lambda = 1064.2nm$								
E GeV	1.0	2.0	3.0	4.0	5.0	6.0	7.0	8.0
rate Khz	0.0	357.8	477.1	544.3	581.8	604.1	613.0	621.8

Table 27: ***Compton rate in the electron detector.*** *For various beam energies E at 100 μA . The rate is given for the energy range ($[p_{min},p_{max}]$) covered by the electron detector of size 3 cm with a safety gap of 5 mm wrt beam. The experimental parameters are those of table (8).*

7.5 Bremsstrahlung for the electron detector

The bremsstrahlung seen by the electron detector is due to

- bremsstrahlung photons generated between the end of the dipole 3 and the electron detector. The useful length is only $L \simeq 3.6\ m$ and the photons are seen under an angle $\theta > 1.4\ mrad$ larger than the characteristics bremsstrahlung angle $\theta_{brem} \simeq m/E < 0.25\ mrad$. So this background is very weak compared to the Compton rate.
  We also assume here that the photons generated between the end of the last dipole of the bending arc and the first dipole of the magnetic chicane are not seen by the electron detector.

- electrons having emitted a bremsstrahlung photon between the dipole 2 and 3 and with an energy in the energy range ($[p_{min},p_{max}]$) covered by the electron detector. The useful length for bremsstrahlung is the same ($L \simeq 2.5\ m$) than for the photon detector (Section 6.4).

  Outgoing bremsstrahlung electrons are emitted with angles $\theta \simeq 1/\gamma = m/E$ (Appendix D.2). These angles are small ($\theta < 0.25\ mrad$) and can be neglected : the corresponding deviation at the electron detector is $< 1\ mm$. So the electron detector will see the bremsstrahlung electrons in the energy range covered by the sensitive area.

For computing the bremsstrahlung rate, we have used the Tsai cross section (Appendix D.1) integrated from $k'_c = E - p_{max}$ to $k'_{max} = E - p_{min}$. The energy threshold due to the safety gap $E_{gap} = p_{max}$ is given in table (23). For p_{min}, we have used an electron detector size of 3 cm.

Table (26) gives the energy integration range and the integrated bremsstrahlung rate. The rates are given for a residual vacuum with a mean Z of $Z = 1$ and for a residual vacuum with a mean Z of $Z = 6$ and a STP density $\rho_0 = 1.08\ g/l$. These rates of order of 0.1 kHz are independent of the incident energy and had to be compared to the Compton rate in the same kinematic range (Tab. 27). The compton rate reported in this table stands for the experimental parameters of table (8).

8 Optical Cavity

8.1 Principle

The idea is to trap the Laser beam in a resonant Fabry-Perot cavity made of two highly reflective mirrors. Due to constructive interferences, the light power circulating in the cavity will be enhanced by a factor G with respect to the power of the Laser. If the interaction region of the LASER with the electron beam is located in this cavity, then the luminosity will have an amplification by the gain G. Optical Cavities used with IR and visible Lasers with a gain of order $G \simeq 10000$ are currently used for experiments on gravitational waves detection by laser interferometry [13], [14] and by measurement of photon-photon scattering parameters [15].

In this section, the resonance conditions for a Fabry-Perot cavity will be derived. The relation between the mirror quality and the gain of the cavity will be explained. The mirror specifications needed to obtain a 10 000 gain will be listed. After a short presentation of the Laser that we plan to use, the feed back system between the Laser and the cavity will be explained. More details of the various items treated in this section, can be found in appendix G. The expected radiation rates on the cavity will end this section.

8.2 Gaussian Beam and Fabry-Perot cavity

The complex electric field of a Gaussian beam propagating along the z direction at frequency ω, in a medium of refractive index $n = \frac{kc}{\omega}$, at a wavelength $\lambda = \frac{2\pi}{k}$ is given by [21]:

$$E(x,y,z)_{mn} = A\frac{d_0}{d(z)}e^{-ikz}e^{i\omega t}e^{i(m+n+1)\Psi(z)}e^{-ik\frac{x^2+y^2}{2R^2(z)}}e^{-\frac{x^2+y^2}{d^2(z)}}H_m(\sqrt{2}\frac{x}{d(z)})H_n(\sqrt{2}\frac{y}{d(z)}). \tag{93}$$

The waist spot size d_0, the beam size $d(z)$, the phase $\Psi(z)$ and the radius of curvature $R(z)$ are related to the Rayleigh range z_R which characterize the longitudinal evolution of the Gaussian beam by

$$d_0^2 = \frac{\lambda}{\pi}z_R, \qquad d(z) = d_0\sqrt{1+\frac{z^2}{z_R^2}}, \tag{94}$$

$$\Psi(z) = \tan^{-1}\frac{z}{z_R}, \tag{95}$$

$$R(z) = z(1+\frac{z_R^2}{z^2}). \tag{96}$$

H_m and H_n are Hermite Polynomials and $m.n$ are two integers that define the **transverse mode** of the Gaussian beam. The intensity profiles for different transverse modes are represented on figure 24. One can see that the best focalisation is achieved for the lowest order transverse mode.

When a Gaussian beam is trapped in a resonator consisting of two identical mirrors with radius of curvature R_M separated by a distance L, the following boundary conditions on the curvature radius have to be fulfilled:

$$R(z=-L/2) = -R_M \ ; \ R(z=L/2) = R_M.$$

Defining

$$g = 1 - \frac{L}{R_M}, \tag{97}$$

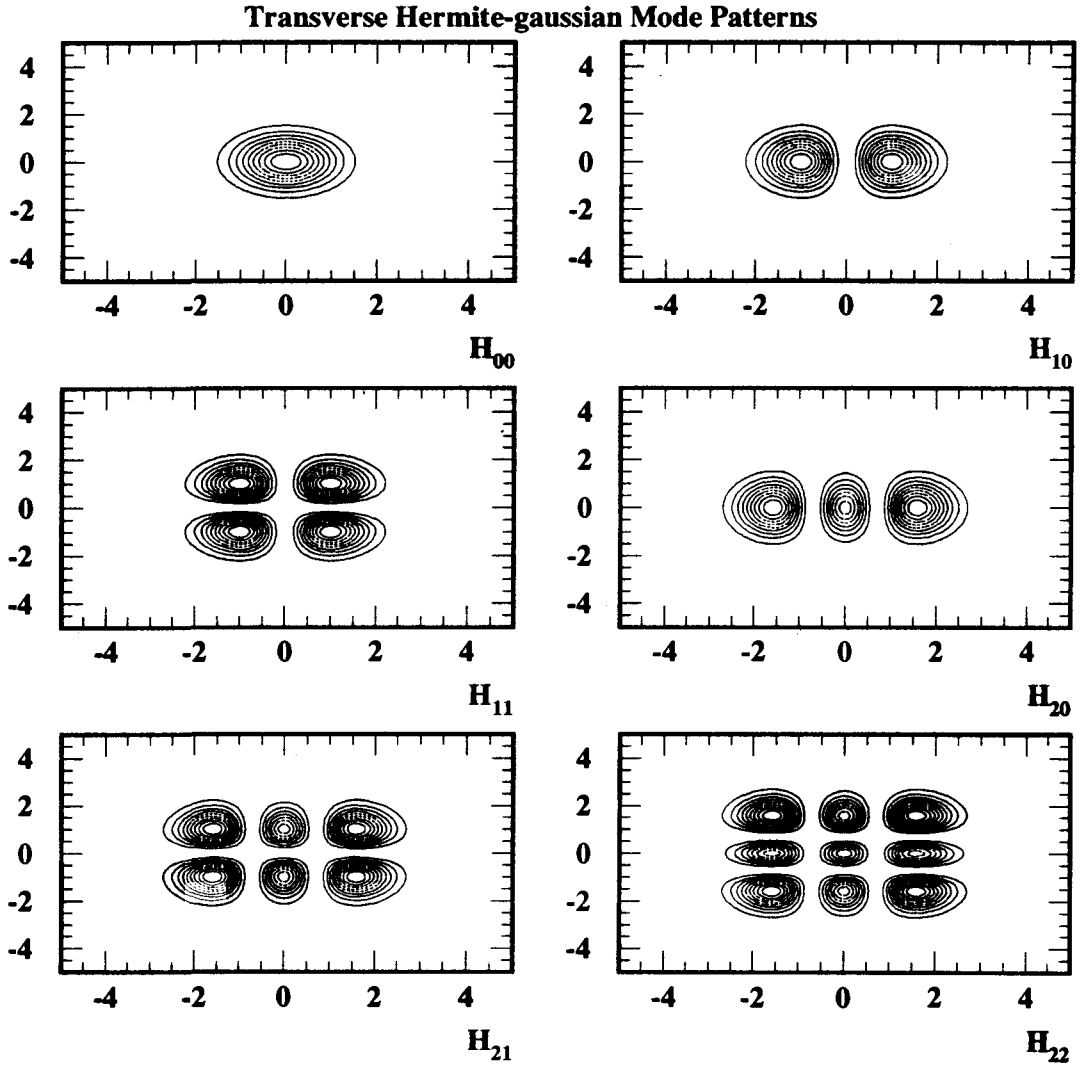

Figure 24: ***Transverse Hermite-Gaussian mode.*** *Intensity Profile versus x/σ and y/σ, The highest focalisation is obtained for the lowest mode TE_{00}.*

the Rayleigh range and the beam waist size are:

$$z_R = \frac{L}{2}\sqrt{\frac{1+g}{1-g}} \quad , \quad d_0^2 = \frac{\lambda}{\pi}\frac{L}{2}\sqrt{\frac{1+g}{1-g}}. \tag{98}$$

The diameters of the beam on each mirror are (see figure 25):

$$d_1^2 = d_2^2 = \frac{\lambda}{\pi}L\sqrt{\frac{1}{1-g^2}} = \frac{2d_0^2}{1+g}. \tag{99}$$

The stability of the resonator requires that (See G.1.3)

$$-1 \leq g \leq 1. \tag{100}$$

To find out what are the allowed **longitudinal modes** in such a cavity, we request that the electric field does not change in a round trip, i.e, that the phase $\theta(z) = kz - \tan^{-1}(\frac{z}{z_R})$ difference is $\theta(z_1) - \theta(z_2) = n\pi$ $(n = 1, 2, 3...)$. This gives the allowed frequencies (or longitudinal modes) in the cavity.

For the transverse mode defined by n, m the frequency of longitudinal mode l must be:

$$\boxed{\nu_l(mn) = \nu_{FSR}\left(l + \frac{1}{\pi}(m+n+1)\cos^{-1}\sqrt{g^2}\right);\ l = 0, 1, ...} \tag{101}$$

where the Free Spectral Range of the cavity is given by

$$\boxed{\nu_{FSR} = \frac{c}{2L}}. \tag{102}$$

8.3 Gain and losses in a Fabry-Perot Cavity

In this section we gives the relations between the gain of the cavity and the cavity parameters: size of the cavity, shape of the mirrors, reflectivity, absorption and scattering of the mirrors, ... We consider here a cavity with 2 mirrors M_1 and M_2 with transmission and reflection coefficients t_i, r_i, $(i = 1, 2)$ separated by a distance L (see Fig. 26).

The reflection r_i and transmission t_i coefficients of the mirrors are defined by [22]:

$$r = \frac{E_R}{E_I} \qquad t = \frac{E_T}{E_I},$$

where E_I, E_R and E_T are the electric field of the incident, reflected and transmitted light. In terms of energy, we define the reflectivity R and the transmission T of the mirror by :

$$R = \frac{J_R}{J_I} \qquad T = \frac{J_T}{J_I},$$

where J_k , $(k = I, R, T)$, the amount of energy per unit area per second, is proportional to $|E_k|^2$:

$$R = |r|^2 \qquad T = |t|^2\frac{q_2}{q_1}.$$

In the equation of the transmission T, q_i is given for a Transverse Electric wave TE by (q_1 is for initial and q_2 for final medium) :

$$q_i = \sqrt{\frac{\epsilon_i}{\mu_i}}\cos\theta_i, \tag{103}$$

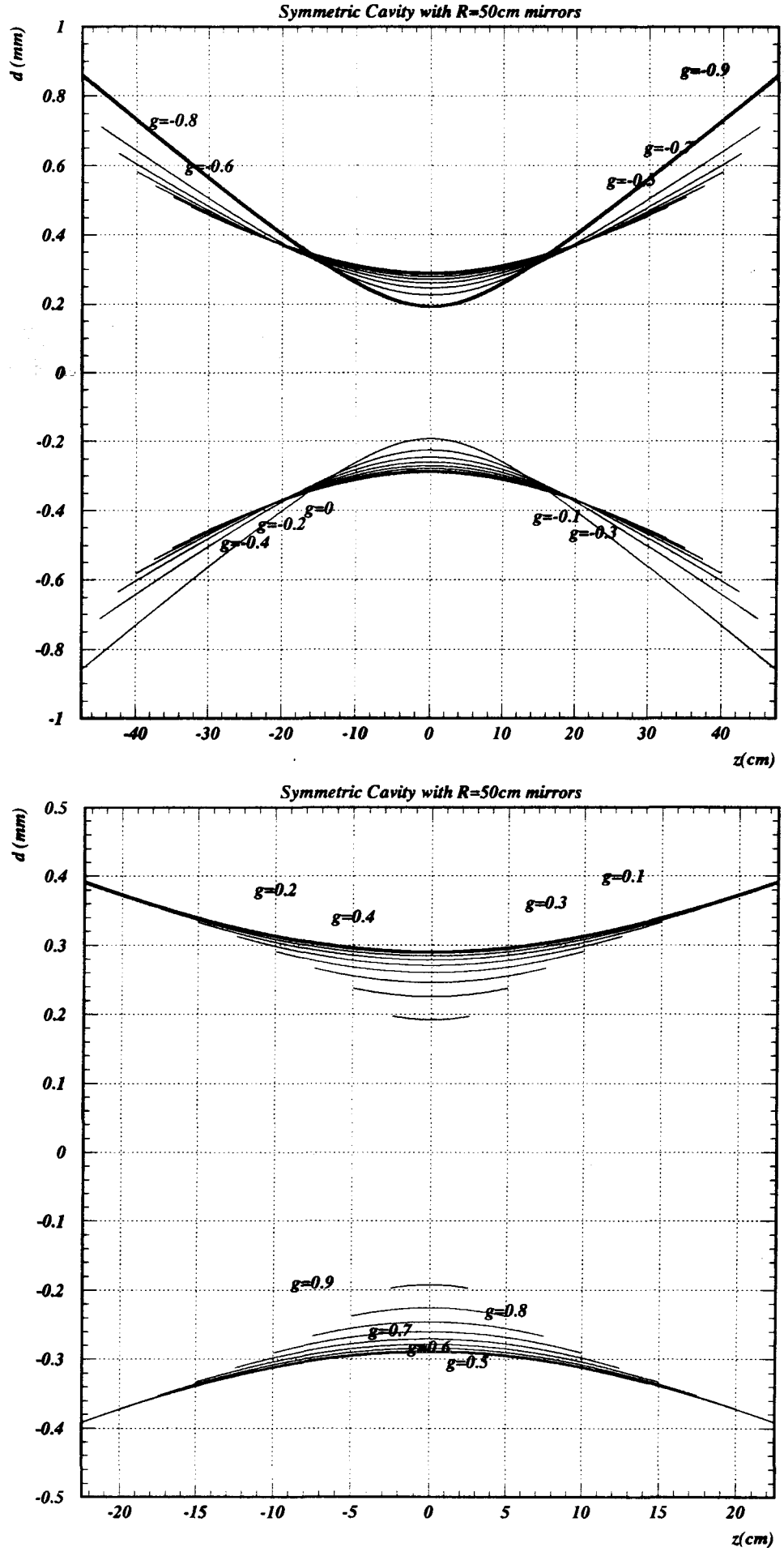

Figure 25: ***Beam Shape in a symmetric cavity.*** *$d(z)$ versus position along the cavity axis z for symmetric mirrors with 1m curvature radius and for a cavity length L=1.95,1.75,...,0.15m*

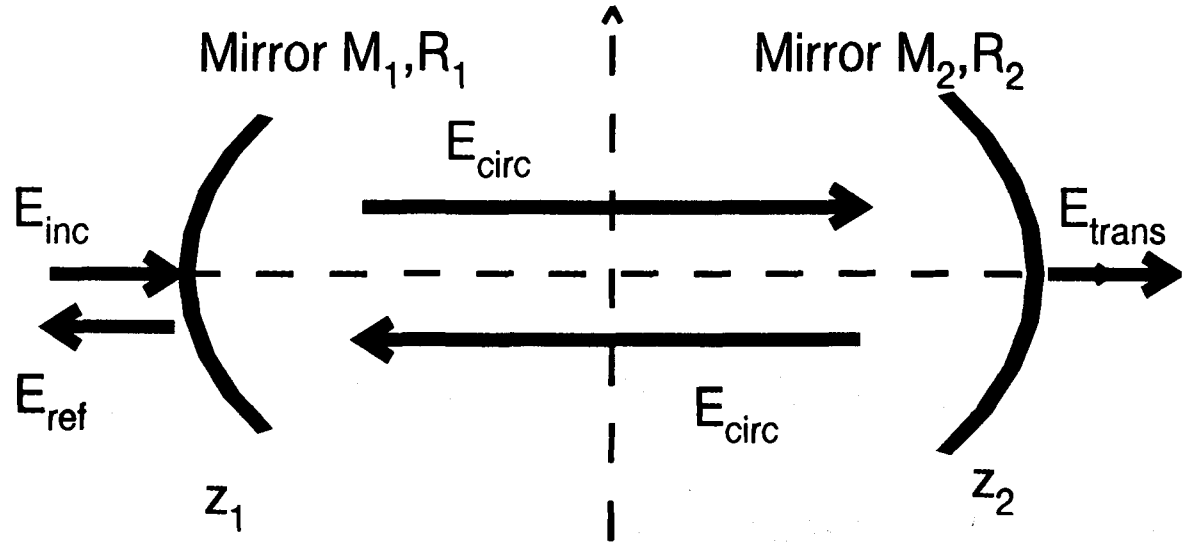

Figure 26: ***A 2 Mirrors Resonator.*** *Incoming electric field E_I, circulating E_{circ}, transmitted E_{trans} and reflected E_{refl}.*

whereas for a Transverse Magnetic wave TM, q_i is given by (r and t being the ratio of amplitude of magnetic and not electric field) :

$$q_i = \sqrt{\frac{\mu_i}{\epsilon_i}} \cos\theta_i. \tag{104}$$

In our case, the initial and final media are the same.

The round trip gain $g_{rt}(\omega)$ of a cavity for an incident light with frequency ω relates the circulating field inside the cavity just after mirror M_1 at time t, $E_{circ}(t)$, to the circulating field just after mirror M_1 one round trip earlier, at time $t - 2\tau = t - 2\frac{L}{c}$. We have :

$$E_{circ}(t) = it_1 E_I(t) + g_{rt}(\omega) E_{circ}(t - 2\tau). \tag{105}$$

In steady state, $E_{circ}(t - 2\tau) = E_{circ}(t)$ and thus [23]:

$$E_{circ} = it_1 E_I + g_{rt}(\omega) E_{circ}; \qquad \frac{E_{circ}}{E_I} = \frac{it_1}{1 - g_{rt}(\omega)}. \tag{106}$$

The round trip gain depends on medium absorption. We introduce α_0 the electric absorption coefficient of the medium inside the cavity, so that the electric field and power at $z = l$ are related to field and power at $z = 0$ by :

$$E(l) = E(0)e^{-\alpha_0 l} \qquad J(l) = J(0)e^{-2\alpha_0 l}.$$

For a round trip $l = 2L$, this gives an attenuation :

$$E(l) = E(0)e^{-2\,\alpha_0\,L} = E(0)e^{-\frac{\delta_0}{2}} \qquad J(l) = J(0)e^{-4\,\alpha_0\,L} = J(0)e^{-\delta_0}, \tag{107}$$

where $\delta_0 = 4\alpha_0\, L$ represents the round trip absorption of the cavity medium.

Therefore the round trip gain includes medium absorption on a round trip ($e^{-\frac{\delta_0}{2}}$), reflection on mirror M_2 (r_2), reflection on mirror M_1 (r_1) and also a global phase $e^{-ik2L} = e^{-i\omega\frac{2L}{c}} = e^{-i\omega 2\tau}$, (with c the velocity of light in the material inside the cavity) according to :

$$g_{rt}(\omega) = r_1 r_2 e^{-\frac{\delta_0}{2}} e^{-i2L\frac{\omega}{c}}. \tag{108}$$

Identically the transmitted field E_{trans} (after mirror M_2) is given by (medium absorption on the cavity length $e^{-\frac{\delta_0}{4}}$, global phase $e^{-ikL} = e^{-iL\frac{\omega}{c}}$ and transmission through mirror M_2):

$$E_{trans} = it_2 e^{-\frac{\delta_0}{4}} e^{-iL\frac{\omega}{c}} E_{circ}, \tag{109}$$

and thus

$$\frac{E_{trans}}{E_I} = -\frac{t_1 t_2 e^{-\frac{\delta_0}{4}} e^{-iL\frac{\omega}{c}}}{1 - r_1 r_2 e^{-\frac{\delta_0}{2}} e^{-i2L\frac{\omega}{c}}} = -\frac{t_1 t_2}{\sqrt{r_1 r_2}} \frac{\sqrt{g_{rt}(\omega)}}{1 - g_{rt}(\omega)}. \tag{110}$$

For a symmetric cavity $r_1 = r_2 = r$ and $t_1 = t_2 = t$, one gets :

$$\frac{E_{circ}}{E_I} = \frac{it}{1 - r^2 e^{-\frac{\delta_0}{2}} e^{-i2L\frac{\omega}{c}}}; \qquad \frac{E_{trans}}{E_I} = -\frac{t^2 e^{-\frac{\delta_0}{4}} e^{-iL\frac{\omega}{c}}}{1 - r^2 e^{-\frac{\delta_0}{2}} e^{-i2L\frac{\omega}{c}}}. \tag{111}$$

In terms of power, this gives for the cavity gain G and for the cavity transmission $\mathcal{T}$ (with $R = r^2$ and $T = t^2$, at normal incidence):

$$G = \frac{J_{circ}}{J_I} = \frac{T}{1 - 2R\cos(\frac{\omega}{c}2L)e^{-\frac{\delta_0}{2}} + (Re^{-\frac{\delta_0}{2}})^2} = \frac{T}{(1 - Re^{-\frac{\delta_0}{2}})^2 + 4Re^{-\frac{\delta_0}{2}}\sin^2(\frac{\omega}{2c}2L)} \tag{112}$$

$$\mathcal{T} = \frac{J_{trans}}{J_I} = \frac{T^2 e^{-\frac{\delta_0}{2}}}{1 - 2R\cos(\frac{\omega}{c}2L)e^{-\frac{\delta_0}{2}} + (Re^{-\frac{\delta_0}{2}})^2} = \frac{T^2 e^{-\frac{\delta_0}{2}}}{(1 - Re^{-\frac{\delta_0}{2}})^2 + 4Re^{-\frac{\delta_0}{2}}\sin^2(\frac{\omega}{2c}2L)} \tag{113}$$

One sees that for frequencies such that $\frac{\omega}{c}(2L) = l\,2\pi$, $l = 1, 2, 3...$ i.e

$$\omega_l = l\frac{2\pi c}{2L} = l\Delta\omega_{FSR} \;\; or \;\; \nu_l = l\Delta\nu_{FSR}, \tag{114}$$

where

$$\Delta\omega_{FSR} = \omega_{l+1} - \omega_l = \frac{2\pi c}{2L} \;\; or \;\; \Delta\nu_{FSR} = \frac{c}{2L}, \tag{115}$$

is the axial mode interval, also called "free spectral range of the cavity", the cavity has maximum gain G_l and transmission T_l :

$$\boxed{G_l = \frac{T}{(1 - Re^{-\frac{\delta_0}{2}})^2} = \frac{1 - R - P}{(1 - Re^{-\frac{\delta_0}{2}})^2} \qquad , T_l = \frac{T^2 e^{-\frac{\delta_0}{2}}}{(1 - Re^{-\frac{\delta_0}{2}})^2} = \frac{(1 - R - P)^2 e^{-\frac{\delta_0}{2}}}{(1 - Re^{-\frac{\delta_0}{2}})^2}}, \tag{116}$$

where we have used the energy conservation for the reflection on a mirror with transmission $T = |t|^2$, reflectivity $R = |r|^2 = e^{-\delta_r}$ and total loss P due to absorption ($A = 1 - e^{-\delta_a}$) and scattering ($D = 1 - e^{-\delta_d}$)

$$\begin{aligned} 1 &= T + R + A + D; \quad 1 = T + R + P \\ T &= 1 - R - A - D \simeq \quad \delta_r - (\delta_a + \delta_d)\,. \end{aligned} \tag{117}$$

For high reflectivity mirrors ($1 - R \simeq \delta_r \ll 1$), negligible scattering and absorption on the mirrors and negligible absorption in the cavity medium ($\delta_d, \delta_a, \delta_0 \ll \delta_r$), the maximum gain is

$$G_l \simeq \frac{1}{\delta_r} \frac{\left(1 - \left(\frac{\delta_a + \delta_d}{\delta_r}\right)\right)}{\left(1 + \frac{\delta_0}{2\delta_r}\right)^2}.$$

Equations (112) and (113) can also be written:

$$G(\omega) = G_l \frac{1}{1 + \frac{4Re^{-\frac{\delta_0}{2}}}{\left(1 - Re^{-\frac{\delta_0}{2}}\right)^2} \sin^2\left(\pi \frac{\omega}{\Delta\omega_{FSR}}\right)}, \tag{118}$$

$$\mathcal{T}(\omega) = T_l \frac{1}{1 + \frac{4Re^{-\frac{\delta_0}{2}}}{\left(1 - Re^{-\frac{\delta_0}{2}}\right)^2} \sin^2\left(\pi \frac{\omega}{\Delta\omega_{FSR}}\right)}. \tag{119}$$

Using the definition of the finesse of the cavity $\mathcal{F}$,

$$\boxed{\frac{\mathcal{F}}{\pi} = \frac{\sqrt{Re^{-\frac{\delta_0}{2}}}}{1 - Re^{-\frac{\delta_0}{2}}}} = \frac{\sqrt{e^{-\left[\delta_r + \frac{\delta_0}{2}\right]}}}{1 - e^{-\left[\delta_r + \frac{\delta_0}{2}\right]}} \simeq \frac{1}{\delta_r + \frac{\delta_0}{2}}, \tag{120}$$

we get

$$\boxed{G(\omega) = G_l \frac{1}{1 + \left(\frac{2\mathcal{F}}{\pi}\right)^2 \sin^2\left(\pi \frac{\omega}{\Delta\omega_{FSR}}\right)}, \qquad \mathcal{T}(\omega) = T_l \frac{1}{1 + \left(\frac{2\mathcal{F}}{\pi}\right)^2 \sin^2\left(\pi \frac{\omega}{\Delta\omega_{FSR}}\right)}}. \tag{121}$$

The gain of the cavity is presented on figures 27 and 30 for various cavity parameters.

The bandwidth $\Delta\omega_{cav}$ of the cavity is defined so that the gain G of the cavity or its transmission will decrease by a factor 2 when the frequency will change from the resonance $\omega = \omega_l$ to $\omega = \omega_l \pm \frac{\Delta\omega_{cav}}{2}$ and is related to the finesse by:

$$\boxed{\frac{\Delta\omega_{cav}}{\Delta\omega_{FSR}} = \frac{2}{\pi} \sin^{-1}\left(\frac{\pi}{2\mathcal{F}}\right)}. \tag{122}$$

For a cavity with high finesse this equation becomes:

$$\frac{\Delta\omega_{cav}}{\Delta\omega_{FSR}} \simeq \frac{1}{\mathcal{F}}. \tag{123}$$

The higher the finesse, the smaller the bandwidth of the resonance peaks. On the other hand, the maximum gain G_l at resonance is

$$\boxed{G_l = \frac{\mathcal{F}}{\pi} \frac{1}{\sqrt{Re^{-\frac{\delta_0}{2}}}} \frac{T}{1 - Re^{-\frac{\delta_0}{2}}} = \frac{\mathcal{F}}{\pi} \frac{1}{\sqrt{Re^{-\frac{\delta_0}{2}}}} \frac{1 - R - P}{1 - Re^{-\frac{\delta_0}{2}}}} \simeq \frac{\mathcal{F}}{\pi} \frac{\delta_r - (\delta_a + \delta_d)}{\delta_r + \frac{\delta_0}{2}}. \tag{124}$$

One can see (Fig. 27) the two main applications of a cavity with high finesse:

- High amplification for the circulating power inside the cavity, in which we are interested;
- Very precise frequency selection for the transmitted field.

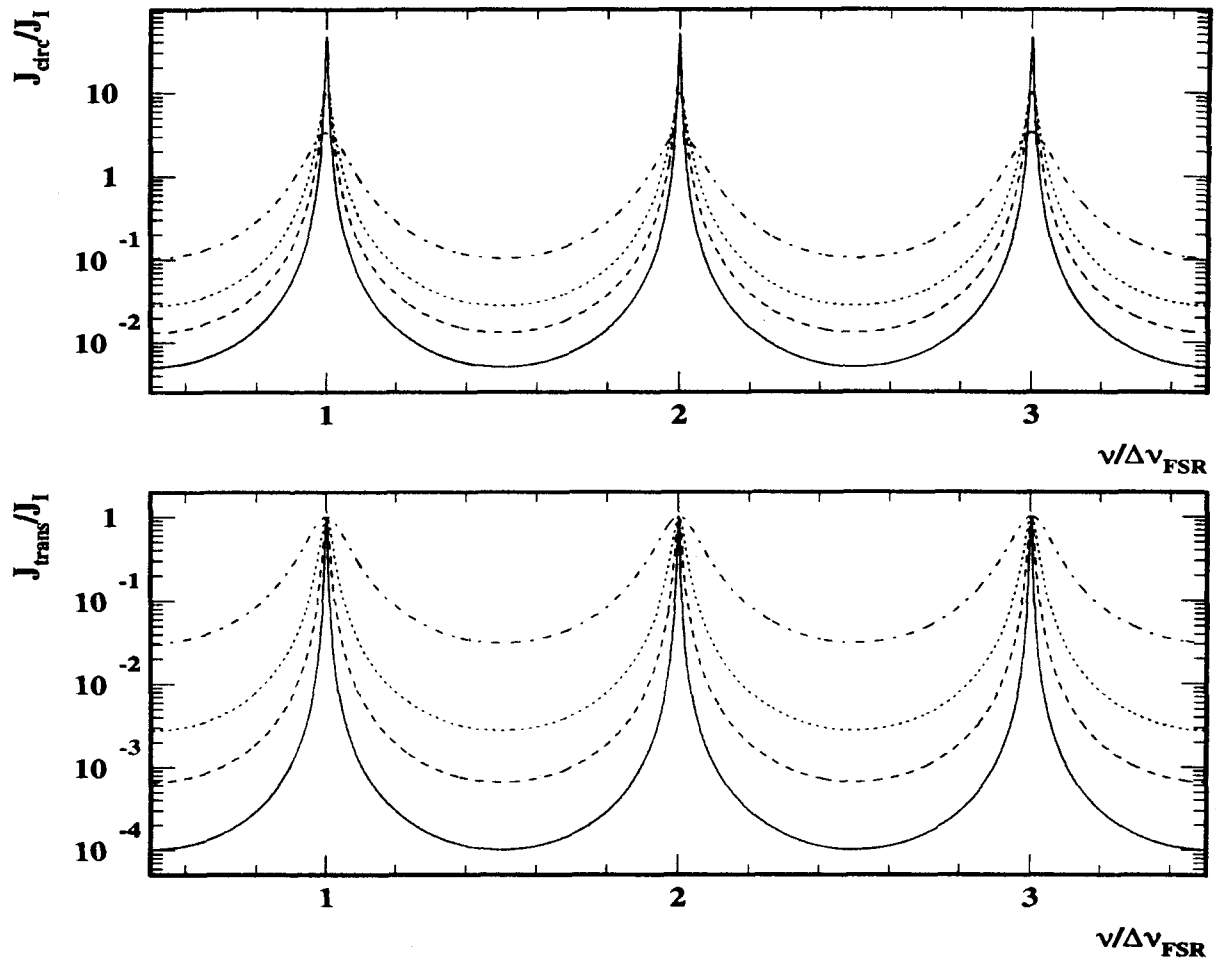

Figure 27: ***Circulating (up) and transmitted (down) power in a cavity.*** *For reflectivity R=0.98, 0.95, 0.90, 0.70 and mirrors with no absorption and scattering $\delta_a = \delta_d = 0$ versus frequency in free spectral range unit*

		L = 1 m	L = 10 cm
$\Delta\nu_{FSR} = \frac{c}{2L}$		150 MHz	1.5 GHz
$\Delta\nu_{cav} = \frac{1}{\mathcal{F}}\Delta\nu_{FSR}$	$\mathcal{F} = 300$	500 kHz	5 MHz
	$\mathcal{F} = 3000$	50 kHz	500 kHz
	$\mathcal{F} = 30000$	5 kHz	50 kHz

Table 28: ***Typical Free spectral range*** $\Delta\nu_{FSR}$ ***and bandwidth*** $\Delta\nu_{cav}$ *for a* $L = 1m$ *and* $L = 10cm$ *cavity with various finesse* $\mathcal{F}$.

λ(nm)	δ_a(ppm)	δ_d(ppm)	δ_p(ppm)	δ_r(ppm)	G
1064	3	2	5	105	9070
633	12	6	18	118	7182

Table 29: ***Specifications for the IPN Lyon Mirrors***

8.4 High reflectivity, low absorption and scattering mirrors

Super-Mirrors available from industry [24] have now a good reflectivity ($R \simeq 99.97\%$), low transmission ($T \simeq 0.12\%$), and reasonable losses $P \leq 100ppm$. One can thus expect to reach a finesse of $\mathcal{F} \simeq 10000$, and a gain of $G_l \simeq 2000$. This could be acceptable for our cavity, unfortunately these Super-Mirrors have a too low maximum power density ($1kW/cm^2$). For a Laser of 0.5 W, trapped in a 1 meter cavity with $g = -0.95$, i.e a beam diameter on the mirrors close to $1mm$, with a gain of $G_l = 2000$ (resp. $G_l = 10000$), the power density is $100kW$ (resp. $500kW$). Such a power density is not yet available from industry, that's why, J.M. Makowsky from IPNL at Lyon, the laboratory responsible for the VIRGO mirror construction, will build and characterize our mirrors.

The mirrors [25] have the structure $LL(HL)_N HS$ where L (resp. H) stands for a $\lambda/4$ layer of low (resp. high) index material and S for the substrate. The mirrors that will be constructed for our polarimeter are made of Ditantalium pentoxyde (Ta_2O_5) layer with (High) index $n \simeq 2.1$, and Silica (SiO_2) with (Low) index $n \simeq 1.47$ deposited on a super polished silica substrate using the technology of Ion beam sputtering. The diameter of the mirrors will be $\frac{1}{4}$ inch ($7.75mm$). To minimize the scattering, the layers are made of amorphous deposit. The reflectivity of the mirror is governed by the design of the layers (See appendix G). We will use $(HL)_{14}$ mirrors with the following specifications:

- Residual transmission $T = 1 - R - A - D \simeq \delta_r - (\delta_a + \delta_d) \simeq 100ppm$,
- Scattering $D \simeq \delta_d \simeq 2ppm$ (resp. $D \simeq 6ppm$) at $1064nm$ (resp. at $633nm$),
- Absorption $A \simeq \delta_a \simeq 3ppm$ (resp. $A \simeq 12ppm$) at $1064nm$ (resp. at $633nm$).

The cavity medium will be vacuum to reduce absorption (e.g $\delta_0 = 0$, for comparison $50cm$ of air has an absorption of $3ppm$). We thus expect a maximum cavity gain

$$G_l \simeq \frac{(\delta_r - (\delta_a + \delta_d))}{\left(\delta_r + \frac{\delta_0}{2}\right)^2} \tag{125}$$

$G \simeq 9070$ at $1064\,nm$ and $G \simeq 7182$ at $633\,nm$. To keep scattering very low one need to manipulates the mirror under laminar flux (velocity $v = 0.5m/s$), since one dust of $1\mu m$ corresponds to $\frac{1}{2}ppm$. Perfect surface state is also mandatory, one needs to start with a super polished substrate (with RMS roughness $0.5A$) and a peak/valley of $15A$ to end up after coating to a RMS roughness of $0.3A$ and a peak/valley of $4A$. The question of damage by irradiation (synchrotron light, neutron background) will be discussed in section 8.10.2.

8.5 The LightWave Series 126 NdYAG Laser

Solid-state Lasers [26] contain a lasing medium which consists of light emitting atoms, the dopant, in our case Neodymium (Nd), fixed in a crystalline or glassy material, the host, in our case Yttrium Aluminum Garnet (YAG). The laser crystal is pumped by a semiconductor diode laser. The resonator for the 126 Series is a non planar ring oscillator (NPRO) promoting single unidirectional longitudinal mode operation (TEM_{00}). The direction of oscillation is set by designing an "optical diode" into the resonator, by applying a magnetic field to the crystal. The stability of the Series 126 is obtained on one hand through a monolithic design: the mirrors of the laser cavity are the polished surfaces of the crystal. On the other hand, using a laser diode for pumping gives an even greater stability due to the stable output power of the diode. The optical layout of the laser head is shown on fig. 28. The laser Ga-Al-As diode normally emitting at 810 nm is cooled by a Thermo-electric cooler (TEC) resulting in a frequency drop of 0.3nm/°C to reach 808.5 nm, a highly efficient wavelength for NdYAG pumping.

There is two ways to tune the Laser frequency [26] :

- **Slow Frequency Tuning.**
  By applying a voltage to a thermoelectric cooler under the laser crystal the temperature of the crystal can be varied. Two primary effects of heating the crystal occur: the crystal physically expands and the index of refraction of the NdYAG increases. The crystal expansion leads to a longer cavity length, slightly decreasing the frequency of the Laser. The increase in the index of refraction also makes the optical cavity length appear longer, and this lead to a further decrease in the output frequency. This allows for a tuning range of tens of GHz with a relatively slow time constant (1 to 10 s). The input impedance is 10 kΩ and the maximum design-case voltage is ± **10 V**. Between mode hops, the tuning coefficient is **+5.0 GHz/V**, and averaged to include mode hops effect, this coefficient is **+1.6 GHz/V**.

- **Fast Frequency Tuning.**
  By applying a voltage to a piezoelectric bonded onto the crystal, the later is expanded or contracted. This strains the crystal sufficiently to vary the frequency by tens of MHz at rates up to **30 kHz**. The tuning coefficient is **+3.2 MHz/V at 10 V DC**, and **+3.1 MHz/V at 10 Vpp AC at 5kHz**. The piezo can operates at frequencies greater than 30 kHz, but the tuning coefficient can vary substantially above 30 kHz.

The spectral distribution of the noise content of the laser (RIN, residual noise intensity) is given in figure 29. For frequency above 20 MHz, the Laser is below the shot noise limit of most photo-diodes. The major source of noise is the spike around 300 kHz due to relaxation oscillations, occurring because of the noise of the pump diode. This noise is reduced by the noise reduction electronics. The rms noise, i.e the amplitude modulation (AM) noise content integrated over 10Hz to 10 MHz is less than 0.1 %. Some parameters of the laser are listed in table 30.

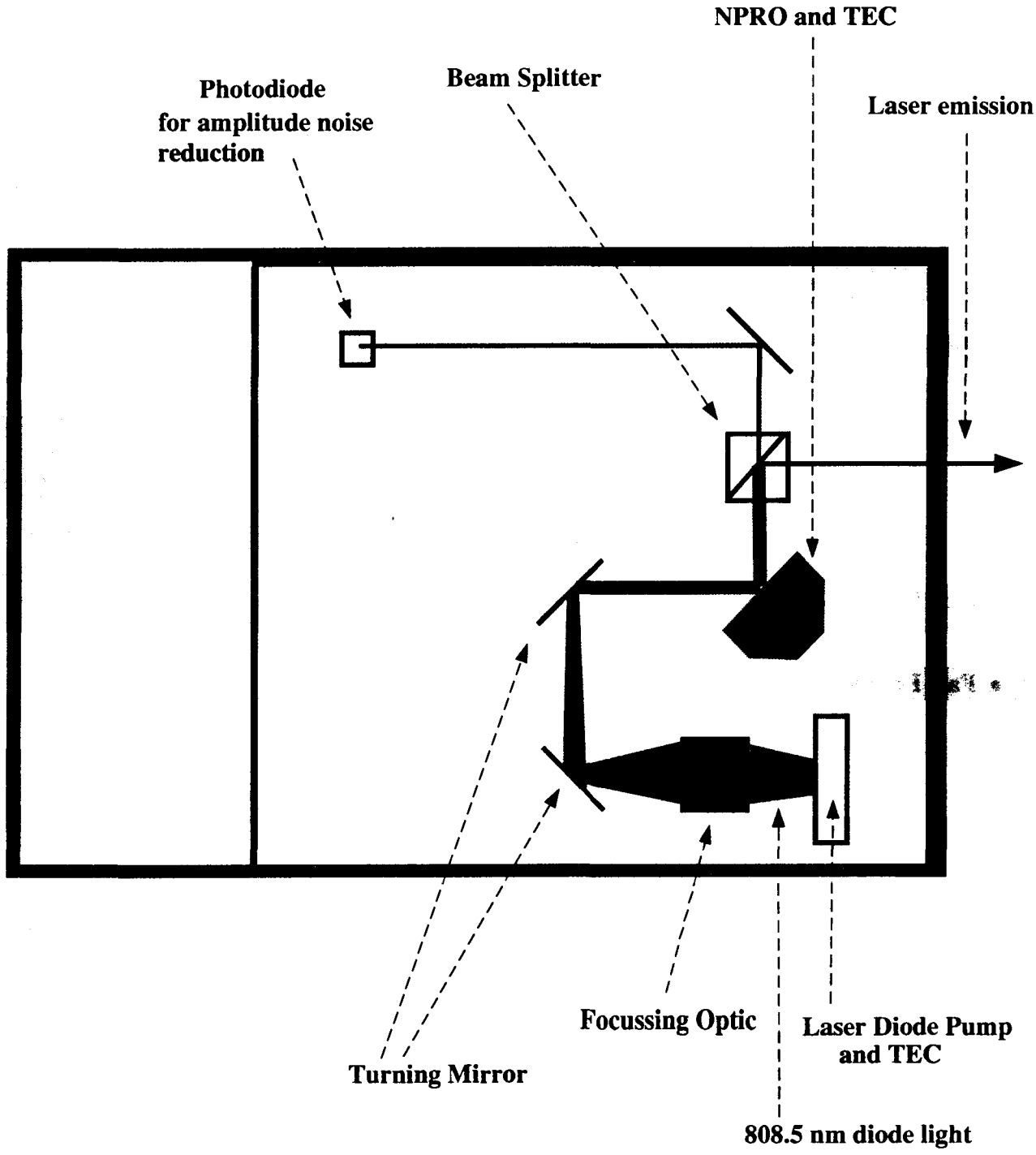

Figure 28: *Top View of the Series 126 Laser Head*

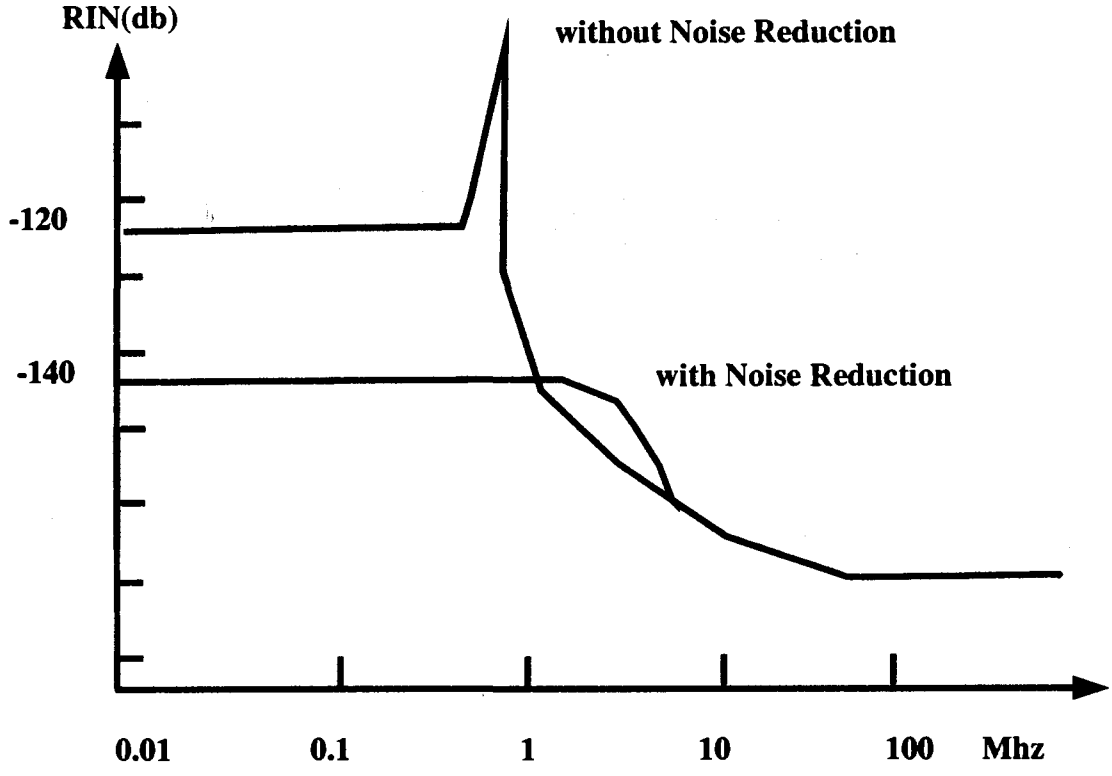

Figure 29: ***Residual Noise Intensity of the Series 126 Laser Head***

CW Power	300 mW
Spatial Mode	TEM_{00}
AM noise [10 Hz, 10 MHz]	<0.1 %
Line width, over 1ms	5 kHz
Coherence length	1000 m
Frequency Jitter	75 kHz/sec
Frequency Drift	50 MHz/hour
Polarization	300:1
Waist Location	5cm outside
Waist diameter $1/e^2 vertical$	0.43 mm
Waist diameter $1/e^2 horizontal$	0.54 mm
Beam divergence Vertical	3.1 mrad
Beam divergence Horizontal	2.5 mrad

Table 30: ***Laser parameters***

8.6 Need for a feedback between the laser and the cavity

On top of the laser noise described in section 8.5, the main source of noise is the vibration of the cavity. Indeed, assume that the laser frequency ν_L is tuned on a cavity mode so that

$$\nu_L = (n + \eta)\Delta\nu_{cav},$$

where $\eta \ll 1$. To keep the tuning at this level one has to guarantee that the cavity length is

$$L = L_0 + \eta\frac{\lambda}{2\mathcal{F}}$$

Various mechanic noises can produce change in length greater than a fraction of $\frac{\lambda}{2\mathcal{F}}$. One thus have to setup a feedback system that will change the laser frequency to follow the change in resonance frequency of the cavity due to this noise.

8.7 Field Reflected by the cavity

The feedback system between the Laser and the cavity [27], [28], [29] is based on the analysis of the phase of the reflected field E_{ref} (see also appendix G). This field is given by [23] :

$$E_R = r_1 E_I + i t_1 E_{circ}\frac{g_{rt}(\omega)}{r_1}. \tag{126}$$

Using Eq. (106) this becomes :

$$\frac{E_R}{E_I} = r_1 - \frac{t_1^2}{r_1}\frac{g_{rt}(\omega)}{1 - g_{rt}(\omega)} = r_1\left[1 - \frac{t_1^2}{r_1^2}\frac{g_{rt}(\omega)}{1 - g_{rt}(\omega)}\right], \tag{127}$$

with the round trip gain given by:

$$g_{rt}(\omega) = r_1 r_2 e^{-\frac{\delta_0}{2}} e^{-2i\pi\frac{\omega}{\Delta\omega_{FSR}}}. \tag{128}$$

Let ω be the frequency of the incident field and $\omega_c = n\Delta\omega_{FSR}$ the nearest resonance to the incident field ($\delta\omega = \omega - \omega_c$):

$$\omega = (n + \epsilon)\Delta\omega_{FSR} \text{ or } \boxed{\epsilon = \frac{\omega - \omega_c}{\Delta\omega_{FSR}} = \frac{\delta\omega}{\Delta\omega_{FSR}}}, \tag{129}$$

where $|\epsilon| < 1$, **the detuning parameter**, is the shift wrt the resonance in Free spectral range unit ($\Delta\omega_{FSR}$). This can also be parametrized by the shift η wrt the resonance in bandwidth unit (ω_{cav}) as

$$\omega = n\Delta\omega_{FSR} + \eta\Delta\omega_{cav} \text{ or } \eta = \frac{\omega - \omega_c}{\Delta\omega_{cav}} = \frac{\delta\omega}{\Delta\omega_{FSR}}\frac{\Delta\omega_{FSR}}{\Delta\omega_{cav}} = \epsilon\frac{\Delta\omega_{FSR}}{\Delta\omega_{cav}} \simeq \epsilon\mathcal{F}. \tag{130}$$

The round trip gain becomes as a function of the detuning parameter

$$g_{rt}(\omega) = r_1 r_2 e^{-\frac{\delta_0}{2}} e^{-2i\pi\epsilon}. \tag{131}$$

The intensity reflection coefficient of the cavity $\mathcal{R}$ (**cavity reflectivity**) is deduced from the field reflection coefficient ρ of the cavity given by :

$$\rho = \frac{E_R}{E_I} = r\left[\frac{1 - (r^2 + t^2)\, e^{-\frac{\delta_0}{2}} e^{-2i\pi\epsilon}}{1 - r^2 e^{-\frac{\delta_0}{2}} e^{-2i\pi\epsilon}}\right], \tag{132}$$

through the equation:

$$\mathcal{R}(\epsilon) = \rho\rho^* = R\left[\frac{1-(R+T)\,e^{-\frac{\delta_0}{2}}}{1-Re^{-\frac{\delta_0}{2}}}\right]^2 \left[\frac{1+4\frac{(R+T)e^{-\frac{\delta_0}{2}}}{\left(1-(R+T)e^{-\frac{\delta_0}{2}}\right)^2}\sin^2\pi\epsilon}{1+4\frac{Re^{-\frac{\delta_0}{2}}}{\left(1-Re^{-\frac{\delta_0}{2}}\right)^2}\sin^2\pi\epsilon}\right]. \tag{133}$$

For vacuum $\delta_0 = 0$, introducing P the total losses of a mirror

$$P = A + D = 1 - (R+T), \tag{134}$$

the cavity reflectivity reads

$$\boxed{\mathcal{R}(\epsilon) = R\left[\frac{P^2 + 4(1-P)\sin^2\pi\epsilon}{(1-R)^2 + 4R\sin^2\pi\epsilon}\right]}, \tag{135}$$

and for small detuning parameter

$$\boxed{\mathcal{R}(\epsilon) \simeq R\left[\frac{P^2}{(1-R)^2}\right]}. \tag{136}$$

The phase Φ_R of the field reflection coefficient

$$\rho = \sqrt{\mathcal{R}}e^{i\Phi_R}, \tag{137}$$

is given by

$$\tan\Phi_R(\epsilon) = \frac{Te^{-\frac{\delta_0}{2}}\sin 2\pi\epsilon}{1-2Re^{-\frac{\delta_0}{2}}\cos 2\pi\epsilon + R(R+T)e^{-\delta_0} - Te^{-\frac{\delta_0}{2}}\cos 2\pi\epsilon}. \tag{138}$$

For small detuning parameter we have

$$\tan\Phi_R(\epsilon) \simeq 2\pi\epsilon\frac{Te^{-\frac{\delta_0}{2}}}{1-2Re^{-\frac{\delta_0}{2}} + R(R+T)e^{-\delta_0} - Te^{-\frac{\delta_0}{2}}}, \tag{139}$$

and in vacuum $\delta_0 = 0$, so that

$$\boxed{\tan\Phi_R(\epsilon) \simeq 2\pi\epsilon\left\{\frac{1-R-P}{P(1-R)}\right\}}. \tag{140}$$

The phase and the module of the reflection coefficient are presented on figure 30 for various cavity parameters.

For small detuning parameter, the phase of the Fabry-Perot is proportional to the detuning parameter: $\tan\Phi_R \propto \epsilon$, and vary very rapidly around the resonance; so that a measurement of this phase may be used to correct for the detuning. This is the idea of the Pound-Drever method used for the cavity feedback system.

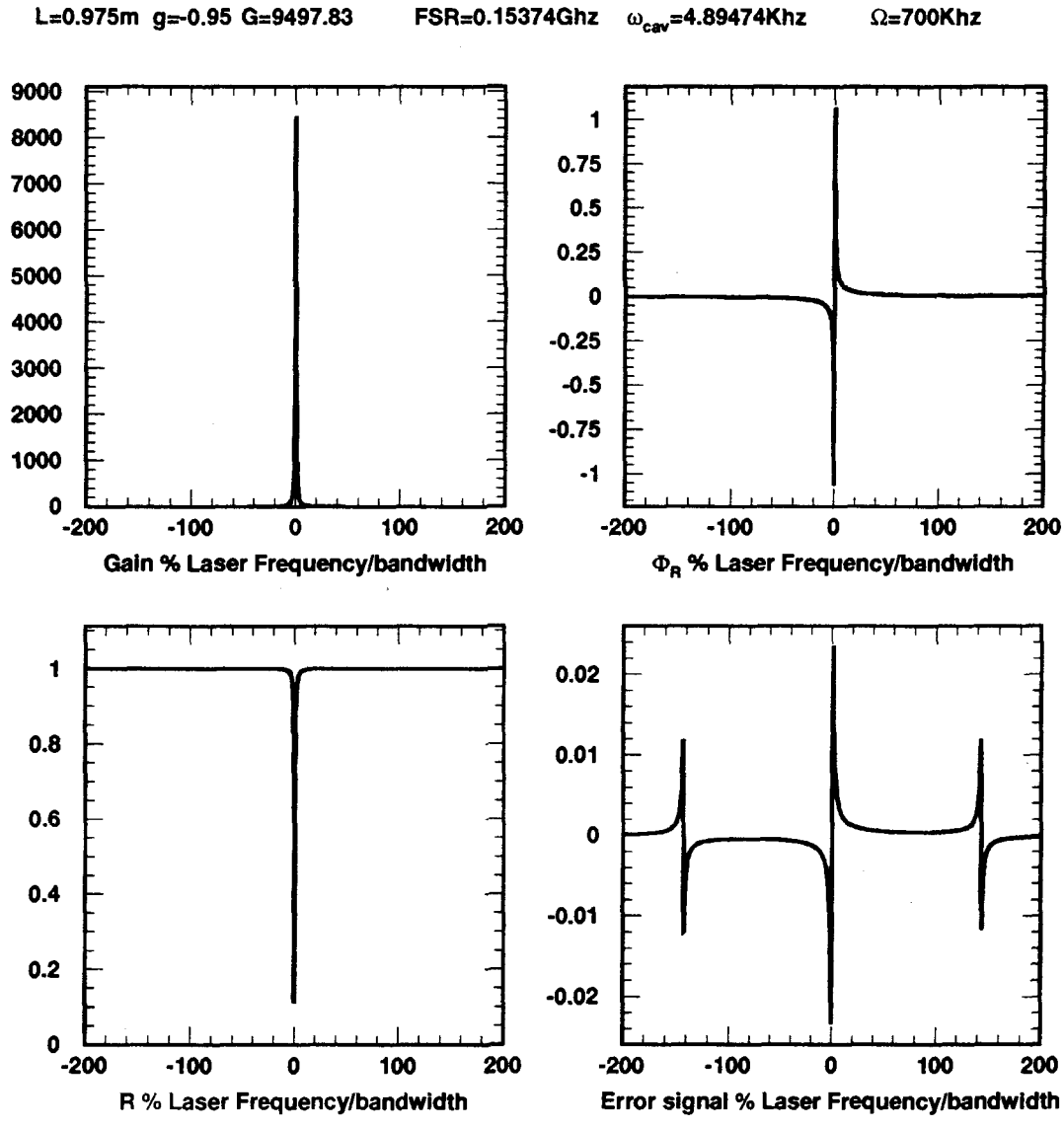

Figure 30: ***Cavity Gain*** G***, Phase*** Φ_R***, Module of the reflection coefficient*** $\mathcal{R}$ ***and discriminator signal from the Pound Drever Method*** *for a 97.5 cm cavity, with* $g = -0.95$ *and maximum Gain 9497. The frequency modulation* Ω *is 700 kHz large compared to the cavity bandwidth* ω_{cav} *=4.9 kHz and small wrt the free spectral range* $\Delta\omega_{FSR} = 0.15Ghz$.

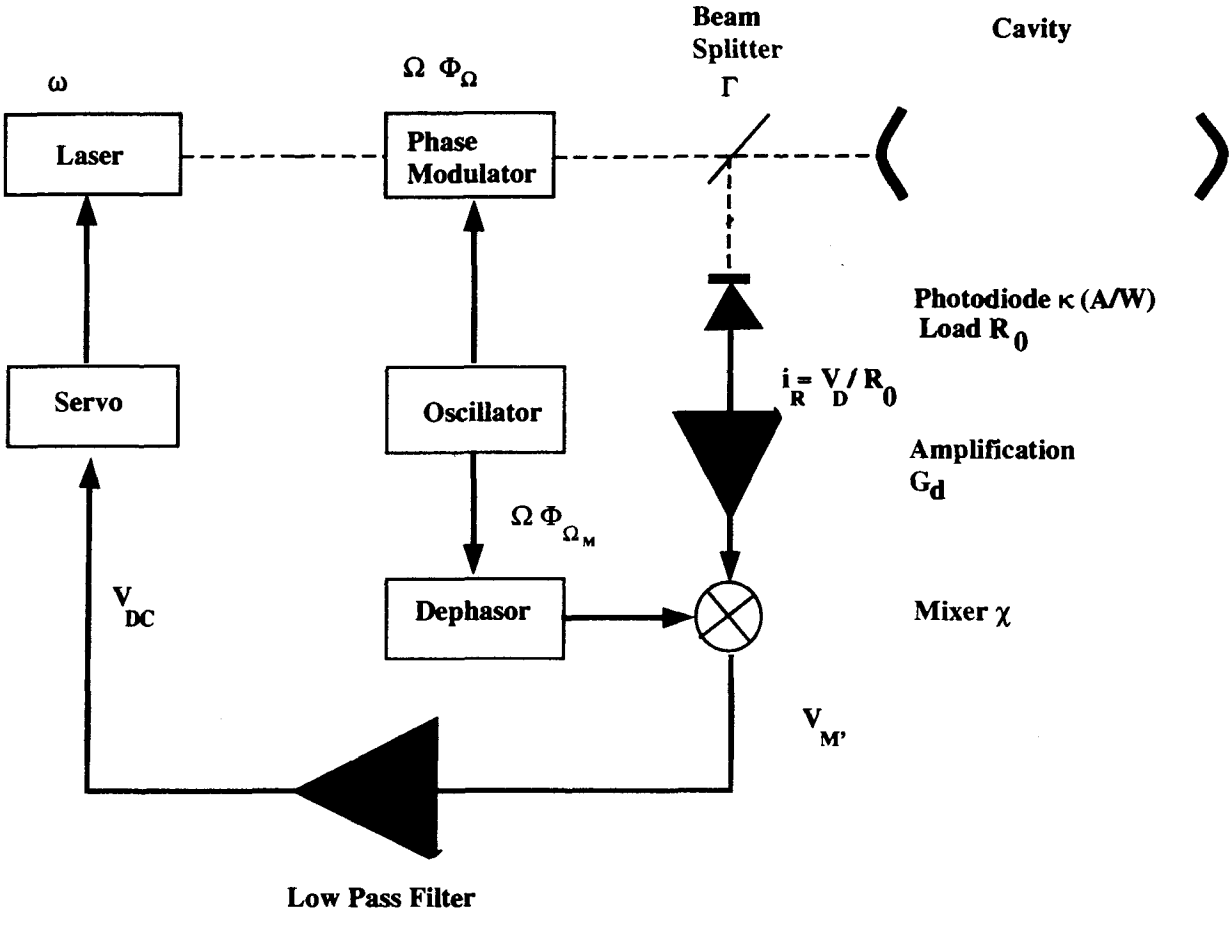

Figure 31: ***Pound Drever Method.*** *The Laser frequency ω is modulated at frequency Ω. This modulated field after reflection on the Fabry Perot Cavity is sent to a photodiode. The photodiode signal, after amplification, is mixed with the Oscillator at frequency Ω. After a low pass filter, this will be the discriminator signal sent to the servo system.*

8.8 Getting the discriminator signal

In this section, the method to extract the phase of the reflected field, i.e the discriminator signal, is presented. A schema is displayed on Fig. 31.

The Laser incident field E_I at frequency $\nu = \frac{c}{\lambda}$ is phase modulated by an oscillator at frequency Ω and with a small phase modulation amplitude m.

$$E_I = E_0 e^{i\omega t} e^{im\cos(\Omega t + \Phi_\Omega)}. \tag{141}$$

Using Bessel functions, it can be shown that a field at frequency ω phase modulated at frequency Ω and amplitude m has a frequency spectrum given by $\omega_k^{\pm} = \omega \pm k\Omega$, each frequency component having a strength given by the kth Bessel function $J_k(m)$ and a phase given by $k(\frac{\pi}{2} \pm \Phi_\Omega)$:

$$E_I = E_0 \left[J_0(m) e^{i\omega t} + \sum_{k=1}^{\infty} J_k(m) \left(e^{ik\left(\frac{\pi}{2}+\Phi_\Omega\right)} e^{i\omega_k^+ t} + e^{ik\left(\frac{\pi}{2}-\Phi_\Omega\right)} e^{i\omega_k^- t} \right) \right]. \tag{142}$$

For small value of the amplitude of the phase modulation, the incident field is

$$E_I \simeq E_0 e^{i\omega t} \left[J_0(m) + (i) J_1(m) e^{+i(\Omega t + \Phi_\Omega)} + (i) J_1(m) e^{-i(\Omega t + \Phi_\Omega)} \right]. \tag{143}$$

Using the cavity reflection coefficient ρ, the (complex) field reflected by the cavity can be expressed as

$$\begin{aligned} E_R \simeq\ & E_0 e^{i\omega t} \left[J_0(m) \sqrt{\mathcal{R}(\omega)} e^{i\Phi_R(\omega)} \right. \\ +\ & (i) J_1(m) \sqrt{\mathcal{R}(\omega+\Omega)} e^{i\Phi_R(\omega+\Omega)} e^{+i(\Omega t + \Phi_\Omega)} \\ +\ & \left. (i) J_1(m) \sqrt{\mathcal{R}(\omega-\Omega)} e^{i\Phi_R(\omega-\Omega)} e^{-i(\Omega t + \Phi_\Omega)} \right]. \end{aligned} \tag{144}$$

Note that for a laser frequency $\omega = (n + \epsilon)\Delta\omega_{FSR}$ close to a cavity resonance frequency ω_c and a modulation frequency

$$\Delta\omega_{FSR} \ll \Omega \ll \Delta\omega_{cav}, \tag{145}$$

we have $\sqrt{\mathcal{R}(\omega \pm \Omega)} \simeq 1$ and $\Phi_R(\omega \pm \Omega) \simeq 0$, so that the electric field is

$$\begin{aligned} E_R \simeq\ & E_0 e^{i\omega t} \left[J_0(m) \sqrt{\mathcal{R}(\omega)} e^{i\Phi_R(\omega)} \right. \\ +\ & (i) J_1(m) e^{i(+\Omega t + \Phi_\Omega)} \\ +\ & \left. (i) J_1(m) e^{i(-\Omega t + \Phi_\Omega)} \right]. \end{aligned} \tag{146}$$

A fraction $\Gamma(1-\Gamma)$ (Γ transitivity of the beam splitter) of the intensity of the reflected field is directed through a photodiode with a conversion factor κ in (A/W). The photodiode is not fast enough to detect the intensity variation at frequency ω and above, the current delivered by the photodiode is thus

$$\begin{aligned} i_{ph} \simeq\ & \frac{1}{2}\Gamma(1-\Gamma)\kappa|E_0|^2 \left[J_0^2(m) \sqrt{\mathcal{R}(\omega)}^2 \right. \\ -\ & 2J_0(m)J_1(m)\sqrt{\mathcal{R}(\omega)}\sqrt{\mathcal{R}(\omega+\Omega)} \sin\left(\Omega t + \Phi_\Omega + \Phi_R(\omega+\Omega) - \Phi_R(\omega)\right) \\ +\ & \left. 2J_0(m)J_1(m)\sqrt{\mathcal{R}(\omega)}\sqrt{\mathcal{R}(\omega-\Omega)} \sin\left(\Omega t + \Phi_\Omega - \Phi_R(\omega-\Omega) + \Phi_R(\omega)\right) \right]. \end{aligned}$$

(where E_0^2 is now expressed in $Watt$). The resulting voltage is

$$V_d = \Gamma(1-\Gamma)R_0 I_{ph}, \tag{147}$$

where R_0 is the load resistance of the photodiode.

After amplification (gain G_d), the photodiode voltage is mixed with an oscillator at frequency Ω (phase Φ_Ω) and amplitude V_O. At the mixer output, one gets the following voltage (χ Mixer efficiency, see appendix G):

$$\begin{aligned} V_{M'} &= \frac{1}{2}\chi V_O G_d R_0 \Gamma(1-\Gamma)\kappa|E_0|^2 \left[J_0^2(m)\sqrt{\mathcal{R}(\omega)}^2 \cos(\Omega t + \Phi_{\Omega_M}) \right. \\ &+ J_0(m)J_1(m)\sqrt{\mathcal{R}(\omega)}\sqrt{\mathcal{R}(\omega+\Omega)} \\ &\left[\sin(+2\Omega t + \Phi_\Omega + \Phi_R(\omega+\Omega) - \Phi_R(\omega) + \Phi_{\Omega_M}) + \sin(+\Phi_\Omega - \Phi_{\Omega_M} + \Phi_R(\omega+\Omega) - \Phi_R(\omega)) \right] \\ &+ J_0(m)J_1(m)\sqrt{\mathcal{R}(\omega)}\sqrt{\mathcal{R}(\omega-\Omega)} \\ &\left[\sin(-2\Omega t - \Phi_\Omega + \Phi_R(\omega-\Omega) - \Phi_R(\omega) - \Phi_{\Omega_M}) + \sin(-\Phi_\Omega + \Phi_{\Omega_M} + \Phi_R(\omega-\Omega) - \Phi_R(\omega)) \right] \left. \right]. \end{aligned}$$

This voltage is sent to a low pass filter, cutting all frequencies above Ω resulting in a DC voltage

$$\begin{aligned} V_{DC} &\simeq \frac{1}{2}\chi V_O G_d \Gamma(1-\Gamma)\kappa R_0 |E_0|^2 J_0(m)J_1(m)\sqrt{\mathcal{R}(\omega)} \\ &\left[\sqrt{\mathcal{R}(\omega+\Omega)}\sin(\Phi_R(\omega+\Omega) - \Phi_R(\omega) + (\Phi_\Omega - \Phi_{\Omega_M})) \right. \\ &+ \left. \sqrt{\mathcal{R}(\omega-\Omega)}\sin(\Phi_R(\omega-\Omega) - \Phi_R(\omega) - (\Phi_\Omega - \Phi_{\Omega_M})) \right]. \end{aligned} \tag{148}$$

Again, for a laser frequency $\omega = (n+\epsilon)\Delta\omega_{FSR}$ close to a cavity resonance frequency ω_c and a modulation frequency

$$\Delta\omega_{FSR} \ll \Omega \ll \Delta\omega_{cav},$$

we have $\sqrt{\mathcal{R}(\omega \pm \Omega)} \simeq 1$ and $\Phi_R(\omega \pm \Omega) \simeq 0$, so that the voltage after the low pass filter is

$$V_{DC} \simeq \cos(\Phi_\Omega - \Phi_{\Omega_M})\,\chi V_O G_d R_0 \Gamma(1-\Gamma)\kappa|E_0|^2 J_0(m)J_1(m)\sqrt{\mathcal{R}(\omega)}\sin(\Phi_R(\omega)). \tag{149}$$

For small detuning parameter ϵ, using Eq. (136) and (139), one gets :

$$\boxed{V_{DC} \simeq \cos(\Phi_\Omega - \Phi_{\Omega_M})\,\chi V_O G_d \Gamma(1-\Gamma)\kappa|E_0|^2 R_0 J_0(m)J_1(m)2\pi\epsilon\left\{\sqrt{R}\frac{1-R-P}{(1-R)^2}\right\}}, \tag{150}$$

or similarly using the finesse :

$$V_{DC} \simeq 2\cos(\Phi_\Omega - \Phi_{\Omega_M})\,\chi V_O G_d R_0 \Gamma(1-\Gamma)\kappa\|E_0|^2 J_0(m)J_1(m)\mathcal{F}\epsilon\left\{\frac{1-R-P}{(1-R)}\right\}. \tag{151}$$

The DC voltage is then a good discriminator signal proportional to the phase Φ_R of the reflected field (Eq. 149 or Fig 30b and 30d) and so to the detuning parameter $\epsilon \propto (\omega - \omega_c)$. The electronic servo that we will use in conjunction with this discriminator is discussed in appendix G.4.

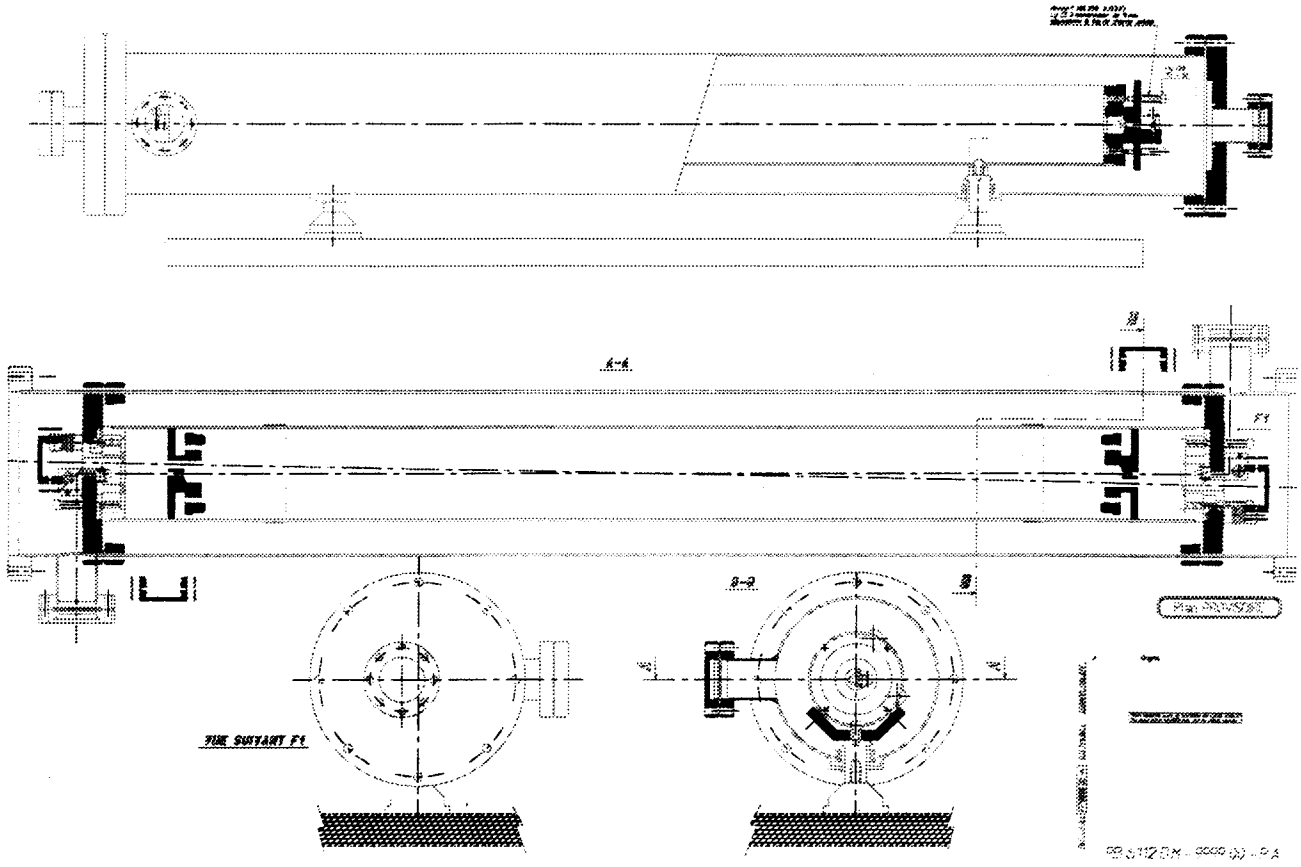

Figure 32: ***Preliminary design of the cavity mechanic***

8.9 Mechanic of the Cavity

The mechanic of the cavity has to include the following parameters

- good vacuum
- Isolation from vibrations
- good mechanical resistivity
- Crossing with the electron beam at small angle
- allow Laser and/or mirror alignment.

A preliminary design of the cavity mechanic is presented on figure 32. In this solution, the optical alignment is obtained by moving the mirrors. An alternative solution, in which the mirrors are fixed, and the Laser is aligned on the cavity optical axis is currently under study.

8.10 Radiations for the cavity mirrors

8.10.1 Neutron radiation seen by the cavity mirrors

Neutrons originating from the interaction of the electron beam with the target in ESA will diffuse also in the Compton Tunnel. Measurements performed in Hall C at a luminosity of $\mathcal{L} = 153\mu A - g/cm^2 - hr$ gave a dose of $8rem$ in the polarimeter tunnel. Careful shielding of the Polarimeter will thus be very important.

8.10.2 Synchrotron radiation seen by the cavity mirrors

The radiation to be considered here are the synchrotron photons emitted by the end of the dipole 2 of the magnetic chicane ($B = 0.75T$ at 4 GeV and $L = 1\,m$).
We recall (see figures 33 and 34) that the cavity mirrors of diameter $d_m = 8mm$ are centered on the beam axis z in the dipole bending plane y, z and are distant of $D_m = 1m$ from each other. In the transverse plane x, z, the centers of the mirrors are at a distance of $\pm 10mm$ from the beam z axis. So the angle with the z axis is $\alpha = 20\,mrad$ and the safety distance between the edge of the mirrors and the beam is $d_s = \pm 6mm$.
The cavity mirrors see a piece $\Delta\theta$ (y,z plane) of the dipole of the chicane under an angle ψ (angle in the x,z plane between the bending plane and the observation point). The synchrotron radiation is given by equation 215 of section C

$$\frac{\partial P}{\partial \Omega} = \frac{P_0}{2\pi}\,\frac{21}{32}\,\frac{\gamma}{(1+\gamma^2\psi^2)^{5/2}}\left[1+\frac{5}{7}\frac{\gamma^2\psi^2}{1+\gamma^2\psi^2}\right]$$

$$\frac{\partial P}{\partial(\gamma\psi)} = P_0\,\frac{21}{32}\,\frac{1}{(1+\gamma^2\psi^2)^{5/2}}\left[1+\frac{5}{7}\frac{\gamma^2\psi^2}{1+\gamma^2\psi^2}\right]$$

where P_0 is given by

$$P_0 = \frac{2r_0 c m_e c^2}{3}\,\frac{\beta^4\gamma^4}{R^2}\,\frac{R\Delta\theta}{\beta c}\,\frac{I_e}{e}$$

The first (resp. second) mirror will be located at a distance $D_1 = 0.65\,m$ (resp. $D_2 = 1.65\,m$) from the end of the dipole, which corresponds to a $\psi\gamma > 72.2$ at 4 GeV (resp. $\psi\gamma > 28.4$). As a consequence of large angles, the synchrotron power seen by the mirrors is very small (See tables 31 and 32), i.e less than $.02\mu\,W$, and its mean energy ranges from .008 eV (155 μm) to 0.14 eV (8.8 μm). The power is almost independent of the beam energy. For large synchrotron radiation angles, the power increases with energy as $P \simeq \gamma^5/\rho$ but the fraction seen by the mirrors decreases as $F \simeq 1./\psi^3/\gamma^5$. The power seen by the mirrors is then $P \simeq 1./\psi^3/\rho$.
Always due to large angles, the power on the mirrors is maximum on the edge of the mirror near the electron beam as shown on figure 35.

Some data exists on the synchrotron radiation damage to Ta_2O_5/SiO_2 multi-layer mirrors[30],[31]. At the Super ACO accelerator at Orsay, the Free Electron Laser (FEL) is operated in the UV at $\lambda = 350nm$ using a cavity with $10m$ curvature radius, with losses $P \leq 1\%$ and transmission $T \simeq 5\,10^{-4}$. The Super ACO FEL synchrotron radiation has a critical wave length $\lambda_c = 71A$. In ultra-high vacuum (UHV) (10^{-8} to 10^{-10} torr), a certain quantity of residual hydrocarbon gases exists, out-gassing from the vacuum chamber walls. It is known[30] that the interaction between hydrocarbons and X-UV radiation produces the cracking of the chemical bonds, and a subsequent progressive contamination of the optic surface by carbon atoms. Measurements at Super-ACO have shown that a raise of mirror losses of order of 0.5% per $40mAh$ dose have to be expected.

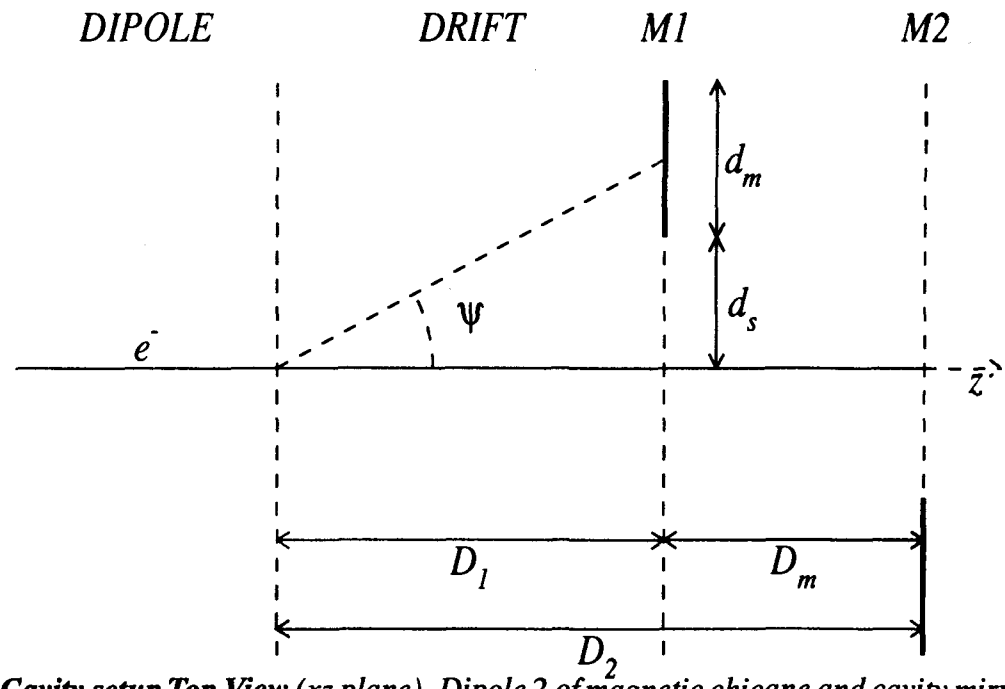

Figure 33: ***Cavity setup Top View*** *(xz plane). Dipole 2 of magnetic chicane and cavity mirrors M1 and M2*

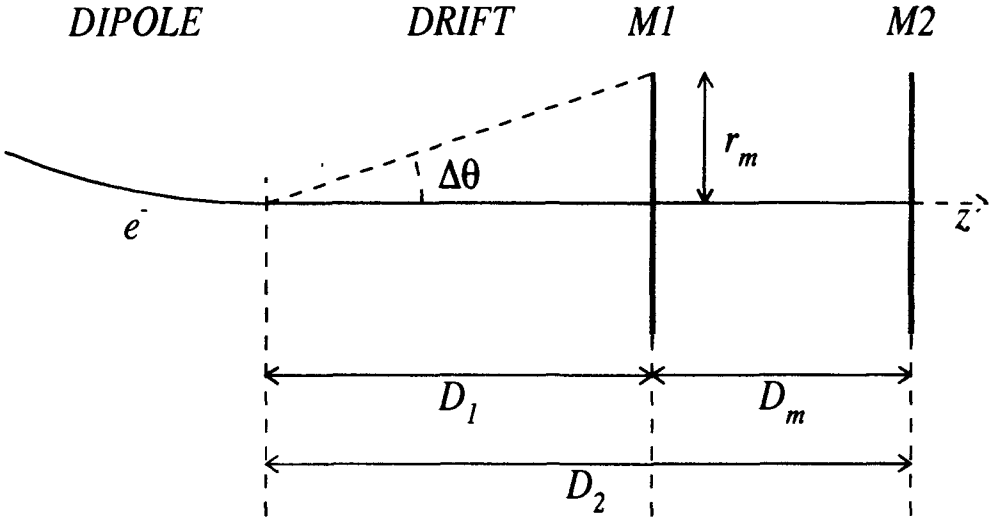

Figure 34: ***Cavity setup Side View*** *(yz plane). Dipole 2 of magnetic chicane and cavity mirrors M1 and M2*

This mirror degradation is for direct exposure, it is obvious that for mirror located a few mm off the ondulator axis (this is the case for our cavity) the mirror degradation will be less important. A measurement is anyway mandatory. This will be done at CEBAF by the "Laser backscattering Facility" collaboration at CEBAF [32]. Procedures exist to partially recover the mirror losses by an RF oxygen plasma cleaning apparatus [31] or baking at 300° C with oxygen (Air) atmosphere.

E	GeV	1.0	2.0	3.0	4.0	5.0	6.0	7.0	8.0
B	Tesla	-0.19	-0.37	-0.56	-0.75	-0.94	-1.12	-1.31	-1.50
Power	μW	0.0012	0.0012	0.0012	0.0012	0.0012	0.0012	0.0012	0.0012
N_γ	$10^{12}s^{-1}$	0.935	0.932	0.928	0.926	0.923	0.921	0.919	0.917
$< \epsilon >$	eV	0.008	0.008	0.008	0.008	0.008	0.008	0.008	0.008

Table 31: ***Synchrotron radiation seen by the first mirror.*** *For a beam of* $100\,\mu A$ *and a mirror of diameter* $8.0mm$ *located at a distance from downstream of dipole 2 of magnetic chicane of* $0.65m$. *The mirror center is at* $1.0cm$ *wrt the beam axis* ($\Delta\theta = 6.1mrad$).

E	GeV	1.0	2.0	3.0	4.0	5.0	6.0	7.0	8.0
B	Tesla	-0.19	-0.37	-0.56	-0.75	-0.94	-1.12	-1.31	-1.50
Power	μW	0.0196	0.0201	0.0202	0.0203	0.0203	0.0203	0.0203	0.0203
N_γ	$10^{12}s^{-1}$	0.929	0.935	0.935	0.933	0.932	0.930	0.929	0.928
$< \epsilon >$	eV	0.131	0.134	0.135	0.136	0.136	0.136	0.137	0.137

Table 32: ***Synchrotron radiation seen by the second mirror.*** *For a beam of* $100\,\mu A$ *and a mirror of diameter* $8.0mm$ *located at a distance from downstream of dipole 2 of magnetic chicane of* $1.65m$. *The mirror center is at* $1.0cm$ *wrt the beam axis* ($\Delta\theta = 2.4mrad$).

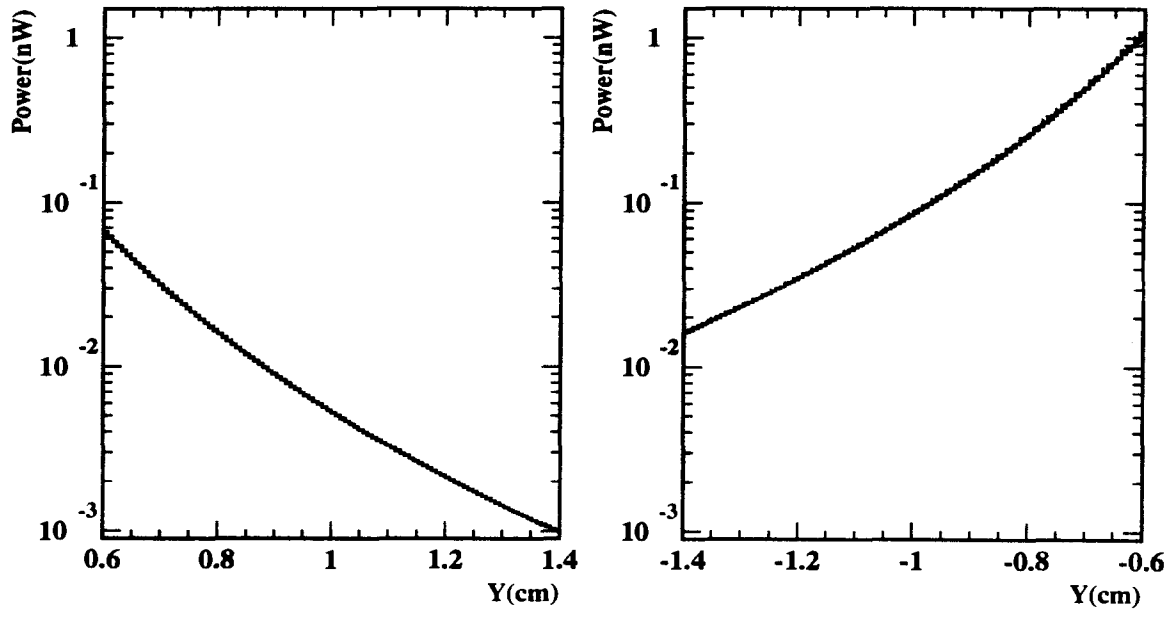

Figure 35: ***Synchrotron power seen by the first (left) and second (right) mirror versus position on the mirror wrt beam position.*** *At 1 GeV (solid line) and 8 GeV (dashed line).*

9 Laser Polarization

The measurement of the electron beam longitudinal polarization by Compton scattering requires a source of longitudinal photons. The possibility to reverse frequently the sign of this polarization minimize the sensitivity of our measurement to the time variation of the experimental setup. The light from the NdYAG laser is (vertically) linearly polarized at the 99.66 % level. This section describes two possible ways to obtain and reverse circular polarization from the NdYAG Laser and the method to measure the Laser polarization.

9.1 Getting circular polarization from linear polarization

The x axis is defined as the direction in which the electric field is pointing at the exit of the Laser. To obtain a circular polarization, a quarter wave plate (birefringent crystal), with its slow axis at 45° from the x axis could be used. In this case the ellipticity of the light after this plates is given by $\tan\theta$, where θ is the angle between the quarter wave plate slow axis and the incident linear polarization direction [33]. "Newport" catalog reference for the quarter wave plate $10RP04$ quotes a reflectivity $R < 0.25\%$, a maximum power density of $2MW/cm^2$.

9.2 Reversals of the Polarization

To reverse the polarization helicity, one can flip the linear polarization by a Pockels Cell, before entering a quarter-wave plate. Or one can used directly the Pockels Cell as a quarter-wave. After a brief introduction of the Pockels effect, these two possible methods will be detailed.

The Pockels effect is one of the possible electro-optical properties of matter. For any material with an index ellipsoid defined by n_{ij}^2, the modification of the ellipsoid when an electric field is applied to the materiel can be written [33]:

$$\frac{1}{n_{ij}^2}(E) = \frac{1}{n_{ij}^2}(0) + \Delta\left[\frac{1}{n_{ij}^2}\right], \tag{152}$$

with

$$\Delta\left[\frac{1}{n_{ij}^2}\right] = r_{ijk}E_k + S_{ijkl}E_kE_l. \tag{153}$$

The linear electro-optic tensor (r_{ijk}) describes the Pockels effect, whereas the quadratic electro-optic tensor (S_{ijkl}) the Kerr effect. In what follows the Voigt notation will be used, reducing to a 6x3 matrix (r_{ij}) the original Pockels tensor (r_{ijk}).

The Pockels coefficients (r_{ij}) being very small ($\simeq 10^{-10}$ to $10^{-12}mV^{-1}$), the voltage to apply to get a significant Pockels effect is important (a few hundred volts). In the IR range, K*DP (Potassium dideuterium Phosphate) could be a good crystal candidate. When no field is applied, this is a uni-axis crystal (index n_0 and n_e). Let Z and X, Y be the principal axis of the crystal with zero electric field, Z is the optical axis (with index n_e), and X,Y have associated n_0 index. Let $Z' = Z$, X' and Y' be the new principal axis when an electric field is applied in the optical axis (Z') direction. The indices with non zero voltage are given by

$$n_{x'} = n_0 - \frac{1}{2}n_0^3 r_{63}E, \tag{154}$$

$$n_{y'} = n_0 + \frac{1}{2} n_0^3 r_{63} E, \tag{155}$$

and thus the crystal is now bi-axis, with principal axis with field X', Y' are $\pi/4$ rotated with respect to the axis without field X, Y.

When propagating in the Y' direction, light polarized in the X' and Z' directions will have a phase difference after traveling a distance e in the Y' crystal direction submitted to a voltage V on a thickness d given by

$$\phi = \frac{2\pi}{\lambda} e \Delta n = \frac{2\pi}{\lambda} e \left(n_{z'} - n_{x'}\right) = \frac{2\pi}{\lambda} \left(n_e - n_0 + \frac{1}{2} n_0^3 r_{63} \frac{V}{d}\right) e. \tag{156}$$

If the length of the crystal e is a multiple of $\frac{\lambda}{(n_e - n_0)}$, this phase difference becomes

$$\phi = \frac{2\pi}{\lambda} \Delta n e = \frac{1}{2} n_0^3 r_{63} \frac{2\pi}{\lambda} V \frac{e}{d}. \tag{157}$$

This phase-shift is equal to π for a voltage given by

$$V_{\frac{\lambda}{2}} = \frac{d}{e} \frac{\lambda}{n_0^3 r_{63}}.$$

When propagating in the Z' direction, light polarized in the X' and Y' directions will have a phase difference after traveling a distance e in the Z' crystal direction submitted to a voltage V on a thickness $d = e$ given by

$$\phi = \frac{2\pi}{\lambda} e \Delta n = \frac{2\pi}{\lambda} e \left(n_{y'} - n_{x'}\right) = \frac{2\pi}{\lambda} \left(n_0^3 r_{63} \frac{V}{d}\right) d = \frac{2\pi}{\lambda} n_0^3 r_{63} V \tag{158}$$

This phase-shift is equal to $\pi/2$ for a voltage given by

$$V_{\frac{\lambda}{4}} = \frac{\lambda}{4 n_0^3 r_{63}},$$

9.2.1 Transverse field design

For an applied voltage of $V_{\frac{\lambda}{2}}$, resulting in an electric field along the optical Z axis, transverse to the light propagation direction, the cell is equivalent to a half-wave plate. Consequently, entering the cell in the Y' direction with a linear polarization orthogonal to the X' axis (e.g along Z) would result in a polarization flip if the voltage $V_{\frac{\lambda}{2}}$ is applied to crystal. If the Pockels cell is followed by a quarter-wave plate, then according to the value of the voltage (0 or $V_{\frac{\lambda}{2}}$), one then ends with light right or left circularly polarized (See Fig. 36).

9.2.2 Longitudinal field design

For an applied voltage of $V_{\frac{\lambda}{4}}$, resulting in an electric field along the optical Z axis, parallel to the light propagation direction, the cell is equivalent to a quarter-wave plate. Consequently, entering the cell in the Z direction with a linear polarization at $\pm\frac{\pi}{4}$ to the slow axis (Y' or X' axis) would result in a circular right or left polarization (See Fig. 37).

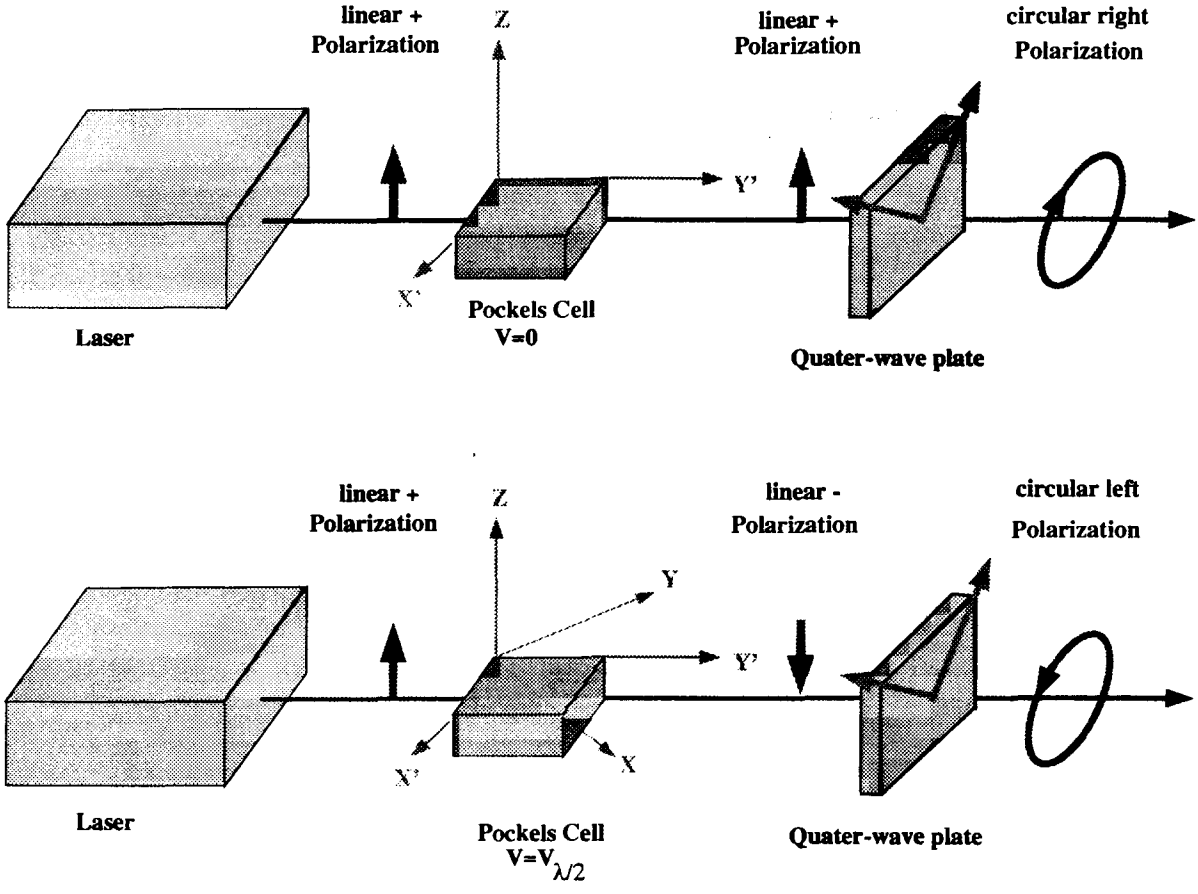

Figure 36: ***Getting right and left circular polarization from the linearly (vertically) polarized light of the NdYAG Laser.*** *If the Pockels cell voltage is set to zero (resp. $V_{\frac{\lambda}{2}}$), the light after the quarter-wave plate is circularly right (resp. left) polarized.*

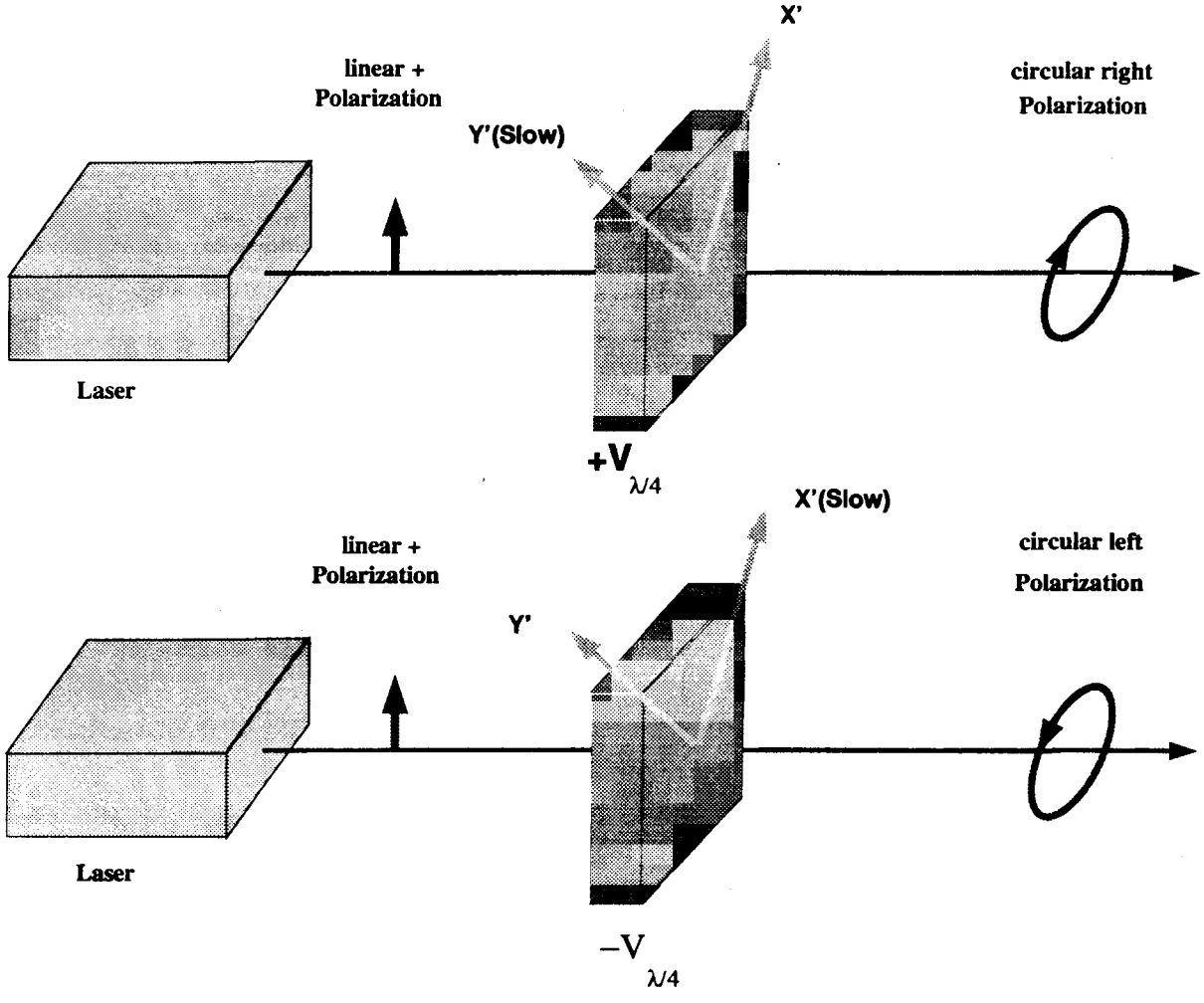

Figure 37: ***Getting right and left circular polarization from the linearly (vertically) polarized light of the NdYAG Laser.*** *If the Pockels cell voltage is set $+V_{\frac{\lambda}{4}}$ (resp. $-V_{\frac{\lambda}{4}}$), the light is circularly right (resp. left) polarized.*

9.2.3 Possible Technical Solution

The Lasermetrics LMA-1 (transverse field) or LMA-3 (longitudinal Field) modulators might be a possible choice [34]. The crystal is K*DP. They have 2.3 mm clear aperture diameter and a 1000:1 typical extinction ratio, with a 94 % transmittance and a rise time less than 5 ns. They must be used with a 8403 HV amplifier, which can drive the Pockels cell from DC to 24 kHz.

9.3 Polarization Measurement

The Laser light is linearly polarized at the 300/1 level (light Wave 126 Specifications). The light polarization P_γ is extracted from the measurement of the light polarization P'_γ at the exit of the cavity, assuming that the exiting light is a random sample of the cavity circulating light. To measure P'_γ, we plan to use the standard technique of linear polarization separation [35], where a small part of the circularly polarized light is sent by a canted glass window to a Wollaston Prism. This Wollaston Prism splits the two perpendicular linear light, and one measures via Joule meters the intensity of the two polarization I_x and I_y. From their ratio $R = \frac{I_x}{I_y}$, the polarization could be easily extracted.

This method could be explained by considering the electric field of an elliptic polarization light

$$E = \begin{bmatrix} a\cos(\omega t - kz) = \sqrt{I_x}\cos(\omega t - kz) \\ b\sin(\omega t - kz) = \sqrt{I_y}\sin(\omega t - kz) \\ 0 \end{bmatrix}$$

Introducing the right (resp. left) handed circularly polarized electric field E_+ (resp E_-):

$$E_+ = e_+ \begin{bmatrix} \cos(\omega t - kz) \\ \sin(\omega t - kz) \\ 0 \end{bmatrix}$$

$$E_- = e_- \begin{bmatrix} +\cos(\omega t - kz) \\ -\sin(\omega t - kz) \\ 0 \end{bmatrix}$$

with the number of right (resp. left) handed photons given by $N_+ = \beta < E_+^2 >$, $N_- = \beta < E_-^2 >$ and the total number of photons given by $N = N_+ + N_- = \beta\frac{1}{2}(a^2 + b^2) = \beta\frac{1}{2}b^2(R+1)$. So that the coefficient of the elliptic field can be expressed in terms of the right and left handed field:

$$a = e_+ + e_- = \beta(\sqrt{N_+} + \sqrt{N_-})$$
$$b = e_+ - e_- = \beta(\sqrt{N_+} - \sqrt{N_-})$$

e.g

$$ab = \sqrt{R}b^2 = N_+ - N_- \tag{159}$$

and finally

$$P_\gamma = \frac{N_+ - N_-}{N_+ + N_-} = \frac{2\sqrt{R}}{1+R} \tag{160}$$

Using this technique the Compton polarimeter group at SLC has obtained a measurement of the light polarization at the 2 % level [35].

Detector	Number of "channels"	Total	Base time
BPM	3 BPM x 2 (x,y) x 2 Voltage	12	Slow
γ Calorimeter	25 crystals (25 PM, 25 ADC)	25	
EMCAl T Monitoring	6 thermal monitors x 1 Voltage	6	Slow
e^- detector	3 Silicon-Strip planes(128 channels) x 4PU (32bits)	12	
e^- detector trigger	2 plane of 6 Scintillators (6 PM, 6ADC)	12	
Magnetic Chicane	Power supply intensity	1	Slow
Laser	Power	1	Slow
Cavity	Pressure	1	Slow
Beam Pipe	Pressure	1	Slow
Diode for reflected Light	Intensity	1	Slow
Diode for transmitted Light	Intensity for the 2 polarization state	2	Slow

Table 33: ***Type of data for the Polarimeter Acquisition***

10 Data taking

As explained in section 3, we expect counting rate of a few hundred kHz. Table 33 gives an idea of the various data that will be written on tape.

11 Systematic errors

Equations (30),(41) and (50) of section 2.3 give the relationships between the electron polarization P_e and the measured (Laser polarization P_γ and asymmetry of number of Compton events A_{exp}) or theoretical (Compton longitudinal asymmetry A_l) quantities. For instance, equation (30) for one energy bin of the differential method gives

$$P_e \;=\; \frac{A_{exp}}{P_\gamma\ A_l} \;=\; \frac{(n^+ - n^-)}{(n^+ + n^-)}\ \frac{1}{P_\gamma\ A_l}\,, \tag{161}$$

where n^+ and n^- are the numbers of Compton events normalized to the same integrated luminosity $\mathcal{LT}$ for the two measurements with parallel or anti parallel polarizations of the electron and Laser beams. We will now look at the systematic effects limiting the precision on the P_e measurement : false asymmetry induced by the variation of some physical parameters between the two measurements, systematic effects on the Laser polarization P_γ and on the theoretical Compton longitudinal asymmetry A_l. We will conclude this section with the study of the change of polarization between the interacting point of the Compton polarimeter where the electron polarization is measured at the target interacting point.

11.1 False asymmetry

Equations (30),(41) and (50) are a simplification of the relationships between the electron polarization P_e and the measured quantities. The measured numbers of Compton events are given by

$$n^+ \;=\; \mathcal{L}^+\,T^+\,\epsilon^+\,\sigma^+\,(1 + P_e P_\gamma^+ A_l^+) \;=\; \mathcal{E}^+\ (1 + P_e P_\gamma^+ A_l^+)\,, \tag{162}$$

$$n^- \;=\; \mathcal{L}^-\,T^-\,\epsilon^-\,\sigma^-\ (1 - P_e P_\gamma^- A_l^-) \;=\; \mathcal{E}^-\ (1 - P_e P_\gamma^- A_l^-)\,, \tag{163}$$

where $\mathcal{E}$, the overall efficiency, stands for $\mathcal{E} = \mathcal{L}\ T\ \epsilon\ \sigma$.

To obtain equation (161), we have assumed that the integrated luminosity $\mathcal{L}T$, the efficiency ϵ, the incident energies (which act on the unpolarized cross section σ and on the Compton longitudinal asymmetry A_l) are the same for the two measurements with parallel or anti parallel polarizations as we have assumed the same amplitude for the reversed polarization P_γ.

We will now take into account the variations of these quantities which can be parametrized by the asymmetries of the overall efficiency $A_\mathcal{E}$, Laser polarization A_{P_γ} and Compton longitudinal asymmetry A_{A_l}, respectively

$$A_\mathcal{E} = \frac{\mathcal{E}^+ - \mathcal{E}^-}{\mathcal{E}^+ + \mathcal{E}^-}, \qquad A_{P_\gamma} = \frac{P_\gamma^+ - P_\gamma^-}{P_\gamma^+ + P_\gamma^-}, \qquad A_{A_l} = \frac{A_l^+ - A_l^-}{A_l^+ + A_l^-},$$

around the mean values of the overall efficiency $\mathcal{E}$, Laser polarization P_γ and mean Compton longitudinal asymmetry A_l,

$$\mathcal{E} = \frac{\mathcal{E}^+ + \mathcal{E}^-}{2}, \qquad P_\gamma = \frac{P_\gamma^+ + P_\gamma^-}{2}, \qquad A_l = \frac{A_l^+ + A_l^-}{2}.$$

The numbers of events can be rewritten as

$$n^\pm = \mathcal{E}\Big[1 \pm A_\mathcal{E}\Big] \pm \mathcal{E} P_e P_\gamma A_l \Big[1 \pm (A_\mathcal{E} + A_{P_\gamma} + A_{A_l}) + A_\mathcal{E} A_{P_\gamma} + A_\mathcal{E} A_{A_l} + A_{P_\gamma} A_{A_l} \pm A_\mathcal{E} A_{P_\gamma} A_{A_l}\Big] \tag{164}$$

and the electron polarization is now given by

$$P_e = \frac{1}{P_\gamma A_l} \frac{A_{exp} - A_\mathcal{E}}{1 + A_\mathcal{E} A_{P_\gamma} + A_\mathcal{E} A_{A_l} + A_{P_\gamma} A_{A_l} - A_{exp} A_\mathcal{E} - A_{exp} A_{P_\gamma} - A_{exp} A_{A_l} - A_{exp} A_\mathcal{E} A_{P_\gamma} A_{A_l}} \quad (165)$$

where $A_{exp} = (n^+ - n^-)/(n^+ + n^-)$ is the measured asymmetry of the number of Compton events.

When the asymmetries $A_\mathcal{E}$, A_{P_γ} and A_{A_l} are small, the equation (165) can be expanded to first order in the relative contributions of each effect :

$$P_e \simeq \frac{A_{exp}}{P_\gamma A_l} + \frac{1}{P_\gamma A_l} \left(-A_\mathcal{E} + {A_{exp}}^2 A_{P_\gamma} + {A_{exp}}^2 A_{A_l} \right). \quad (166)$$

Each term in the parenthesis is a correction to the simple expression in equation (161) and the uncertainty translates into a systematic uncertainty in electron polarization P_e.

The required precision on the overall efficiency asymmetry $\Delta A_\mathcal{E}$ is then related to the required precision on the electron polarization $\Delta P_e / P_e$ by

$$\Delta A_\mathcal{E} \leq \frac{\Delta P_e}{P_e} P_\gamma A_l P_e \simeq \frac{\Delta P_e}{P_e} A_{exp} , \quad (167)$$

while the requirement on the Laser polarization (or Compton longitudinal asymmetry) asymmetry is given by

$$\Delta A_{P_\gamma} \leq \frac{\Delta P_e}{P_e} \frac{P_\gamma A_l P_e}{A_{exp}^2} \simeq \frac{\Delta P_e}{P_e} \frac{1}{A_{exp}}. \quad (168)$$

For this experiment, we have a Laser polarization $P_\gamma = 100\%$, a Compton longitudinal asymmetry which is given roughly as a function of the beam energy by $\sqrt{< A_l^2 >} = 0.84\, E\,\%$ (Table 2) and we assume an electron polarization $P_e = 50\%$. Then for a 1 % measurement of the electron polarization $\Delta P_e / P_e$, **the requirements on the uncertainties of the asymmetries of the Laser polarization A_{P_γ}, Compton asymmetry A_{A_l} and overall efficiency $A_\mathcal{E}$** are the following :

- **uncertainty on the polarization asymmetry :** $\Delta A_{P_\gamma} \leq 2.4 \;/\; E(GeV)$,
- **uncertainty on the asymmetry of the Compton asymmetry :** $\Delta A_{A_l} \leq 2.4 \;/\; E(GeV)$,
- **uncertainty on the overall efficiency asymmetry :** $\Delta A_\mathcal{E} \leq 4\, 10^{-5}\, E(GeV)$.

The first two requirements are quite large (30 % at 8 GeV) and can be disregarded. Only the last requirement on the overall efficiency asymmetry can introduce sizeable systematic effects in our measurement. We recall here the expression of this overall efficiency using the approximated formula of the luminosity given by equation (69)

$$\mathcal{E} = \mathcal{L}\, T\, \epsilon\, \sigma \simeq \frac{2}{\sqrt{2\pi}} \frac{I_e}{e} \frac{P_L\, G}{h\, c^2} \frac{\lambda}{\sqrt{\sigma_e^2 + \sigma_\gamma^2}} \frac{1}{sin(\alpha_c)} T\, \epsilon\, \sigma , \quad (169)$$

where I_e, P_L and G are the electron beam intensity, the Laser beam power and the cavity gain, λ is the Laser wavelength, σ_e and σ_γ are the electron and laser beam size at the interacting point and where α_c is the beam crossing angle and σ the unpolarized Compton cross section. We will now distinguish between asymmetry correlated or not with the Laser polarization reversals. The second one are concerned by the general stability of each term of equation (169) and by a variation of the alignment of the two beams. The effect of such uncorrelated asymmetry can be reduced by frequent Laser polarization reversals while the correlated asymmetry had to be at the level given by equation (167).

11.1.1 False asymmetry not correlated with the Laser polarization reversals

The asymmetries which are not correlated with the Laser polarization can be reduced to an acceptable level by high frequency polarization reversals and suitable randomization of polarization reversal. Let's the overall efficiency asymmetry $A_\mathcal{E}$ be zero with a fluctuation per unit of time $dA_\mathcal{E}/dt$. The systematic and statistical (Eq. 78) errors on the polarization deduced from a pair of pulse of length Δt are

$$\frac{\Delta P_e{}^{syst}}{P_e} \simeq \frac{1}{A_{exp}} \frac{dA_\mathcal{E}}{dt} \Delta t \,, \tag{170}$$

$$\frac{\Delta P_e{}^{stat}}{P_e} \simeq \frac{1}{A_{exp}} \frac{1}{\sqrt{2\,\mathcal{L}\epsilon\sigma\,\Delta t}} \,. \tag{171}$$

After N^p pulse pairs, since the errors are uncorrelated, these equations become

$$\frac{\Delta P_e{}^{syst}}{P_e} \simeq \frac{1}{A_{exp}} \frac{\Delta t}{\sqrt{N^p}} \frac{dA_\mathcal{E}}{dt} \,, \tag{172}$$

$$\frac{\Delta P_e{}^{stat}}{P_e} \simeq \frac{1}{A_{exp}} \frac{1}{\sqrt{N^p\,\Delta t}} \frac{1}{\sqrt{2\,\mathcal{L}\epsilon\sigma}} \tag{173}$$

giving a ratio α between systematic and statistical errors

$$\alpha = \frac{\Delta P_e{}^{syst}}{\Delta P_e{}^{stat}} \simeq \frac{dA_\mathcal{E}}{dt} \Delta t^{\frac{3}{2}} \sqrt{2\,\mathcal{L}\epsilon\sigma}. \tag{174}$$

Introducing the reversal frequency $f = \frac{1}{\Delta t}$ and the Compton rate $\frac{dN_c}{dt} = \mathcal{L}\epsilon\sigma$, we get

$$\alpha = \frac{\Delta P_e{}^{syst}}{\Delta P_e{}^{stat}} \simeq \frac{dA_\mathcal{E}}{dt} \frac{1}{f^{\frac{3}{2}}} \sqrt{2\frac{dN_c}{dt}}. \tag{175}$$

Then the level of systematic error wrt the statistical error can be reduced by higher frequency reversal or by lower Compton rate (but with a longer time for the same statistical error). **For systematic error less than statistical one** ($\alpha \leq 1$)**, the fluctuation of the overall efficiency asymmetry per unit of time** $dA_\mathcal{E}/dt$ **must verify**

$$\frac{dA_\mathcal{E}}{dt} \leq f^{\frac{3}{2}} \frac{1}{\sqrt{2\frac{dN_c}{dt}}}. \tag{176}$$

Assuming the experimental conditions of section 3.4, the Compton rate is approximatively $\frac{dN_c}{dt} = 800kHz$ (Table 8) for a 100 μA electron beam intensity and for a $G = 10000$ cavity gain . Then the fluctuation of the overall efficiency $A_\mathcal{E}$ must be kept under $dA_\mathcal{E}/dt \leq 8\,10^{-4}/s$ for a reversal frequency $f = 1Hz$. For a reversal frequency $f = 10Hz(100Hz)$, this upper limit is increased to $dA_\mathcal{E}/dt \leq 2.5\,10^{-2}/s\ (8\,10^{-1}/s)$.
For lower Compton rate, the limits are still increased. For example, for a 100 nA electron beam intensity and a $G = 1000$ cavity gain (giving a Compton rate of $80Hz$), the required efficiency stability for a reversal frequency $f = 1Hz$ decreases from $dA_\mathcal{E}/dt \leq 8\,10^{-4}/s$ to $dA_\mathcal{E}/dt \leq 8\,10^{-2}/s$.
We can estimate the fluctuation of the overall efficiency $A_\mathcal{E}$ by looking at the asymmetry between two pulses of same Laser polarization. The expected statistical error, given by

$$dA = \frac{1}{\sqrt{2\frac{dN_c}{dt}\,\Delta t}}. \tag{177}$$

is the same than the error on the measured experimental asymmetry A_{exp}. Thus the final statistical errors will be the same for the Compton asymmetry A_{exp} from pulses of opposite polarization and for asymmetry from pulses of same polarization. Thus the systematic error due to the fluctuation of the overall efficiency $A_\mathcal{E}$ can be controlled with the same accuracy than the statistical errors on the electron polarization.

11.1.2 False asymmetry correlated with the Laser polarization reversals

For the asymmetries which are correlated with the Laser polarization, we need the previous limit on the overall efficiency asymmetry (Eq. 167) between two pulses of opposite polarization i.e.

$$\Delta A_\mathcal{E} \leq \frac{\Delta P_e}{P_e} P_\gamma A_l P_e \simeq \frac{\Delta P_e}{P_e} A_{exp}$$

giving, for a 1 % measurement, an uncertainty on the overall efficiency asymmetry $\Delta A_\mathcal{E} \leq 4\,10^{-5}\, E(GeV)$.
In the previous equation of the overall efficiency (Eq. 169), the electron beam intensity I_e, the electron beam spot size σ_e and the efficiency ϵ are not correlated with the Laser polarization.
The Compton cross section σ (Eq.23), given at first order by $\sigma = \pi\, {r_0}^2\, a$ where $a = 1/(1 + \frac{4kE}{m^2})$, depend on the energy k of the Laser beam and so can be correlated to the polarization reversal.
Taking into account only terms which may depend on the Laser polarization, the uncertainty on the overall efficiency asymmetry can be expressed as

$$\begin{aligned}\Delta A_\mathcal{E} &= \Delta P_L + \Delta G - \Delta\alpha_c - \Delta\sigma_\gamma \frac{1}{1+\frac{\sigma_e^2}{\sigma_\gamma^2}} + \Delta\lambda + \Delta\sigma \\ &= \Delta P_L + \Delta G - \Delta\alpha_c - \Delta\sigma_\gamma \frac{1}{1+\frac{\sigma_e^2}{\sigma_\gamma^2}} + \Delta\lambda\left(1 + \frac{4Ek}{4Ek+m^2}\right). \qquad (178)\end{aligned}$$

This uncertainty depends on the asymmetries of the Laser intensity P_L, cavity gain G, crossing angle α_c, Laser spot size σ_γ and Laser wavelength λ. We have not include here the effect of a change of the Laser beam position at the interacting point.
Each term of equation (178) has to be measured within the previous limit of $4\,10^{-5}\, E(GeV)$.

11.2 Photon beam polarization

The experimental electron polarization P_e is proportional to the photon polarization P_γ (Eq. 161). So the level of systematic in the photon polarization measurement has to be the same as the required precision on the electron polarization i.e. 1%.

11.3 Longitudinal asymmetry

The term A_l of equation (161) or (166) is in fact a more complicated function of the theoretical Compton longitudinal asymmetry. As shown in section 2.3, it has to be the mean value of the theoretical Compton longitudinal asymmetry on the scattered energy range weighted by the unpolarized Compton cross section and by the detector efficiency (Eq. 29, 39 or 49). So it depends on the resolution and on the calibration of the scattered particle detector. These effects are detailed in appendix E where approximated detector performances to reach the required precision are given. The final study of these systematic effects will be done when experimental results on the detector characteristics will be available.

Here we will only look at the effects due to the calibration of the incident beam energies. The mean asymmetries used in equations (29), (39) or (49) are, in our kinematic range, roughly proportional to the Laser and electron beam energies $A_l \propto k\,E$.
The required resolution on the Laser and electron beam energies is low : $\sigma k/k \simeq 1\,\%$ **and** $\sigma E/E \simeq 1\,\%$.

11.4 Precession of the Polarization in the Chicane

It is well known [36, 37] that the magnetic moment of an electron of spin $\vec{s}$, ($\vec{\mu} = -g\frac{e}{2m}\vec{s}$), precesses in a static magnetic field $\vec{B}$ perpendicular to the particle momentum by an angle θ_P around $\vec{B}$ given by

$$\theta_P = \theta_m \gamma \frac{g-2}{2}, \tag{179}$$

where θ_m is the electron trajectory rotation and g is the gyro-magnetic ratio for the electron,

$$\frac{g-2}{2} \simeq 1.16\ 10^{-3}. \tag{180}$$

Since our measurement of the electron beam longitudinal polarization is performed at a point followed by magnetic elements of magnetic length $\int Bdl$, the electron trajectory will be rotated by a magnetic angle $\theta_m = \frac{0.3}{p} \int Bdl$. The resulting change of the direction of the polarization θ_R is then

$$\theta_R = \theta_P + \theta_m = \theta_m \left(\gamma \frac{g-2}{2} + 1\right). \tag{181}$$

and gives for the longitudinal polarization at the target $P^T_{e||}$

$$P^T_{e||} = P^m_{e||} \cos\theta_R + P^m_{e\perp} \sin\theta_R, \tag{182}$$

where $P^m_{e||}$ and $P^m_{e\perp}$ are the measured longitudinal polarization and the transverse polarization at the Compton interacting point. According to Eq. (182), the measurement of the longitudinal polarization $P^m_{e||}$, of the transverse polarization $P^m_{e\perp}$ and of the polarization rotation angle θ_R are needed to determine the polarization on the Target. The systematic uncertainty is given by

$$\sigma(P^T_{e||}) = \sqrt{\sigma^2(\theta_R)\left[-P^m_{e||}\sin\theta_R + P^m_{e\perp}\cos\theta_R\right]^2 + \sigma^2(P^m_{e\perp})\sin^2\theta_R}. \tag{183}$$

The transverse polarization $P^m_{e\perp}$ is not measured at the Compton interaction point. If the measured longitudinal polarization $P^m_{e||}$ is high (> 50 %), we can only assume $\frac{P^m_{e\perp}}{P^m_{e||}} \leq 1$, ($P^2_{e\perp} + P^2_{e||} \leq 1$) and $\sigma(P^m_{e\perp}) = P^m_{e\perp}$.
Furthermore we plan to set to zero the magnetic rotation angle θ_m of the elements after the Compton interaction point within a measured accuracy $\sigma(\theta_m)$ close to the $0.5\ mrad$. For the resulting polarization rotation angle, this gives $\sigma(\theta_R)$ between $1.6\ mrad$ at $1\ GeV$ and $9.6\ mrad$ at $8\ GeV$.
Then, assuming $\theta_R \simeq \sigma(\theta_R) << 1$ and $\sigma(P^m_{e\perp}) = P^m_{e\perp}$, Eq. 183 can be rewritten as

$$\begin{aligned}\frac{\sigma(P^T_{e||})}{P^T_{e||}} &= \sqrt{\sigma^2(\theta_R)\left[-\tan\theta_R + \frac{P^m_{e\perp}}{P^m_{e||}}\right]^2 + \left[\frac{P^m_{e\perp}}{P^m_{e||}}\right]^2 \tan^2\theta_R} \\ &\leq \sqrt{\sigma^2(\theta_R)\left[\frac{P^m_{e\perp}}{P^m_{e||}}\right]^2 + \left[\frac{P^m_{e\perp}}{P^m_{e||}}\right]^2 \sigma^2(\theta_R)}\end{aligned} \tag{184}$$

So even with a relative transverse polarization as high as $\frac{P^m_{e\perp}}{P^m_{e\parallel}} = 1$, the systematic effect due to the precession,

$$\frac{\sigma(P^T_{e\parallel})}{P^T_{e\parallel}} \leq \sqrt{2}\,\sigma(\theta_R)\left[\frac{P^m_{e\perp}}{P^m_{e\parallel}}\right], \tag{185}$$

can be kept under the required precision if the electron trajectory rotation after the Compton interacting point is small.

For a zero magnetic rotation angle θ_m within a measured accuracy $\sigma(\theta_m) = 0.5\ mrad$, the relative error on the polarization lies between $\frac{\sigma(P^T_e)}{P^T_e} = 0.2\%$ at $1\ GeV$ to 1.3% at $8\ GeV$.

A CEBAF beam in Hall A

A.1 Beam Parameters

First estimates of the beam size at the Compton polarimeter location [38] in the normal mode (i.e. achromatic mode) give a beam spot size approximately the same as that on the target i.e. $4\,\sigma_e = 140\mu$.

In the dispersive mode, since the dispersion is quite large at this point (nearly $12m$), the beam spot size at the position of the Compton polarimeter will be quite large, roughly a little more than $1.2mm$.

In the normal mode, 4 Quads (Q17, Q18, Q19 and Q20) are located upstream the Compton Polarimeter. They can easily be tuned so that the size of the electron beam at the Compton IP is close to $\sigma_e = 50\ \mu m$. The question of the focalisation at the same time on the target ($\sigma_e = 35\ \mu m$) has been investigated by V. Lebedev from the accelerator division. After the Möller polarimeter commissioning, there will be 10 m downstream the Compton polarimeter, 3 (and may be 4) Möller Quads QA1H01, QA1H02 and QA1H03 (QA1H04). QA1H01 is a standard Cebaf Quad, whereas QA1H02 and QA1H03 are 4" Quads. QA1H01, QA1H02 and QA1H03 (but not QA1H04) will be used also as beam line quads[39]. The study performed by V. Lebedev assumed a beam emittance of $\epsilon_x = \epsilon_y = 10^{-9}\ mrad$ and an energy dispersion $\frac{\Delta p}{p} = 2.5\,10^{-5}$. The four 30 cm upstream Quads (Q17, Q18, Q19 and Q20) were tuned to the field values $1.53\ kG/cm$, $-0.92\ kG/cm$, $-2.31\ kG/cm$ and $2\ kG/cm$. Downstream the Compton polarimeter, 4 Quads (Q23, Q24, Q25 and Q26) with 30 cm, 35.92 cm, 35.92 cm, and 35.92 cm length were used to refocus on the target in ESA. The field gradients were $1.05\ kG/cm$, $-0.91\ kG/cm$, $-0,91\ kG/cm$ and $1.05\ kG/cm$. As depicted on figure 38, (See also table 34) the focalisation at the compton IP and at the target is $\sigma_x = \sigma_y \simeq 60\mu m$.

A.2 Beam Stability

An other important feature is the beam stability. V. Lebedev from the accelerator division states that the beam stability in Arc 1 is about 100 μ (for 10m) at 60 Hz. In one to two years time frame, a feedback system will be installed to suppress the 60 Hz noise and reach a level of about 10-20 μ (per 10m). At any particular point (say, at Compton entrance), the feedback can be adjusted to be at least this level, and maybe better for shorter distance.

A.3 Beam Requirements at the target in ESA

The Physic division beam requirement to the accelerator division are summarized in table 35. The beam emittance is quite good $0.4\,10^{-9} mrad \leq \epsilon_{x,y} = \sigma_{x,y}\sigma_{x',y'} \leq 2.5\,10^{-9} mrad$. The beam halo at 5σ being only $\leq 1\,10^{-6}$ of total current, we are confident that the location of the mirrors cavity (5mm away from the electron beam) is a safe position.

A.4 Beam Position Monitor Specifications

The BPM specifications are summarized in table 36. These specifications are in good agreement with our requirements for beam direction and position localization at Compton IP.

A.5 Polarized source

The source[40] is a classic GaAs that is a first cousin of the Peggy II source at SLAC, but it will be enhanced considerably with the latest important change being an RF laser drive that produces the charge

```
OptiM
# CEBAF Hall A beam Line
Energy[MeV]=4050   Mass[MeV]=0.511   Hr[kG*cm]=13511
Emittance: ex[cm]=1e-07  ey[cm]=1e-07  DP/P=2.5e-05
Initial: BetaX[cm]=1000  BetaY[cm]=1000
AlfaX=0  AlfaY=0
DispersX[cm]=0  DispersY[cm]=0
Dsp_PrimeX=0  DspPrimeY=0
X[cm]=0  Y[cm]=0  Z[cm]=0  S[cm]=0
tetaX[deg]=0  tetaY[deg]=0
#
begin lattice. Number of periods=1
o1a  dMLA1C02 be1  o1b QA1C01 o2 QA1C02 o3 QA1C03 o4a   be1 dMBN1C04  o4b
#AMATCH
QA1C04 o5 QA1C05 o6 QA1C06 o7 QA1C07 o8
#ACHRO360
 QF o9a SD  o9b  be dMBA1C  be  o9c    QD o9a SF  o9b  be  dMBA1C  be o9c
 QF o9a SD  o9b  be dMBA1C  be  o9c    QD o9a SF  o9b  be  dMBA1C  be o9c
 QF o9a SD  o9b  be dMBA1C  be  o9c    QD o9a SF  o9b  be  dMBA1C  be o9c
 QF o9a SD  o9b  be dMBA1C  be  o9c    QD o9a SF  o9b  be  dMBA1C  be
# Match and S-Harps
O17 ds1 O17a Q17 O18 Q18 O19
#   Compton polarimeter focusing
Q19 O20 Q20
#CHICANE, 12 m
O21 bp O23b bm O23c bm O23b bp
#  Final Focus
O23d O23e Q23 O24 Q24 O25 Q25 O26 Q26 O27
#odump
end lattice
#-----------------------------------------------
begin list
O17          L[cm]=60
ds1          L[cm]=60     B[kG]=0
O17a         L[cm]=205
O18          L[cm]=50
Q17          L[cm]=30     G[kG/cm]=1.52901  Tilt[deg]=0
Q18          L[cm]=30     G[kG/cm]=-0.92  Tilt[deg]=0
Q19          L[cm]=30     G[kG/cm]=-2.31  Tilt[deg]=0
Q20          L[cm]=30     G[kG/cm]=2  Tilt[deg]=0
O19          L[cm]=490
O20          L[cm]=50
O21          L[cm]=105.7
bp           L[cm]=100    B[kG]=7.5    G[kG/cm]=0   Tilt[deg]=90
bm           L[cm]=100    B[kG]=-7.5    G[kG/cm]=0   Tilt[deg]=90
O23b         L[cm]=440
O23c         L[cm]=230
O23d         L[cm]=250
O23e         L[cm]=495
Q23          L[cm]=30     G[kG/cm]=1.05 Tilt[deg]=0
O24          L[cm]=87.04
Q24          L[cm]=35.92     G[kG/cm]=-0.91  Tilt[deg]=0
O25          L[cm]=54.08
Q25          L[cm]=35.92     G[kG/cm]=-0.91  Tilt[deg]=0
O26          L[cm]=54.08
Q26          L[cm]=35.92     G[kG/cm]=1.05  Tilt[deg]=0
O27          L[cm]=1512.04
odump        L[cm]=5000
# Match and Arc drifts
o1a          L[cm]=45
o1b          L[cm]=1200
o2           L[cm]=200
o3           L[cm]=200
o4a          L[cm]=1200
o4b          L[cm]=100
o5           L[cm]=300
o6           L[cm]=700
o7           L[cm]=500
o8           L[cm]=580
o9a          L[cm]=34.5
o9b          L[cm]=60.5
o9c          L[cm]=80
# Match and Arc Dipoles
dMLA1C02     L[cm]=99     B[kG]=3.76786
dMBN1C04     L[cm]=99     B[kG]=3.76786
be1          L[cm]=1     B[kG]=3.76786     G[kG/cm]=-0.10524
Tilt[deg]=0
dMBA1C       L[cm]=298     B[kG]=3.36557
be           L[cm]=1     B[kG]=3.36557     G[kG/cm]=-0.12598
Tilt[deg]=0
#  QUADRUPOLES for Match
QA1C01       L[cm]=30     G[kG/cm]=0.883351  Tilt[deg]=0
QA1C02       L[cm]=30     G[kG/cm]=-1.38964  Tilt[deg]=0
QA1C03       L[cm]=30     G[kG/cm]=0.883351  Tilt[deg]=0
QA1C04       L[cm]=30     G[kG/cm]=1.11014  Tilt[deg]=0
QA1C05       L[cm]=30     G[kG/cm]=-1.20162  Tilt[deg]=0
QA1C06       L[cm]=30     G[kG/cm]=1.05151  Tilt[deg]=0
QA1C07       L[cm]=30     G[kG/cm]=-1.46159  Tilt[deg]=0
#QUAD VALS FOR 90 DEGREE ACHROMATIC ARC
QF           L[cm]=30     G[kG/cm]=1.26988  Tilt[deg]=0
QD           L[cm]=30     G[kG/cm]=-1.36836  Tilt[deg]=0
#SEXTUPOLES FOR ARC TO ACHIEVE SECOND ORDER ACHROMAT
SD           L[cm]=15     S[kG/cm/cm)]=-0.0082733
SF           L[cm]=15     S[kG/cm/cm)]=0.0144618
end list of elements
```

Table 34: ***Beam line description*** *from V. Lebedev, showing focalisation both at Compton IP and the ESA target.*

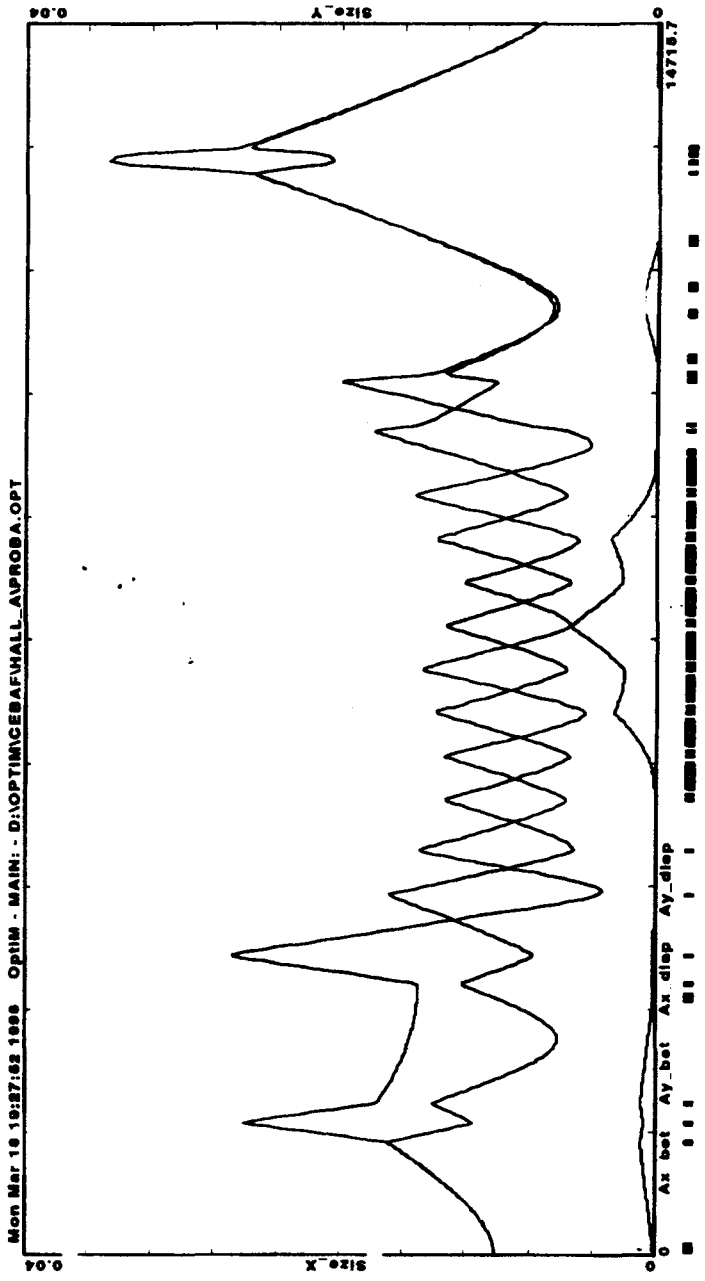

Figure 38: ***Beam envelope*** *from V. Lebedev, showing focalisation both at Compton IP and the ESA target.*

Parameter	Nominal value and Range	Stability (hours)
RMS spot size [1]	$20\mu m \leq \sigma_x \leq 50\mu m$	25 % of value
$1\,\sigma$	$20\mu m \leq \sigma_y \leq 50\mu m$	25 % of value
Angular divergence	$\sigma_{x'} \leq 100\mu r$	25 % of value
$1\,\sigma$	$\sigma_{y'} \leq 100\mu r$	25 % of value
Beam Position	$0\mu m$ wrt optic axis	25 % RMS spot size
Beam Direction	$0\mu r$ wrt optic axis	25 % RMS angular divergence
Energy (average)	0.5-4 GeV	$3\,10^{-4}$
Energy Spectrum (1σ)	$\sigma_E/E = 5\,10^{-5}$	25 % of value
Beam Halo	$\leq 1\,10^{-6}$ of total current at 5σ	
Current	$40nA \leq I_e \leq 190\mu A$	$\pm 10\%$
Polarization	$\geq 35\%$ bulk GaAs $I_e = 100\mu A$	$\pm 10\%$
	$\geq 75\%$ strained cathode $I_e = 30\mu A$	$\pm 10\%$
Duty Cycle	90 %	
rastering	$\geq 100\mu m$ rastered beam spot size	
	$\leq 1cm$ beam position stability	

Table 35: ***Physic Division Beam requirements***

Quantity	Description	Specification
Relative accuracy	$1\,\sigma$	50 μm
Absolute accuracy	$1\,\sigma$	Calibrate to $\leq$ 50 μm
Measurement time		1 s (8 $msec$ required for Parity, $100\mu s$ desired)
Time scale	time over which the specifications must hold	1 hour
Operating current		1-200 μA
Operating position		$\pm 5mm$
X-Y coupling		$\leq 50\mu m$ *per* mmX

Table 36: ***BPM Specifications***

bunches directly at the photo-cathode.

As for the characteristics of the beam - it will have the same (or possibly better) emittance, energy spread etc as the "standard" CEBAF beam, and the nominal helicity structure will probably be "flipping" at 1/30 of a second (the usual randomized pattern with an equal number of groups with each helicity so the average is zero). Other helicity flip rates can in principle be accommodated, but doing it much faster than proposed here may cause difficulties that should be discussed.

B Luminosity generalities

The total luminosity for the interaction of the laser and the electron beams is (eq. 61)

$$\mathcal{L} = \int\int\int v_{rel}\, \rho_e\, \rho_\gamma\, dz\, dx\, dy\,, \tag{186}$$

where the relative velocity of the two beams is $v_{rel} = c(1+cos(\alpha_c))$ with α_c crossing angle and where ρ_e, ρ_γ are the electron and laser beam's densities.

As already mentioned in the section 3.1, **the beam density in beam frame** (x', y', z' where z' is along the beam axis) (eq. 56) is taken as the product of two normalized gaussians in x' and y' with a normalization factor N_0 i.e.

$$\rho(x', y', z') = N_0\ \frac{1}{\sqrt{2\pi}\sigma_x(z')}\ exp\left(-\frac{x'^2}{2\sigma_x^2(z')}\right)\ \frac{1}{\sqrt{2\pi}\sigma_y(z')}\ exp\left(-\frac{y'^2}{2\sigma_y^2(z')}\right), \tag{187}$$

where $\sigma_x(z')$ and $\sigma_y(z')$ are the x' and y' beam sizes at z'.

The evolution along z' of these beam sizes (Eq. 57) is characterized by the waist beam sizes $\sigma(0)$ (taking the beam waist as the origin of the beam frame) and the angular divergence ϵ (parametrized by the Rayleigh range Z).

$$\sigma_{x,y}^2(z') = \sigma_{x,y}^2(0)\quad \left(1. + \frac{z'^2}{Z_{x,y}^2}\right). \tag{188}$$

So that the waist size and the asymptotic angular divergence are

$$d(0)\ =\ 2\sigma(0)\qquad ,\qquad tan(\epsilon)\ =\ \sigma(0)/Z\,. \tag{189}$$

The normalization factors for the electron beam (intensity I_e) and for the Laser beam (power P_L and wavelength λ) are deduced from :

$$\frac{dN_\gamma}{dt} = \frac{P_L}{h\,\nu} = \frac{N_{0\gamma}\ \int\int\int \rho_\gamma\, dz\, dx\, dy}{dt} = \frac{N_{0\gamma}\int dz}{dt} = \frac{N_{0\gamma}\, c\, dt}{dt} = N_{0\gamma}\, c, \tag{190}$$

$$\frac{dN_e}{dt} = \frac{I_e}{e} = \frac{N_{0e}\ \int\int\int \rho_e\, dz\, dx\, dy}{dt} = \frac{N_{0e}\int dz}{dt} = \frac{N_{0e}\, c\, dt}{dt} = N_{0e}\, c, \tag{191}$$

leading to (also referenced as Eq. 60 and 59)

$$N_{0e}\ =\ \frac{I_e}{e\,c}\qquad ,\qquad N_{0\gamma}\ =\ \frac{P_L\,\lambda}{h\,c^2}\,. \tag{192}$$

B.1 Luminosity for zero beam crossing angle

When the crossing angle α_c between the electron and Laser beams is zero, the electron and Laser beam frames are the same. Assuming that the Laser and electron beam waists are the same and using $\sigma_{x,y}(0) = \sigma_{x,y}$, the differential luminosity is thus given by

$$\begin{aligned}\frac{d\mathcal{L}}{dz\,dx\,dy}\ &=\ c(1+cos\alpha_c)\, N_{0e}\, N_{0\gamma}\\ &\frac{1}{2\pi}\frac{1}{\sigma_e^x\sigma_\gamma^x}\ \frac{1}{\sqrt{1+\frac{z^2}{Z_e^{x2}}}}\ \frac{1}{\sqrt{1+\frac{z^2}{Z_\gamma^{x2}}}}\ exp\left[-\frac{x^2}{2}\left(\frac{1}{\sigma_e^{x2}\left(1+\frac{z^2}{Z_e^{x2}}\right)}+\frac{1}{\sigma_\gamma^{x2}\left(1+\frac{z^2}{Z_\gamma^{x2}}\right)}\right)\right]\\ &\frac{1}{2\pi}\frac{1}{\sigma_e^y\sigma_\gamma^y}\ \frac{1}{\sqrt{1+\frac{z^2}{Z_e^{y2}}}}\ \frac{1}{\sqrt{1+\frac{z^2}{Z_\gamma^{y2}}}}\ exp\left[-\frac{y^2}{2}\left(\frac{1}{\sigma_e^{y2}\left(1+\frac{z^2}{Z_e^{y2}}\right)}+\frac{1}{\sigma_\gamma^{y2}\left(1+\frac{z^2}{Z_\gamma^{y2}}\right)}\right)\right].\end{aligned} \tag{193}$$

The differential luminosity along the beam axis z is obtained after integration over the transverse coordinates x and y of the beam densities $\frac{d\mathcal{L}}{dz} = \int\int v_{rel}\,\rho_e\,\rho_\gamma\,dx\,dy$ giving :

$$\frac{d\mathcal{L}}{dz} = 2c\,N_{0e}\,N_{0\gamma}\,\frac{1}{2\pi}\frac{1}{\sigma_e^x\sigma_\gamma^x}\,\frac{1}{\sqrt{1+\frac{z^2}{Z_e^{x2}}}}\,\frac{1}{\sqrt{1+\frac{z^2}{Z_\gamma^{x2}}}}\,\sqrt{2\pi}\,\frac{1}{\sqrt{\frac{1}{\sigma_e^{x2}\left(1+\frac{z^2}{Z_e^{x2}}\right)}+\frac{1}{\sigma_\gamma^{x2}\left(1+\frac{z^2}{Z_\gamma^{x2}}\right)}}}$$

$$\frac{1}{2\pi}\frac{1}{\sigma_e^y\sigma_\gamma^y}\,\frac{1}{\sqrt{1+\frac{z^2}{Z_e^{y2}}}}\,\frac{1}{\sqrt{1+\frac{z^2}{Z_\gamma^{y2}}}}\,\sqrt{2\pi}\,\frac{1}{\sqrt{\frac{1}{\sigma_e^{y2}\left(1+\frac{z^2}{Z_e^{y2}}\right)}+\frac{1}{\sigma_\gamma^{y2}\left(1+\frac{z^2}{Z_\gamma^{y2}}\right)}}},$$

and finally

$$\frac{d\mathcal{L}}{dz} = 2c\,N_{0e}\,N_{0\gamma}\,\frac{1}{2\pi}\,\frac{1}{\sqrt{\sigma_e^{x2}+\sigma_\gamma^{x2}+z^2\left(\frac{\sigma_e^{x2}}{Z_e^{x2}}+\frac{\sigma_\gamma^{x2}}{Z_\gamma^{x2}}\right)}}\,\frac{1}{\sqrt{\sigma_e^{y2}+\sigma_\gamma^{y2}+z^2\left(\frac{\sigma_e^{y2}}{Z_e^{y2}}+\frac{\sigma_\gamma^{y2}}{Z_\gamma^{y2}}\right)}}. \quad (194)$$

Assuming now that the electron and Laser beams are symmetric in x and y (i.e. $\sigma^x = \sigma^y = \sigma$ and $Z^x = Z^y = Z$), we obtain finally the differential luminosity along the beam direction $\frac{d\mathcal{L}}{dz}$ for zero crossing beams

$$\boxed{\frac{d\mathcal{L}}{dz} = 2c\,N_{0e}\,N_{0\gamma}\,\frac{1}{2\pi}\,\frac{1}{\sigma_e^2+\sigma_\gamma^2+z^2\left(\frac{\sigma_e^2}{Z_e^2}+\frac{\sigma_\gamma^2}{Z_\gamma^2}\right)}.} \quad (195)$$

The total luminosity $\mathcal{L}_T$ is given in this case (beams symmetric in x and y) by

$$\mathcal{L}_T = 2c\,N_{0e}\,N_{0\gamma}\,\frac{1}{2\pi}\,\frac{1}{\left(\frac{\sigma_e^2}{Z_e^2}+\frac{\sigma_\gamma^2}{Z_\gamma^2}\right)}\int\frac{1}{z^2+\frac{\sigma_e^2+\sigma_\gamma^2}{\left(\frac{\sigma_e^2}{Z_e^2}+\frac{\sigma_\gamma^2}{Z_\gamma^2}\right)}}\,dz;$$

$$\mathcal{L}_T = 2c\,N_{0e}\,N_{0\gamma}\,\frac{1}{2\pi}\,\frac{1}{\left(\frac{\sigma_e^2}{Z_e^2}+\frac{\sigma_\gamma^2}{Z_\gamma^2}\right)}\,\frac{\pi}{\sqrt{\frac{\sigma_e^2+\sigma_\gamma^2}{\left(\frac{\sigma_e^2}{Z_e^2}+\frac{\sigma_\gamma^2}{Z_\gamma^2}\right)}}}. \quad (196)$$

Using equation (192) for the beam normalization, one gets for the total luminosity at zero crossing angle and for beams symmetric in x and y

$$\boxed{\mathcal{L}_T = \frac{I_e}{e}\,\frac{P_L\,\lambda}{h\,c^2}\,\frac{1}{\sqrt{\left(\sigma_e^2+\sigma_\gamma^2\right)\left(\frac{\sigma_e^2}{Z_e^2}+\frac{\sigma_\gamma^2}{Z_\gamma^2}\right)}}.} \quad (197)$$

The partial luminosity $\mathcal{L}_p(L)$ (luminosity for 2 beams crossing over a length L) can be written using equation (195)

$$\mathcal{L}_p(L) = 2c\,N_{0e}\,N_{0\gamma}\,\frac{1}{2\pi}\,\frac{1}{\left(\frac{\sigma_e^2}{Z_e^2}+\frac{\sigma_\gamma^2}{Z_\gamma^2}\right)}\int_{-L/2}^{L/2}\frac{1}{z^2+\frac{\sigma_e^2+\sigma_\gamma^2}{\left(\frac{\sigma_e^2}{Z_e^2}+\frac{\sigma_\gamma^2}{Z_\gamma^2}\right)}}\,dz.$$

The integration gives

$$\mathcal{L}_p(L) = 2c\,N_{0e}\,N_{0\gamma}\,\frac{1}{2\pi}\,\frac{2}{\sqrt{\left(\frac{\sigma_e^2}{Z_e^2}+\frac{\sigma_\gamma^2}{Z_\gamma^2}\right)(\sigma_e^2+\sigma_\gamma^2)}}\,\tan^{-1}\left(\frac{L}{2}\sqrt{\frac{\sigma_e^2+\sigma_\gamma^2}{\left(\frac{\sigma_e^2}{Z_e^2}+\frac{\sigma_\gamma^2}{Z_\gamma^2}\right)}}\right);$$

$$\mathcal{L}_p(L) = \frac{I_e}{e}\,\frac{P_L\,\lambda}{h\,c^2}\,\frac{1}{\pi}\,\frac{2}{\sqrt{\left(\frac{\sigma_e^2}{Z_e^2}+\frac{\sigma_\gamma^2}{Z_\gamma^2}\right)(\sigma_e^2+\sigma_\gamma^2)}}\,\tan^{-1}\left(\frac{L}{2}\sqrt{\frac{\sigma_e^2+\sigma_\gamma^2}{\left(\frac{\sigma_e^2}{Z_e^2}+\frac{\sigma_\gamma^2}{Z_\gamma^2}\right)}}\right). \tag{198}$$

The interaction length $L_{int}(\kappa)$ is defined as the length containing a fraction κ of the total luminosity (Eq. 197). This fraction is given by

$$\kappa = \frac{\mathcal{L}(L)}{\mathcal{L}} = \frac{2}{\pi}\,\tan^{-1}\left(\frac{L}{2}\sqrt{\frac{\sigma_e^2+\sigma_\gamma^2}{\left(\frac{\sigma_e^2}{Z_e^2}+\frac{\sigma_\gamma^2}{Z_\gamma^2}\right)}}\right), \tag{199}$$

so that one gets for the interaction length

$$\boxed{L_{int}(\kappa) = tan\left(\frac{\pi\kappa}{2}\right)\sqrt{\frac{\left(\frac{\sigma_e^2}{Z_e^2}+\frac{\sigma_\gamma^2}{Z_\gamma^2}\right)}{\sigma_e^2+\sigma_\gamma^2}}.} \tag{200}$$

B.2 Luminosity for non zero beam crossing angle

When the crossing angle α_c between the electron and Laser beams differs from zero, we define the xz plane of the laboratory frame as the crossing plane and the z axis as the mean beam axis. The angle between the electron (resp. Laser) beam and the z axis is $\alpha = \alpha_c/2$ (resp. -α). Thus the differential luminosity is given by

$$\frac{d\mathcal{L}}{dz\,dx\,dy} = c\,(1+cos\alpha_c)\,N_{0e}\,N_{0\gamma}$$
$$\frac{1}{2\pi}\,\frac{1}{\sigma_e^x\sigma_\gamma^x}\,exp\left[-\frac{(xcos\alpha+zsin\alpha)^2}{2\sigma_e^{x2}}\right]exp\left[-\frac{(xcos\alpha-zsin\alpha)^2}{2\sigma_\gamma^{x2}}\right]$$
$$\frac{1}{2\pi}\,\frac{1}{\sigma_e^y\sigma_\gamma^y}\,exp\left[-\frac{y^2}{2}\left(\frac{1}{\sigma_e^{y2}}+\frac{1}{\sigma_\gamma^{y2}}\right)\right]. \tag{201}$$

In these equations, the beam sizes depend on the coordinates x and z according to

$$\sigma_e^2 = \sigma_e^2(0)\left(1.+\frac{(-xsin\alpha+zcos\alpha)^2}{Z_e^2}\right) \quad , \quad \sigma_\gamma^2 = \sigma_\gamma^2(0)\left(1.+\frac{(xsin\alpha+zcos\alpha)^2}{Z_\gamma^2}\right).$$

The integration over y gives

$$\frac{d\mathcal{L}}{dz\,dx} = c(1+cos\alpha_c)\,N_{0e}\,N_{0\gamma}\;\frac{1}{2\pi}\frac{1}{\sigma_e^y\sigma_\gamma^y}\;\sqrt{2\pi}\sqrt{\frac{1}{\frac{1}{\sigma_e^{y2}}+\frac{1}{\sigma_\gamma^{y2}}}}$$
$$\frac{1}{2\pi}\frac{1}{\sigma_e^x\sigma_\gamma^x}\;exp\left[-\frac{(xcos\alpha+zsin\alpha)^2}{2\sigma_e^{x2}}\right]\;exp\left[-\frac{(xcos\alpha-zsin\alpha)^2}{2\sigma_\gamma^{x2}}\right];$$

$$\frac{d\mathcal{L}}{dz\,dx} = c(1+cos\alpha_c)\,N_{0e}\,N_{0\gamma}\;\frac{1}{\sqrt{2\pi}}\sqrt{\frac{1}{\sigma_e^{y2}+\sigma_\gamma^{y2}}}$$
$$\frac{1}{2\pi}\frac{1}{\sigma_e^x\sigma_\gamma^x}\;exp\left[-\frac{(xcos\alpha+zsin\alpha)^2}{2\sigma_e^{x2}}\right]\;exp\left[-\frac{(xcos\alpha-zsin\alpha)^2}{2\sigma_\gamma^{x2}}\right];$$

$$\frac{d\mathcal{L}}{dz\,dx} = c(1+cos\alpha_c)\,N_{0e}\,N_{0\gamma}\;\frac{1}{\sqrt{2\pi}}\sqrt{\frac{1}{\sigma_e^{y2}+\sigma_\gamma^{y2}}}\;\frac{1}{2\pi}\frac{1}{\sigma_e^x\sigma_\gamma^x}\;exp\left[-\frac{z^2sin^2\alpha}{2}\left(\frac{1}{\sigma_e^{x2}}+\frac{1}{\sigma_\gamma^{x2}}\right)\right]$$
$$exp\left[-\frac{x^2cos^2\alpha}{2}\left(\frac{1}{\sigma_e^{x2}}+\frac{1}{\sigma_\gamma^{x2}}\right)\right]\;exp\left[-xzcos\alpha sin\alpha\left(\frac{1}{\sigma_e^{x2}}-\frac{1}{\sigma_\gamma^{x2}}\right)\right]. \qquad (202)$$

We assume now that the beam sizes $\sigma^{x,y}$ are constant over the crossing length (i.e. the beam angular divergences are small wrt to the crossing angle α_c). This is the case in our experiment where the beam angular divergences are $\leq 100\ \mu rad$ (See appendix A) while the crossing angle is equal to $\alpha_c = 20\ mrad$.

The integration over the transverse coordinate x gives the differential luminosity along the beam axis $\frac{d\mathcal{L}}{dz}$:

$$\frac{d\mathcal{L}}{dz} = c(1+cos\alpha_c)\,N_{0e}\,N_{0\gamma}\frac{1}{\sqrt{2\pi}}\sqrt{\frac{1}{\sigma_e^{y2}+\sigma_\gamma^{y2}}}\frac{1}{2\pi}\frac{1}{\sigma_e^x\sigma_\gamma^x}\;exp\left[-\frac{z^2sin^2\alpha}{2}\left(\frac{1}{\sigma_e^{x2}}+\frac{1}{\sigma_e^{x2}}\right)\right]$$
$$\sqrt{\frac{2\pi}{cos^2\alpha\left(\frac{1}{\sigma_e^{x2}}+\frac{1}{\sigma_e^{x2}}\right)}}\;exp\left[\frac{z^2sin^2\alpha}{2\left(\sigma_e^{x2}+\sigma_\gamma^{x2}\right)}\frac{\left(\sigma_e^{x2}-\sigma_\gamma^{x2}\right)^2}{\sigma_e^{x2}\sigma_\gamma^{x2}}\right].$$

where we have used

$$\int exp\left(-ax^2\right)\;exp(-2bx)\,dx = \sqrt{\frac{\pi}{a}}\,exp\left(\frac{b^2}{a}\right).$$

Finally one gets for **the differential luminosity along the beam axis**

$$\boxed{\frac{d\mathcal{L}}{dz} = c\frac{1+cos\alpha_c}{cos\alpha}\,N_{0e}\,N_{0\gamma}\frac{1}{2\pi}\;\sqrt{\frac{1}{\sigma_e^{y2}+\sigma_\gamma^{y2}}}\;\sqrt{\frac{1}{\sigma_e^{x2}+\sigma_\gamma^{x2}}}\;exp\left[-\frac{2z^2sin^2\alpha}{\sigma_e^{x2}+\sigma_\gamma^{x2}}\right].} \qquad (203)$$

The total luminosity is given by the integration over z

$$\begin{aligned}
\mathcal{L} &= c\,\frac{1+cos\alpha_c}{cos\alpha}\,N_{0e}\,N_{0\gamma}\,\frac{1}{2\pi}\,\sqrt{\frac{1}{\sigma_e^{y2}+\sigma_\gamma^{y2}}}\,\sqrt{\frac{1}{\sigma_e^{x2}+\sigma_\gamma^{x2}}}\,\sqrt{2\pi}\sqrt{\frac{\sigma_e^{x2}+\sigma_\gamma^{x2}}{4sin^2\alpha}} \\
\mathcal{L} &= c\,\frac{1+cos\alpha_c}{2sin\alpha cos\alpha}\,N_{0e}\,N_{0\gamma}\,\frac{1}{\sqrt{2\pi}}\,\sqrt{\frac{1}{\sigma_e^{y2}+\sigma_\gamma^{y2}}} \\
\mathcal{L} &= c(1+cos\alpha_c)\,N_{0e}\,N_{0\gamma}\,\frac{1}{\sqrt{2\pi}}\,\sqrt{\frac{1}{\sigma_e^{y2}+\sigma_\gamma^{y2}}}\,\frac{1}{sin\alpha_c}.
\end{aligned}$$

Using equation (192) for the beam normalization, one gets for **the total luminosity**

$$\boxed{\mathcal{L} = \frac{I_e}{e}\,\frac{P_L\,\lambda}{h\,c^2}\,\frac{(1+cos\alpha_c)}{\sqrt{2\pi}}\,\sqrt{\frac{1}{\sigma_e^{y2}+\sigma_\gamma^{y2}}}\,\frac{1}{sin\alpha_c}.} \tag{204}$$

The differential luminosity (Eq. 203) can be rewritten as

$$\frac{d\mathcal{L}}{dz} = c\,\frac{1+cos\alpha_c}{cos\alpha}\,N_{0e}\,N_{0\gamma}\,\frac{1}{2\pi}\,\sqrt{\frac{1}{\sigma_e^{y2}+\sigma_\gamma^{y2}}}\,\sqrt{\frac{1}{\sigma_e^{x2}+\sigma_\gamma^{x2}}}\,exp\left[-\frac{z^2}{2\sigma_I^2}\right];$$

where the gaussian width σ_I, related to the interaction length L_{int}, is given by

$$\sigma_I = \frac{L_{int}}{2} = \frac{\sqrt{\sigma_e^{x2}+\sigma_\gamma^{x2}}}{2sin\alpha}. \tag{205}$$

Without the previous assumptions about the z evolution of the beam sizes, the differential luminosity $\frac{d\mathcal{L}}{dz}$ was obtained by the numerical integration of $\frac{d\mathcal{L}}{dzdx}$ given by equation (202). A second numerical integration over z gives in this case the total luminosity. In our case, the results obtained with these numerical integrations are well approximated (within 10^{-3}) by the equations 203 and 204.

C Synchrotron generalities

In this section devoted to the synchrotron radiation, we give, with the main characteristics of the radiation, the angular and spectral power density. More precise information can be found in the article of A. Hofmann [41].

C.1 Total Power

For an electron of energy E and mass m on a circular trajectory of bending radius $R(m) = p(eV)/cB(T)$, the total power radiated by the electron is :

$$P_0 = \frac{2r_0 c m_e c^2}{3} \frac{\beta^4 \gamma^4}{R^2}, \tag{206}$$

corresponding to a number of gamma per second dn_γ/dt of mean energy $< \epsilon >$ given by

$$\frac{dn_\gamma}{dt} = \frac{P_0}{< \epsilon > e} = \frac{5 r_0 m_e c^2}{2\sqrt{3}} \frac{2\pi}{he} \frac{\beta^4 \gamma}{R}, \tag{207}$$

$$< \epsilon >= \frac{4}{5\sqrt{3}} \frac{hc}{2\pi} \frac{\gamma^3}{R}. \tag{208}$$

We can also define the critical energy as :

$$\epsilon_c = \frac{15\sqrt{3}}{8} < \epsilon > . \tag{209}$$

C.2 Full Angular Power Density

The full angular power density radiated by the electron is :

$$\frac{\partial^2 P}{\partial \phi \partial cos\theta} = P_0 \frac{3}{8\pi} \frac{1}{\gamma^4} \frac{1}{(1 - \beta \cos\theta)^3} \left[1 - \frac{\sin^2\theta \cos^2\phi}{\gamma^2 (1 - \beta \cos\theta)^2} \right], \tag{210}$$

where θ and ϕ are the polar angles wrt beam direction. The total power radiated by the electron P_0, the mean energy $< \epsilon >$ and the critical energy ϵ_c are given by equations 206, 208 and 209.

For the ultra relativistic case, we get approximatively :

$$\frac{\partial^2 P}{\partial \phi \partial cos\theta} = P_0 \frac{3\gamma^2}{\pi} \left[\frac{(1 + 2\gamma^2\theta^2(1 - 2cos^2\phi) + \gamma^4\theta^4)}{(1 + \gamma^2\theta^2)^5} \right]. \tag{211}$$

The figure 39 presents power densities for various ϕ range and the figures 40 and 41 for various $\theta\gamma$ range.

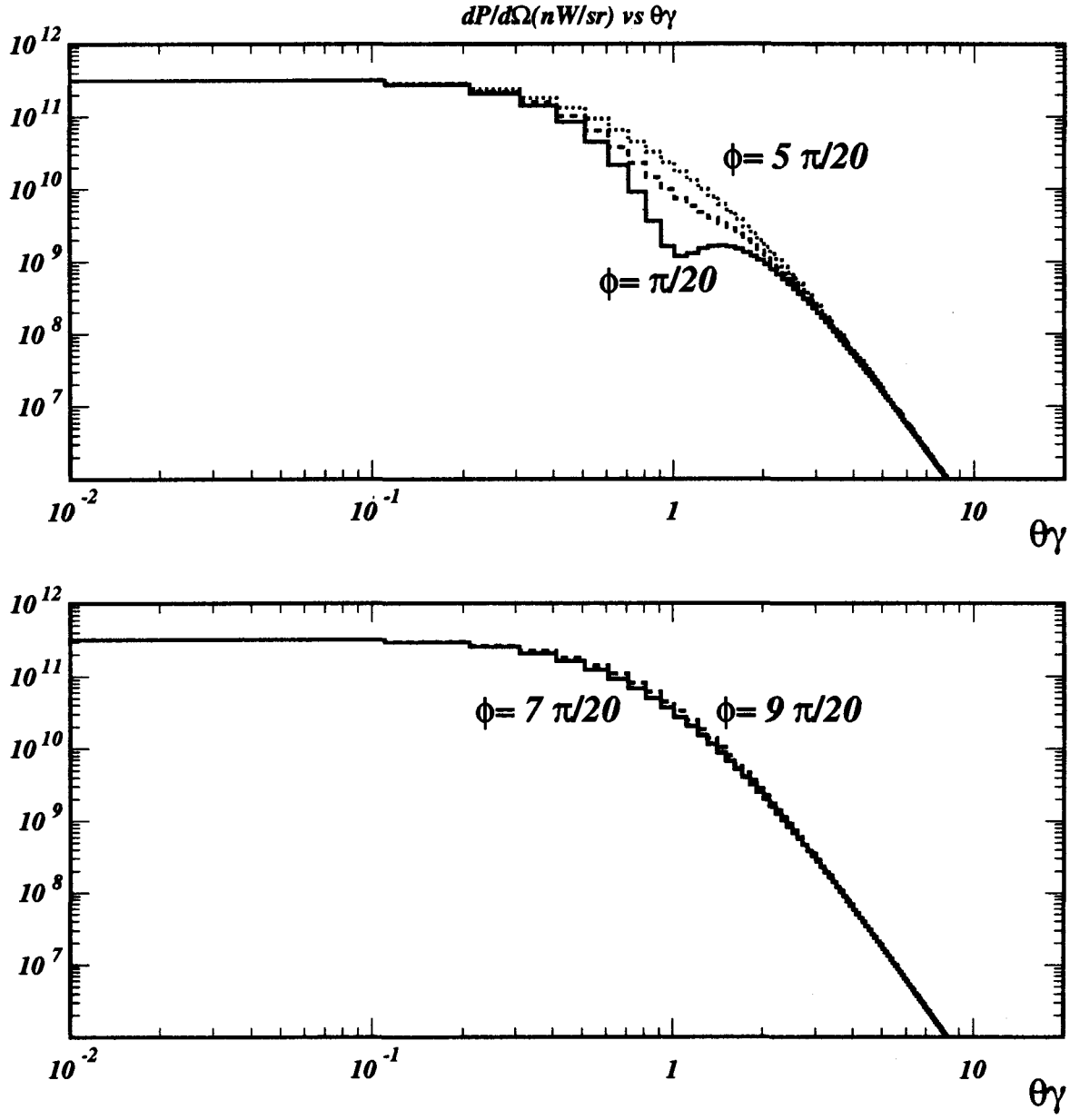

Figure 39: ***Full Power Density*** (nW/sr) ***at 4 GeV for various azimuthal angles*** ϕ ***(from 0 to*** $\pi/2$.***).***

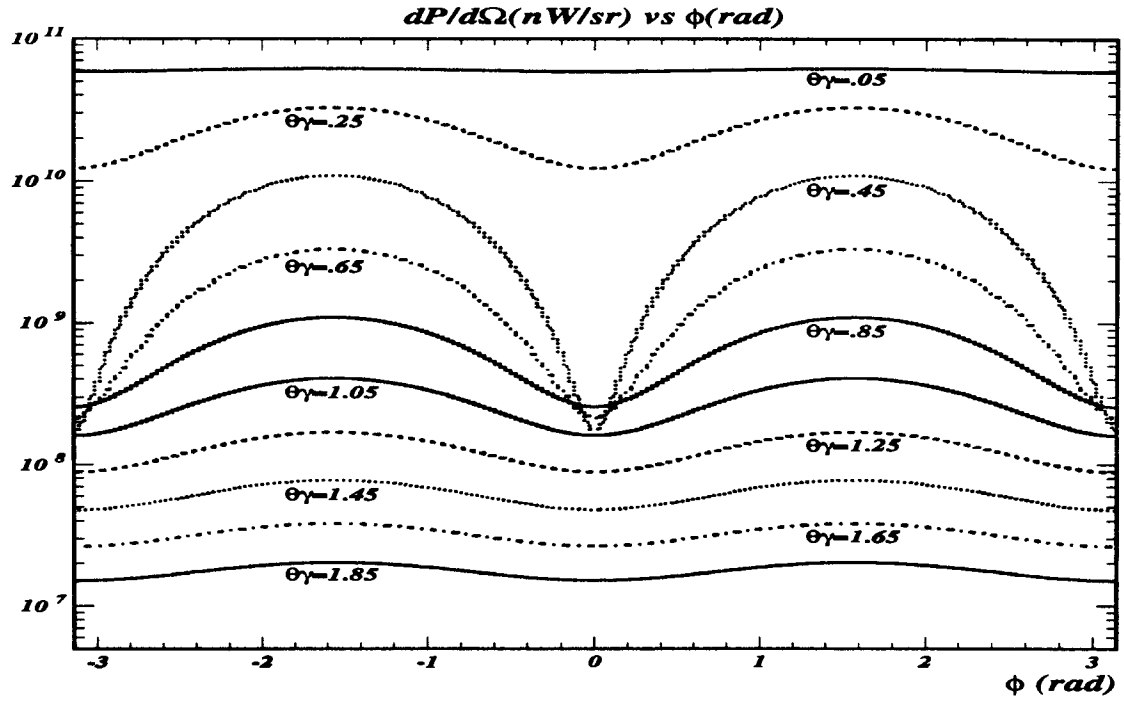

Figure 40: ***Full Power Density*** (nW/sr) ***at 4 GeV for various polar angles*** $\theta\gamma$ ***(from 0. to 1.9).***

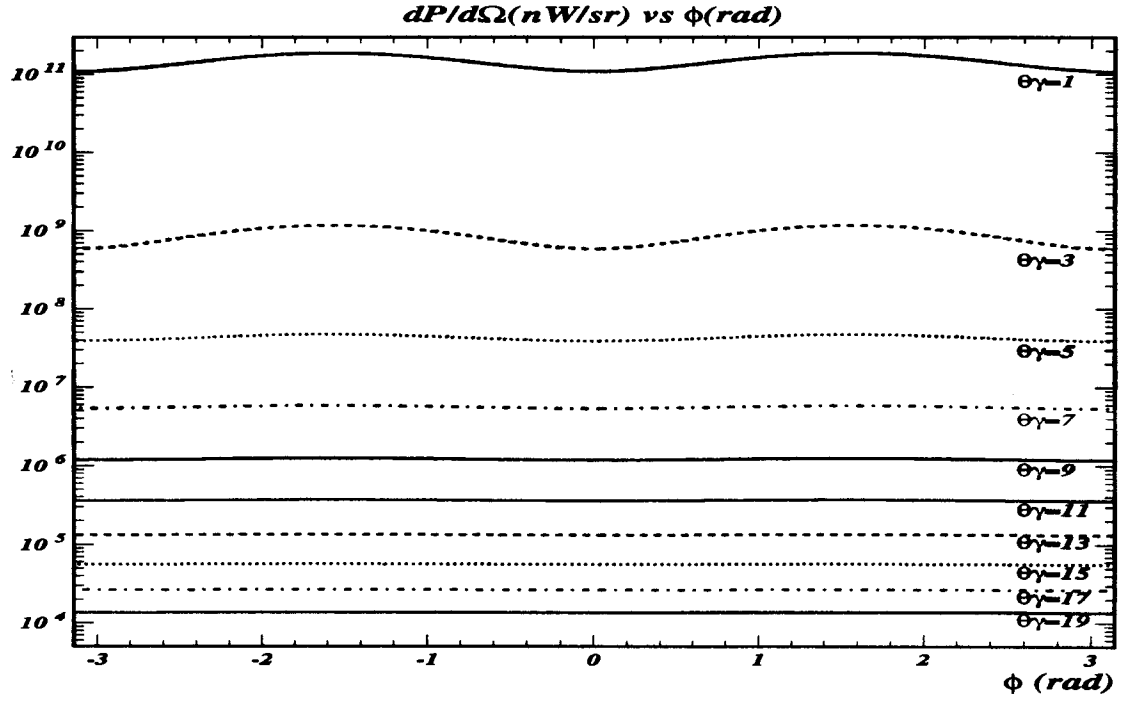

Figure 41: ***Full Power Density*** (nW/sr) ***at 4 GeV for various polar angles*** $\theta\gamma$ ***(from 0. to 20.).***

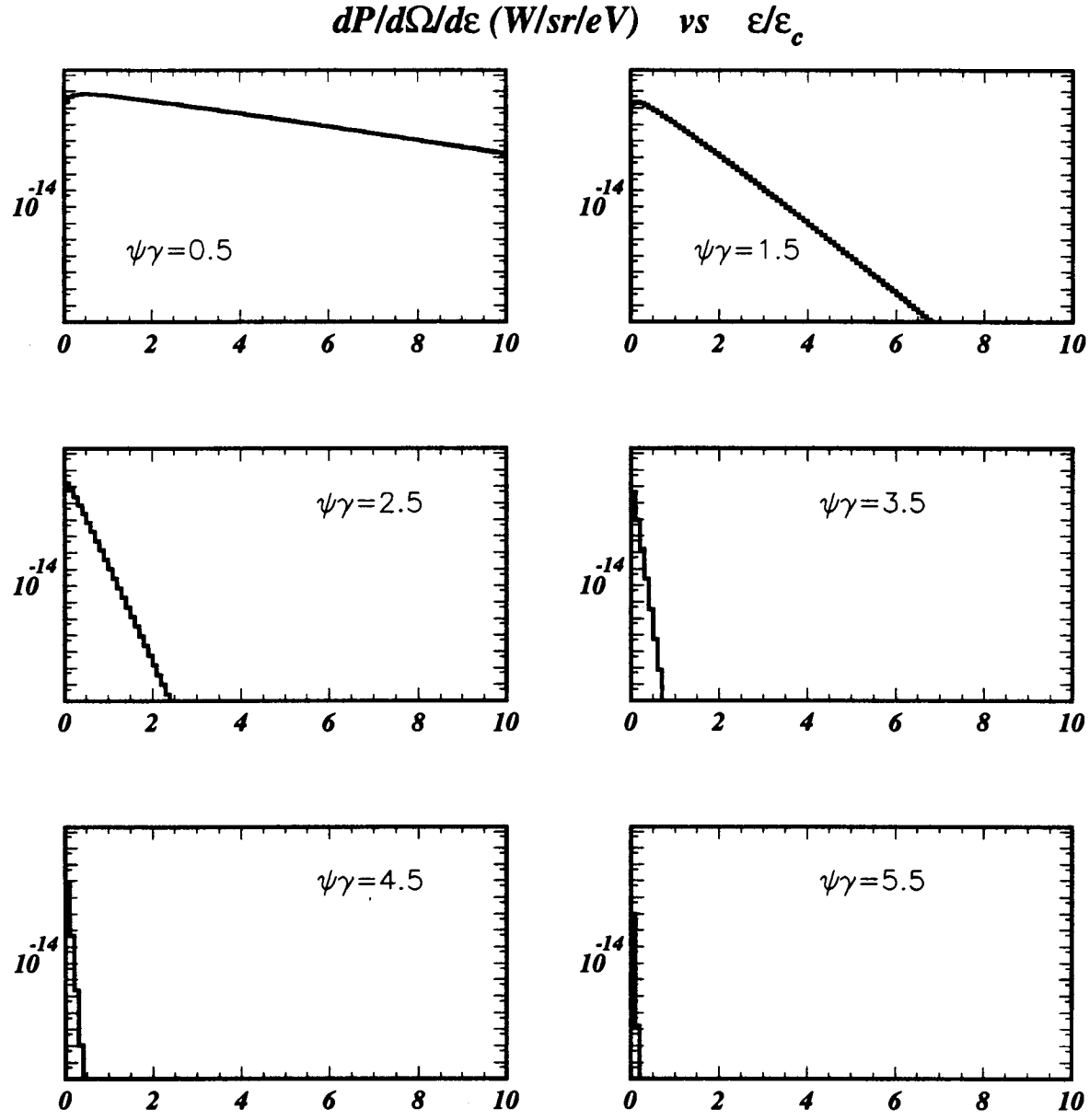

Figure 42: ***Partial Spectral Power Density for various angular range at 4 GeV.***

C.3 Partial Angular Spectral Power Density

We use here a partial angular dependence : the angle ψ between the bending plane and the vector pointing from the particle to the observation point. The angle with respect to the electron trajectory was included in the integration along the electron path, assuming all the radiation was emitted tangential to this path.

The partial angular spectral power density radiated by the electron is :

$$\frac{\partial^2 P}{\partial\Omega\partial\epsilon} = \frac{P_0}{\epsilon_c}\,\gamma\,F(\frac{\epsilon}{\epsilon_c},\psi), \tag{212}$$

where

$$F(x,\psi) = \left(\tfrac{3}{2\pi}\right)^3 \left(\tfrac{x}{2}\right)^2 (1+\gamma^2\psi^2), \tag{213}$$
$$\left[(1+\gamma^2\psi^2)\;K^2_{2/3}(\tfrac{x}{2}(1+\gamma^2\psi^2)^{3/2}) \;+\; \gamma^2\psi^2\,K^2_{1/3}\,(\tfrac{x}{2}(1+\gamma^2\psi^2)^{3/2}).\right]$$

K are the modified Bessel functions .

The total power radiated by the electron P_0, the mean energy $< \epsilon >$ and the critical energy ϵ_c are given

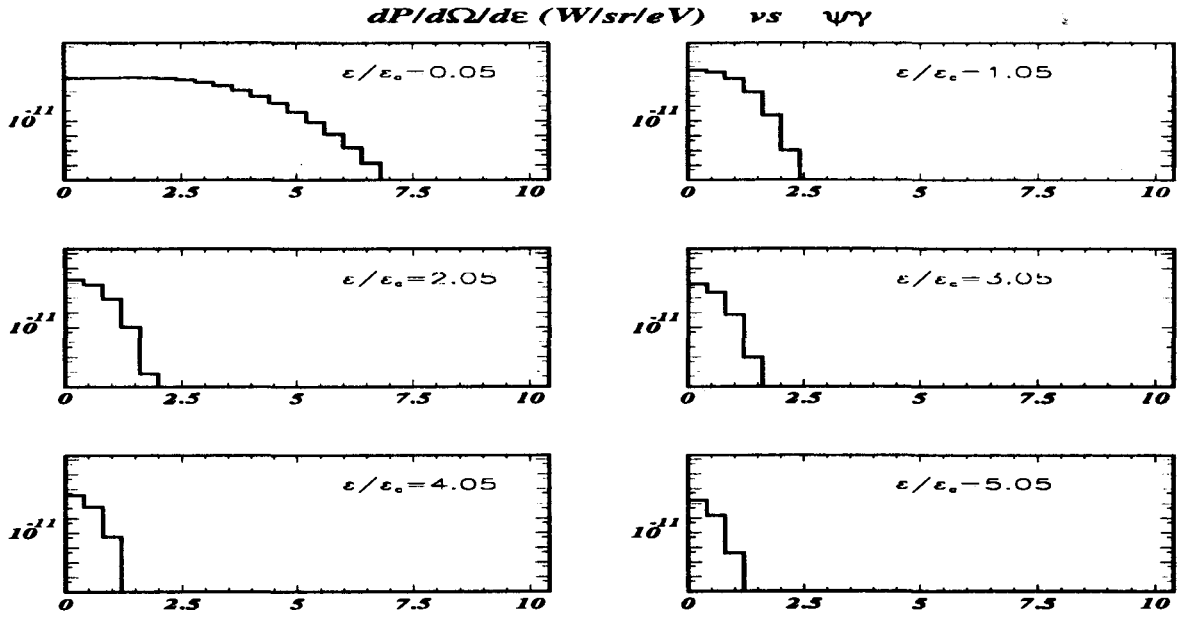

Figure 43: ***Partial Angular Power Density for various energy range at 4 GeV.***

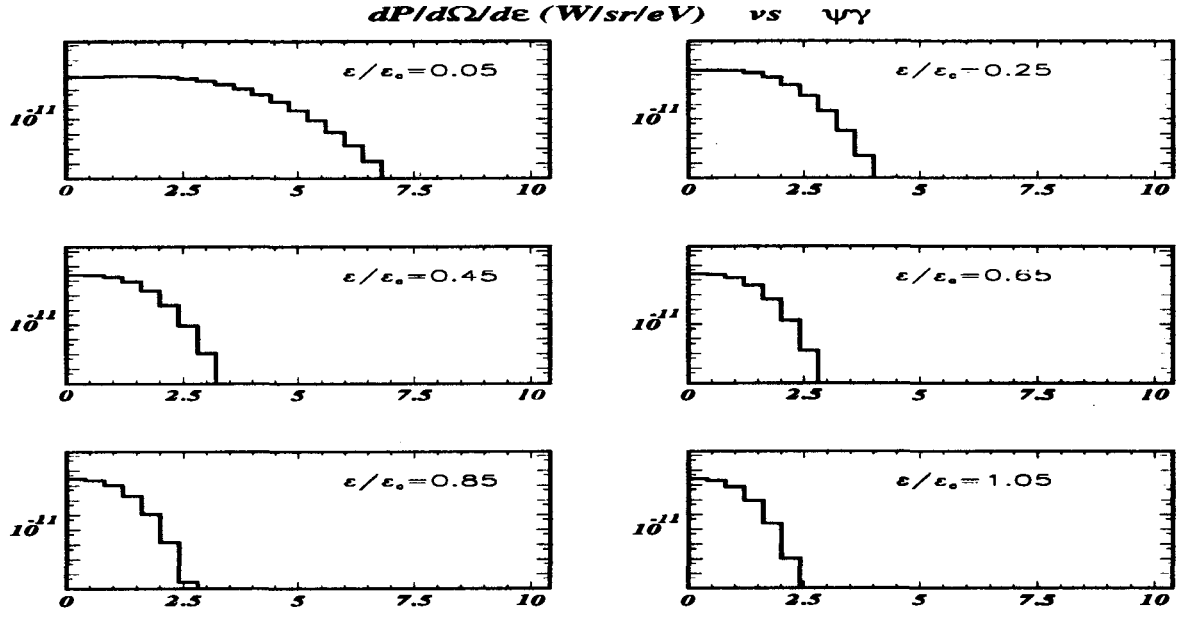

Figure 44: ***Partial Angular Power Density for various energy range at 4 GeV.***

by equations 206,208 and 209.

The behavior of equation 212 is a universal function of $\psi\gamma$ and ϵ/ϵ_c, the power density is only modulated by a factor $\beta^4\gamma^2/\rho$.
Figure 42 presents power density for various angular range and figures 43 and 44 for various gamma energy range. We can see from these figures that **for large angles, only gammas with small energies are emitted.**

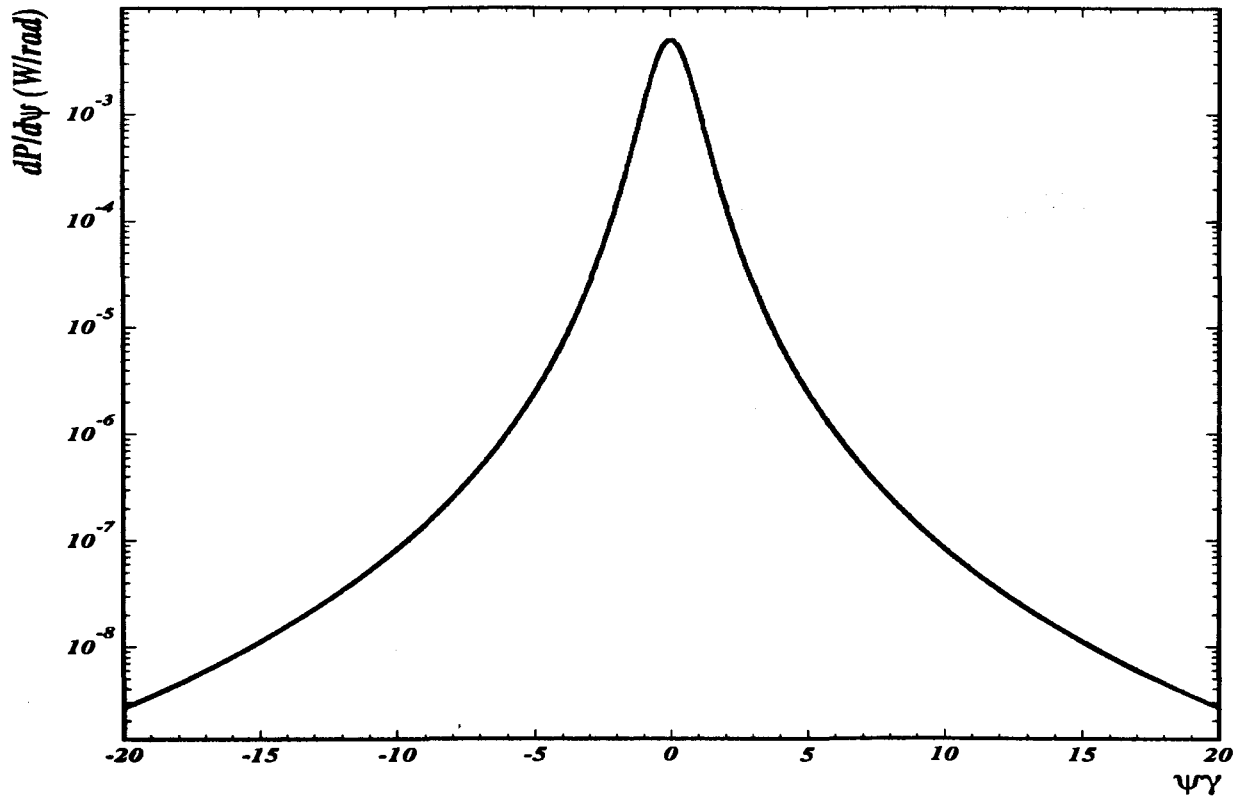

Figure 45: ***Partial Angular Power Density at 4 GeV.***

C.4 Partial Angular Power Density

By integrating the partial angular spectral power density (Eq. 212) over the gamma energy, we obtain the partial angular power density (see figure 45)

$$\frac{\partial P}{\partial \Omega} = \frac{P_0}{2\pi}\,\frac{21}{32}\,\frac{\gamma}{(1+\gamma^2\psi^2)^{5/2}}\,\left[1+\frac{5}{7}\frac{\gamma^2\psi^2}{1+\gamma^2\psi^2}\right], \tag{214}$$

or

$$\frac{\partial P}{\partial(\gamma\psi)} = P_0\,\frac{21}{32}\,\frac{1}{(1+\gamma^2\psi^2)^{5/2}}\,\left[1+\frac{5}{7}\frac{\gamma^2\psi^2}{1+\gamma^2\psi^2}\right]. \tag{215}$$

The total power radiated by the electron P_0 is given by equation 206.

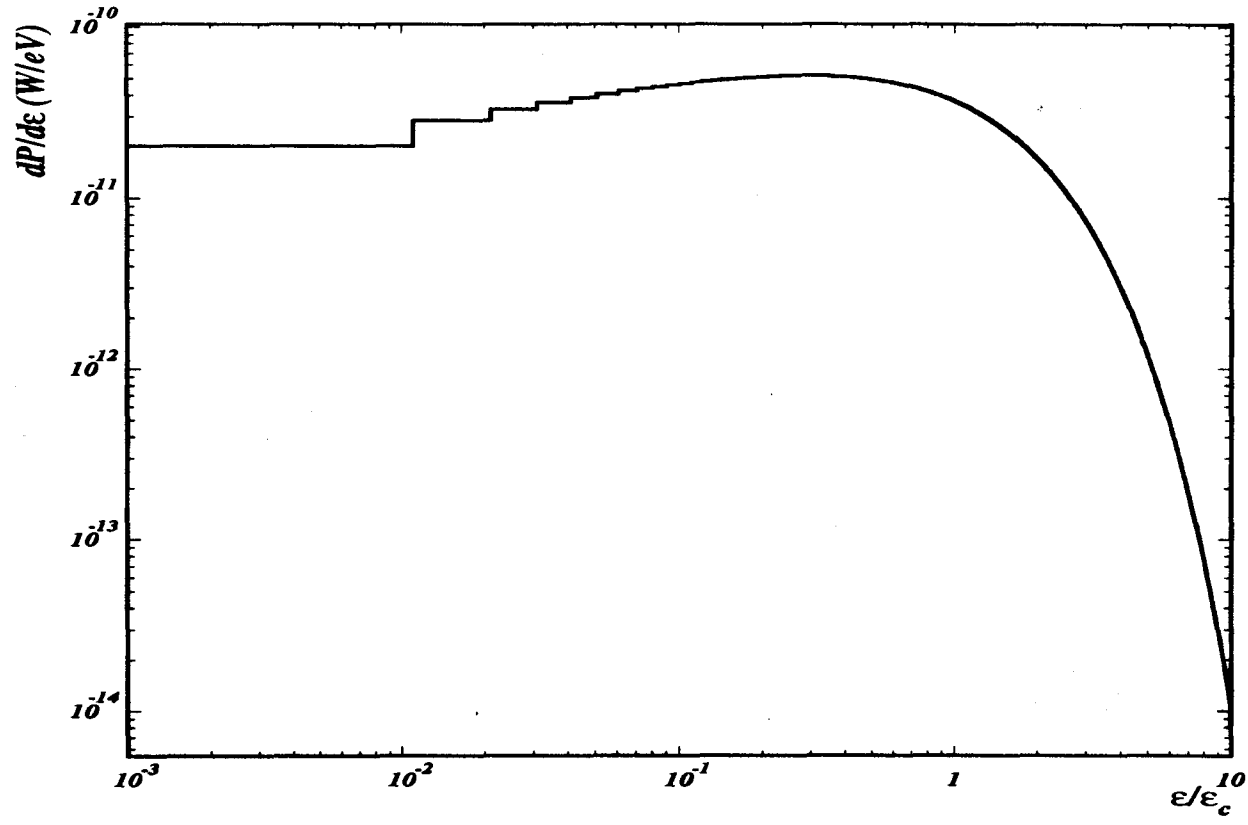

Figure 46: ***Partial Spectral Power Density at 4 GeV.***

C.5 Partial Spectral Power Density

By integrating the partial angular spectral power density (Eq. 212) over the ψ angle, we obtain the partial spectral power density (Fig. 46)

$$\frac{dP}{d\epsilon} = \frac{P_0}{\epsilon_c} S(\frac{\epsilon}{\epsilon_c}), \tag{216}$$

or

$$\frac{\partial \frac{dn}{dt}}{\partial \frac{\epsilon}{\epsilon_c}} = \frac{P_0}{\epsilon_c} \frac{S(\frac{\epsilon}{\epsilon_c})}{\frac{\epsilon}{\epsilon_c}}, \tag{217}$$

with

$$S(x) = \frac{9\sqrt{3}}{8\pi} x \int_x^\infty K_{5/3}(u)du. \tag{218}$$

K are the modified Bessel functions .
The total power radiated by the electron P_0 and the critical energy ϵ_c are given by equations 206 and 209.

D Bremsstrahlung generalities

D.1 Tsai cross section

According to Y.S. TSAI[42], the bremsstrahlung cross section σ_b for production of a photon of energy k' by an electron of energy E in the field of an atom of charge Z is given by (See figure 47):

$$\frac{d\sigma_b}{dk'} = \frac{\alpha r_0^2}{k'}\left\{\left[\left(\frac{4}{3}-\frac{4}{3}y+y^2\right)\left(Z^2\left(\phi_1(\eta_1)-\frac{4}{3}\ln Z-4f(\eta_3)\right)+Z\left(\psi_1(\eta_2)-\frac{8}{3}\ln Z\right)\right)\right. \quad (219)$$
$$\left.+\frac{2}{3}(1-y)\left(Z^2(\phi_1(\eta_1)-\phi_2(\eta_1))+Z(\psi_1(\eta_2)-\psi_2(\eta_2)\ln Z)\right)\right]\Big\},$$

where $y = \frac{k'}{E}$ and Z is the charge of the medium. Using

$$\eta_1 = \frac{100mk'}{E(E-k')Z^{1/3}}, \qquad \eta_2 = \frac{100mk'}{E(E-k')Z^{2/3}}, \qquad \eta_3 = (\alpha Z)^2 \quad (220)$$

The functions $\phi_1, \phi_2, \psi_1, \psi_2$ are given by

$$\begin{aligned}
\phi_1(x) &= 20.863x - 2\ln\left[1+(0.55846x)^2\right] - 4\left[1-0.6e^{-0.9x}-0.4e^{-1.5x}\right], \quad (221)\\
\phi_2(x) &= \phi_1(x) - \frac{2}{3}\frac{1}{1+6.5x+6x^2},\\
\psi_1(x) &= 28.340x - 2\ln\left[1+(3.621x)^2\right] - 4\left[1-0.7e^{-8x}-0.3e^{-29.2x}\right],\\
\psi_2(x) &= \psi_1(x) - \frac{2}{3}\frac{1}{1+40x+400x^2},
\end{aligned}$$

and the Coulomb correction by

$$f(z) = z\sum_{n=1}^{\infty}\frac{1}{n(n^2+z)} \simeq 1.202z - 1.0369z^2 + \frac{1.008z^3}{1+z}. \quad (222)$$

For a total material with thickness L , with atomic number A whose density is ρ_0 at normal pressure $P_0 = 760\ Torr$, the bremsstrahlung rate $\dot{n}_b$ at pressure P is given by

$$\frac{d\dot{n}_b}{dk'} = \frac{I_e}{e}\left(\rho_0\frac{P}{P_0}\frac{N_a}{A}\right)L\frac{d\sigma_b}{dk'}. \quad (223)$$

D.2 GEANT parametrization

S.M. Seltzer and M.J. Berger have given [43] a set of bremsstrahlung cross sections which have been parametrized in the GEANT code. The parametrization for production of a photon of energy k' by an electron of energy E in the field of an atom of charge Z integrated above an energy cut off k'_c has the form

$$\sigma(k'_c) = \int_{k'_c}^{E-m} = \frac{Z(Z+\xi)E^2}{(E-m)(E+m)}\left[\ln\left(\frac{E-m}{k'_c}\right)\right]^{\alpha} F(Z,X,Y), \quad (224)$$

where

$$X = \ln\left(\frac{E}{m}\right) \qquad Y = \ln\left(\frac{v\,E}{k'_c}\right) \qquad F(Z,X,Y) = \sum_{i=0,5\ ;\ j=0,5} C^0_{ij}\,X^iY^j + Z\,C^1_{ij}\,X^iY^j.$$

The parameters ξ, α, v, C_{ij}^0 and C_{ij}^1 have been fitted for

$$Z = 6; 13; 29; 47; 74; 92 \qquad 10\ KeV \leq (E-m) \leq 10\ TeV \qquad 10\ KeV \leq k'_c \leq (E-m).$$

This parametrization gives results in good agreement (within 10 %) with the Tsai or the Seltzer Berger results. Figure 47 shows the differential Tsai cross section and the total Tsai cross section integrated from k' to the incident energy E. Plotted as the function of the radiated photon energy k' normalized to the incident energy E, these cross section do not depend on the incident energy.

The angular dependence is contained mainly in the variable $u = \gamma\theta$ with $\gamma = E/m$. For a given value of u, the dependence of the shape of $d\sigma/dk'/d\Omega$ is very weak. Thus the distribution is approximated by

$$f(u) = \left(\frac{9a^2}{9+d}\right)\left(u\, e^{-au} + d\, u\, e^{-3au}\right), \tag{225}$$

with

$$a = 0.625 \qquad d = 0.13\ \left(0.8 + \tfrac{1.3}{Z}\right)\left(100 + \tfrac{1}{E}\right)\left(1 + \tfrac{k'}{E}\right).$$

Figure 48 gives the angular distribution and shows the weak dependence on Z,E and k'. The angular distribution is peaked around $u = \gamma\theta \simeq 0.5$.

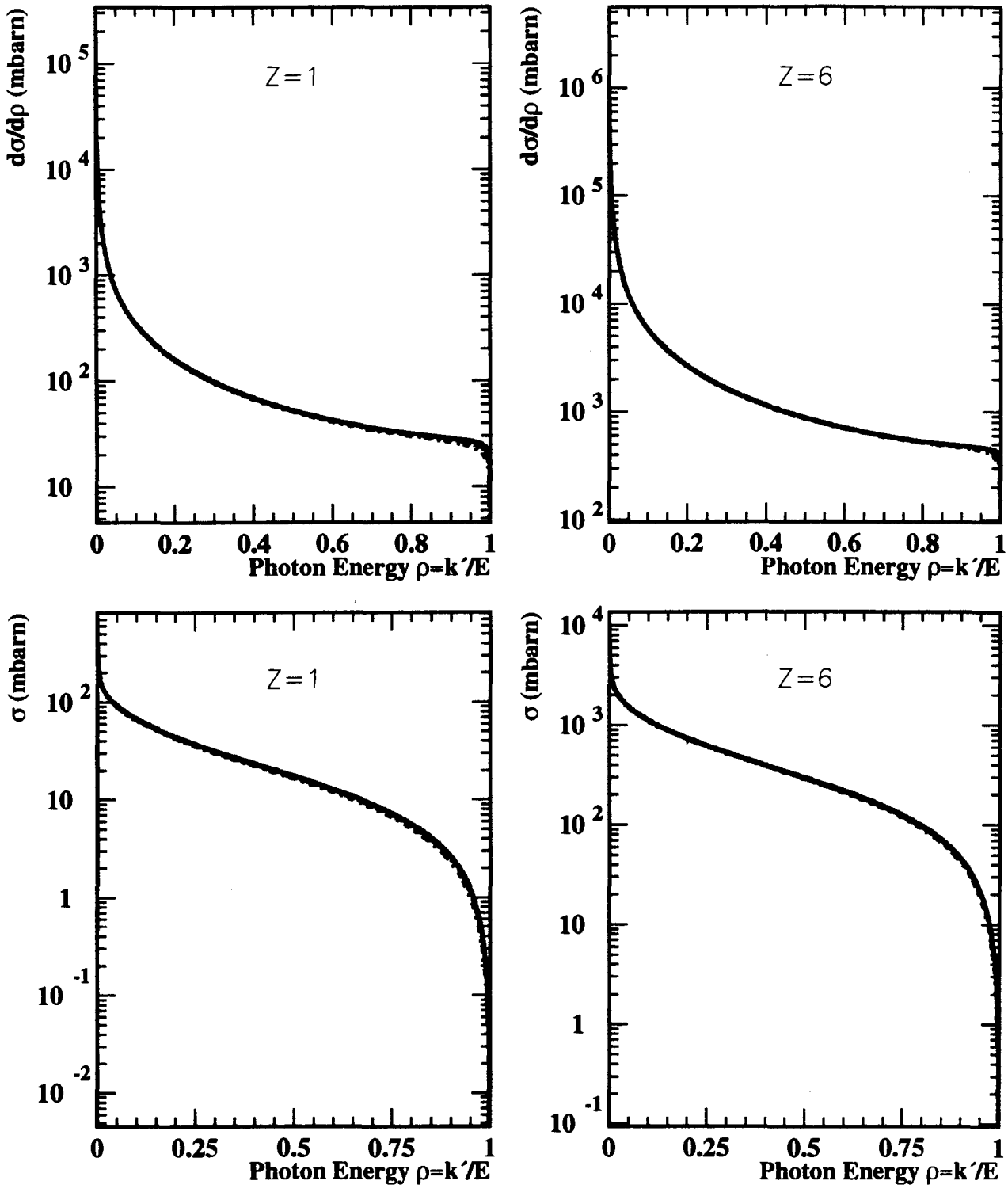

Figure 47: ***Bremsstrahlung TSAI cross section for Z=1 and Z=6.*** *The upper curves give the differential cross section $d\sigma/d\rho$ where ρ is the radiated photon energy k' normalized to the incident energy E. The lower curves give the total cross section σ integrated from the energy threshold $k'_c = 0.1\,MeV$ to the maximum energy E. For each curve, results for $E = 8, 6, 4, 2\,GeV$ are superposed.*

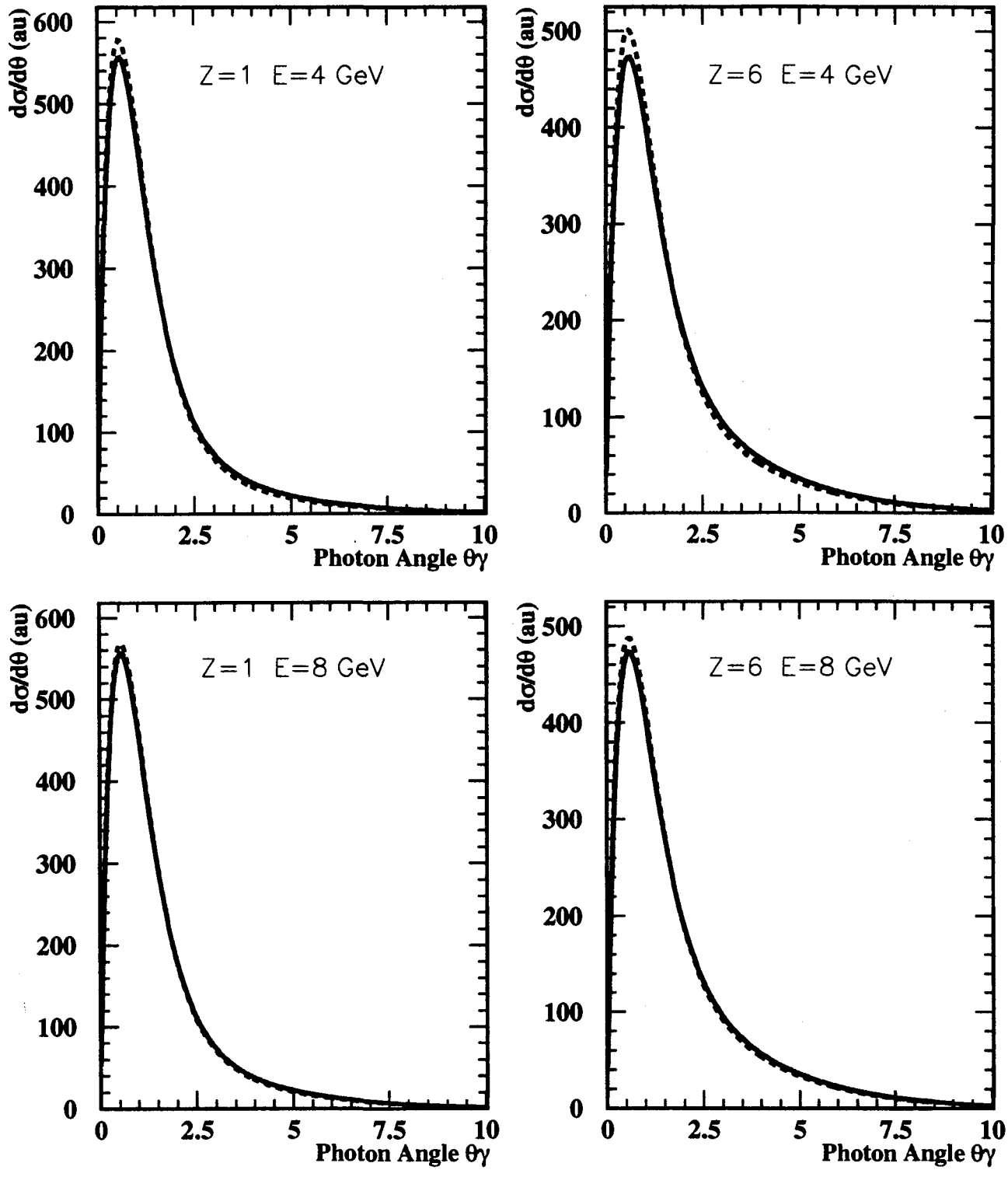

Figure 48: ***Bremsstrahlung angular distribution for Z=1,6 and E=4,8 GeV.*** *Each curve shows results for* $k' = 0.1\,MeV$ *(solid line) and for* $k' = 1\,GeV$ *(dashed line) as a function of* $\theta\gamma$ *where* $\gamma = E/m$.

E Effect of the detector resolution

In section 2.3, we have compared different methods (integrated or differential) to extract the electron polarization from the experimental asymmetry. In particular, we have seen that the differential method gives a better statistical error than the integrated method especially when the threshold ρ_t on the scattered Compton γ energy is lower than $\simeq 0.5$. For a higher threshold, the two methods give similar precisions. These conclusions don't take into account the response function of the detector.

In this section, we try to estimate the effect of resolution and calibration of the gamma or electron detector. The results will be given for incident electron energy E in the range [1 , 8] GeV and for different values of the energy threshold ρ_t.

E.1 Polarization measurement

E.1.1 Experimental asymmetry and polarization

The electron polarization P^i_{ex} measured in the scattered γ energy ρ bin i of range $[\rho_i , \rho_{i+1}]$ is deduced from the experimental asymmetry A^i_{ex} by

$$P^i_{ex} = \frac{A^i_{ex}}{A^i_{th}\ P_\gamma} \tag{226}$$

In this equation

- ρ is the energy of the scattered gamma normalized to the maximum energy : $\rho = k/k_{max}$.
- P_γ is the Laser beam polarization.
- A^i_{ex} the experimental asymmetry is a function of the normalized number of Compton events $N^i_\pm$ (measured number of Compton events divided by the luminosity $N^i_\pm = n^i_\pm/\mathcal{L}_\pm$).

$$A^i_{ex} = \frac{N^i_+ - N^i_-}{N^i_+ + N^i_-} \qquad with \qquad N^i_\pm = \int_{\rho_i}^{\rho_{i+1}} \frac{d\sigma^m_\pm}{d\rho}\, d\rho \tag{227}$$

  where $d\sigma^m_\pm\ /\ d\rho$ is the measured polarized Compton cross section.

- A^i_{th} the theoretical asymmetry is a function of the longitudinal asymmetry A_l and of the unpolarized Compton cross section $d\sigma_c\ /\ d\rho$. The expression of A^i_{th} will be derived later.

These experimental polarizations P^i_{ex} are then used to extract the final measured electron polarization according to the chosen method (integrated or differential) :

- For the integrated method, there is only one energy bin of range $[\rho_{min}\ :\ \rho_{max}]$ and the final experimental electron polarization P^{IM}_{ex} is given by

$$P^{IM}_{ex} = \frac{A_{ex}}{A_{th}\ P_\gamma} \tag{228}$$

- For the differential method, the energy range $[\rho_{min} : \rho_{max}]$ is divided into N bins $[\rho_i : \rho_{i+1}]$ and the final experimental electron polarization P^{DM}_{ex} is the weighted mean of the bin polarization $P^i_{ex} \pm dP^i_{ex}$

$$P^{DM}_{ex} = \sum_{i=1}^{N} \frac{P^i_{ex}}{(dP^i_{ex})^2}\ /\ \sum_{i=1}^{N} \frac{1}{(dP^i_{ex})^2} \tag{229}$$

E.1.2 Response function of the detector

With a perfect detector (resolution and calibration), the measured polarized Compton cross section $\sigma^m_\pm$ is equal to the polarized Compton cross section

$$\frac{d\sigma^m_\pm}{d\rho}(\rho) = \frac{d\sigma_c}{d\rho}(\rho)\ (1 \pm P_\gamma P_e\ A_l(\rho)) \qquad with \qquad P_e = electron\ polarization \tag{230}$$

Using equation 226, the experimental asymmetry leads to the electron polarization

$$P^i_{ex} = \frac{A^i_{ex}}{A^i_{th}\,P_\gamma} = \frac{1}{A^i_{th}\,P_\gamma}\frac{N^i_+ - N^i_-}{N^i_+ + N^i_-} = \frac{1}{A^i_{th}\,P_\gamma} P_\gamma P_e \frac{\int_{\rho_i}^{\rho_{i+1}} A_l \frac{d\sigma_c}{d\rho}\,d\rho}{\int_{\rho_i}^{\rho_{i+1}} \frac{d\sigma_c}{d\rho}\,d\rho} = \frac{P_e}{A^i_{th}} \frac{\int_{\rho_i}^{\rho_{i+1}} A_l \frac{d\sigma_c}{d\rho}\,d\rho}{\int_{\rho_i}^{\rho_{i+1}} \frac{d\sigma_c}{d\rho}\,d\rho} \tag{231}$$

provided that the theoretical asymmetry A^i_{th} be defined by

$$A^i_{th} = \frac{\int_{\rho_i}^{\rho_{i+1}} A_l \frac{d\sigma_c}{d\rho}\,d\rho}{\int_{\rho_i}^{\rho_{i+1}} \frac{d\sigma_c}{d\rho}\,d\rho} \tag{232}$$

In fact, the energy distribution of Compton events $d\sigma_c/d\rho$ is first smeared with a resolution $\sigma(\rho)$ due to the response of the detector. For instance for a Gaussian law, the **smeared energy distribution taking into account only the detector resolution** becomes

$$\frac{d\sigma_s}{d\rho_s} = \int_0^1 \frac{d\sigma_c}{d\rho}(\rho) \frac{1}{\sqrt{2\pi}\sigma(\rho)} e^{-\frac{(\rho-\rho_s)^2}{2\sigma(\rho)^2}}\,d\rho \tag{233}$$

where the mean value of the smeared energy ρ_s is equal to the incident energy ρ.
Moreover, the energy calibration of the detector gives the relation between the measured energy ρ_m and the smeared energy ρ_s, which at first order can be written

$$\rho_s = \rho_0 + s\,\rho_m \tag{234}$$

and the **measured energy spectrum** $d\sigma_m\,/\,d\rho_m$ **taking into account the detector resolution and calibration** is given in this case by

$$\frac{d\sigma_m}{d\rho_m}(\rho_m) = s\ \frac{d\sigma_m}{d\rho_s}(\rho_m) = s\ \frac{d\sigma_s}{d\rho_s}(\rho_s) \tag{235}$$

This measured differential Compton cross section is no longer equal to the polarized Compton cross section. This will introduce a systematic effect in the electron polarization measurement unless we have only one energy bin covering the whole energy distribution since the smearing does not change the total cross section. However, for the other cases (limited energy range, more than one energy bin), this bias can be removed if the resolution and the calibration of the detector are perfectly known. In this case, we can reproduce for given electron and gamma polarizations (P^S_e and P^S_γ) the distribution of the number of events $N^S_\pm$ and the experimental polarization P^i_{ex} of equation 226 becomes

$$P^{i\,S}_{ex} = \frac{A^i_{ex}}{A^{i\,S}_{th}\ P_\gamma} \tag{236}$$

with the smeared theoretical asymmetry $A^{i\,S}_{th}$ defined by

$$A^{i\,S}_{th} = \frac{N^S_+ - N^S_-}{N^S_+ + N^S_-}\frac{1}{P^S_e\ P^S_\gamma} \tag{237}$$

We use now the smeared theoretical asymmetry $A^{i\,S}_{th}$ instead of the theoretical asymmetry A^i_{th} of equation 232 to extract the electron polarization P_e.

E.1.3 Method to estimate systematic errors from detector calibration or resolution

Actually, the resolution or the calibration of the detector are only known within some errors and it remains a residual bias. To study the systematic effect on P_e measurement induced by these errors on the knowledge of the resolution or of the calibration of the detector, we

- try to reproduce the **experimental asymmetry** A^i_{ex} for given electron and gamma polarizations (P_e and P_γ). For this, we use a simulation of the detector resolution to obtain the smeared Compton cross section $\sigma^0_\pm$. This simulation depends on a set of parameters $P = [a, b, , ...]$.
  Using now the calibration equation 234, we determine the measured Compton cross section $\sigma^m_\pm$ by equation 235 and the number of events

$$N^{i\,0}_\pm = \int_{\rho^i_s}^{\rho^{i+1}_s} \frac{d\sigma^0_\pm}{d\rho}\, d\rho = \int_{\rho^i_m}^{\rho^{i+1}_m} \frac{d\sigma^m_\pm}{d\rho}\, d\rho \tag{238}$$

  from which we deduce the experimental asymmetry A^i_{ex} by equation 227.

- compute the **smeared theoretical asymmetry** $A^{i\,S}_{th}$ following equation 237 with simulated number of events given by

$$N^{i\,S}_\pm = \int_{\rho^i_m}^{\rho^{i+1}_m} \frac{d\sigma^S_\pm}{d\rho}\, d\rho \tag{239}$$

  which depends only of the smeared Compton cross section $\sigma^S_\pm$ where we have used an estimated set of the resolution parameters $P^S = [a^S, b^S, , ...]$

- deduce the **experimental polarization** $P^{i\,S}_{ex}$ with equation 236 and the measured electron polarizations P^{IM}_{ex} and P^{DM}_{ex} with equations 228 and 229.

- compare the **measured electron polarizations** P^{IM}_{ex} **and** P^{DM}_{ex} with the **initial electron polarization** P_e.

Using the same set of resolution parameters and a perfect calibration for the experimental and smeared theoretical asymmetry, the measured and initial electron polarizations are the same since

$$\frac{d\sigma^0_\pm}{d\rho} = \frac{d\sigma^S_\pm}{d\rho} \qquad (\ set\ P\ =\ set\ P^S\ )$$
$$\rho^i_m = \rho^i_s \qquad (\ perfect\ calibration\ )$$

For each detector (gamma or electron), we will now look at the difference when varying one of the estimated parameters. Simple simulation of the response of the detectors have been used for this study (see section E.2.1 and E.3.1 for the γ and electron detectors).

E.2 Effect of the Gamma detector resolution and calibration

E.2.1 Simulation of the γ detector resolution

In order to study the effect of the detector resolution and calibration on the electron polarization measurement, the Compton cross section $d\sigma_c/dk$ has first to be smeared to give the smeared energy distribution $d\sigma_s\ /\ dk_s$. The usual parametrization of the overall resolution $\sigma'(k)$ for an electromagnetic calorimeter has the standard form

$$\frac{\sigma'(k)}{k} = a' \oplus \frac{b'}{\sqrt{k}} \oplus \frac{c'}{k} \tag{240}$$

or using $\rho = k/k_{max}$

$$\frac{\sigma(\rho)}{\rho} = a' \oplus \frac{b'}{\sqrt{k_{max}}}\frac{1}{\sqrt{\rho}} \oplus \frac{c'}{k_{max}}\frac{1}{\rho} = a \oplus b\frac{1}{\sqrt{\rho}} \oplus c\frac{1}{\rho} \tag{241}$$

To simulate the response of the γ detector, we have used here a three steps process following the physical phenomena to combine the 3 terms of equation 240 and we have neglected the lead absorber effect. More detailed procedure (GEANT based) will be done later when experimental results on the γ detector used in this experiment will be available.

- For the deposited energy or light output in the crystal, the scattered γ energy was distributed according to a Gaussian law with a resolution $\sigma'_1(k)$. We consider here for the resolution the following process :
  - physics noise (fluctuation of the electron shower)
  - shower leakage
  - non uniformity of light response

  We have assumed in this step that all these terms gives a resolution $\sigma'_1(k) = a'_1\ k$, i.e. only a contribution to the constant a' term of the resolution. We neglect the irrelevant conversion factors (γ energy - deposited energy - light output) and express the distribution in term of **deposited energy** k_d, i.e. we assume that the mean deposited energy was equal to the incident energy $k_d = k$. After integration over the scattered γ energy spectrum given by the Compton cross section $d\sigma_c/dk$ (Fig 49a), we obtain the deposited energy distribution (Fig 49b) :

$$\frac{d\sigma_s^a}{dk_d} = \int_0^{k_{max}} \frac{d\sigma_c}{dk}\frac{1}{\sqrt{2\pi}\,a'_1\,k}\,e^{-\frac{(k-k_d)^2}{2\,(a'_1\,k)^2}}\,dk \tag{242}$$

- This light output or deposited energy k_d was then converted into a **number of photoelectrons** distributed according to a Poisson law of mean value $N_{\gamma e}(k_d)$ proportional to the energy deposited in the crystal. These conversion contribute to the statistical term of the resolution b' and can be written

$$N_{\gamma e}(k_d) = \frac{k_d}{b'^2_2} \qquad with \qquad \frac{1}{b'^2_2} = Number\ of\ photoelectrons/GeV \tag{243}$$

  After integration over the deposited energy spectrum, we obtain the distribution of the number of photoelectrons N_e (Fig 49c) :

$$\frac{dN_e^s}{dN_e} = \int_0^{\infty} \frac{d\sigma_s^a}{dk_d}\frac{N_{\gamma e}(k_d)^{N_e}\ e^{-N_{\gamma e}(k_d)}}{N_e!}\,dk_d \tag{244}$$

- We have now to take into account the smearing due to the electronic noise contributing to the linear term of the resolution c'. We add also a term for the one photoelectron resolution which contributes to the statistical term b' and which can not be neglected for low γ energy. A Gaussian law was used with a resolution

$$\sigma'_3(k_d = b'^2_2\, N_e) \;=\; \sqrt{(c'_3\, k_{max})^2 + (b'_3\, b'_2)^2\, k_d} \tag{245}$$

where

  - the electronic noise c'_3 (photo detector and ADC noise,ADC non linearities, pedestals variations,..) was taken proportional to k_{max}
  - the one photoelectron resolution was given by b'_3.

This resolution, expressed in term of number of photoelectrons becomes

$$\sigma_n(N_e) \;=\; \frac{\sigma'_3(k_d = b'^2_2\, N_e)}{b'^2_2} \tag{246}$$

We integrate over the number of photoelectrons spectrum to obtain the final smeared number of photoelectrons distribution N (Fig 49d where we can see the peaks corresponding to zero and one photoelectron) :

$$\frac{dN_s}{dN} \;=\; \int_0^\infty \frac{dN_e^s}{dN_e}\, \frac{1}{\sqrt{2\pi}\,\sigma_n(N_e)}\, e^{-\frac{(N_e - N)^2}{2\,\sigma_n(N_e)^2}}\, dN_e \tag{247}$$

We use the number of photoelectrons rather than the electric charge at the exit of the PM or the ADC channel neglecting here the irrelevant gain of the electronic chain.
To obtain the smeared cross section $d\sigma_s\ /\ dk_s$ independent of the calibration of the detector, we have only to convert this smeared number of photoelectrons into smeared energy k_s with the same conversion law of equation 243. In this case, the mean value of the smeared energy k_s is equal to the energy k of the incident γ. Figure 50 gives the cross section at 1,2,4 and 8 GeV

For this study, we have used conservative values for the different terms of the resolution (equation 240) for a $PbWO_4$ crystal viewed by a photomultiplicator i.e.

$$a'_1 \;=\; 1\% \qquad b'_2 \;=\; 3\% \qquad c'_3 \;=\; 1\% \qquad b'_3 \;=\; 50\% \qquad (\ k\ in\ GeV\ ) \tag{248}$$

The statistical term $b'_2 \;=\; 3\%$ corresponds to a number of collected photoelectrons of $N_{\gamma e} = 1.11/MeV$.

Table 37 gives the different terms contributing to the resolution in equation 241 and the resolution for some values of ρ.

E	GeV	1.00	2.00	3.00	4.00	5.00	6.00	7.00	8.00
k_{max}	MeV	17.5	68.9	152.4	266.5	409.6	580.3	777.3	999.4
$\sigma(\rho_{max})$	%	25.4	12.9	8.7	6.6	5.4	4.6	4.1	3.6
$\sigma(\rho_{max}/2)$	%	17.9	9.1	6.2	4.7	3.9	3.3	2.9	2.6
$\sigma(0)$	%	1.0	1.0	1.0	1.0	1.0	1.0	1.0	1.0
a	%	1.0	1.0	1.0	1.0	1.0	1.0	1.0	1.0
b	%	25.3	12.8	8.6	6.5	5.2	4.4	3.8	3.4
c	%	1.0	1.0	1.0	1.0	1.0	1.0	1.0	1.0

Table 37: γ ***detector resolution*** *for the maximum, half and minimum energy* $\rho = \rho_{max}$, $\rho_{max}/2$ *and* 0. *Contributions of the different terms of Eq. 241.*

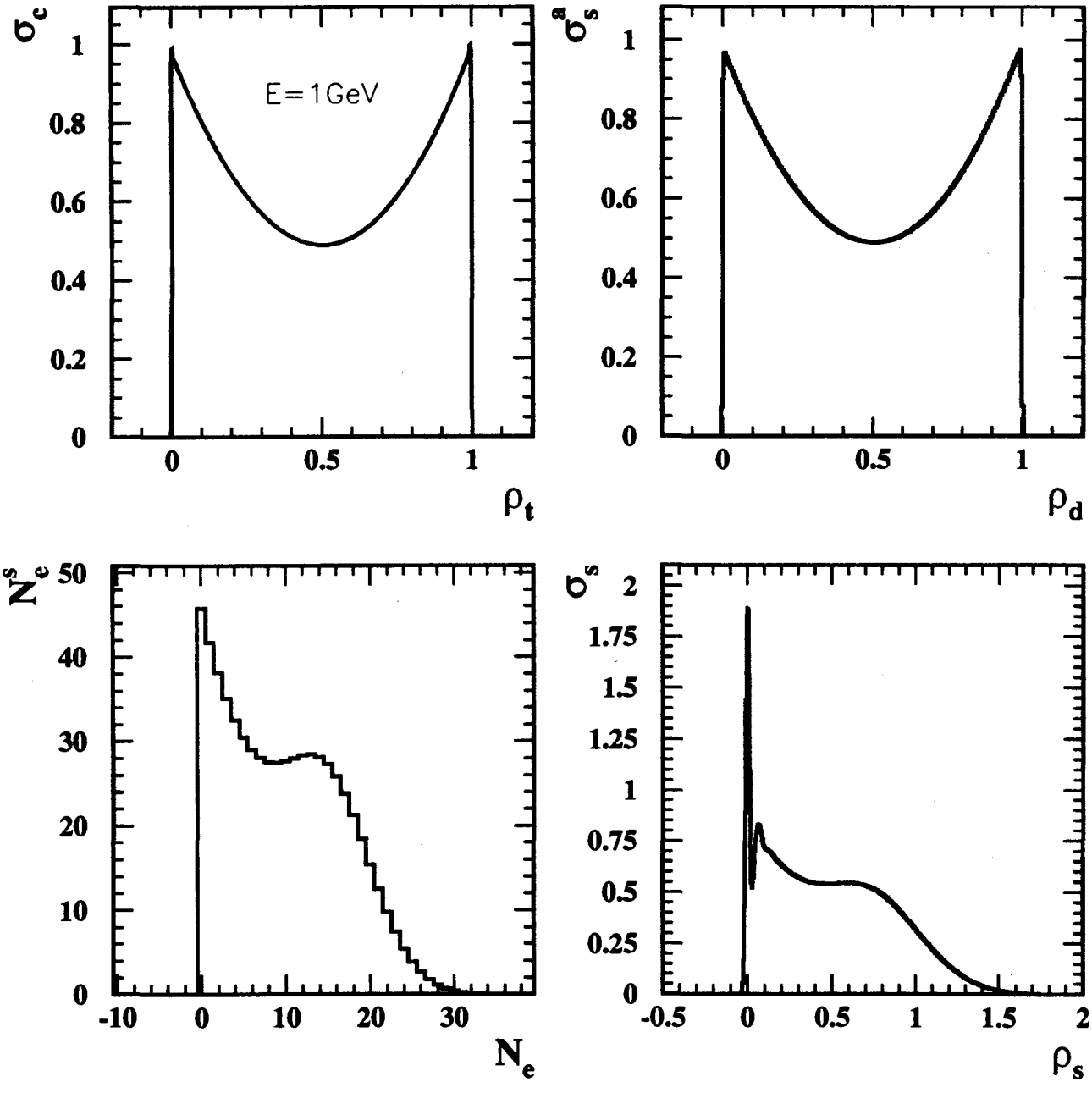

Figure 49: ***Energy distribution in the*** γ ***detector :*** *Compton cross section (up left). Energy deposited in the crystal (up right). Number of photoelectrons (down left). Smeared Compton cross section (down right). Incident electron energy is* $E = 1\ GeV$. *Laser and electron polarizations are* $P_\gamma = 1.$ *and* $P_e = +0.5$

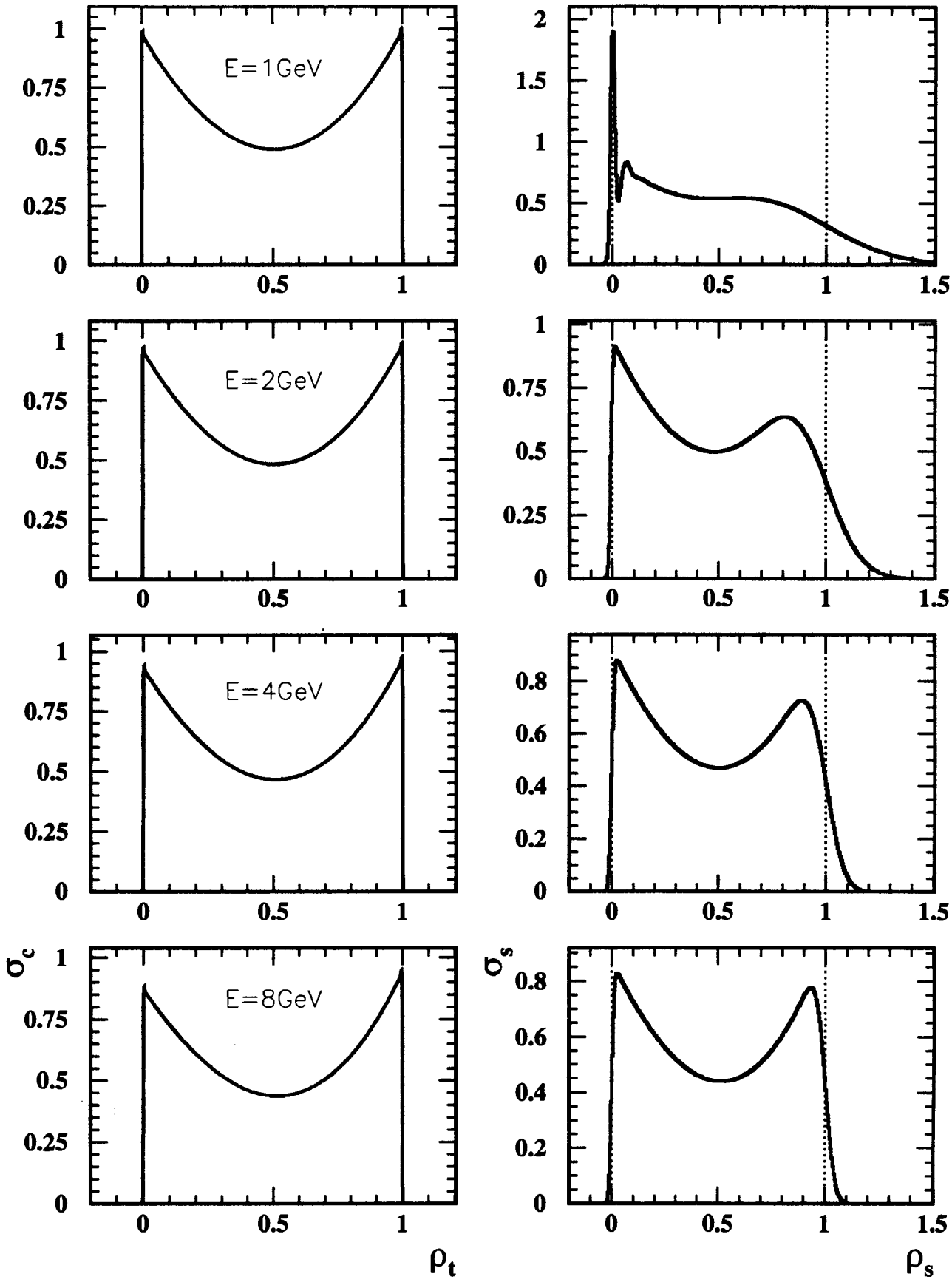

Figure 50: ***Compton cross section (left) and smeared Compton cross section (right) for incident electron energy*** $E = 1, 2, 3, 4\ GeV$. ***Laser and electron polarizations are*** $P_\gamma = 1.$ ***and*** $P_e = +0.5$

E.2.2 Energy bining, variation of threshold, calibration simulation

For the differential method, we have used 10 scattered γ **energy** ρ **bins** of width $w_b = 0.1$ except for an incident energy of 1 GeV where we use only 5 bins of width $w_b = 0.2$. These values have been chosen to have a bin width at least equal to the mean resolution of the detector (see Table 37). The first and last bins have been enlarged to cover the whole energy distribution.

The **energy threshold** ρ_{min} follows the previous bining i.e.

- 10 values [-∞ , 0.1 , 0.2 , 0.3 , 0.4 , 0.5 , 0.6 , 0.7 , 0.8 , 0.9] for $E_{inc} \geq 2\ GeV$
- 5 values [-∞ , 0.2 , 0.4 , 0.6 , 0.8] for $E_{inc} = 1\ GeV$

The **calibration** of the detector was parametrized following equation 234

$$\rho_s = \rho_0 + s\,\rho_m$$

where ρ_m and ρ_s are the measured and smeared energy. Having neglected the irrelevant conversion factors (γ energy - deposited energy - light output - electronic chain gain), a perfect calibration would give $\rho_0 = 0$ and $s = 1$.
In order to have the same absolute error ρ_t on the measured energy for all energy thresholds t, i.e. $\rho_s - \rho_m = \rho_t$, the parameter ρ_0 of the previous equation varies with the threshold according to

$$\rho_0 = \rho_t + (1 - s)\,t \tag{249}$$

E.2.3 Results and discussion

1. **Error on the resolution**

   As expected for low γ energies, the resolution of the γ detector is dominated by the quadratic term b' (see table 37).

   The main systematic effect on P_e measurement due to the finite resolution comes from the knowledge of this **statistical term**. The relative error on the electron polarization $\Delta P_e/P_e$ for a ± 10 % relative error on the knowledge of the statistical term b'_2 is given in tables 38,39,40 and 41 for respectively (Differential method,-10 %), (Integrated method,-10 %), (Differential method,+10 %) and (Integrated method,+10 %). Such an error would affect the P_e measurement at a level less than 1% for all thresholds and all energies except for an incident energy of 1 GeV where the resolution is worst. For this energy, the systematic effect would be 2 % for the differential method (almost independent of the threshold) and 1 % for the integrated method (for a threshold ρ=0.5). The integrated method is only sensitive to the smearing near the threshold since the upper threshold has been enlarged to cover the whole upper part of the energy distribution. This method gives lower systematic errors than the differential method where the smearing acts on all bins.

   We are almost insensitive to an error on the **constant** (a'_1) **or linear** (c'_3) **terms**. An error of ± 10 % on these terms gives an relative error on the polarization below $\frac{\Delta P_e}{P_e} \leq 0.1$ % as shown in tables 42,43 and 44,45 for the constant and the linear term.

   Measurement of the quadratic term of the resolution at a 5 % level have been achieved in tests of calorimeter prototype of PWO crystal at γ energies between 0.5 and 2 GeV [20]. Such an error would give a systematic error on the electron polarization less than the required precision of 1 %. We plan to extend these tests at lower energy on the electron beam at Mainz. Moreover the electron detector can be used to control on line the variation of the resolution.

Differential Method Smeared E_γ = 1.17eV P_e =0.500 quadratic term(%) = 2.70								
E(GeV)	1.00	2.00	3.00	4.00	5.00	6.00	7.00	8.00
k_m(MeV)	17.5	68.9	152.4	266.5	409.6	580.3	777.3	999.4
ρ	Δ%	Δ%	Δ%	Δ%	Δ%	Δ%	Δ%	Δ%
0.00	1.66±0.72	0.56±0.34	0.23±0.22	0.12±0.17	0.07±0.14	0.04±0.12	0.03±0.10	0.02±0.09
0.10	*****±****	0.56±0.34	0.23±0.22	0.12±0.17	0.07±0.14	0.04±0.12	0.03±0.10	0.02±0.09
0.20	1.68±0.72	0.57±0.34	0.24±0.23	0.12±0.17	0.07±0.14	0.04±0.12	0.03±0.10	0.02±0.09
0.30	*****±****	0.56±0.34	0.24±0.23	0.12±0.17	0.07±0.14	0.04±0.12	0.03±0.10	0.02±0.09
0.40	1.46±0.73	0.53±0.34	0.22±0.23	0.11±0.17	0.06±0.14	0.04±0.12	0.03±0.11	0.02±0.09
0.50	*****±****	0.51±0.34	0.21±0.23	0.10±0.17	0.06±0.14	0.03±0.12	0.02±0.11	0.02±0.09
0.60	1.86±0.74	0.58±0.34	0.23±0.23	0.11±0.17	0.06±0.14	0.04±0.12	0.03±0.11	0.02±0.09
0.70	*****±****	0.79±0.35	0.32±0.24	0.16±0.18	0.09±0.15	0.06±0.12	0.04±0.11	0.03±0.10
0.80	2.00±0.85	0.99±0.39	0.50±0.26	0.28±0.19	0.17±0.16	0.11±0.13	0.08±0.12	0.06±0.10
0.90	*****±****	0.96±0.49	0.59±0.33	0.40±0.25	0.29±0.20	0.21±0.17	0.16±0.15	0.13±0.13

Table 38: ***Relative error Δ on the electron polarization*** *due to a $-$ 10 % error on the quadratic term of the resolution ($b_2' = 3\%$, $b_2'^S = 2.7\%$). For the differential method, incident energies ranging from 1 GeV to 8 GeV and thresholds from 0.0 to 0.9*

Integrated Method Smeared E_γ = 1.17eV P_e =0.500 quadratic term(%) = 2.70								
E(GeV)	1.00	2.00	3.00	4.00	5.00	6.00	7.00	8.00
k_m(MeV)	17.5	68.9	152.4	266.5	409.6	580.3	777.3	999.4
ρ	Δ%	Δ%	Δ%	Δ%	Δ%	Δ%	Δ%	Δ%
0.00	0.00±1.27	0.00±0.66	0.00±0.46	0.00±0.35	0.00±0.29	0.00±0.25	0.00±0.22	0.00±0.20
0.10	*****±****	-0.31±0.59	-0.14±0.41	-0.08±0.32	-0.05±0.26	-0.04±0.23	-0.03±0.20	-0.02±0.18
0.20	-0.76±0.99	-0.26±0.52	-0.13±0.36	-0.08±0.28	-0.05±0.23	-0.04±0.20	-0.03±0.18	-0.02±0.16
0.30	*****±****	-0.15±0.46	-0.08±0.31	-0.05±0.24	-0.03±0.20	-0.02±0.17	-0.02±0.15	-0.02±0.14
0.40	0.39±0.80	0.00±0.41	-0.01±0.28	-0.01±0.21	-0.01±0.18	-0.01±0.15	-0.01±0.13	0.00±0.12
0.50	*****±****	0.18±0.37	0.07±0.25	0.04±0.19	0.02±0.16	0.02±0.14	0.01±0.12	0.01±0.11
0.60	1.49±0.75	0.38±0.36	0.16±0.24	0.09±0.18	0.06±0.15	0.04±0.13	0.03±0.11	0.02±0.10
0.70	*****±****	0.61±0.36	0.27±0.24	0.15±0.18	0.10±0.15	0.07±0.13	0.05±0.11	0.04±0.10
0.80	2.00±0.85	0.83±0.39	0.42±0.26	0.25±0.19	0.16±0.16	0.11±0.13	0.08±0.12	0.07±0.10
0.90	*****±****	0.96±0.49	0.59±0.33	0.40±0.25	0.29±0.20	0.21±0.17	0.16±0.15	0.13±0.13

Table 39: ***Relative error Δ on the electron polarization*** *due to a $-$ 10 % error on the quadratic term of the resolution ($b_2' = 3\%$, $b_2'^S = 2.7\%$). For the integrated method, incident energies ranging from 1 GeV to 8 GeV and thresholds from 0.0 to 0.9*

Differential Method Smeared E_γ = 1.17eV P_e =0.500 quadratic term(%) = 3.30								
E(GeV)	1.00	2.00	3.00	4.00	5.00	6.00	7.00	8.00
k_m(MeV)	17.5	68.9	152.4	266.5	409.6	580.3	777.3	999.4
ρ	Δ%	Δ%	Δ%	Δ%	Δ%	Δ%	Δ%	Δ%
0.00	-1.64±0.74	-0.61±0.34	-0.26±0.23	-0.14±0.17	-0.08±0.14	-0.05±0.12	-0.03±0.10	-0.03±0.09
0.10	*****±****	-0.61±0.34	-0.26±0.23	-0.14±0.17	-0.08±0.14	-0.05±0.12	-0.04±0.10	-0.03±0.09
0.20	-1.65±0.75	-0.63±0.34	-0.27±0.23	-0.14±0.17	-0.08±0.14	-0.05±0.12	-0.04±0.10	-0.03±0.09
0.30	*****±****	-0.61±0.34	-0.27±0.23	-0.14±0.17	-0.08±0.14	-0.05±0.12	-0.04±0.10	-0.03±0.09
0.40	-1.50±0.75	-0.57±0.35	-0.25±0.23	-0.13±0.17	-0.08±0.14	-0.05±0.12	-0.03±0.11	-0.02±0.09
0.50	*****±****	-0.56±0.35	-0.23±0.23	-0.12±0.17	-0.07±0.14	-0.04±0.12	-0.03±0.11	-0.02±0.09
0.60	-1.97±0.77	-0.66±0.35	-0.26±0.23	-0.13±0.18	-0.08±0.14	-0.05±0.12	-0.03±0.11	-0.02±0.09
0.70	*****±****	-0.88±0.36	-0.37±0.24	-0.19±0.18	-0.11±0.15	-0.07±0.12	-0.05±0.11	-0.04±0.10
0.80	-2.05±0.88	-1.05±0.40	-0.56±0.26	-0.32±0.20	-0.19±0.16	-0.13±0.13	-0.09±0.12	-0.07±0.10
0.90	*****±****	-0.99±0.49	-0.61±0.33	-0.42±0.25	-0.31±0.20	-0.23±0.17	-0.18±0.15	-0.14±0.13

Table 40: ***Relative error Δ on the electron polarization*** *due to a + 10 % error on the quadratic term of the resolution (b'_2 = 3% , b'^S_2 = 3.3%). For the differential method, incident energies ranging from 1 GeV to 8 GeV and thresholds from 0.0 to 0.9*

Integrated Method Smeared E_γ = 1.17eV P_e =0.500 quadratic term(%) = 3.30								
E(GeV)	1.00	2.00	3.00	4.00	5.00	6.00	7.00	8.00
k_m(MeV)	17.5	68.9	152.4	266.5	409.6	580.3	777.3	999.4
ρ	Δ%	Δ%	Δ%	Δ%	Δ%	Δ%	Δ%	Δ%
0.00	0.00±1.27	0.00±0.66	0.00±0.46	0.00±0.35	0.00±0.29	0.00±0.25	0.00±0.22	0.00±0.20
0.10	*****±****	0.33±0.59	0.16±0.41	0.09±0.32	0.06±0.26	0.04±0.23	0.03±0.20	0.03±0.18
0.20	0.75±0.97	0.29±0.52	0.14±0.36	0.08±0.28	0.06±0.23	0.04±0.20	0.03±0.18	0.02±0.16
0.30	*****±****	0.16±0.45	0.09±0.31	0.05±0.24	0.04±0.20	0.03±0.17	0.02±0.15	0.02±0.14
0.40	-0.50±0.81	-0.01±0.41	0.01±0.28	0.01±0.21	0.01±0.18	0.01±0.15	0.01±0.13	0.01±0.12
0.50	*****±****	-0.21±0.37	-0.08±0.25	-0.04±0.19	-0.02±0.16	-0.02±0.14	-0.01±0.12	-0.01±0.11
0.60	-1.58±0.78	-0.43±0.36	-0.18±0.24	-0.10±0.18	-0.06±0.15	-0.04±0.13	-0.03±0.11	-0.03±0.10
0.70	*****±****	-0.68±0.36	-0.30±0.24	-0.17±0.18	-0.11±0.15	-0.08±0.13	-0.06±0.11	-0.04±0.10
0.80	-2.05±0.88	-0.89±0.40	-0.47±0.26	-0.27±0.20	-0.18±0.16	-0.13±0.13	-0.09±0.12	-0.07±0.10
0.90	*****±****	-0.99±0.49	-0.61±0.33	-0.42±0.25	-0.31±0.20	-0.23±0.17	-0.18±0.15	-0.14±0.13

Table 41: ***Relative error Δ on the electron polarization*** *due to a + 10 % error on the quadratic term of the resolution (b'_2 = 3% b'^S_2 = 3.3%). For the integrated method, incident energies ranging from 1 GeV to 8 GeV and thresholds from 0.0 to 0.9*

Differential Method Smeared E_γ = 1.17eV P_e =0.500 constant term(%) = 1.10								
E(GeV)	1.00	2.00	3.00	4.00	5.00	6.00	7.00	8.00
k_m(MeV)	17.5	68.9	152.4	266.5	409.6	580.3	777.3	999.4
ρ	Δ%	Δ%	Δ%	Δ%	Δ%	Δ%	Δ%	Δ%
0.00	0.00±0.73	0.00±0.34	0.00±0.22	0.00±0.17	0.00±0.14	0.00±0.12	0.00±0.10	0.00±0.09
0.10	*****±****	0.00±0.34	0.00±0.23	0.00±0.17	0.00±0.14	0.00±0.12	0.00±0.10	0.00±0.09
0.20	0.00±0.73	0.00±0.34	0.00±0.23	0.00±0.17	0.00±0.14	0.00±0.12	0.00±0.10	0.00±0.09
0.30	*****±****	0.00±0.34	0.00±0.23	0.00±0.17	0.00±0.14	0.00±0.12	0.00±0.10	0.00±0.09
0.40	0.00±0.74	0.00±0.34	0.00±0.23	0.00±0.17	0.00±0.14	0.00±0.12	0.00±0.11	0.00±0.09
0.50	*****±****	0.00±0.34	0.00±0.23	0.00±0.17	0.00±0.14	0.00±0.12	0.00±0.11	0.00±0.09
0.60	0.00±0.75	0.00±0.35	0.00±0.23	0.00±0.18	0.00±0.14	0.00±0.12	0.00±0.11	0.00±0.09
0.70	*****±****	0.00±0.36	0.00±0.24	0.00±0.18	0.00±0.15	0.00±0.12	0.00±0.11	0.00±0.10
0.80	0.00±0.86	-0.01±0.40	-0.01±0.26	-0.01±0.19	-0.01±0.16	0.00±0.13	0.00±0.12	0.00±0.10
0.90	*****±****	-0.01±0.49	-0.01±0.33	-0.01±0.25	-0.01±0.20	-0.01±0.17	-0.01±0.15	-0.01±0.13

Table 42: ***Relative error Δ on the electron polarization*** *due to a* 10 % *error on the constant term of the resolution* ($a_1' = 1\%$, $a_1'^{S} = 1.1\%$). *For the differential method, incident energies ranging from 1 GeV to 8 GeV and thresholds from 0.0 to 0.9*

Integrated Method Smeared E_γ = 1.17eV P_e =0.500 constant term(%) = 1.10								
E(GeV)	1.00	2.00	3.00	4.00	5.00	6.00	7.00	8.00
k_m(MeV)	17.5	68.9	152.4	266.5	409.6	580.3	777.3	999.4
ρ	Δ%	Δ%	Δ%	Δ%	Δ%	Δ%	Δ%	Δ%
0.00	0.00±1.27	0.00±0.66	0.00±0.46	0.00±0.35	0.00±0.29	0.00±0.25	0.00±0.22	0.00±0.20
0.10	*****±****	0.00±0.59	0.00±0.41	0.00±0.32	0.00±0.26	0.00±0.23	0.00±0.20	0.00±0.18
0.20	0.00±0.98	0.00±0.52	0.00±0.36	0.00±0.28	0.00±0.23	0.00±0.20	0.00±0.18	0.00±0.16
0.30	*****±****	0.00±0.45	0.00±0.31	0.00±0.24	0.00±0.20	0.00±0.17	0.00±0.15	0.00±0.14
0.40	0.00±0.81	0.00±0.41	0.00±0.28	0.00±0.21	0.00±0.18	0.00±0.15	0.00±0.13	0.00±0.12
0.50	*****±****	0.00±0.37	0.00±0.25	0.00±0.19	0.00±0.16	0.00±0.14	0.00±0.12	0.00±0.11
0.60	0.00±0.76	0.00±0.36	0.00±0.24	0.00±0.18	0.00±0.15	0.00±0.13	0.00±0.11	0.00±0.10
0.70	*****±****	0.00±0.36	0.00±0.24	0.00±0.18	0.00±0.15	0.00±0.13	0.00±0.11	0.00±0.10
0.80	0.00±0.86	0.00±0.40	0.00±0.26	-0.01±0.20	0.00±0.16	0.00±0.13	0.00±0.12	0.00±0.10
0.90	*****±****	-0.01±0.49	-0.01±0.33	-0.01±0.25	-0.01±0.20	-0.01±0.17	-0.01±0.15	-0.01±0.13

Table 43: ***Relative error Δ on the electron polarization*** *due to a* 10 % *error on the constant term of the resolution* ($a_1' = 1\%$, $a_1'^{S} = 1.1\%$). *For the integrated method, incident energies ranging from 1 GeV to 8 GeV and thresholds from 0.0 to 0.9*

Differential Method Smeared E_γ = 1.17eV P_e =0.500 linear term(%) = 1.10								
E(GeV)	1.00	2.00	3.00	4.00	5.00	6.00	7.00	8.00
k_m(MeV)	17.5	68.9	152.4	266.5	409.6	580.3	777.3	999.4
ρ	Δ%	Δ%	Δ%	Δ%	Δ%	Δ%	Δ%	Δ%
0.00	-0.01±0.73	-0.01±0.34	-0.01±0.22	-0.01±0.17	-0.01±0.14	-0.01±0.12	-0.01±0.10	-0.01±0.09
0.10	*****±****	-0.01±0.34	-0.01±0.23	-0.01±0.17	-0.01±0.14	-0.01±0.12	-0.01±0.10	-0.01±0.09
0.20	-0.01±0.73	-0.01±0.34	-0.01±0.23	-0.01±0.17	-0.01±0.14	-0.01±0.12	-0.01±0.10	-0.01±0.09
0.30	*****±****	-0.01±0.34	-0.01±0.23	-0.01±0.17	-0.01±0.14	-0.01±0.12	-0.01±0.10	-0.01±0.09
0.40	-0.01±0.74	-0.01±0.34	-0.01±0.23	-0.01±0.17	-0.01±0.14	-0.01±0.12	-0.01±0.11	-0.01±0.09
0.50	*****±****	-0.01±0.34	-0.01±0.23	-0.01±0.17	-0.01±0.14	-0.01±0.12	-0.01±0.11	-0.01±0.09
0.60	-0.01±0.75	-0.01±0.35	-0.01±0.23	-0.01±0.18	-0.01±0.14	-0.01±0.12	-0.01±0.11	-0.01±0.09
0.70	*****±****	-0.01±0.36	-0.01±0.24	-0.01±0.18	-0.01±0.15	-0.01±0.12	-0.01±0.11	-0.01±0.10
0.80	-0.01±0.86	-0.01±0.40	-0.01±0.26	-0.01±0.19	-0.01±0.16	-0.01±0.13	-0.01±0.12	-0.01±0.10
0.90	*****±****	-0.01±0.49	-0.01±0.33	-0.01±0.25	-0.01±0.20	-0.01±0.17	-0.01±0.15	-0.02±0.13

Table 44: ***Relative error Δ on the electron polarization*** *due to a* 10 % *error on the linear term of the resolution* ($c_3' = 1\%$, $c_3'^{S} = 1.1\%$). *For the differential method, incident energies ranging from 1 GeV to 8 GeV and thresholds from 0.0 to 0.9*

Integrated Method Smeared E_γ = 1.17eV P_e =0.500 linear term(%) = 1.10								
E(GeV)	1.00	2.00	3.00	4.00	5.00	6.00	7.00	8.00
k_m(MeV)	17.5	68.9	152.4	266.5	409.6	580.3	777.3	999.4
ρ	Δ%	Δ%	Δ%	Δ%	Δ%	Δ%	Δ%	Δ%
0.00	0.00±1.27	0.00±0.66	0.00±0.46	0.00±0.35	0.00±0.29	0.00±0.25	0.00±0.22	0.00±0.20
0.10	*****±****	0.00±0.59	0.00±0.41	0.00±0.32	0.00±0.26	0.00±0.23	0.00±0.20	0.00±0.18
0.20	0.00±0.98	0.00±0.52	0.00±0.36	0.00±0.28	0.00±0.23	0.00±0.20	0.00±0.18	0.00±0.16
0.30	*****±****	0.00±0.45	0.00±0.31	0.00±0.24	0.00±0.20	0.00±0.17	0.00±0.15	0.00±0.14
0.40	-0.01±0.81	0.00±0.41	0.00±0.28	0.00±0.21	0.00±0.18	0.00±0.15	0.00±0.13	0.00±0.12
0.50	*****±****	-0.01±0.37	-0.01±0.25	-0.01±0.19	-0.01±0.16	-0.01±0.14	-0.01±0.12	-0.01±0.11
0.60	-0.01±0.76	-0.01±0.36	-0.01±0.24	-0.01±0.18	-0.01±0.15	-0.01±0.13	-0.01±0.11	-0.01±0.10
0.70	*****±****	-0.01±0.36	-0.01±0.24	-0.01±0.18	-0.01±0.15	-0.01±0.13	-0.01±0.11	-0.01±0.10
0.80	-0.01±0.86	-0.01±0.40	-0.01±0.26	-0.01±0.20	-0.01±0.16	-0.01±0.13	-0.01±0.12	-0.01±0.10
0.90	*****±****	-0.01±0.49	-0.01±0.33	-0.01±0.25	-0.01±0.20	-0.01±0.17	-0.01±0.15	-0.02±0.13

Table 45: ***Relative error Δ on the electron polarization*** *due to a* 10 % *error on the linear term of the resolution* ($c_3' = 1\%$, $c_3'^{S} = 1.1\%$). *For the integrated method, incident energies ranging from 1 GeV to 8 GeV and thresholds from 0.0 to 0.9*

2. **Error on the calibration**

The total number of Compton events above the threshold only depends on the resolution of the detector and on the upper energy range. Having enlarged this upper limit to cover the whole energy spectrum, this number is insensitive to the **slope of the calibration**. So an error on the slope would not affect the experimental polarization measured by the integrated method (assuming that the resolution and the threshold are known).

For the differential method, the relative error on the electron polarization $\Delta P_e/P_e$ for a $\pm 1\,\%$ relative error on the knowledge of the slope is given in tables 46 ($-1\,\%$) and 47 ($+1\,\%$). For an energy threshold of $\rho = 0.5$, the systematic error should be close to 0.5 %. To reach a systematic error on the electron polarization less than the required precision of 1 %, the slope had to be known at a 2% level.

The last parameter is the error on the **measured energy at threshold** ρ_t of equation 249. Tables 48 and 49 show that the required precision would be close to 0.5 %. This requires an absolute measurement of the γ energy.

Such precisions in the calibration seem achievable thanks to the electron detector.

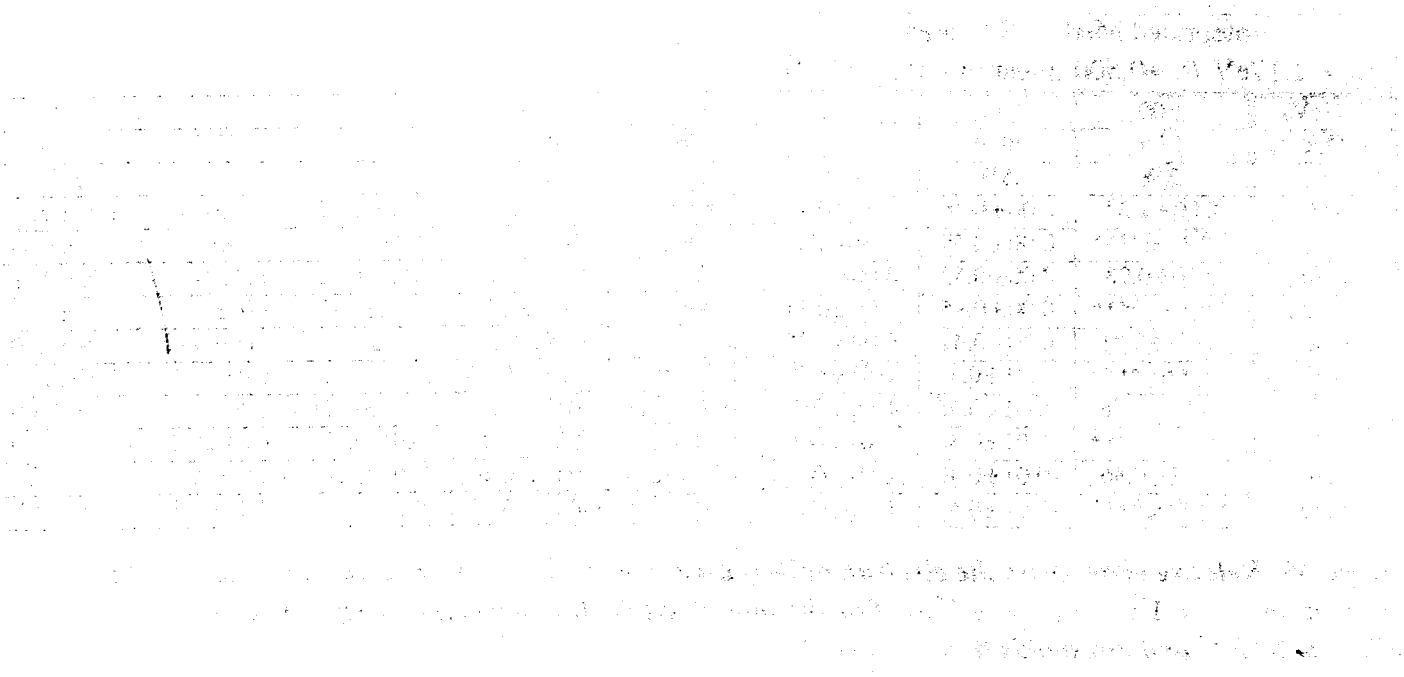

Differential Method Smeared E_γ = 1.17eV P_e =0.500 slope term = 0.99								
E(GeV)	1.00	2.00	3.00	4.00	5.00	6.00	7.00	8.00
k_m(MeV)	17.5	68.9	152.4	266.5	409.6	580.3	777.3	999.4
ρ	Δ%	Δ%	Δ%	Δ%	Δ%	Δ%	Δ%	Δ%
0.00	0.84±0.72	1.16±0.33	1.28±0.22	1.35±0.17	1.39±0.14	1.43±0.12	1.45±0.10	1.47±0.09
0.10	*****±****	1.00±0.33	1.11±0.22	1.18±0.17	1.22±0.14	1.24±0.12	1.27±0.10	1.28±0.09
0.20	0.61±0.73	0.86±0.34	0.96±0.22	1.01±0.17	1.05±0.14	1.08±0.12	1.09±0.10	1.11±0.09
0.30	*****±****	0.72±0.34	0.81±0.23	0.86±0.17	0.89±0.14	0.91±0.12	0.93±0.10	0.94±0.09
0.40	0.36±0.73	0.57±0.34	0.65±0.23	0.69±0.17	0.72±0.14	0.74±0.12	0.76±0.10	0.77±0.09
0.50	*****±****	0.41±0.34	0.48±0.23	0.52±0.17	0.54±0.14	0.56±0.12	0.57±0.11	0.59±0.09
0.60	0.14±0.75	0.26±0.34	0.30±0.23	0.34±0.17	0.36±0.14	0.37±0.12	0.38±0.11	0.39±0.09
0.70	*****±****	0.13±0.36	0.16±0.24	0.18±0.18	0.19±0.15	0.20±0.12	0.21±0.11	0.22±0.10
0.80	0.00±0.86	0.05±0.40	0.06±0.26	0.07±0.19	0.07±0.16	0.08±0.13	0.08±0.12	0.09±0.10
0.90	*****±****	0.00±0.49	0.00±0.33	0.00±0.25	0.00±0.20	0.00±0.17	0.00±0.15	0.00±0.13

Table 46: ***Relative error Δ on the electron polarization*** *due to a $-$ 1 % error on the slope of the calibration ($s = 0.99$). For the differential method, incident energies ranging from 1 GeV to 8 GeV and thresholds from 0.0 to 0.9*

Differential Method Smeared E_γ = 1.17eV P_e =0.500 slope term = 1.01								
E(GeV)	1.00	2.00	3.00	4.00	5.00	6.00	7.00	8.00
k_m(MeV)	17.5	68.9	152.4	266.5	409.6	580.3	777.3	999.4
ρ	Δ%	Δ%	Δ%	Δ%	Δ%	Δ%	Δ%	Δ%
0.00	-0.85±0.74	-1.18±0.34	-1.31±0.23	-1.39±0.17	-1.44±0.14	-1.48±0.12	-1.51±0.10	-1.53±0.09
0.10	*****±****	-1.02±0.34	-1.14±0.23	-1.21±0.17	-1.26±0.14	-1.29±0.12	-1.31±0.10	-1.33±0.09
0.20	-0.61±0.74	-0.87±0.34	-0.98±0.23	-1.04±0.17	-1.08±0.14	-1.11±0.12	-1.13±0.11	-1.15±0.09
0.30	*****±****	-0.73±0.34	-0.82±0.23	-0.88±0.17	-0.91±0.14	-0.94±0.12	-0.96±0.11	-0.97±0.09
0.40	-0.36±0.74	-0.58±0.35	-0.66±0.23	-0.71±0.18	-0.74±0.14	-0.76±0.12	-0.78±0.11	-0.79±0.09
0.50	*****±****	-0.41±0.35	-0.48±0.23	-0.52±0.18	-0.55±0.14	-0.57±0.12	-0.59±0.11	-0.60±0.10
0.60	-0.14±0.75	-0.26±0.35	-0.31±0.23	-0.34±0.18	-0.36±0.14	-0.38±0.12	-0.39±0.11	-0.40±0.09
0.70	*****±****	-0.13±0.36	-0.16±0.24	-0.18±0.18	-0.20±0.15	-0.21±0.12	-0.21±0.11	-0.22±0.10
0.80	0.00±0.86	-0.05±0.40	-0.06±0.26	-0.07±0.19	-0.08±0.16	-0.08±0.13	-0.08±0.12	-0.09±0.10
0.90	*****±****	0.00±0.49	0.00±0.33	0.00±0.25	0.00±0.20	0.00±0.17	0.00±0.15	0.00±0.13

Table 47: ***Relative error Δ on the electron polarization*** *due to a + 1 % error on the slope of the calibration ($s = 1.01$). For the differential method, incident energies ranging from 1 GeV to 8 GeV and thresholds from 0.0 to 0.9*

Differential Method Smeared E_γ = 1.17eV P_e =0.500 threshold term =-1.00								
E(GeV)	1.00	2.00	3.00	4.00	5.00	6.00	7.00	8.00
k_m(MeV)	17.5	68.9	152.4	266.5	409.6	580.3	777.3	999.4
ρ	Δ%	Δ%	Δ%	Δ%	Δ%	Δ%	Δ%	Δ%
0.00	1.23±0.72	1.58±0.33	1.70±0.22	1.77±0.17	1.82±0.14	1.85±0.12	1.87±0.10	1.89±0.09
0.10	*****±****	1.57±0.33	1.69±0.22	1.76±0.17	1.81±0.14	1.84±0.12	1.86±0.10	1.88±0.09
0.20	1.23±0.73	1.53±0.33	1.66±0.22	1.73±0.17	1.77±0.14	1.80±0.12	1.82±0.10	1.84±0.09
0.30	*****±****	1.54±0.34	1.66±0.22	1.72±0.17	1.77±0.14	1.80±0.12	1.82±0.10	1.83±0.09
0.40	1.30±0.73	1.59±0.34	1.71±0.23	1.77±0.17	1.82±0.14	1.85±0.12	1.87±0.10	1.88±0.09
0.50	*****±****	1.62±0.34	1.75±0.23	1.83±0.17	1.87±0.14	1.91±0.12	1.93±0.10	1.95±0.09
0.60	1.03±0.74	1.50±0.34	1.67±0.23	1.76±0.17	1.82±0.14	1.86±0.12	1.89±0.10	1.92±0.09
0.70	*****±****	1.20±0.35	1.40±0.23	1.51±0.18	1.58±0.14	1.63±0.12	1.66±0.11	1.69±0.09
0.80	0.56±0.85	0.81±0.39	0.97±0.25	1.09±0.19	1.17±0.15	1.22±0.13	1.26±0.11	1.29±0.10
0.90	*****±****	0.45±0.47	0.48±0.32	0.53±0.24	0.56±0.19	0.60±0.16	0.63±0.14	0.65±0.12

Table 48: ***Relative error Δ on the electron polarization*** *due to a* -0.01 *error on the threshold of the calibration* ($\rho_t = 0.01$). *For the differential method, incident energies ranging from 1 GeV to 8 GeV and thresholds from 0.0 to 0.9*

Integrated Method Smeared E_γ = 1.17eV P_e =0.500 threshold term =-1.00								
E(GeV)	1.00	2.00	3.00	4.00	5.00	6.00	7.00	8.00
k_m(MeV)	17.5	68.9	152.4	266.5	409.6	580.3	777.3	999.4
ρ	Δ%	Δ%	Δ%	Δ%	Δ%	Δ%	Δ%	Δ%
0.00	0.00±1.27	0.00±0.66	0.00±0.46	0.00±0.35	0.00±0.29	0.00±0.25	0.00±0.22	0.00±0.20
0.10	*****±****	1.89±0.59	1.90±0.41	1.90±0.32	1.91±0.26	1.92±0.23	1.93±0.20	1.93±0.18
0.20	1.83±0.97	2.00±0.51	2.04±0.36	2.06±0.28	2.08±0.23	2.10±0.20	2.12±0.17	2.14±0.16
0.30	*****±****	1.91±0.45	1.97±0.31	2.01±0.24	2.04±0.20	2.07±0.17	2.09±0.15	2.12±0.14
0.40	1.43±0.80	1.71±0.40	1.78±0.28	1.83±0.21	1.86±0.18	1.89±0.15	1.92±0.13	1.95±0.12
0.50	*****±****	1.46±0.37	1.54±0.25	1.58±0.19	1.61±0.16	1.64±0.14	1.67±0.12	1.70±0.11
0.60	0.94±0.76	1.19±0.35	1.27±0.24	1.31±0.18	1.35±0.15	1.37±0.13	1.40±0.11	1.42±0.10
0.70	*****±****	0.92±0.36	1.01±0.24	1.06±0.18	1.09±0.15	1.11±0.12	1.13±0.11	1.15±0.10
0.80	0.56±0.85	0.66±0.39	0.75±0.25	0.80±0.19	0.84±0.15	0.87±0.13	0.89±0.11	0.91±0.10
0.90	*****±****	0.45±0.47	0.48±0.32	0.53±0.24	0.56±0.19	0.60±0.16	0.63±0.14	0.65±0.12

Table 49: ***Relative error Δ on the electron polarization*** *due to a* -0.01 *error on the threshold of the calibration* ($\rho_t = 0.01$). *For the integrated method, incident energies ranging from 1 GeV to 8 GeV and thresholds from 0.0 to 0.9*

E.3 Effect of the Electron detector resolution and calibration

The scattered γ energy k is here measured by the deviation of the scattered electron through the first dipole magnet. Using the dispersion of this dipole, the transverse deviation from the beam axis is related to the difference between the electron momentum p and the electron beam momentum p_0 and so to the γ energy $k = p_0 - p$.

E.3.1 Simulation of the electron detector resolution

The **total transverse deviation** d for an electron of momentum p after a dipole (length L, field B) and a drift (length l) is for a perfect dipole and neglecting the incident electron angle

$$d = R(1 - \cos\theta) + l\,\tan\theta = R\sin\theta\,\tan(\frac{\theta}{2}) + l\,\tan\theta = \sin\theta\left(\frac{L}{1+\cos\theta} + \frac{l}{\cos\theta}\right) \tag{250}$$

where the characteristics of the helix describing the electron trajectory in the dipole, deviation angle θ and radius of curvature R, are

$$\sin\theta = \frac{0.3\,B}{p}L \quad ; \quad R = \frac{p}{0.3\,B} \quad ; \quad R\sin\theta = L \tag{251}$$

For small deviation angle θ, the transverse deviation can be approximated by

$$d \simeq \sin\theta\left(\frac{L}{2}+l\right) \simeq \frac{0.3\,B}{p}L\left(\frac{L}{2}+l\right) \simeq \frac{A}{p} \qquad with \qquad A = 0.3BL\left(\frac{L}{2}+l\right) \tag{252}$$

The **displacement** Δx for an electron of momentum p from the beam of momentum p_0 is given by

$$\Delta x = d - d_0 = -\frac{A}{p_0}\frac{p - p_0}{p} = \alpha\frac{\Delta p}{p} \tag{253}$$

and depends on the dispersion α

$$\alpha = \frac{\Delta x}{\Delta p\,/\,p} \simeq -\frac{A}{p_0} = -\frac{0.3\,B}{p_0}L\left(\frac{L}{2}+l\right) \tag{254}$$

The **energy k of the scattered photon** is then measured by the displacement Δx of the scattered electron (momentum $p = p_0 - k$) through equation 253 with $\Delta p = p - p_0 = -k$

$$k = p_0\frac{\Delta x}{\Delta x - \alpha} \tag{255}$$

The **resolution on the γ energy** k, given by

$$\frac{\sigma(k)}{k} = \frac{\sigma(p_0)}{p_0} \bigoplus \sigma(\Delta x)\frac{(p_0 - k)^2}{\alpha\,p_0\,k} \bigoplus \sigma(\alpha)\frac{(p_0 - k)}{\alpha\,p_0} \tag{256}$$

is due to

- the energy resolution of the beam $\sigma(p_0)$ which can be neglected here: $\sigma(p_0) = 0$.
- the transverse size of the interaction between the Laser beam and the electron beam $\sigma(\Delta x)$. This size will be close to $\sigma(\Delta x) = 100\ \mu$.
- the resolution on the dispersion $\sigma(\alpha)$ which includes higher order magnetic effects neglected in the parametrization of the dispersion (Eq. 254), angular divergence of the electron beam and scattering angle of the Compton electron. For this preliminary study, we have taken $\sigma(\alpha)\,/\,\alpha = 1\%$ a very conservative value for magnetic system.

E	GeV	1.00	2.00	3.00	4.00	5.00	6.00	7.00	8.00
B	Tesla	0.19	0.37	0.56	0.75	0.94	1.12	1.31	1.50
α	$cm/\%$	0.230	0.230	0.230	0.230	0.230	0.230	0.230	0.230
k_{max}	MeV	17.5	68.9	152.4	266.5	409.6	580.3	777.3	999.4
k_{gap}	MeV	21.2	42.5	63.7	84.9	106.2	127.4	148.6	169.9
k_{end}	MeV	131.8	263.7	395.5	527.4	659.2	791.1	922.9	1054.8
$\sigma(\rho_{max})$	%	2.58	1.52	1.22	1.09	1.02	0.97	0.94	0.91
$\sigma_x(\rho_{max})$	%	2.39	1.17	0.77	0.57	0.45	0.37	0.31	0.27
$\sigma_\alpha(\rho_{max})$	%	0.98	0.97	0.95	0.93	0.92	0.90	0.89	0.88
$\sigma(\rho_{gap})$	%	2.65	1.35	0.91	0.70	0.57	0.48	0.42	0.37
$\sigma_x(\rho_{gap})$	%	2.37	1.21	0.82	0.62	0.51	0.43	0.37	0.33
$\sigma_\alpha(\rho_{gap})$	%	1.19	0.60	0.41	0.31	0.25	0.21	0.19	0.17
$< \Delta\rho >$	%	0.00	2.97	1.98	1.49	1.19	0.99	0.85	0.74

Table 50: ***Contribution to the electron detector resolution*** *for an electron detector of size $D_e = 3\ cm$ with a safety gap of $d_g = 5\ mm$ after a dipole ($L = 1\ m$, B) and a drift length ($l = 3.6\ m$). Maximal Compton γ energy k_{max}. γ energy range $[\,k_{gap}\,,\,k_{end}\,]$ covered by the electron detector. Resolution $\sigma(\rho)$ on $\rho = k/k_{max}$ for scattered γ energy k_{max} and k_{gap}. σ_x gives the contribution coming from the beam position resolution $\sigma(\Delta x) = 100\ \mu$ while σ_α gives the contribution coming from the resolution on the dispersion $\sigma(\alpha)/\alpha = 1\%$. Bin width $\Delta\rho$ for the mean energy $(k_{gap} + k_{max})/2$. and for a silicon detector pitch of* $250\ \mu$.

The scattered γ energy was distributed according to a Gaussian law with a resolution $\sigma(k)$ given by equation 256. After integration over the scattered γ energy spectrum given by the Compton cross section $d\sigma_c/dk$, we obtain the smeared energy distribution :

$$\frac{d\sigma_a}{dk_s} = \int_0^{k_{max}} \frac{d\sigma_c}{dk}\ \frac{1}{\sqrt{2\pi}\,\sigma(k)\,k}\ e^{-\frac{(k-k_s)^2}{2\,(\sigma(k))^2}}\ dk \tag{257}$$

The electron detector of size $D_e = 3\ cm$ has to be set out of the electron beam. A safety gap of $d_g = 5mm$ prevents the detector from the beam. The energy range covered by the electron detector $[k_{gap}\,;\,k_{end}]$ is given in table 50 for incident electron energies E ranging from 1 to 8 GeV. These energies have been deduced from equation 255 with $\Delta x = d_g$ and $\Delta x = d_g + D_e$. The magnetic dispersion (Eq. 254) stands for a $L = 1\ m$ dipole, a drift length $l = 3.6\ m$ and the magnetic field given in the second line of table 50.

The gap energy k_{gap} has to be lower than the maximal Compton γ energy k_{max} to allow Compton cross section measurements. From the table, we see that polarization measurements with this electron detector are only feasible for $E \geq 2\ GeV$.

This table gives also the resolution on $\rho = k/k_{max}$ for k_{max} and k_{gap} with the contributions coming from the beam size $\sigma(\Delta x) = 150\ \mu$ and from the resolution on the dispersion $\sigma(\alpha)/\alpha = 1\ \%$.

Finally, the bin energy width $\Delta\rho$ for the mean detected energy is quoted for a silicon detector pitch of $250\ \mu$. This width is about twice the resolution.

The figure 51 gives the smeared cross section $d\sigma_s\ /\ dk_s$ for incident energies $E = 2, 4, 6$ and $8\ GeV$ as well as the threshold due to the safety gap.

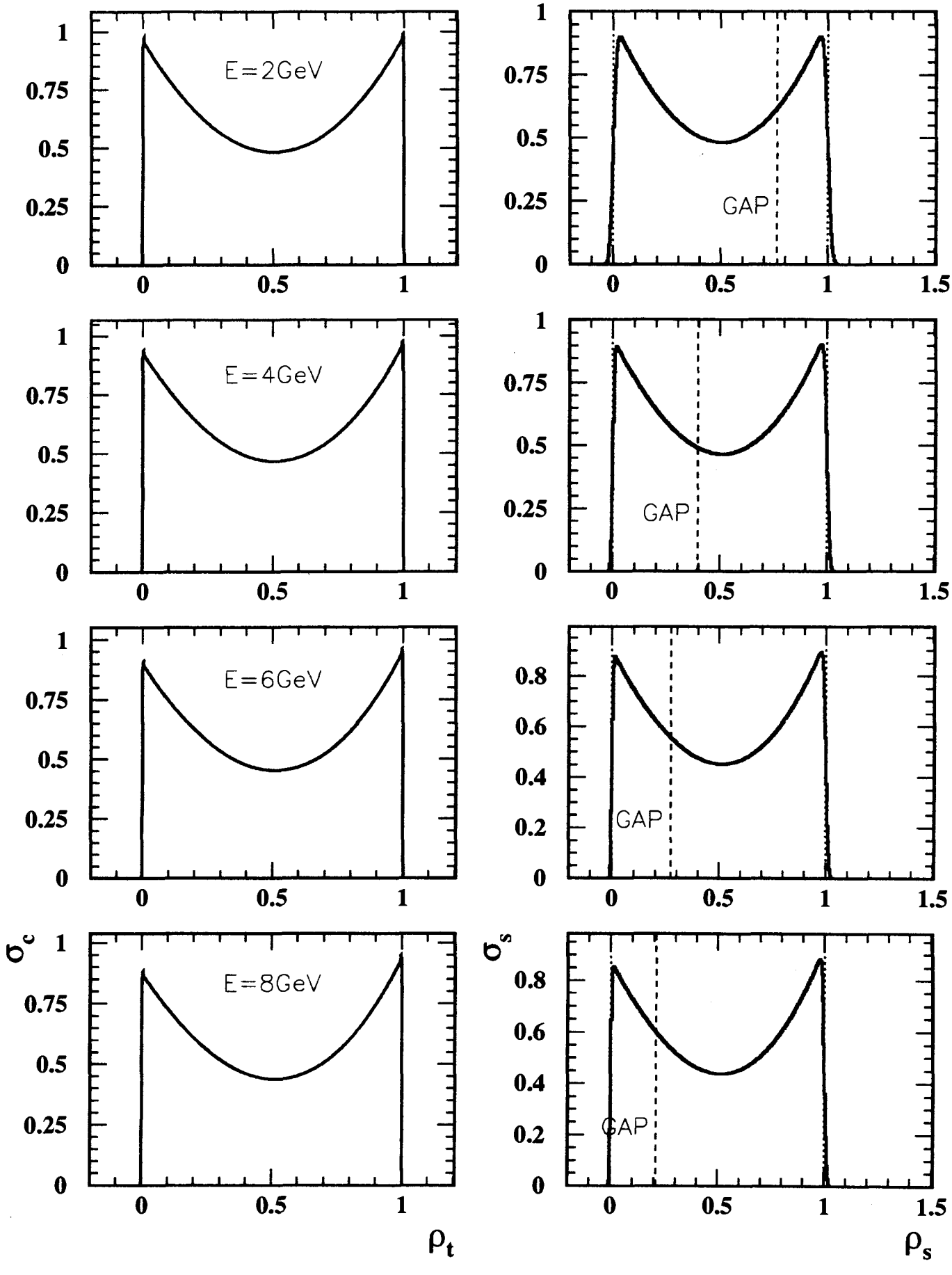

Figure 51: ***Compton cross section (left) and smeared Compton cross section (right)*** *for incident electron energy* $E = 2, 4, 6, 8, GeV$. *Laser and electron polarizations are* $P_\gamma = 1.$ *and* $P_e = +0.5$

E (GeV)	1.00	2.00	3.00	4.00	5.00	6.00	7.00	8.00
Number of bins	0	13	15	16	16	16	20	19
$\rho_s(1)$	*****	0.616	0.418	0.319	0.259	0.220	0.191	0.170
$\rho_s(2)$	*****	0.646	0.459	0.365	0.310	0.273	0.238	0.220
$\rho_s(3)$	*****	0.676	0.499	0.412	0.360	0.326	0.284	0.269
$\rho_s(4)$	*****	0.706	0.540	0.458	0.410	0.378	0.329	0.317
$\rho_s(5)$	*****	0.736	0.580	0.504	0.459	0.430	0.375	0.365
$\rho_s(6)$	*****	0.766	0.620	0.549	0.508	0.481	0.419	0.412
$\rho_s(7)$	*****	0.796	0.660	0.594	0.556	0.532	0.463	0.458
$\rho_s(8)$	*****	0.826	0.700	0.639	0.604	0.582	0.507	0.504
$\rho_s(9)$	*****	0.855	0.740	0.684	0.652	0.632	0.550	0.550
$\rho_s(10)$	*****	0.885	0.779	0.728	0.699	0.681	0.593	0.595
$\rho_s(11)$	*****	0.915	0.818	0.772	0.746	0.730	0.636	0.639
$\rho_s(12)$	*****	0.944	0.858	0.816	0.793	0.778	0.678	0.683
$\rho_s(13)$	*****	0.974	0.897	0.860	0.839	0.826	0.719	0.726
$\rho_s(14)$	*****	3.826	0.935	0.903	0.884	0.873	0.760	0.769
$\rho_s(15)$	*****	*****	0.974	0.946	0.930	0.920	0.801	0.812
$\rho_s(16)$	*****	*****	2.595	0.989	0.975	0.966	0.841	0.853
$\rho_s(17)$	*****	*****	*****	1.979	1.610	1.363	0.881	0.895
$\rho_s(18)$	*****	*****	*****	*****	*****	*****	0.921	0.936
$\rho_s(19)$	*****	*****	*****	*****	*****	*****	0.960	0.976
$\rho_s(20)$	*****	*****	*****	*****	*****	*****	0.999	1.055
$\rho_s(21)$	*****	*****	*****	*****	*****	*****	1.187	*****

E	GeV	1.00	2.00	3.00	4.00	5.00	6.00	7.00	8.00
Number of thresholds		0	4	6	7	7	8	8	8
ρ_t	$\simeq 0.200$	*****	*****	*****	*****	*****	0.220	0.191	0.170
ρ_t	$\simeq 0.300$	*****	*****	*****	0.319	0.259	0.326	0.284	0.317
ρ_t	$\simeq 0.400$	*****	*****	0.418	0.412	0.410	0.378	0.419	0.412
ρ_t	$\simeq 0.500$	*****	*****	0.499	0.504	0.508	0.481	0.507	0.504
ρ_t	$\simeq 0.600$	*****	0.616	0.580	0.594	0.604	0.582	0.593	0.595
ρ_t	$\simeq 0.700$	*****	0.706	0.700	0.684	0.699	0.681	0.719	0.683
ρ_t	$\simeq 0.800$	*****	0.796	0.818	0.816	0.793	0.778	0.801	0.812
ρ_t	$\simeq 0.900$	*****	0.915	0.897	0.903	0.884	0.920	0.881	0.895

Table 51: ***Energy bin range. Energy threshold values.***

E.3.2 Energy bining, variation of threshold, calibration simulation

The **energy bins** are fixed by the safety gap $d_g = 5\ mm$ and the width of the silicon strips $d_s = 250\ \mu$. We have in fact used larger bins $d_b = n_r\ d_s$ in order to have energy bins of order $dk^i \simeq .05\ k_{max}$. All bins above k_{max} have been also grouped. The **smeared energy** k_s corresponding to a perfect calibration is then (Eq. 255)

$$k_s^i = p_0 \frac{\Delta x^i}{\Delta x^i - \alpha} \qquad with \qquad \Delta^i x = d_g + (i-1)\, d_b \tag{258}$$

The perfect calibration means that the safety gap and the dispersion are perfectly known.

Due to the errors d_x on the measured safety gap $d_m = d_g + d_x$ and $d\alpha/\alpha$ on the measured dispersion $\alpha_m = \alpha\,(1 + d\alpha/\alpha)$, the **measured energy** k_m is

$$k_m^i = p_0 \frac{\Delta x_m^i}{\Delta x_m^i - \alpha_m} \quad with \quad \Delta x_m^i = d_g + d_x + (i-1)d_b \quad and \quad \alpha_m = \alpha(1 + \frac{d\alpha}{\alpha}) \tag{259}$$

The **energy thresholds** are the bin energy closest to some predefined values ρ_t:

$$\rho_t \simeq [\,0.\,,\ 0.1\,,\ 0.2\,,\ 0.3\,,\ 0.4\,,\ 0.5\,,\ 0.6\,,\ 0.7\,,\ 0.8\,,\ 0.9\,]$$

The number of bins and the bin range are listed in table 51. Also are given the number and the values of the useful thresholds. We have only given the smeared energy ρ_s independent of the calibration.

E.3.3 Results and discussion

1. **Error on the resolution**
   We have seen that the resolution on the γ energy k (Eq. 256) was mainly due to the transverse size of the interaction region and to the resolution on the dispersion. The contributions of these terms in the resolution are quite similar as seen in table 50.
   We will now look at the systematic effects induced by an error on the knowledge of these parameters :

   - the transverse size of the interaction between the Laser beam and the electron beam $\sigma(\Delta x)$ whose expected value has been taken as $\sigma(\Delta x) = 100\ \mu$.
     The relative error on the electron polarization $\Delta P_e/P_e$ for a $+50$ % relative error on the knowledge of the beam size is given in tables 52 and 53 for respectively the differential method and the integrated method. Such an error would affect the P_e measurement at a level less than 0.25 % for all thresholds and all energies.
   - the resolution on the dispersion $\sigma(\alpha)$ taken as $\sigma(\alpha)\ /\ \alpha = 1$ %
     The relative error on the electron polarization $\Delta P_e/P_e$ for a $+50$ % relative error on the knowledge of the dispersion is given in tables 54 and 55 for respectively the differential method and the integrated method. The systematic effect on the P_e measurement is less than 0.1 % for all thresholds and all energies.

   The systematic effects due to the kwnoledge of the resolution are small. This comes from the fact that the resolution is good (better than 2%) inducing a weak smearing. A relative precision of ± 50 % on both the interaction size and the resolution on the dispersion ensures systematic effects less than 0.25 %. Such precision can be easily reached.

2. **Error on the calibration**
   The calibration of the electron detector (Eq. 259) depends on 2 parameters :

   - the error d_x on the measured safety gap $d_m = d_g + d_x$ which differs from the real one $d_g = 5\ mm$.
     The relative error on the electron polarization $\Delta P_e/P_e$ for a $d_x = \pm 50\ \mu$ error on the safety gap is given in tables 56, 57,58 and 59 for respectively $d_x = -50\ \mu$ (differential and integrated method) and $d_x = 50\ \mu$ (differential and integrated method). The systematic effect is close to 1 %.
     So we have to measure and control the safety gap between the beam and the electron detector with an absolute precision better than $50\ \mu$. Beam position monitors associated to the electron detector will have to give this precision.
   - the error $d\alpha$ on the estimated dispersion $\alpha_m = \alpha + d\alpha$ which differs from the true dispersion α.
     The relative error on the electron polarization $\Delta P_e/P_e$ for a ± 50 % relative error on the knowledge of the dispersion is given in tables 60,61,62 and 63 for respectively $d\alpha/\alpha = -50$ % (differential and integrated method) and $d\alpha/\alpha = +50$ % (differential and integrated method). The systematic effect is close to 1 %.
     We have then to know the dispersion with an relative precision better than 0.5 %. There is no peculiar problem to reach this level for magnetic system.

Differential Method Smeared : E_γ = 1.17eV P_e =0.500 σ_x = 150.0μ							
$E(GeV)$	2.00	3.00	4.00	5.00	6.00	7.00	8.00
$k_m(MeV)$	68.9	152.4	266.5	409.6	580.3	777.3	999.4
ρ	Δ%	Δ%	Δ%	Δ%	Δ%	Δ%	Δ%
0.20	*****±****	*****±****	*****±****	*****±****	-0.01±0.12	-0.01±0.10	0.00±0.09
0.30	*****±****	*****±****	-0.02±0.17	-0.01±0.14	-0.01±0.12	-0.01±0.10	0.00±0.09
0.40	*****±****	-0.02±0.22	-0.02±0.17	-0.01±0.14	-0.01±0.12	-0.01±0.10	0.00±0.09
0.50	*****±****	-0.02±0.22	-0.02±0.17	-0.01±0.14	-0.01±0.12	-0.01±0.10	0.00±0.09
0.60	-0.06±0.33	-0.02±0.22	-0.02±0.17	-0.01±0.14	-0.01±0.12	-0.01±0.11	0.00±0.09
0.70	-0.06±0.34	-0.03±0.23	-0.02±0.17	-0.01±0.14	-0.01±0.12	-0.01±0.11	0.00±0.09
0.80	-0.08±0.36	-0.04±0.25	-0.03±0.19	-0.01±0.15	-0.01±0.13	-0.01±0.11	0.00±0.10
0.90	-0.15±0.49	-0.05±0.31	-0.04±0.24	-0.02±0.18	-0.01±0.18	-0.01±0.13	-0.01±0.13

Table 52: ***Relative error Δ on the electron polarization*** *(differential method) due to a* $+ 50$ % *relative error on the beam size* ($\sigma(\Delta x) = 100\ \mu$, $(\sigma(\Delta x))^S = 150\ \mu$).

Integrated Method Smeared : E_γ = 1.17eV P_e =0.500 σ_x = 150.0μ							
$E(GeV)$	2.00	3.00	4.00	5.00	6.00	7.00	8.00
$k_m(MeV)$	68.9	152.4	266.5	409.6	580.3	777.3	999.4
ρ	Δ%	Δ%	Δ%	Δ%	Δ%	Δ%	Δ%
0.20	*****±****	*****±****	*****±****	*****±****	0.00±0.19	0.00±0.18	0.00±0.17
0.30	*****±****	*****±****	-0.01±0.24	0.00±0.21	0.00±0.17	0.00±0.16	0.00±0.13
0.40	*****±****	-0.02±0.27	-0.01±0.21	-0.01±0.17	0.00±0.16	0.00±0.13	0.00±0.12
0.50	*****±****	-0.02±0.25	-0.01±0.19	-0.01±0.16	-0.01±0.14	0.00±0.12	0.00±0.11
0.60	-0.05±0.34	-0.02±0.24	-0.01±0.18	-0.01±0.15	-0.01±0.13	0.00±0.11	0.00±0.10
0.70	-0.06±0.34	-0.03±0.23	-0.01±0.18	-0.01±0.15	-0.01±0.12	-0.01±0.11	0.00±0.10
0.80	-0.07±0.36	-0.03±0.26	-0.02±0.19	-0.01±0.15	-0.01±0.13	-0.01±0.12	0.00±0.10
0.90	-0.13±0.49	-0.05±0.31	-0.03±0.24	-0.02±0.18	-0.01±0.18	-0.01±0.13	-0.01±0.13

Table 53: ***Relative error Δ on the electron polarization*** *(integrated method) due to a* $+ 50$ % *relative error on the beam size* ($\sigma(\Delta x) = 100\ \mu$, $(\sigma(\Delta x))^S = 150\ \mu$).

Differential Method Smeared : E_γ = 1.17eV P_e =0.500 σ_α/α = 1.5%							
$E(GeV)$	2.00	3.00	4.00	5.00	6.00	7.00	8.00
$k_m(MeV)$	68.9	152.4	266.5	409.6	580.3	777.3	999.4
ρ	Δ%	Δ%	Δ%	Δ%	Δ%	Δ%	Δ%
0.20	*****±****	*****±****	*****±****	*****±****	0.00±0.12	-0.02±0.10	0.00±0.09
0.30	*****±****	*****±****	-0.01±0.17	0.00±0.14	0.00±0.12	-0.02±0.10	0.00±0.09
0.40	*****±****	0.00±0.22	-0.01±0.17	0.00±0.14	0.00±0.12	-0.02±0.10	0.00±0.09
0.50	*****±****	0.00±0.22	-0.01±0.17	0.00±0.14	0.01±0.12	-0.01±0.10	0.00±0.09
0.60	0.00±0.33	0.00±0.22	-0.01±0.17	0.00±0.14	0.00±0.12	-0.02±0.11	0.00±0.09
0.70	-0.01±0.34	-0.01±0.23	-0.02±0.17	0.00±0.14	0.00±0.12	-0.02±0.11	0.00±0.09
0.80	-0.02±0.36	-0.02±0.25	-0.04±0.19	-0.02±0.15	-0.01±0.13	-0.04±0.12	-0.02±0.10
0.90	-0.08±0.49	-0.06±0.31	-0.08±0.24	-0.05±0.18	-0.06±0.18	-0.07±0.13	-0.05±0.13

Table 54: ***Relative error Δ on the electron polarization*** *(differential method) due to a* $+ 50$ % *relative error on the dispersion* ($\sigma(\alpha)/\alpha = 1$ % , $(\sigma(\alpha)/\alpha)^S = 1.5$ %).

Integrated Method Smeared : E_γ = 1.17eV P_e =0.500 σ_α/α = 1.5%							
$E(GeV)$	2.00	3.00	4.00	5.00	6.00	7.00	8.00
$k_m(MeV)$	68.9	152.4	266.5	409.6	580.3	777.3	999.4
ρ	Δ%	Δ%	Δ%	Δ%	Δ%	Δ%	Δ%
0.20	*****±****	*****±****	*****±****	*****±****	0.01±0.19	0.00±0.18	0.00±0.17
0.30	*****±****	*****±****	0.01±0.24	0.01±0.21	0.01±0.17	0.01±0.16	0.01±0.13
0.40	*****±****	0.00±0.27	0.00±0.21	0.00±0.17	0.01±0.16	0.00±0.13	0.00±0.12
0.50	*****±****	0.00±0.25	0.00±0.19	0.00±0.16	0.00±0.14	0.00±0.12	0.00±0.11
0.60	0.00±0.34	0.00±0.24	0.00±0.18	0.00±0.15	0.00±0.13	0.00±0.11	0.00±0.10
0.70	-0.01±0.34	-0.01±0.23	-0.01±0.18	-0.01±0.15	-0.01±0.12	-0.01±0.11	-0.01±0.10
0.80	-0.02±0.36	-0.03±0.26	-0.03±0.19	-0.02±0.15	-0.02±0.13	-0.02±0.12	-0.02±0.10
0.90	-0.07±0.49	-0.05±0.31	-0.06±0.24	-0.04±0.18	-0.07±0.18	-0.04±0.13	-0.05±0.13

Table 55: ***Relative error Δ on the electron polarization*** *(integrated method) due to a* $+ 50$ % *relative error on the dispersion* ($\sigma(\alpha)/\alpha = 1$ % , $(\sigma(\alpha)/\alpha)^S = 1.5$ %).

Differential Method Smeared : E_γ = 1.17eV P_e =0.500 dx = -50.0μ							
$E(GeV)$	2.00	3.00	4.00	5.00	6.00	7.00	8.00
$k_m(MeV)$	68.9	152.4	266.5	409.6	580.3	777.3	999.4
ρ	Δ%	Δ%	Δ%	Δ%	Δ%	Δ%	Δ%
0.20	*****±****	*****±****	*****±****	*****±****	0.42±0.12	0.37±0.10	0.31±0.09
0.30	*****±****	*****±****	0.58±0.17	0.46±0.14	0.42±0.12	0.37±0.10	0.31±0.09
0.40	*****±****	0.79±0.22	0.60±0.17	0.47±0.14	0.42±0.12	0.38±0.10	0.32±0.09
0.50	*****±****	0.81±0.22	0.61±0.17	0.49±0.14	0.44±0.12	0.39±0.10	0.33±0.09
0.60	1.19±0.33	0.79±0.22	0.60±0.17	0.47±0.14	0.44±0.12	0.38±0.10	0.33±0.09
0.70	1.06±0.33	0.69±0.23	0.54±0.17	0.42±0.14	0.40±0.12	0.35±0.11	0.30±0.09
0.80	0.87±0.36	0.51±0.25	0.40±0.19	0.36±0.15	0.33±0.13	0.28±0.11	0.20±0.10
0.90	0.55±0.49	0.42±0.31	0.32±0.24	0.28±0.18	0.20±0.18	0.20±0.13	0.12±0.13

Table 56: ***Relative error Δ on the electron polarization*** *(differential method) due to a $d_x = -50\ \mu$ error on the safety gap ($d_g = 5\ mm$, $d_g{}^S = 4.95\ mm$).*

Integrated Method Smeared : E_γ = 1.17eV P_e =0.500 dx = -50.0μ							
$E(GeV)$	2.00	3.00	4.00	5.00	6.00	7.00	8.00
$k_m(MeV)$	68.9	152.4	266.5	409.6	580.3	777.3	999.4
ρ	Δ%	Δ%	Δ%	Δ%	Δ%	Δ%	Δ%
0.20	*****±****	*****±****	*****±****	*****±****	0.43±0.19	0.43±0.18	0.43±0.17
0.30	*****±****	*****±****	0.60±0.24	0.63±0.21	0.41±0.17	0.43±0.16	0.42±0.13
0.40	*****±****	0.71±0.27	0.55±0.21	0.37±0.17	0.39±0.15	0.38±0.13	0.19±0.12
0.50	*****±****	0.63±0.25	0.48±0.19	0.32±0.16	0.34±0.14	0.33±0.12	0.34±0.11
0.60	0.74±0.34	0.54±0.24	0.40±0.18	0.40±0.15	0.29±0.13	0.28±0.11	0.14±0.10
0.70	0.61±0.34	0.42±0.23	0.34±0.18	0.22±0.15	0.23±0.12	0.22±0.11	0.24±0.10
0.80	0.50±0.36	0.32±0.25	0.25±0.19	0.18±0.15	0.19±0.13	0.18±0.12	0.09±0.10
0.90	0.37±0.49	0.20±0.31	0.20±0.24	0.21±0.18	0.13±0.18	0.15±0.13	0.07±0.13

Table 57: ***Relative error Δ on the electron polarization*** *(integrated method) due to a $d_x = -50\ \mu$ error on the safety gap ($d_g = 5\ mm$, $d_g{}^S = 4.95\ mm$).*

Differential Method Smeared : E_γ = 1.17eV P_e =0.500 dx = 50.0μ							
$E(GeV)$	2.00	3.00	4.00	5.00	6.00	7.00	8.00
$k_m(MeV)$	68.9	152.4	266.5	409.6	580.3	777.3	999.4
ρ	Δ%	Δ%	Δ%	Δ%	Δ%	Δ%	Δ%
0.20	*****±****	*****±****	*****±****	*****±****	-0.42±0.12	-0.35±0.10	-0.31±0.09
0.30	*****±****	*****±****	-0.63±0.17	-0.48±0.14	-0.42±0.12	-0.35±0.10	-0.31±0.09
0.40	*****±****	-0.85±0.23	-0.65±0.17	-0.50±0.14	-0.43±0.12	-0.36±0.11	-0.32±0.09
0.50	*****±****	-0.87±0.23	-0.67±0.17	-0.52±0.14	-0.44±0.12	-0.37±0.11	-0.33±0.09
0.60	-1.22±0.33	-0.86±0.23	-0.65±0.17	-0.51±0.14	-0.44±0.12	-0.37±0.11	-0.32±0.09
0.70	-1.09±0.34	-0.76±0.23	-0.60±0.18	-0.46±0.14	-0.40±0.12	-0.31±0.11	-0.30±0.10
0.80	-0.90±0.37	-0.60±0.26	-0.46±0.19	-0.38±0.15	-0.34±0.13	-0.26±0.12	-0.26±0.10
0.90	-0.62±0.49	-0.46±0.31	-0.35±0.24	-0.25±0.18	-0.21±0.18	-0.24±0.13	-0.21±0.13

Table 58: ***Relative error Δ on the electron polarization*** *(differential method) due to a $d_x = 50\ \mu$ error on the safety gap ($d_g = 5\ mm$, $d_g{}^S = 5.05\ mm$).*

Integrated Method Smeared : E_γ = 1.17eV P_e =0.500 dx = 50.0μ							
$E(GeV)$	2.00	3.00	4.00	5.00	6.00	7.00	8.00
$k_m(MeV)$	68.9	152.4	266.5	409.6	580.3	777.3	999.4
ρ	Δ%	Δ%	Δ%	Δ%	Δ%	Δ%	Δ%
0.20	*****±****	*****±****	*****±****	*****±****	-0.64±0.19	-0.43±0.18	-0.43±0.17
0.30	*****±****	*****±****	-0.61±0.24	-0.42±0.21	-0.41±0.17	-0.43±0.16	-0.42±0.13
0.40	*****±****	-0.72±0.27	-0.55±0.21	-0.56±0.18	-0.39±0.16	-0.38±0.13	-0.39±0.12
0.50	*****±****	-0.64±0.25	-0.48±0.19	-0.48±0.16	-0.34±0.14	-0.33±0.12	-0.17±0.11
0.60	-0.76±0.35	-0.55±0.24	-0.41±0.18	-0.27±0.15	-0.29±0.13	-0.29±0.11	-0.29±0.10
0.70	-0.63±0.35	-0.43±0.23	-0.34±0.18	-0.22±0.15	-0.23±0.12	-0.22±0.11	-0.12±0.10
0.80	-0.51±0.37	-0.33±0.26	-0.25±0.20	-0.27±0.15	-0.19±0.13	-0.18±0.12	-0.18±0.10
0.90	-0.37±0.49	-0.27±0.31	-0.20±0.24	-0.14±0.18	-0.13±0.18	-0.07±0.13	-0.14±0.13

Table 59: ***Relative error Δ on the electron polarization*** *(integrated method) due to a $d_x = 50\ \mu$ error on the safety gap ($d_g = 5\ mm$, $d_g{}^S = 5.05\ mm$).*

Differential Method Smeared : E_γ = 1.17eV P_e =0.500 $d\alpha/\alpha$ = -0.5%							
$E(GeV)$	2.00	3.00	4.00	5.00	6.00	7.00	8.00
$k_m(MeV)$	68.9	152.4	266.5	409.6	580.3	777.3	999.4
ρ	Δ%	Δ%	Δ%	Δ%	Δ%	Δ%	Δ%
0.20	*****±****	*****±****	*****±****	*****±****	0.74±0.12	0.80±0.10	0.79±0.09
0.30	*****±****	*****±****	0.80±0.17	0.80±0.14	0.75±0.12	0.80±0.10	0.81±0.09
0.40	*****±****	0.82±0.22	0.82±0.17	0.82±0.14	0.76±0.12	0.83±0.10	0.82±0.09
0.50	*****±****	0.83±0.22	0.83±0.17	0.83±0.14	0.78±0.12	0.84±0.10	0.84±0.09
0.60	0.84±0.33	0.82±0.22	0.82±0.17	0.82±0.14	0.78±0.12	0.83±0.10	0.83±0.09
0.70	0.76±0.34	0.76±0.23	0.77±0.17	0.76±0.14	0.72±0.12	0.75±0.11	0.78±0.09
0.80	0.64±0.36	0.64±0.25	0.60±0.19	0.66±0.15	0.62±0.13	0.64±0.11	0.62±0.10
0.90	0.44±0.49	0.53±0.31	0.45±0.24	0.52±0.18	0.40±0.18	0.51±0.13	0.49±0.12

Table 60: ***Relative error Δ on the electron polarization*** *(differential method) due to a* $d\alpha/alpha = -0.5$ % *relative error on the dispersion.*

Integrated Method Smeared : E_γ = 1.17eV P_e =0.500 $d\alpha/\alpha$ = -0.5%							
$E(GeV)$	2.00	3.00	4.00	5.00	6.00	7.00	8.00
$k_m(MeV)$	68.9	152.4	266.5	409.6	580.3	777.3	999.4
ρ	Δ%	Δ%	Δ%	Δ%	Δ%	Δ%	Δ%
0.20	*****±****	*****±****	*****±****	*****±****	0.21±0.19	0.21±0.18	0.21±0.17
0.30	*****±****	*****±****	0.20±0.24	0.42±0.21	0.21±0.17	0.21±0.16	0.21±0.13
0.40	*****±****	0.36±0.27	0.36±0.21	0.37±0.17	0.39±0.15	0.38±0.13	0.39±0.12
0.50	*****±****	0.47±0.25	0.32±0.19	0.32±0.16	0.51±0.14	0.33±0.12	0.51±0.11
0.60	0.37±0.34	0.41±0.24	0.40±0.18	0.40±0.15	0.43±0.13	0.43±0.11	0.43±0.10
0.70	0.41±0.34	0.32±0.23	0.34±0.18	0.33±0.15	0.35±0.12	0.33±0.11	0.36±0.10
0.80	0.33±0.36	0.32±0.25	0.33±0.19	0.27±0.15	0.37±0.13	0.36±0.12	0.27±0.10
0.90	0.24±0.49	0.26±0.31	0.26±0.24	0.35±0.18	0.26±0.18	0.29±0.13	0.28±0.13

Table 61: ***Relative error Δ on the electron polarization*** *(integrated method) due to a* $d\alpha/alpha = -0.5$ % *relative error on the dispersion.*

Differential Method Smeared : E_γ = 1.17eV P_e =0.500 $d\alpha/\alpha$ = 0.5%							
$E(GeV)$	2.00	3.00	4.00	5.00	6.00	7.00	8.00
$k_m(MeV)$	68.9	152.4	266.5	409.6	580.3	777.3	999.4
ρ	Δ%	Δ%	Δ%	Δ%	Δ%	Δ%	Δ%
0.20	*****±****	*****±****	*****±****	*****±****	-0.81±0.12	-0.79±0.10	-0.79±0.09
0.30	*****±****	*****±****	-0.82±0.17	-0.81±0.14	-0.82±0.12	-0.80±0.10	-0.81±0.09
0.40	*****±****	-0.87±0.23	-0.84±0.17	-0.83±0.14	-0.83±0.12	-0.82±0.11	-0.82±0.09
0.50	*****±****	-0.88±0.23	-0.85±0.17	-0.85±0.14	-0.85±0.12	-0.83±0.11	-0.84±0.09
0.60	-0.79±0.33	-0.87±0.23	-0.84±0.17	-0.83±0.14	-0.85±0.12	-0.83±0.11	-0.83±0.09
0.70	-0.74±0.34	-0.80±0.23	-0.79±0.18	-0.78±0.14	-0.80±0.12	-0.74±0.11	-0.79±0.10
0.80	-0.66±0.37	-0.68±0.26	-0.68±0.20	-0.69±0.15	-0.68±0.13	-0.65±0.12	-0.66±0.10
0.90	-0.47±0.49	-0.53±0.31	-0.57±0.24	-0.55±0.18	-0.41±0.18	-0.55±0.14	-0.57±0.13

Table 62: ***Relative error Δ on the electron polarization*** *(differential method) due to a* $d\alpha/alpha = +0.5$ % *relative error on the dispersion.*

Integrated Method Smeared : E_γ = 1.17eV P_e =0.500 $d\alpha/\alpha$ = 0.5%							
$E(GeV)$	2.00	3.00	4.00	5.00	6.00	7.00	8.00
$k_m(MeV)$	68.9	152.4	266.5	409.6	580.3	777.3	999.4
ρ	Δ%	Δ%	Δ%	Δ%	Δ%	Δ%	Δ%
0.20	*****±****	*****±****	*****±****	*****±****	-0.43±0.19	-0.21±0.18	-0.21±0.17
0.30	*****±****	*****±****	-0.40±0.24	-0.21±0.21	-0.41±0.17	-0.43±0.16	-0.42±0.13
0.40	*****±****	-0.36±0.27	-0.37±0.21	-0.37±0.17	-0.39±0.16	-0.38±0.13	-0.39±0.12
0.50	*****±****	-0.32±0.25	-0.48±0.19	-0.48±0.16	-0.34±0.14	-0.33±0.12	-0.34±0.11
0.60	-0.38±0.35	-0.41±0.24	-0.41±0.18	-0.41±0.15	-0.43±0.13	-0.43±0.11	-0.43±0.10
0.70	-0.31±0.34	-0.32±0.23	-0.34±0.18	-0.33±0.15	-0.35±0.12	-0.33±0.11	-0.36±0.10
0.80	-0.34±0.37	-0.24±0.26	-0.33±0.20	-0.36±0.15	-0.38±0.13	-0.36±0.12	-0.36±0.10
0.90	-0.31±0.49	-0.33±0.31	-0.27±0.24	-0.29±0.18	-0.26±0.18	-0.30±0.13	-0.29±0.13

Table 63: ***Relative error Δ on the electron polarization*** *(integrated method) due to a* $d\alpha/alpha = +0.5$ % *relative error on the dispersion.*

E.4 Conclusions

In order to measure the electron polarization with a 1 % systematic error due to the resolution and the calibration of the detector, we have to control

- **the γ detector resolution at the 5 % level.**
  Tests of a 5*5 matrix of $PbWO_4$ crystal (section 20*20 mm,length 23 cm) viewed by XP1911 photomultiplicators is planned at Mainz for electron energies below 800 MeV. Further studies can be done with the Compton polarimeter using the electron detector for the tagging of the electron energy.

- **the γ detector calibration at the 1 % level.**
  This calibration can also be done with the Compton polarimeter using the electron detector.

- **the position of the relative electron detector and beam position with a 50 μ accuracy.**
  For this, we have to measure the absolute position of the electron detector wrt the beam monitor positions with this precision. We have also to use beam position monitors giving this required precision. Mechanical studies have still to be done.

- **the dispersion of the dipole at the 0.5 % level**
  This needs field map measurement of the first dipole. Measurements with the beam position monitors of the beam deviation for various incident energies of the Cebaf beam can be used to confirm the field map information.

SET UP	ELEMENT	Z(m)	Length(m)	X(cm)	Y(cm)
OPTICAL CAVITY		-40.5	2.	0.	0.
	Mirror 1	-41.		0.	1.
	Mirror 2	-40.		0.	-1.
MAGNETIC CHICANE		-31.5	12.0	0.	0.
	Dipole 1	-36.85	1.	0.	0.
	Dipole 2	-32.25	1.	0.	-25.89
	BPM	-31.5	0.2	0.	-25.89
	Dipole 3	-30.75	1.	0.	-25.89
	Dipole 4	-26.15	1.	0.	0.
γ DETECTOR		-33.15	0.5	0.	0.
	Thick absorber	-33.375	0.05	0.	0.
	Thin absorber	-33.35125	0.0025	0.	0.
	Crystal	-33.235	0.23	0.	0.
e^- DETECTOR		-33.15	0.05	0.	[-21.33;-24.33]

Table 64: ***Alternative Compton polarimeter positioning wrt Hall A target center.*** *Optical cavity before the first dipole of the magnetic chicane*

F Comparison with optical cavity before the first dipole

The optical cavity with its 2 associated beam position monitors could also be installed before the first dipole of the magnetic chicane. In this case, the gamma detector would be located before the dipole 2. The electron detector would be also located before the dipole 2 and its beam position monitor between the dipoles 2 and 3. For this study, space have been left for some extra quadrupoles and beam position monitor. Therefore the length available for the chicane was reduced from 15.1 m (with the optical cavity) to 11.7 m (without the optical cavity).

This alternative layout of the magnetic chicane is shown on Fig. 52 while the positioning of the critical elements of the Compton polarimeter is given in Table 64.

F.1 Magnetic Chicane

For the 2 setups, the magnetic chicane consists of 4 identical dipole magnets with magnetic length $L_i = 1m$ running with a magnetic field B_i. The field scales with incident energy up to 8 GeV where the saturation field of $1.5T$ is reached. This gives bending angles $\theta_i = 3.222\,\text{deg} = 0.056rad$, bending radii $R_i = 17.79m$ and transverse deviation $h_i = 2.81cm$. In this case, we have **the same energy lost by synchrotron radiation in the magnetic chicane** (see Table 13 and Fig. 14).

For the alternative setup, the total available length is $11.7m$ and we keep a distance of $0.5m$ between dipoles 2 and 3 for a beam position monitor (i.e. $D_{23} = 0.5m$). So the remaining drift length $D_{12} = D_{34} = 3.6m$ are smaller than for the chosen setup (resp. $D_{12} = D_{34} = 4.4m$) as well as the transverse deviation $H_{12} = H_{34} = 20.27cm$ (resp. $H_{12} = H_{34} = 24.77cm$) and the maximal deviation $d_{max} = 25.89\,cm$ (resp. $d_{max} = 30.40\,cm$).

For the 2 setups, **the beam crossing between the electron beam and the laser beam** have to be tune with the beam correctors before the cavity.

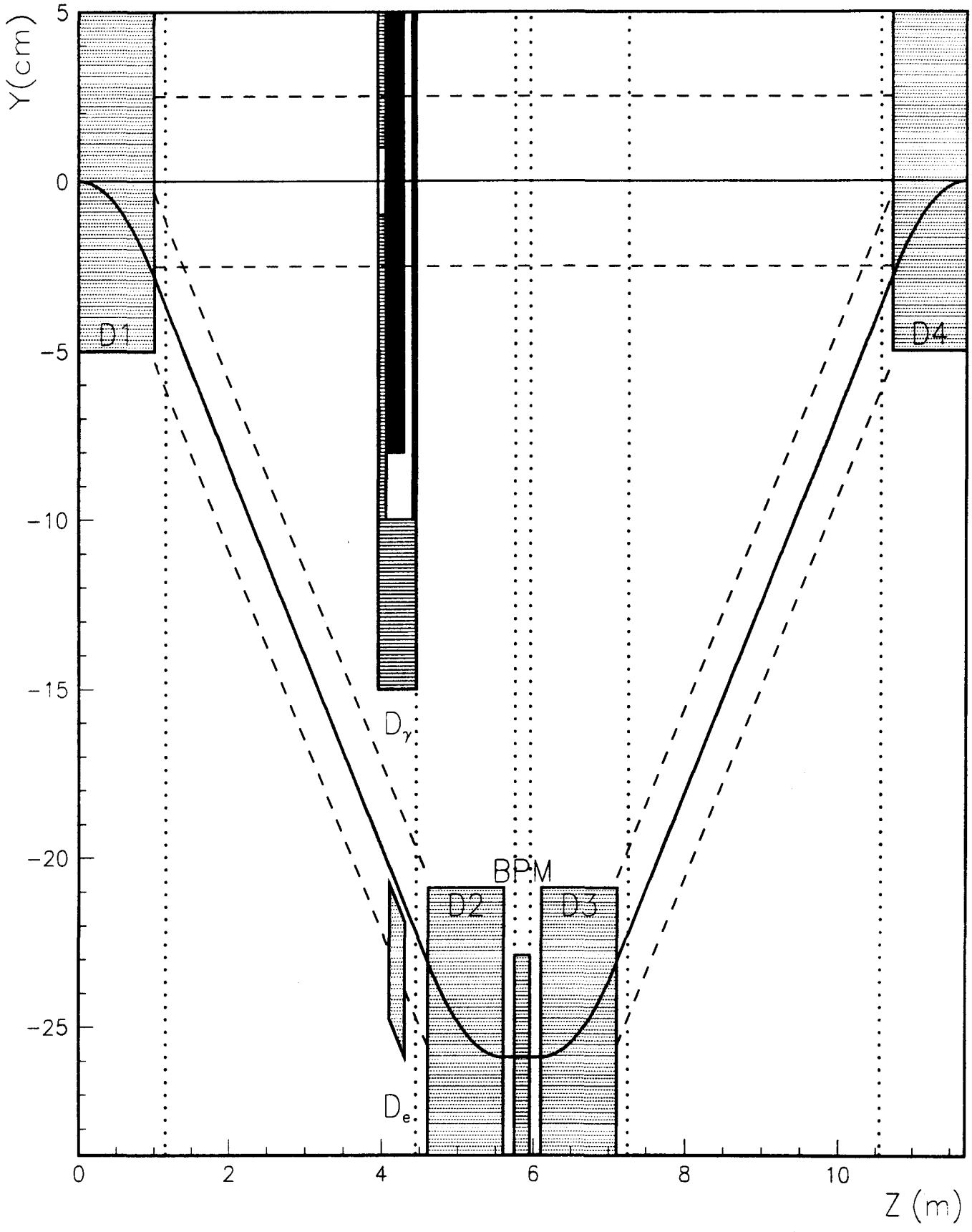

Figure 52: ***Alternative setup (Side View).*** *From Left to right: 1 magnets* (1 m)*; electron and* γ *detectors; 1 magnet* (1 m)*; Beam position monitor; 2 magnets* (1 m)*. The gap between Dipole 1 and 2 or dipole 3 and 4 is* 3.6 m*. The gap between Dipole 2 and 3 is* 0.5 m.

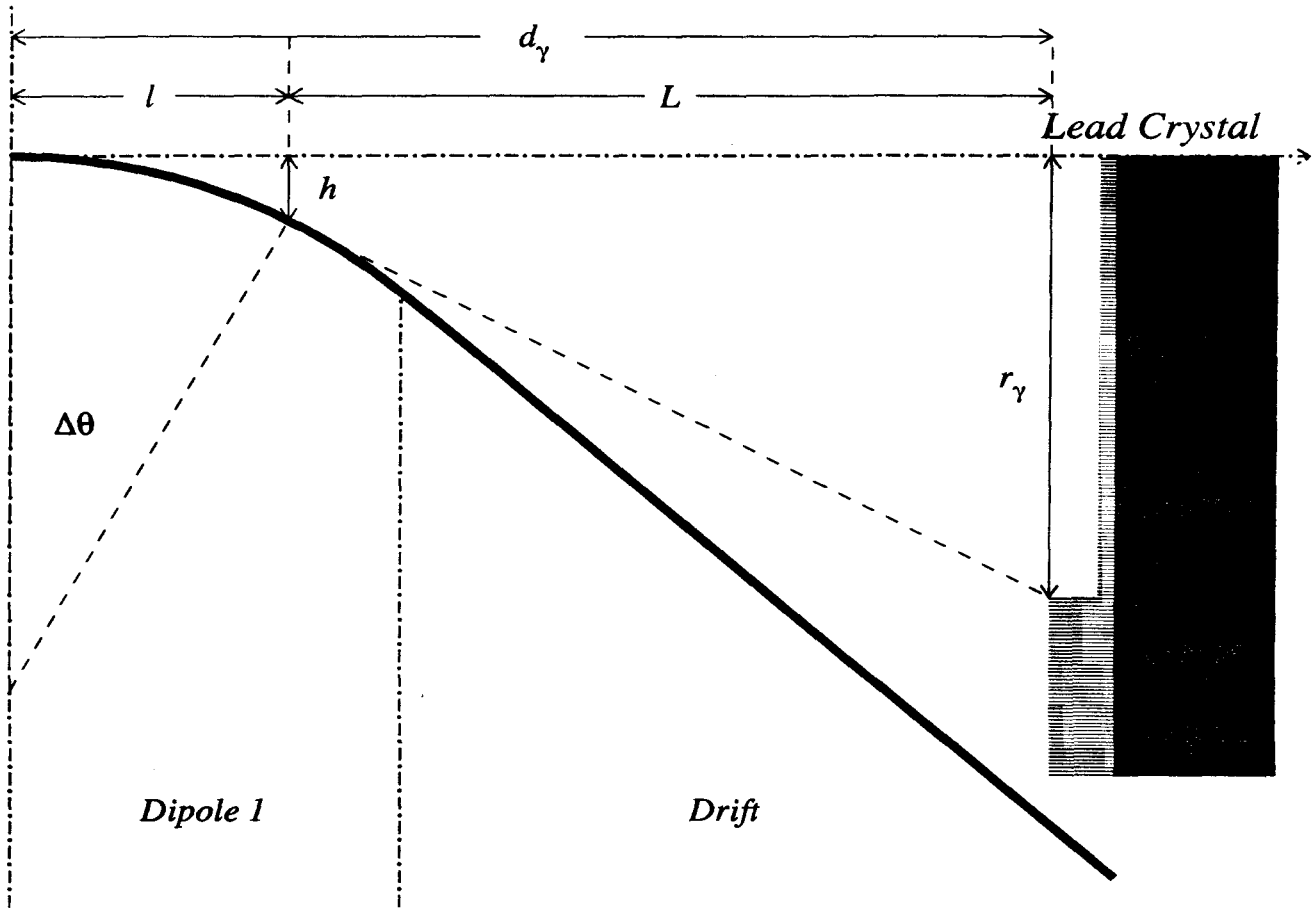

Figure 53: ***Alternative Setup : Useful angle $\Delta\theta$ of the electron trajectory for the synchrotron radiation*** *seen by the photon detector of radius r_γ at a distance d_γ from entrance of Dipole D1.*

$L_1 = L_2$=1.00 m	D_{12}=3.60 m	$D_\gamma = 7.15m$

$\lambda = 1064.2nm$

E	GeV	1.0	2.0	3.0	4.0	5.0	6.0	7.0	8.0
B_1	Tesla	0.187	0.375	0.562	0.750	0.937	1.125	1.312	1.500
k_{max}	MeV	17.5	68.9	152.4	266.5	409.6	580.3	777.3	999.4
k_0	MeV	8.8	35.1	78.2	137.8	213.5	304.9	411.5	533.0
ρ_0	k_0/k_{max}	0.504	0.509	0.513	0.517	0.521	0.525	0.529	0.533
r_c^0 mm	$\rho_{min} = \rho_0$	3.654	1.827	1.218	0.913	0.731	0.609	0.522	0.457
r_c mm	ρ_{min} =0.10	11.058	5.577	3.750	2.836	2.288	1.922	1.661	1.465
r_c mm	ρ_{min} =0.20	7.372	3.718	2.500	1.891	1.525	1.281	1.107	0.976
r_c mm	ρ_{min} =0.30	5.631	2.840	1.909	1.444	1.165	0.979	0.846	0.746
r_c mm	ρ_{min} =0.40	4.515	2.277	1.531	1.158	0.934	0.785	0.678	0.598
r_c mm	ρ_{min} =0.50	3.686	1.859	1.250	0.945	0.763	0.641	0.554	0.488

Table 65: ***Alternative Setup : Photon detector collimator size as a function of the threshold energy.***

F.2 Photon detector

For the alternative setup, the photon detector will be located between dipoles 1 and 2 of the magnetic chicane near dipole 2 where the available transverse deviation of the beam is sufficient. A layout of the photon detector setup is displayed on Fig. 53.

The distance from the interacting point increases from $D_\gamma \simeq 5.80m$ to $D_\gamma \simeq 7.15m$ so we would have to use a **larger gamma detector collimator**. This size is given in Table 65 which had to be compared with Table 14.

F.2.1 Synchrotron Background for the photon detector

The radiation to be considered here are the synchrotron photons emitted by the first dipole of the magnetic chicane instead of by the dipoles 2 and 3 of the magnetic chicane. We neglect the radiation due to the last dipole of the bending arc whose magnetic field is weaker than the chicane field by a factor 2. This gives a factor 2 on the number of synchrotron photons and on the mean photon energy i.e. a factor 4 on the total power. Furthermore, due to lower energy, the photons will be more absorbed in the lead absorber.

As a collimator we will use a 1 cm thick lead foil with a hole of radius r_γ at the entrance of the photon detector. The hole radius varies with incident energy to match the Compton angular distribution and is given in Table 65 without the 2 mm of safety. In front of this hole, the thin absorber will be a $2.5\,mm$ lead foil.

The alternative setup gives slightly lower synchrotron radiation since we have only contribution of dipole 1 (neglecting the last dipole of the bending arc) while dipole 2 and 3 contributes in the other setup . This gives a factor 2 which is reduced later by the smaller size of the collimator in the chosen setup. So the **synchrotron rate in the gamma detector would be reduced by a factor 1.3 for the alternative setup**.

The new values of the number $\frac{dn}{dt}$ and mean energy $< \epsilon >$ of synchrotron photon corresponding to the power P_γ for a hole radius r_γ corresponding to $\Delta\theta$ for the first dipole are listed in Tables 66, 67 and 68. These numbers have to be compared with those of Tables 16, 17 and 18.

Fig. 54 gives the synchrotron rate at 4 and 8 GeV for a lead absorber thickness of 0, 2.5 and 10 mm (to be compared with Fig. 17).

F.2.2 Bremsstrahlung for the photon detector

The bremsstrahlung seen by the photon detector is generated

- for the alternative setup, between the end of the last dipole of the bending arc and the first dipole of the magnetic chicane. The useful length for bremsstrahlung is then of order $L \simeq 15.25\,m$.
- for the chosen setup, between the dipole 2 and 3 of the magnetic chicane. The useful length for bremsstrahlung is then of order $L \simeq 2.5\,m$.

Bremsstrahlung photons are emitted with angles $\theta \simeq 1/\gamma = m/E$ similar to Compton photons (see section D.2). Therefore these photons are fully seen by the photon detector. The thin absorber will cut the low energy ($k' < 0.5\,MeV$) part of the spectrum. For computing the bremsstrahlung rate, we have used the Tsai cross section (section D.1) with a conservative threshold of $k'_c = 0.1\,MeV$.

The chosen setup gives lower bremsstrahlung radiation since the length between dipole 2 and 3 is only 2.5 m while the length between the last dipole of the bending arc and the dipole 1 is 15.25 m. This gives a factor 6. For the alternative setup, the results of Tables 19,20,21,22 and Fig. 18,19 have to be multiplied by this factor. In conclusion, the **bremsstrahlung rate in the gamma detector would be enhanced for the alternative setup by a factor 6.** Nevertheless this rate remains weak compared to the Compton rate.

E	B	r_γ	$\Delta\theta$	P	dn/dt	$< \epsilon >$	$\psi\gamma$	E/100ns
GeV	T	cm	mrad	W	s^{-1}	KeV		GeV/100ns
1.	0.19	1.306	3.26	0.258E-03	0.418E+14	0.386E-01	0.639E+01	0.161E+00
2.	0.37	0.758	1.89	0.240E-02	0.485E+14	0.308E+00	0.741E+01	0.150E+01
3.	0.56	0.575	1.44	0.922E-02	0.552E+14	0.104E+01	0.844E+01	0.575E+01
4.	0.75	0.484	1.21	0.245E-01	0.620E+14	0.247E+01	0.946E+01	0.153E+02
5.	0.94	0.429	1.07	0.530E-01	0.687E+14	0.482E+01	0.105E+02	0.331E+02
6.	1.12	0.392	0.98	0.101E+00	0.754E+14	0.833E+01	0.115E+02	0.628E+02
7.	1.31	0.366	0.92	0.174E+00	0.821E+14	0.132E+02	0.125E+02	0.109E+03
8.	1.50	0.346	0.87	0.281E+00	0.888E+14	0.197E+02	0.136E+02	0.175E+03

Table 66: ***Alternative Setup : Synchrotron radiation without absorber.*** *For various beam energies and magnetic field at 100μA. The power and rate seen by the γ detector located at $d_\gamma = 400\,cm$ from Dipole D1 entrance,are given for a collimator radius r_γ i.e. for $\Delta\theta$. The column $\psi\gamma$ indicates the angular range seen by the detector.*

E	B	r_γ	$\Delta\theta$	P	dn/dt	$< \epsilon >$	$\psi\gamma$	E/100ns
GeV	T	cm	mrad	W	s^{-1}	KeV		GeV/100ns
1.	0.19	1.306	3.26	0.225-131	0.108-116	0.130E+02	0.639E+01	0.140-128
2.	0.37	0.758	1.89	0.196E-32	0.230E-18	0.532E+02	0.741E+01	0.122E-29
3.	0.56	0.575	1.44	0.839E-14	0.697E+00	0.752E+02	0.844E+01	0.524E-11
4.	0.75	0.484	1.21	0.534E-08	0.408E+06	0.818E+02	0.946E+01	0.334E-05
5.	0.94	0.429	1.07	0.830E-06	0.570E+08	0.909E+02	0.105E+02	0.518E-03
6.	1.12	0.392	0.98	0.307E-04	0.118E+10	0.163E+03	0.115E+02	0.192E-01
7.	1.31	0.366	0.92	0.603E-03	0.161E+11	0.234E+03	0.125E+02	0.376E+00
8.	1.50	0.346	0.87	0.481E-02	0.107E+12	0.281E+03	0.136E+02	0.300E+01

Table 67: ***Alternative Setup : Synchrotron radiation with a 2.5 mm lead absorber.*** *For various beam energies and magnetic field at 100μA. The power and rate seen by the γ detector located at $d_\gamma = 400\,cm$ from Dipole D1 entrance are given for a collimator radius r_γ i.e. for $\Delta\theta$. The column $\psi\gamma$ indicates the angular range seen by the detector.*

E	B	r_γ	$\Delta\theta$	P	dn/dt	$< \epsilon >$	$\psi\gamma$	E/100ns
GeV	T	cm	mrad	W	s^{-1}	KeV		GeV/100ns
1.	0.19	1.306	3.26	0.298-211	0.453-197	0.410E+02	0.639E+01	0.186-208
2.	0.37	0.758	1.89	0.159E-47	0.123E-33	0.807E+02	0.741E+01	0.994E-45
3.	0.56	0.575	1.44	0.439E-22	0.319E-08	0.858E+02	0.844E+01	0.274E-19
4.	0.75	0.484	1.21	0.139E-15	0.789E-02	0.110E+03	0.946E+01	0.869E-13
5.	0.94	0.429	1.07	0.561E-10	0.134E+04	0.261E+03	0.105E+02	0.350E-07
6.	1.12	0.392	0.98	0.132E-06	0.262E+07	0.314E+03	0.115E+02	0.823E-04
7.	1.31	0.366	0.92	0.135E-04	0.233E+09	0.361E+03	0.125E+02	0.840E-02
8.	1.50	0.346	0.87	0.268E-03	0.408E+10	0.410E+03	0.136E+02	0.167E+00

Table 68: ***Alternative Setup : Synchrotron radiation with a 1 cm lead absorber.*** *For various beam energies and magnetic field at 100μA. The power and rate seen by the γ detector located at $d_\gamma = 400\,cm$ from Dipole D1 entrance are given for a collimator radius r_γ i.e. for $\Delta\theta$. The column $\psi\gamma$ indicates the angular range seen by the detector.*

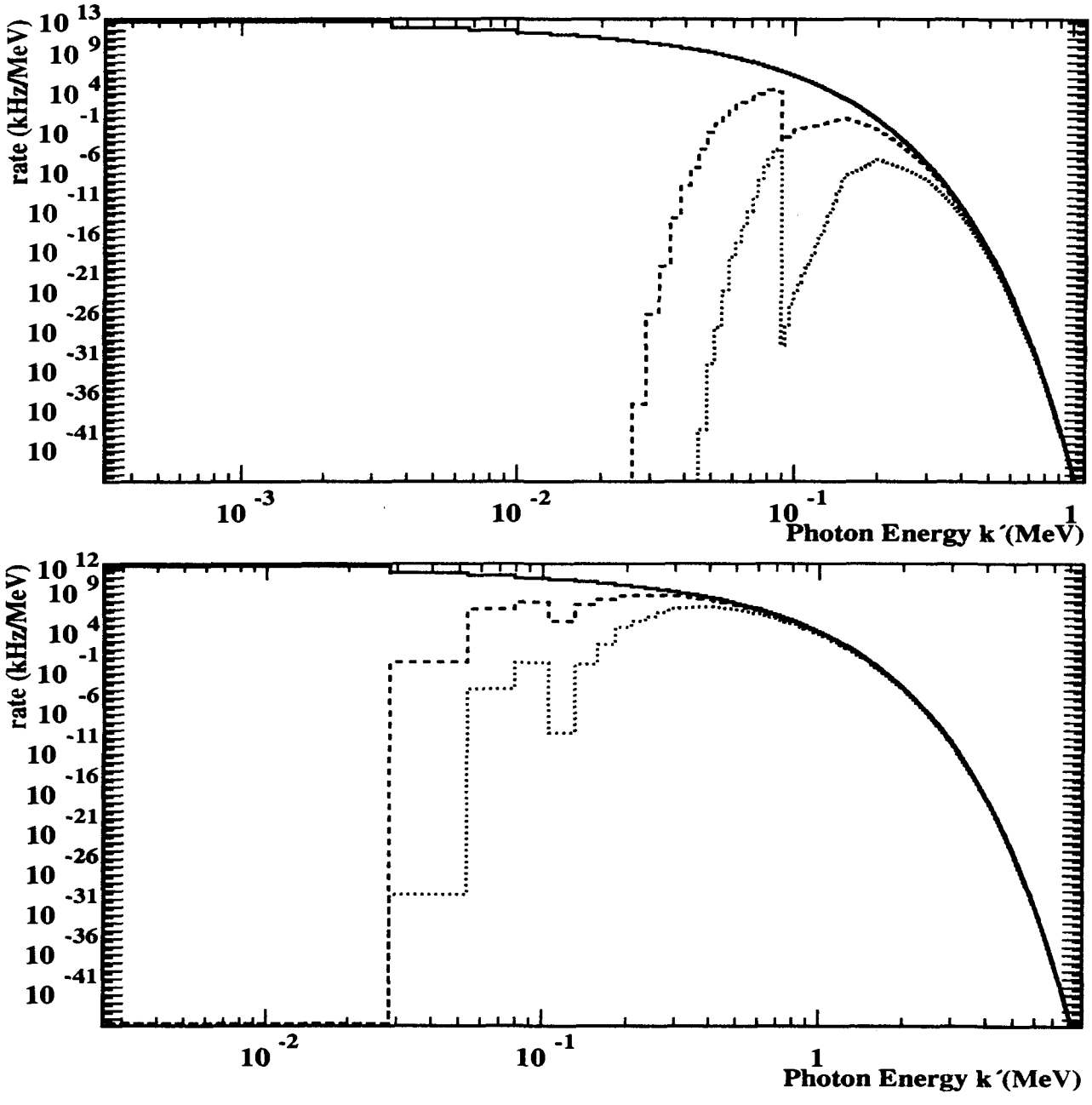

Figure 54: ***Alternative Setup : Synchrotron rate in the photon detector.*** *For* 100μ *A at 4 GeV (up) and 8 GeV (down) with an lead absorber of thickness 0 mm (solid line), 2.5 mm (dashed line) and 10 mm (dotted line).*

$L_1 = L_2$=1.00 m	D_{12}=3.60 m

λ = 1064.2nm	l_e = 3.20m	Gap d_g = 5.0mm

E	GeV	1.0	2.0	3.0	4.0	5.0	6.0	7.0	8.0
k_{max}	MeV	17.5	68.9	152.4	266.5	409.6	580.3	777.3	999.4
B	Tesla	0.187	0.375	0.562	0.750	0.937	1.125	1.312	1.500
Useful size	cm	-0.127	0.246	0.619	0.992	1.365	1.738	2.111	2.484
$< D >$	mm/%	2.178	2.216	2.254	2.293	2.331	2.369	2.408	2.446
$< D >$	mm/MeV	0.218	0.111	0.075	0.057	0.047	0.039	0.034	0.031
$\delta k/k$	%/mm	26.194	13.096	8.730	6.547	5.237	4.364	3.740	3.272
$\partial d/(\partial B/B)$	$\mu/10^{-3}$	212.7	216.5	220.3	224.2	228.1	232.0	235.9	239.9

λ = 532.1nm	l_e = 3.20m	Gap d_g = 5.0mm

E	GeV	1.0	2.0	3.0	4.0	5.0	6.0	7.0	8.0
k_{max}	MeV	34.5	133.2	290.1	499.7	757.1	1058.2	1399.2	1776.8
B	Tesla	0.187	0.375	0.562	0.750	0.937	1.125	1.312	1.500
Useful size	cm	0.246	0.992	1.738	2.484	3.231	3.978	4.725	5.473
$< D >$	mm/%	2.216	2.293	2.369	2.446	2.523	2.600	2.677	2.754
$< D >$	mm/MeV	0.222	0.115	0.079	0.061	0.050	0.043	0.038	0.034
$\delta k/k$	%/mm	13.096	6.547	4.364	3.272	2.617	2.181	1.869	1.635
$\partial d/(\partial B/B)$	$\mu/10^{-3}$	216.5	224.2	232.0	239.9	248.0	256.3	264.7	273.2

Table 69: ***Alternative Setup ; Magnetic dispersion at electron detector location and energy resolution on the scattered Compton photon.*** *The mean dispersion $< D >$ is given from d_{min} to d_{gap}.*

F.3 Scattered electron detector

To reduce radiation damage from synchrotron radiation (see section 7.4), the detector will be located

- for the chosen setup, between dipole 3 and dipole 4. The final position (80 cm before dipole 4) is a compromise between the maximum dispersion and the space left by the vacuum pipe.
- for the alternative setup, between dipole 1 and dipole 2. The final position (40 cm before dipole 2) is a compromise between the maximum dispersion and the effect of the magnetic field of dipole 2.

The drift length between the end of the last dipole before the electron detector and the electron detector is then reduced from 3.6 m to 3.2 m. So the **dispersion at the electron detector location is reduced of 20 %** for the alternative setup.

The new relevant parameters (energies E, E_0, E_{min} and E_{gap} and the corresponding deviations d, d_0, d_{min} and d_{gap}) are given in Tables 69 and 70. Transverse deviations between dipoles 2 and 3 are also given in Table 70. The deviations d_{23} and d_{23}^{min} stand for beam and minimum Compton energy. These values differ slightly from the previous ones (Tables 24 and 23) since the dispersion at the detector location varies only of 20 %. So the results obtained with the electron detector described in section 7 and related to the magnetic dispersion (useful size, energy threshold, k_0 point measurement, effects of the resolution and of the calibration on the P_e polarization measurement, beam pipe size) are similar. So are the requirements on the knowledge of the size of the interaction between the 2 beams, of the magnetic dispersion and of the position of the detector wrt the electron beam and on the power supply stability.

Due to the higher energy threshold, the **Compton rate in the electron detector are lower for the alternative solution**. This rate given in Table 71 have to be compared with those of Table 27.

$L_1 = L_2$=1.00 m	D_{12}=3.60 m
$l_e = 3.20m$	$Gap\ d_g = 5.0mm$

$\lambda = 1064.2nm$

E	GeV	1.0	2.0	3.0	4.0	5.0	6.0	7.0	8.0
B	Tesla	0.187	0.375	0.562	0.750	0.937	1.125	1.312	1.500
E_0	GeV	0.991	1.965	2.922	3.862	4.786	5.695	6.589	7.467
E_{min}	GeV	0.982	1.931	2.848	3.734	4.590	5.420	6.223	7.001
E_{gap}	GeV	0.977	1.953	2.930	3.907	4.883	5.860	6.836	7.813
d	cm	-20.829	-20.829	-20.829	-20.829	-20.829	-20.829	-20.829	-20.829
d_0	cm	-21.015	-21.202	-21.388	-21.574	-21.761	-21.947	-22.134	-22.320
d_{min}	cm	-21.202	-21.574	-21.947	-22.320	-22.693	-23.067	-23.440	-23.813
d_{gap}	cm	-21.329	-21.329	-21.329	-21.329	-21.329	-21.329	-21.329	-21.329
$d_{min} - d_{gap}$	cm	0.127	-0.246	-0.619	-0.992	-1.365	-1.738	-2.111	-2.484
$d_0 - d_{gap}$	cm	0.314	0.127	-0.059	-0.246	-0.432	-0.619	-0.805	-0.992
d_{23}	cm	-25.894	-25.894	-25.894	-25.894	-25.894	-25.894	-25.894	-25.894
d_{23}^{min}	cm	-26.357	-26.820	-27.284	-27.748	-28.211	-28.675	-29.139	-29.603

$\lambda = 532.1nm$

E	GeV	1.0	2.0	3.0	4.0	5.0	6.0	7.0	8.0
B	Tesla	0.187	0.375	0.562	0.750	0.937	1.125	1.312	1.500
E_0	GeV	0.982	1.931	2.848	3.734	4.590	5.420	6.223	7.001
E_{min}	GeV	0.966	1.867	2.710	3.500	4.243	4.942	5.601	6.223
E_{gap}	GeV	0.977	1.953	2.930	3.907	4.883	5.860	6.836	7.813
d	cm	-20.829	-20.829	-20.829	-20.829	-20.829	-20.829	-20.829	-20.829
d_0	cm	-21.202	-21.574	-21.947	-22.320	-22.693	-23.067	-23.440	-23.813
d_{min}	cm	-21.574	-22.320	-23.067	-23.813	-24.560	-25.307	-26.054	-26.802
d_{gap}	cm	-21.329	-21.329	-21.329	-21.329	-21.329	-21.329	-21.329	-21.329
$d_{min} - d_{gap}$	cm	-0.246	-0.992	-1.738	-2.484	-3.231	-3.978	-4.725	-5.473
$d_0 - d_{gap}$	cm	0.127	-0.246	-0.619	-0.992	-1.365	-1.738	-2.111	-2.484
d_{23}	cm	-25.894	-25.894	-25.894	-25.894	-25.894	-25.894	-25.894	-25.894
d_{23}^{min}	cm	-26.820	-27.748	-28.675	-29.603	-30.531	-31.459	-32.388	-33.317

Table 70: ***Alternative Setup ; Transverse deviations at electron detector location.*** *For different beam energy E and Laser wavelength λ. The transverse deviations for the incident energy E and for the minimum scattered energy E_{min} are given by d and d_{min}. The deviation d_0 stands for the scattered energy E_0 where the longitudinal asymmetry vanishes. The deviation $d_{gap} = d - d_g$ is the beam deviation with a security gap d_g and corresponds to a scattered energy E_{gap}. The useful size of the detector is given by $d_{gap} - d_{min}$. The E_0 point can be measured if $d_0 - d_{gap}$ is negative. Between the dipole 2 and the dipole 3, the transverse deviations for the incident energy E and for the minimum scattered energy E_{min} are given by d_{23} and d_{23}^{min}.*

$\lambda = 1064.2nm$

E GeV	1.0	2.0	3.0	4.0	5.0	6.0	7.0	8.0
rate Khz	0.0	308.8	458.1	516.5	561.4	585.4	599.6	611.7

$\lambda = 532.1nm$

E GeV	1.0	2.0	3.0	4.0	5.0	6.0	7.0	8.0
rate Khz	171.7	282.3	317.5	327.3	301.9	241.7	208.8	187.4

Table 71: ***Alternative Setup ; Compton rate in the electron detector.*** *For various beam energies E at $100\mu A$. The rate is given for the energy range ($[p_{min},p_{max}]$) covered by the electron detector of size $3\,cm$ with a safety gap of $5\,mm$ wrt beam. The experimental parameters are those of Table 8.*

E	GeV	1.0	2.0	3.0	4.0	5.0	6.0	7.0	8.0
B	Tesla	0.19	0.37	0.56	0.75	0.94	1.12	1.31	1.50
Power X_c =-2.0cm	nW	102.02	120.42	124.40	125.84	126.51	126.87	127.08	127.21
$\theta\gamma$		6.72	12.92	19.23	25.57	31.92	38.26	44.60	50.92
Power X_c =-2.1cm	nW	61.70	69.58	71.21	71.79	72.06	72.20	72.28	72.32
$\theta\gamma$		7.75	15.10	22.53	29.98	37.44	44.88	52.31	59.72

Table 72: ***Alternative Setup ; Synchrotron power in the electron detector.*** *For a beam of $100\,\mu A$ and an electron detector of size $3.cm * 3.cm$ located at a distance from downstream of Dipole 1 of $3.2m$. The detector center is at $-2.0cm$ or $-2.1cm$ wrt the beam axis. $\theta\gamma$ is the mean polar angle weighted by the power.*

F.3.1 Synchrotron radiation for the electron detector

To compute the synchrotron radiation seen by the electron detector, one uses the full angular dependence of the synchrotron radiation integrated over the electron path and over the polar coordinates of the electron detector for a piece $\Delta\theta$ of

- for the alternative setup, the end of the first dipole of the magnetic chicane.
- for the chosen setup, the end of the dipole 3 of the magnetic chicane. We assume that the synchrotron photons coming from the dipole 1 are not seen by the electron detector.

For the alternative setup, the synchrotron power seen by the electron detector, located $3.2\,m$ downstream the end of dipole 1 and 5 *or* $6\,mm$ away from the beam axis, is given in Table 72. This power of order $130\,nW$ had to be compared with the power of $180\,nW$ obtained for the chosen setup (electron detector located $3.6\,m$ downstream the end of dipole 3). **The lower synchrotron power (factor 1.4) for the alternative setup** is explained by the bigger angles θ_γ seen by the electron detector. But these bigger angles give also a higher energy threshold and lower Compton rate (Table 71).

E	GeV	1.0	2.0	3.0	4.0	5.0	6.0	7.0	8.0
p_{min}	GeV	0.857	1.713	2.570	3.426	4.283	5.140	5.996	6.853
p_{max}	GeV	0.977	1.953	2.930	3.907	4.883	5.860	6.836	7.813
rate Z= 1.	Khz	0.045	0.045	0.045	0.045	0.045	0.045	0.045	0.045
rate Z= 6.	Khz	0.739	0.735	0.734	0.734	0.733	0.733	0.733	0.733

Table 73: ***Alternative Setup ; Bremsstrahlung rate in the electron detector.*** *For various beam energies E at 100μA for a 15.25 m residual vacuum of $10^{-8} Torr$. The rate dn/dt (kHz) is given for the energy range ($[p_{min}, p_{max}]$) covered by the electron detector of size 3 cm with a safety gap of 5 mm wrt beam. The mean Z of the residual vacuum is also given.*

F.3.2 Bremsstrahlung for the electron detector

The bremsstrahlung seen by the electron detector is due for the alternative setup (resp. chosen setup) to

- photons generated between the end of the dipole 1 (3) and the electron detector. The useful length is only $L \simeq 3.2$ (3.6) m and the photons are seen under an angle $\theta > 1.6$ (1.4) $mrad$ larger than the characteristics bremsstrahlung angle $\theta_{brem} \simeq m/E < 0.25\, mrad$. So this background is very weak compared to the Compton rate.
  We assume here that the photons generated between the end of the last dipole of the bending arc and the first dipole of the magnetic chicane are not seen by the electron detector.

- electrons having emitted a bremsstrahlung photon between the end of the last dipole of the bending arc and the first dipole of the magnetic chicane (between the dipoles 2 and 3) and with an energy in the energy range ($[p_{min}, p_{max}]$) covered by the electron detector. The useful length for bremsstrahlung is the same ($L \simeq 15.25$ (2.5) m) than for the photon detector (see section F.2.2).

  Outgoing bremsstrahlung electrons are emitted with angles $\theta \simeq 1/\gamma = m/E$ (see section D.2). These angles are small ($\theta < 0.25\, mrad$) and can be neglected : the corresponding deviation at the electron detector is $< 1\, mm$. So the electron detector will see the bremsstrahlung electrons in the energy range covered by the sensitive area.

For computing the bremsstrahlung rate, we have used the Tsai cross section (section D.1) integrated from $k'_c = E - p_{max}$ to $k'_{max} = E - p_{min}$. The energy threshold due to the safety gap $E_{gap} = p_{max}$ is given in Table 70 (23). For p_{min}, we have used an electron detector size of 3 cm.

Table 73 gives the new energy integration range and the new integrated bremsstrahlung rate. The chosen setup gives lower bremsstrahlung radiation since the length between dipole 2 and 3 is only 2.5 m while the length between the last dipole of the bending arc and the dipole 1 is 15.25 m. The **bremsstrahlung rate would be increased for the alternative setup by a factor 6.1** which is later slightly reduced by the lower energy threshold. Nevertheless this background remains very weak compared to the Compton rate (Table 71).

E	GeV	1.0	2.0	3.0	4.0	5.0	6.0	7.0	8.0
B	Tesla	0.08	0.17	0.25	0.33	0.42	0.50	0.58	0.67
Power	μW	0.7872	1.9497	2.4384	2.6538	2.7634	2.8258	2.8645	2.8901
N_γ	$10^{12}s^{-1}$	0.575	0.811	0.879	0.906	0.919	0.925	0.929	0.932
$< \epsilon >$	eV	8.548	15.007	17.307	18.282	18.776	19.060	19.240	19.363

Table 74: ***Alternative Setup ; Synchrotron radiation seen by the first mirror.*** *For a beam of* $100\,\mu A$ *and a mirror of diameter* $8.0mm$ *located at a distance from downstream of last arc dipole of* $11.4m$. *The mirror center is at* $1.0cm$ *wrt the beam axis* ($\Delta\theta = 0.35mrad$).

E	GeV	1.0	2.0	3.0	4.0	5.0	6.0	7.0	8.0
B	Tesla	0.08	0.17	0.25	0.33	0.42	0.50	0.58	0.67
Power	μW	0.8529	2.3428	3.0320	3.3468	3.5094	3.6028	3.6610	3.6995
N_γ	$10^{12}s^{-1}$	0.537	0.791	0.869	0.900	0.915	0.923	0.927	0.930
$< \epsilon >$	eV	9.908	18.495	21.786	23.219	23.951	24.374	24.642	24.823

Table 75: ***Alternative Setup ; Synchrotron radiation seen by the second mirror.*** *For a beam of* $100\,\mu A$ *and a mirror of diameter* $8.0mm$ *located at a distance from downstream of last arc dipole of* $12.4m$. *The mirror center is at* $-1.0cm$ *wrt the beam axis* ($\Delta\theta = 0.32mrad$).

F.4 Synchrotron radiation seen by the cavity mirrors

The radiation to be considered here would be the synchrotron photons emitted by the end of the last dipole of the arc ($B = 0.33T$ at 4 GeV and $L = 3\,m$) instead of the synchrotron photons emitted by the end of the dipole 2 of the magnetic chicane ($B = 0.75T$ at 4 GeV and $L = 1\,m$).
The first (resp. second) mirror will be located at a distance $D_1 = 11.4\,m$ (resp. $D_2 = 12.4\,m$) from the end of the arc, which corresponds to a $\psi\gamma > 4.1$ at 4 GeV (resp. $\psi\gamma > 3.8$). As a consequence of large angles, the synchrotron power seen by the mirrors is very small (See Tables 74 and 75), i.e less than $3.7\mu\,W$, and its mean energy ranges from 8.54 eV (145 nm) to 24.8 eV (50 nm). The power is almost independent of the beam energy.
For the chosen setup, the first (resp. second) mirror are located at a distance $D_1 = 0.65\,m$ (resp. $D_2 = 1.65\,m$) from the end of the dipole, which corresponds to a $\psi\gamma > 72.2$ at 4 GeV (resp. $\psi\gamma > 28.4$).
Due to smaller angles for the alternative setup, the **synchrotron power in cavity mirrors would be increased by a huge factor : 2400 for mirror 1 and 180 for mirror 2** (see Tables 31 and 32). Moreover the mean energy of the synchrotron photon would also be increased from .008 eV to 20 eV for mirror 1 and from .14 eV to 20 eV for mirror 2. It will be more difficult to reduced these photons by an absorber.

F.5 Conclusions

The comparison between the setup described in this report with the optical cavity between the dipoles 2 and 3 of the magnetic chicane with an alternative setup where the optical cavity would be located before the first dipole shows that the **chosen setup (optical cavity between dipoles 2 and 3) presents over the alternative one** :

- **some major advantages**
  - we can use a smaller gamma detector collimator.
  - the bremsstrahlung rate in the gamma and electron detector is reduced by a factor 6.
  - the synchrotron power in cavity mirrors is reduced by a huge factor : 2400 for mirror 1 and 180 for mirror 2.
  - the dispersion at the electron detector location is enhanced by 20 % giving slightly lower energy threshold and higher Compton rate in the electron detector.
  - larger transverse deviation but this is due only to the larger length of the magnetic chicane (no extra quadrupoles in the chosen geometry).
- **some minor advantages**
  - the synchrotron rate in the gamma detector is increased by a factor 1.3.
  - the synchrotron rate in the electron detector is enhanced by a factor 1.4 but with a higher Compton rate.
- **while**
  - the energy lost by synchrotron radiation in the magnetic chicane are the same.

Moreover, the chosen setup has also practical and mechanical advantages since the gamma detector has not to be removed when the chicane is not used. Only some points not yet studied (focusing of the electron beam on the cavity center, general beam line optics) can change the previous conclusions.

G Optical Cavity for Photon Flux Amplifier

This appendix is a detailed version of section 8 devoted to the Laser-cavity system. Basics of Gaussian beams and standard optical resonators are given. It is explained how high reflectivity can be obtained using quarter-wave multi-layer dielectric mirrors. The time responses of the cavity are derived, and it is shown that the measurement of the emptying time of the cavity is a convenient way to access its reflectivity. The way to extract a discriminator signal for the feedback system between the laser and the cavity is detailed, along with a possible associated electronic servo.

G.1 Gaussian Beams and Resonators

G.1.1 Gaussian Beams

Electromagnetic fields in free space (or in any uniform and isotropic medium) obey the scalar wave equation:

$$\left[\Delta^2 + k^2\right] E(x,y,z) = 0,$$

where E is the complex electric field. For wave propagating along z, we look for solution $E = u(x,y,z)e^{-ikz}$, e.g

$$\frac{\partial^2 u}{\partial x^2} + \frac{\partial^2 u}{\partial y^2} + \frac{\partial^2 u}{\partial z^2} - 2ik\frac{\partial u}{\partial z} = 0.$$

In the paraxial approximation (valid for field description close to the z axis),

$$|\frac{\partial^2 u}{\partial z^2}| \ll |2k\frac{\partial u}{\partial z}|,$$

$$|\frac{\partial^2 u}{\partial z^2}| \ll |\frac{\partial^2 u}{\partial x^2}|,$$

$$|\frac{\partial^2 u}{\partial z^2}| \ll |\frac{\partial^2 u}{\partial y^2}|,$$

this equation becomes

$$\frac{\partial^2 u}{\partial x^2} + \frac{\partial^2 u}{\partial y^2} + -2ik\frac{\partial u}{\partial z} = 0.$$

Solutions to this equation have been given in Eq. (93), (95), (94) and (96).

The evolution equation for the beam size $d(z)$ and the radius of curvature $R(z)$ can be packed together, introducing the "complex radius of curvature", $q(z)$, following the simple propagation law

$$q(z) = q_0 + z \quad ; \quad q_0 = iz_R,$$
$$\frac{1}{q(z)} = \frac{1}{R(z)} + i\frac{\lambda}{\pi d^2(z)}.$$

In term of intensity, the field of Eq. (93) gives ($r^2 = x^2 + y^2$):

$$I(r) = \frac{2}{\pi}\frac{1}{d^2(z)}\exp\left(-2\frac{r^2}{d^2(z)}\right). \tag{260}$$

Since

$$\int_0^{2\pi} d\phi \int_0^{\infty} r dr I(r) = 1,$$

- Free space region index n_0 length L :

$$\begin{bmatrix} 1 & \frac{L}{n_0} \\ 0 & 1 \end{bmatrix}.$$

- Thin lens with focal f :

$$\begin{bmatrix} 1 & 0 \\ -\frac{1}{f} & 1 \end{bmatrix}.$$

- Curved mirror with radius R :

$$\begin{bmatrix} 1 & 0 \\ -\frac{2}{R} & 1 \end{bmatrix}.$$

For a Gaussian beam incident on a optical device with initial complex curvature radius q_i and final complex curvature radius q_f, it can be shown that [21]:

$$q_f = \frac{Aq_i + B}{Cq_i + D}, \tag{268}$$

where $\begin{bmatrix} A & B \\ C & D \end{bmatrix}$ is the ray matrix of the optical device. Consider now our cavity, the ray matrix corresponding to a round trip is :

$$\begin{bmatrix} A & B \\ C & D \end{bmatrix} = \begin{bmatrix} 1 & 0 \\ \frac{-2}{R_1} & 0 \end{bmatrix} \begin{bmatrix} 1 & L \\ 0 & 1 \end{bmatrix} \begin{bmatrix} 1 & 0 \\ \frac{-2}{R_2} & 0 \end{bmatrix} \begin{bmatrix} 1 & L \\ 0 & 1 \end{bmatrix}, \tag{269}$$

and for N round trips, the ray matrix $\mathcal{R}$ will be

$$\mathcal{R} = \begin{bmatrix} A & B \\ C & D \end{bmatrix}^N,$$

so that the ray displacement r_N and slope r'_N after N round trips are given by

$$\begin{bmatrix} r_N \\ r'_N \end{bmatrix} = \mathcal{R} \begin{bmatrix} r_i \\ r'_i \end{bmatrix},$$

requesting that r_N and r'_N stay finite gives the stability condition given in equation (100) :

$$0 \leq g_1 g_2 \leq 1. \tag{270}$$

G.1.4 Reflectivity of a quarter-wave multi layer dielectric mirror

The purpose of our cavity is to allow the LASER light to perform a maximum number of round trips N_{rt}. This means that one needs to use mirrors with high reflectivity, low absorption and low scattering. The high reflectivity is obtained using multi layer "$\lambda/4$ " mirrors, that we now introduce.

Let E_I be the amplitude of the incident electric field $\mathcal{E}_I$ on a mirror with incident angle θ_1 at frequency ω.

$$\mathcal{E}_I = E_I e^{i(\omega t - kz)}.$$

The mirror extends from $z = 0$ to $z = z_1$, and E_R and E_T are the amplitudes of the reflected and transmitted electric field. The optical index of the medium (See Fig. 55) before the mirror $z \leq 0$ (resp. after $z \geq z_1$) are defined by $n_1 = \sqrt{\epsilon_1 \mu_1}$ (resp. $n_l = \sqrt{\epsilon_l \mu_l}$).

this is a normalized intensity. If we compare with the usual Gaussian distribution

$$I(r) = \frac{1}{\sqrt{2\pi}\sigma} e^{-\frac{r^2}{2\sigma^2}},$$

we see that the beam diameter $d(z)$ is related to the standard $\sigma(z)$ via

$$d(z) = 2\sigma(z). \tag{261}$$

G.1.2 Gaussian beam inside a Resonator

To trap a Gaussian beam in a resonator consisting of two mirrors with radius of curvature R_1 and R_2, located at z_1 and z_2, with a separation length $L = z_2 - z_1$ (See Fig. 26), we have to fulfill the boundary conditions: $R(z = z_1) = -R_1$ and $R(z = z_2) = R_2$, where $R(z)$ is given by equation (96). Defining

$$g_i = 1 - \frac{L}{R_i}, i = 1, 2, \tag{262}$$

these boundary conditions lead to [23]

$$z_2 = \frac{g_1(1-g_2)}{g_1 + g_2 - 2g_1g_2} L \quad , \quad z_1 = -\frac{g_2(1-g_1)}{g_1 + g_2 - 2g_1g_2} L, \tag{263}$$

for the mirror location;

$$z_R = \frac{\sqrt{g_1g_2(1-g_1g_2)}}{g_1 + g_2 - 2g_1g_2} L, \tag{264}$$

for the Rayleigh range;

$$d_0^2 = \frac{\lambda}{\pi} \frac{\sqrt{g_1g_2(1-g_1g_2)}}{g_1 + g_2 - 2g_1g_2} L, \tag{265}$$

for the beam waist; and finally for the beam size on each mirror

$$d^2(z = z_1) = d_1^2 = \frac{\lambda}{\pi} \sqrt{\frac{g_2}{g_1(1-g_1g_2)}} L \quad , \quad d^2(z = z_2) = d_2^2 = \frac{\lambda}{\pi} \sqrt{\frac{g_1}{g_2(1-g_1g_2)}} L. \tag{266}$$

G.1.3 Ray Optics and Cavity Stability

In geometrical optic, light propagation is described in terms of ray [21]. For light nearly unidirectional propagating in the z direction, in a medium of index n, the radius r in the transverse plane and its derivative $r'(z) = n(z)\frac{dr}{dz}$ follows linear evolution with z:

$$\begin{aligned} r(z_2) &= AR(z_1) + Br'(z_1), \\ r'(z_2) &= CR(z_1) + Dr'(z_1); \end{aligned}$$

or in matrix notation

$$\begin{bmatrix} r(z_2) \\ r'(z_2) \end{bmatrix} = \begin{bmatrix} A & B \\ C & D \end{bmatrix} \begin{bmatrix} r(z_1) \\ r'(z_1) \end{bmatrix}. \tag{267}$$

This matrix is called *ABCD matrix* or *ray matrix*. For the following standard optical device we have:

Using the formalism of characteristic matrices one can show [22] that if

$$M = \begin{bmatrix} m_{11} & m_{12} \\ m_{21} & m_{22} \end{bmatrix} \tag{271}$$

is the characteristic matrix of the mirror evaluated at $z = z_1$, the reflection and transmission coefficients of that mirror can be expressed as:

$$\begin{aligned} r &= \frac{(m_{11} + m_{12}q_l)\, q_1 - (m_{21} + m_{22}q_l)}{(m_{11} + m_{12}q_l)\, q_1 + (m_{21} + m_{22}q_l)}, \\ t &= \frac{2q_1}{(m_{11} + m_{12}q_l)\, q_1 + (m_{21} + m_{22}q_l)}, \end{aligned}$$

where q_1 and q_l obey Eq. (103, 104). So all the needed information to compute these coefficients is included in the characteristic matrix of a multi layer mirror. For a mirror consisting of N pairs of *quarter-wave films*, i.e with thicknesses given by $h_2 = \frac{\lambda}{4}\frac{1}{n_2}$ and $h_3 = \frac{\lambda}{4}\frac{1}{n_3}$ and indices n_2 and n_3, the characteristic matrix, *for normal incidence* is [22]:

$$M = \begin{bmatrix} -\frac{n_3}{n_2} & 0 \\ 0 & -\frac{n_2}{n_3} \end{bmatrix}^N = \begin{bmatrix} \left(-\frac{n_3}{n_2}\right)^N & 0 \\ 0 & \left(-\frac{n_2}{n_3}\right)^N \end{bmatrix}; \tag{272}$$

so that the reflectivity of our mirror with a layer structure $(n_2, n_3, n_2, n_3, ..., n_2, n_3)$ is :

$$R_{2N} = \left(\frac{1 - \frac{n_l}{n_1}\left(\frac{n_2}{n_3}\right)^{2N}}{1 + \frac{n_l}{n_1}\left(\frac{n_2}{n_3}\right)^{2N}} \right)^2. \tag{273}$$

One can also have mirrors of the type $(n_2, n_3, n_2, n_3, ..., n_2, n_3, n_2)$, where the reflectivity is given by:

$$R_{2N+1} = \left(\frac{1 - \frac{n_2}{n_1}\frac{n_2}{n_l}\left(\frac{n_2}{n_3}\right)^{2N}}{1 + \frac{n_2}{n_1}\frac{n_2}{n_l}\left(\frac{n_2}{n_3}\right)^{2N}} \right)^2. \tag{274}$$

An example of reflectivities that can be obtained is given on figure (56).

G.2 Filling and Emptying time of the cavity

G.2.1 Filling time of the cavity

We have seen that the time evolution of the amplitude of the electric field circulating in the cavity is given by (Eq. 105) :

$$E_{circ}(t) = itE_I(t) + g_{rt}(\omega)E_{circ}(t - 2\tau),.$$

with

$$\boxed{\tau = \frac{L}{c}}. \tag{275}$$

Using Laplace transformations, this equation becomes

$$\hat{E}_{circ}(s) = it\hat{E}_I(s) + g_{rt}(\omega)e^{-2\tau s}\hat{E}_{circ}(s). \tag{276}$$

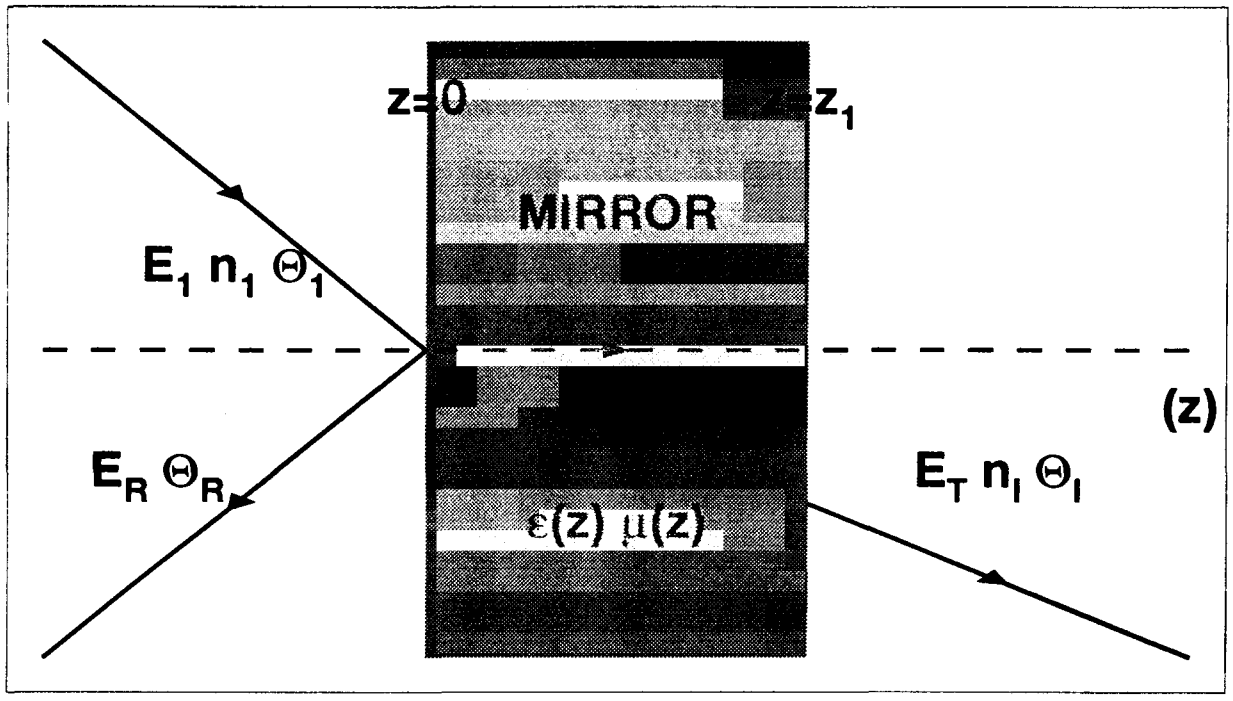

Figure 55: ***A mirror defined by two planes*** $z = 0$ ***and*** $z = z_1$***, with permeability and susceptibility*** $\mu(z)$ ***and*** $\epsilon(z)$.

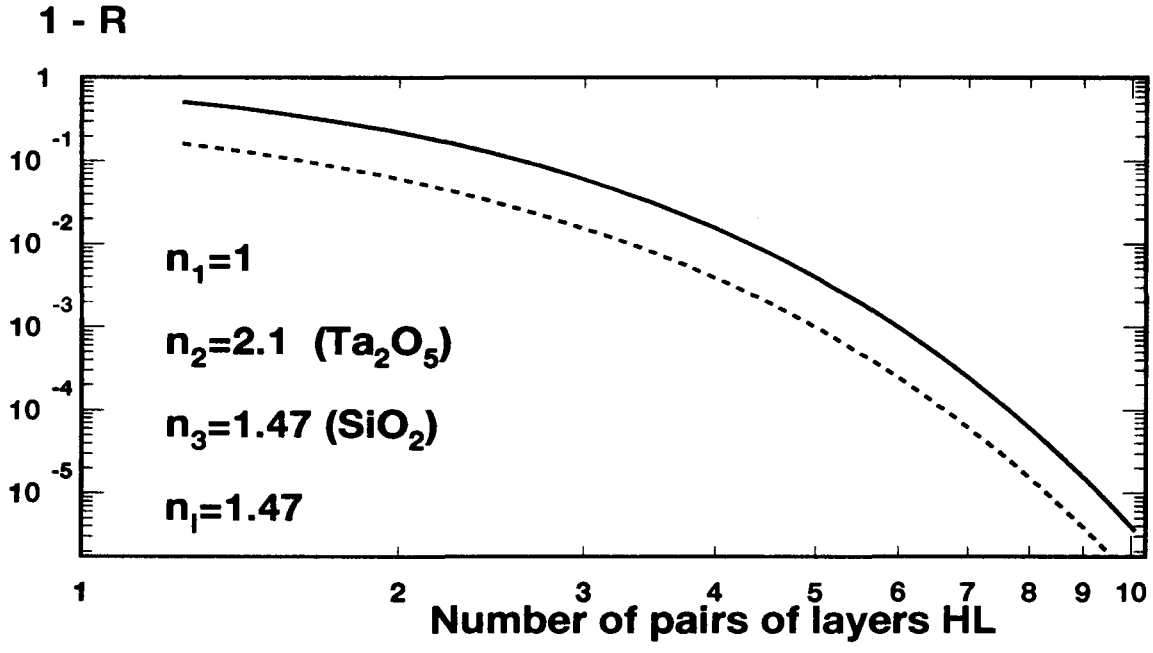

Figure 56: ***Transmission*** $\delta_r = 1 - R = T_r$ ***for*** $(HL)_N$ ***and*** $(HL)_N H$ ***versus number N of layers (HL). High index dielectric is*** Ta_2O_5 ***and low index dielectric is*** SiO_2

Thus the Laplace transforms of the circulating field is given by :

$$\hat{E}_{circ}(s) = it\hat{E}_I(s)\frac{1}{1 - g_{rt}(\omega)e^{-2\tau s}}. \tag{277}$$

Assuming the Laser is switched on at time $t = 0$, so that the incident field $E_I(t)$ is a step function of value E_I starting at time $t = 0$ i.e. $E_I(t) = E_I u(t)$. The Laplace transforms of the incident field is thus $\hat{E}_I(s) = \frac{E_I}{s}$, and Eq. (277) becomes

$$\hat{E}_{circ}(s) = itE_I\frac{1}{s\left(1 - g_{rt}(\omega)e^{-2\tau s}\right)}. \tag{278}$$

Using a Taylor expansion, Eq (278) gives :

$$\hat{E}_{circ}(s) = itE_I\sum_{n=0}^{\infty} g_{rt}^n\frac{e^{-2\tau ns}}{s}. \tag{279}$$

We can now easily perform an inverse Laplace transform, since the inverse Laplace transform of $\frac{e^{-2\tau ns}}{s}$ is a step function starting at time $t = 2\tau n$, we get the time evolution of the circulating field

$$E_{circ}(t) = itE_I\sum_{n=0}^{\infty} g_{rt}^n u(t - 2\tau n). \tag{280}$$

Therefore for $2\tau n \leq t \leq 2\tau\,(n+1)$, the circulating field is

$$E_{circ}(t) = itE_I\left[1 + g_{rt} + g_{rt}^2 + ...g_{rt}^n\right] = itE_I\frac{1 - g_{rt}^{n+1}}{1 - g_{rt}};\ \ for\ \ 2\tau n \leq t \leq 2\tau\,(n+1). \tag{281}$$

We then get the amplitude ratio of circulating and incident field

$$\frac{E_{circ}(t)}{E_I} = \frac{it}{1 - g_{rt}}\left(1 - g_{rt}^{n+1}\right);\ \ for\ \ 2\tau n \leq t \leq 2\tau\,(n+1). \tag{282}$$

We note G the gain (in intensity) in steady state (introduced in Eq. (112))

$$G(t = \infty) = G = \frac{T}{(1 - Re^{-\frac{\delta_0}{2}})^2 + 4Re^{-\frac{\delta_0}{2}}\sin^2(\omega\tau)}. \tag{283}$$

The time evolution of the gain of the cavity is thus

$$G(t) = G\left[1 - g_{rt}^{n+1}\right]\left[1 - g_{rt}^{n+1}\right]^* = G\left[1 - \left(r^2e^{-\frac{\delta_0}{2}}e^{-2i\omega\tau}\right)^{n+1}\right]\left[1 - \left(r^2e^{-\frac{\delta_0}{2}}e^{-2i\omega\tau}\right)^{n+1}\right]^*,$$

$$G(t) = G\left[1 - \left(R^{n+1}e^{-(n+1)\frac{\delta_0}{2}}e^{-2i(n+1)\omega\tau}\right)\right]\left[1 - \left(R^{n+1}e^{-(n+1)\frac{\delta_0}{2}}e^{-2i(n+1)\omega\tau}\right)\right]^*,$$

$$G(t) = G\left[1 - \left(R^{n+1}e^{-(n+1)\frac{\delta_0}{2}}e^{-2i(n+1)\omega\tau}\right)\right]\left[1 - \left(R^{n+1}e^{-(n+1)\frac{\delta_0}{2}}e^{+2i(n+1)\omega\tau}\right)\right],$$

$$G(t) = G\left[1 - 2R^{n+1}e^{-(n+1)\frac{\delta_0}{2}}\cos\left(2\,(n+1)\,\omega\tau\right) + \left(R^{n+1}e^{-(n+1)\frac{\delta_0}{2}}\right)^2\right],$$

$$G(t) = G\left[\left(1 - R^{n+1}e^{-(n+1)\frac{\delta_0}{2}}\right)^2 + 4R^{n+1}e^{-(n+1)\frac{\delta_0}{2}}\sin^2\left((n+1)\omega\tau\right)\right],$$

and with the time t given by $t = (n+1)\tau$,

$$G(t) = G\left[\left(1 - R^{\frac{t}{\tau}}e^{-\frac{t}{\tau}\frac{\delta_0}{2}}\right)^2 + 4R^{\frac{t}{\tau}}e^{-\frac{t}{\tau}\frac{\delta_0}{2}}\sin^2\left(\omega t\right)\right],$$

$$G(t) = G\left[\left(1 - e^{-\frac{t}{\tau}\left(\frac{\delta_0}{2} - \log R\right)}\right)^2 + 4e^{-\frac{t}{\tau}\left(\frac{\delta_0}{2} - \log R\right)}\sin^2\left(\omega t\right)\right].$$

Using T_d (that will be shown to be the decay time of the cavity)

$$\boxed{T_d = \tau\frac{1}{\left(\frac{\delta_0}{2} - \log R\right)} = \tau\frac{1}{\left(\frac{\delta_0}{2} + \delta_r\right)}}, \tag{284}$$

or equivalently

$$\boxed{Re^{-\frac{\delta_0}{2}} = e^{-\frac{\tau}{T_d}}}. \tag{285}$$

the evolution of the cavity gain reads

$$G(t) = G\left[\left(1 - e^{-\frac{t}{T_d}}\right)^2 + 4e^{-\frac{t}{T_d}}\sin^2\left(\omega t\right)\right],$$

$$\boxed{G(t) = G\left[1 - 2e^{-\frac{t}{T_d}}\cos\left(2\omega t\right) + e^{-\frac{t}{T_d/2}}\right]}. \tag{286}$$

For the transmitted field, again using Eq. (105)

$$E_T(t) = it_2e^{-\frac{\delta_0}{4}}e^{-i\omega t}E_{circ}(t-\tau),$$

we get for the ratio of transmitted and incident intensities:

$$\boxed{\mathcal{T}(t) = Te^{-\frac{\delta_0}{2}}G(t-\tau) = \mathcal{T}\left[1 - 2e^{-\frac{t-\tau}{T_d}}\cos\left(2\omega(t-\tau)\right) + e^{-\frac{t-\tau}{T_d/2}}\right]}. \tag{287}$$

G.2.2 Emptying time of the cavity

Assuming now that the Laser is switched on at time $t = 0$, and latter switched off at time $t = t_c$, so that the incident field is $E_I(t) = E_I\left(u(t) - u(t-t_c)\right)$. The Laplace transforms of the incident field is thus $\hat{E}_I(s) = E_I\frac{1-e^{-t_cs}}{s}$, and Eq. (277) becomes

$$\hat{E}_{circ}(s) = itE_I\frac{1 - e^{-t_cs}}{s\left(1 - g_{rt}(\omega)e^{-2\tau s}\right)}, \tag{288}$$

whose inverse Laplace transform is

$$E_{circ}(t) = itE_I\left(\sum_{n=0}^{\infty}g_{rt}^n u(t-2\tau n) - \sum_{n=0}^{\infty}g_{rt}^n u(t-2\tau n - t_c)\right).$$

Let $t_c = 2\tau p$, so that

$$E_{circ}(t) = itE_I \left(\sum_{n=0}^{\infty} g_{rt}^n u\left(t - 2\tau n\right) - \sum_{n=0}^{\infty} g_{rt}^n u\left(t - 2\tau\left(n + p\right)\right) \right).$$

After the laser has been switched off, i.e, for time $t > t_c$, and $2n\tau \leq t \leq 2(n+1)\tau$, with $n > p$, the circulating field is thus

$$E_{circ}(t) = itE_I \left(\frac{1 - g_{rt}^{n+1}}{1 - g_{rt}} - \frac{1 - g_{rt}^{n+1-p}}{1 - g_{rt}} \right) = \frac{itE_I}{1 - g_{rt}} \left(g_{rt}^{\frac{t-t_c}{2\tau}} - g_{rt}^{\frac{t}{2\tau}} \right).$$

Thus the gain in intensity is

$$G(t) = G \left(g_{rt}^{\frac{t-t_c}{2\tau}} - g_{rt}^{\frac{t}{2\tau}} \right) \left(g_{rt}^{\frac{t-t_c}{2\tau}} - g_{rt}^{\frac{t}{2\tau}} \right)^*.$$

Introducing $t' = t - t_c$, so that we start when the laser is switched off,

$$G(t') = G \left(g_{rt}^{\frac{t'}{2\tau}} - g_{rt}^{\frac{t'+t_c}{2\tau}} \right) \left(g_{rt}^{\frac{t'}{2\tau}} - g_{rt}^{\frac{t'+t_c}{2\tau}} \right)^*,$$

and assuming $t_c \to \infty$, e.g the cavity had sufficient time with laser on to reach a steady state, we then can get the evolution of the cavity gain after the laser was switched off. Indeed, $g_{rt}^{\frac{t'+t_c}{2\tau}}$ goes to zero when $t_c \to \infty$ and thus

$$G(t') = G|g_{rt}|^{2\frac{t'}{2\tau}},$$

$$\boxed{G(t') = Ge^{-\frac{t'}{T_d}}}, \tag{289}$$

with the cavity decay time given by Eq. (284).

Using the definition of the cavity Finesse (Eq. 120), we get

$$\frac{\mathcal{F}}{\pi} = \frac{\sqrt{e^{-\frac{\tau}{T_d}}}}{1 - e^{-\frac{\tau}{T_d}}} \simeq \frac{T_d}{\tau} \simeq \frac{1}{\frac{\delta_0}{2} + \delta_r} \tag{290}$$

So that measuring the decay time of the cavity is a convenient way to measure the cavity finesse.

For a cavity with mirror reflectivity $\delta_r = 100ppm$, in vacuum, $\delta_0 = 0$, the decay time is $T_d = 30\mu s$.

G.3 LASER cavity feedback

As explained in section 8.7, the Laser light is phase modulated and the discriminator signal is obtained by demodulation of the signal of a photodiode measuring the reflected field (See Fig. 31).

In this section, the phase modulation principle is first recalled, after what it is shown why the demodulated signal of the photodiode is a good discriminator for a feedback system between the Laser and the cavity.

G.3.1 Phase Modulation

The Laser incident field E_I at frequency $\nu = \frac{c}{\lambda}$ will be phase modulated by an oscillator at frequency Ω and with phase modulation amplitude m.

$$E_I = E_0 \cos\left(\omega t + m\cos(\Omega t + \Phi_\Omega)\right), \tag{291}$$

$$E_I = E_0 e^{i\omega t} e^{im\cos(\Omega t + \Phi_\Omega)}. \tag{292}$$

Using

$$\cos(m\cos\theta) = J_0(m) + 2\sum_{k=1}^{\infty}(-1)^k J_{2k}\cos(2k\theta),$$

$$\sin(m\cos\theta) = 2\sum_{k=0}^{\infty}(-1)^k J_{2k+1}\cos((2k+1)\theta),$$

$$\cos(m\sin\theta) = J_0(m) + 2\sum_{k=1}^{\infty} J_{2k}\cos(2k\theta),$$

$$\sin(m\sin\theta) = 2\sum_{k=0}^{\infty} J_{2k+1}\cos((2k+1)\theta),$$

where J_k are the Bessel functions, the modulated incident field can be written

$$E_I = E_0 e^{i\omega t}\left[J_0(m) + 2\sum_{k=1}^{\infty}(-1)^k J_{2k}\cos\left(2k(\Omega t + \Phi_\Omega)\right) + 2i\sum_{k=0}^{\infty}(-1)^k J_{2k+1}\cos\left((2k+1)(\Omega t + \Phi_\Omega)\right)\right].$$

Leading to the following frequency spectrum

$$E_I = E_0\left[J_0(m)e^{i\omega t} + \sum_{k=1}^{\infty}(i)^k J_k(m)e^{i(\omega t + k(\Omega t + \Phi_\Omega))} + \sum_{k=1}^{\infty}(i)^k J_k(m)e^{i(\omega t - k(\Omega t + \Phi_\Omega))}\right]. \tag{293}$$

In summary a field at frequency ω phase modulated at frequency Ω and amplitude m has a frequency spectrum given by $\omega_k^{\pm} = \omega \pm k\Omega$, each frequency component having a strength given by the kth Bessel function $J_k(m)$ and a phase given by $k(\frac{\pi}{2} \pm \Phi_\Omega)$.

$$E_I = E_0\left[J_0(m)e^{i\omega t} + \sum_{k=1}^{\infty} J_k(m)\left(e^{ik\left(\frac{\pi}{2}+\Phi_\Omega\right)}e^{i\omega_k^+ t} + e^{ik\left(\frac{\pi}{2}-\Phi_\Omega\right)}e^{i\omega_k^- t}\right)\right]. \tag{294}$$

For small value of the amplitude of the phase modulation, one can use

$$J_k(m) \simeq \frac{(\frac{1}{2}m)^k}{k!}.$$

G.3.2 Reflection by the cavity of the Laser Phase Modulated field

Using the cavity reflection coefficient $\rho = \sqrt{\mathcal{R}}e^{i\Phi_R}$, the (complex) field reflected by the cavity can be expressed as

$$E_R = E_0\left[J_0(m)\rho(\omega)e^{i\omega t} + \sum_{k=1}^{\infty} J_k(m)\left(e^{ik\left(\frac{\pi}{2}+\Phi_\Omega\right)}\rho(\omega_k^+)e^{i\omega_k^+ t} + e^{ik\left(\frac{\pi}{2}-\Phi_\Omega\right)}\rho(\omega_k^-)e^{i\omega_k^- t}\right)\right] \tag{295}$$

and the real reflected field is

$$E_R = E_0 \left[J_0(m)\sqrt{\mathcal{R}(\omega)}\cos\left(\omega t+\Phi_R(\omega)\right) + \sum_{k=1}^{\infty} J_k(m)\sqrt{\mathcal{R}\left(\omega_k^+\right)}\cos\left(\omega_k^+ t+\Phi_R\left(\omega_k^+\right)+k\left(\frac{\pi}{2}+\Phi_\Omega\right)\right) + \sum_{k=1}^{\infty} J_k(m)\sqrt{\mathcal{R}\left(\omega_k^-\right)}\cos\left(\omega_k^- t+\Phi_R\left(\omega_k^-\right)+k\left(\frac{\pi}{2}-\Phi_\Omega\right)\right)\right]. \quad (296)$$

The reflected intensity, that will be measured by a photodiode, is thus

$$I_R = E_0^2 \left[J_0(m)\sqrt{\mathcal{R}(\omega)}\cos\left(\omega t+\Phi_R(\omega)\right) + \sum_{k=1}^{\infty} J_k(m)\sqrt{\mathcal{R}\left(\omega_k^+\right)}\cos\left(\omega_k^+ t+\Phi_R\left(\omega_k^+\right)+k\left(\frac{\pi}{2}+\Phi_\Omega\right)\right) + \sum_{k=1}^{\infty} J_k(m)\sqrt{\mathcal{R}\left(\omega_k^-\right)}\cos\left(\omega_k^- t+\Phi_R\left(\omega_k^-\right)+k\left(\frac{\pi}{2}-\Phi_\Omega\right)\right)\right]^2,$$

leading to the lengthy sum

$$\begin{aligned} I_R = E_0^2 \Big[& J_0^2(m)\mathcal{R}(\omega)\cos^2\left(\omega t+\Phi_R(\omega)\right) \\ & + \sum_{k,k'=1}^{\infty} J_k(m)J_{k'}(m)\sqrt{\mathcal{R}\left(\omega_k^+\right)}\sqrt{\mathcal{R}\left(\omega_{k'}^+\right)} \\ & \cos\left(\omega_k^+ t+\Phi_R\left(\omega_k^+\right)+k\left(\frac{\pi}{2}+\Phi_\Omega\right)\right)\cos\left(\omega_{k'}^+ t+\Phi_R\left(\omega_{k'}^+\right)+k\left(\frac{\pi}{2}+\Phi_\Omega\right)\right) \\ & + \sum_{k,k'=1}^{\infty} J_k(m)J_{k'}(m)\sqrt{\mathcal{R}\left(\omega_k^-\right)}\sqrt{\mathcal{R}\left(\omega_{k'}^-\right)} \\ & \cos\left(\omega_k^- t+\Phi_R\left(\omega_k^-\right)+k\left(\frac{\pi}{2}-\Phi_\Omega\right)\right)\cos\left(\omega_{k'}^- t+\Phi_R\left(\omega_{k'}^-\right)+k\left(\frac{\pi}{2}-\Phi_\Omega\right)\right) \\ & +2\sum_{k=1}^{\infty} J_0(m)J_k(m)\sqrt{\mathcal{R}(\omega)}\sqrt{\mathcal{R}\left(\omega_k^+\right)} \\ & \cos\left(\omega t+\Phi_R(\omega)\right)\cos\left(\omega_k^+ t+\Phi_R\left(\omega_k^+\right)+k\left(\frac{\pi}{2}+\Phi_\Omega\right)\right) \\ & +2\sum_{k=1}^{\infty} J_0(m)J_k(m)\sqrt{\mathcal{R}(\omega)}\sqrt{\mathcal{R}\left(\omega_k^-\right)} \\ & \cos\left(\omega t+\Phi_R(\omega)\right)\cos\left(\omega_k^- t+\Phi_R\left(\omega_k^-\right)+k\left(\frac{\pi}{2}-\Phi_\Omega\right)\right) \\ & +2\sum_{k,k'=1}^{\infty} J_k(m)J_{k'}(m)\sqrt{\mathcal{R}\left(\omega_k^+\right)}\sqrt{\mathcal{R}\left(\omega_{k'}^-\right)} \\ & \cos\left(\omega_k^+ t+\Phi_R\left(\omega_k^+\right)+k\left(\frac{\pi}{2}+\Phi_\Omega\right)\right)\cos\left(\omega_{k'}^- t+\Phi_R\left(\omega_{k'}^-\right)+k'\left(\frac{\pi}{2}-\Phi_\Omega\right)\right)\Big]. \end{aligned}$$

By linearisation, we get

$$
\begin{aligned}
I_R = E_0^2 \Bigg[& J_0^2(m)\mathcal{R}(\omega)\frac{1}{2}\left[\cos\left(2\omega t + 2\Phi_R(\omega)\right)+1\right] \\
& + \sum_{k,k'=1}^{\infty} J_k(m)J_{k'}(m)\sqrt{\mathcal{R}\left(\omega_k^+\right)}\sqrt{\mathcal{R}\left(\omega_{k'}^+\right)} \\
& \frac{1}{2}\Bigg[\cos\left(\left(\omega_k^+ + \omega_{k'}^+\right)t + \Phi_R\left(\omega_k^+\right) + \Phi_R\left(\omega_{k'}^+\right) + (k+k')\frac{\pi}{2} + (k+k')\Phi_\Omega\right) + \\
& \quad \cos\left(\left(\omega_k^+ - \omega_{k'}^+\right)t + \Phi_R\left(\omega_k^+\right) - \Phi_R\left(\omega_{k'}^+\right) + (k-k')\frac{\pi}{2} + (k-k')\Phi_\Omega\right)\Bigg] \\
& + \sum_{k,k'=1}^{\infty} J_k(m)J_{k'}(m)\sqrt{\mathcal{R}\left(\omega_k^-\right)}\sqrt{\mathcal{R}\left(\omega_{k'}^-\right)} \\
& \frac{1}{2}\Bigg[\cos\left(\left(\omega_k^- + \omega_{k'}^-\right)t + \Phi_R\left(\omega_k^-\right) + \Phi_R\left(\omega_{k'}^-\right) + (k+k')\frac{\pi}{2} - (k+k')\Phi_\Omega\right) + \\
& \quad \cos\left(\left(\omega_k^- - \omega_{k'}^-\right)t + \Phi_R\left(\omega_k^-\right) - \Phi_R\left(\omega_{k'}^-\right) + (k-k')\frac{\pi}{2} - (k-k')\Phi_\Omega\right)\Bigg] \\
& + 2\sum_{k=1}^{\infty} J_0(m)J_k(m)\sqrt{\mathcal{R}(\omega)}\sqrt{\mathcal{R}\left(\omega_k^+\right)} \\
& \frac{1}{2}\Bigg[\cos\left(\left(\omega + \omega_k^+\right)t + \Phi_R(\omega) + \Phi_R\left(\omega_k^+\right) + k\left(\frac{\pi}{2} + \Phi_\Omega\right)\right) + \\
& \quad \cos\left(\left(\omega - \omega_k^+\right)t + \Phi_R(\omega) - \Phi_R\left(\omega_k^+\right) - k\left(\frac{\pi}{2} + \Phi_\Omega\right)\right)\Bigg] \\
& + 2\sum_{k=1}^{\infty} J_0(m)J_k(m)\sqrt{\mathcal{R}(\omega)}\sqrt{\mathcal{R}\left(\omega_k^-\right)} \\
& \frac{1}{2}\Bigg[\cos\left(\left(\omega + \omega_k^-\right)t + \Phi_R(\omega) + \Phi_R\left(\omega_k^-\right) + k\left(\frac{\pi}{2} - \Phi_\Omega\right)\right) + \\
& \quad \cos\left(\left(\omega - \omega_k^-\right)t + \Phi_R(\omega) - \Phi_R\left(\omega_k^-\right) - k\left(\frac{\pi}{2} - \Phi_\Omega\right)\right)\Bigg] \\
& + 2\sum_{k,k'=1}^{\infty} J_k(m)J_{k'}(m)\sqrt{\mathcal{R}\left(\omega_k^+\right)}\sqrt{\mathcal{R}\left(\omega_{k'}^-\right)} \\
& \frac{1}{2}\Bigg[\cos\left(\left(\omega_k^+ + \omega_{k'}^-\right)t + \Phi_R\left(\omega_k^+\right) + \Phi_R\left(\omega_{k'}^-\right) + (k+k')\frac{\pi}{2} + (k-k')\Phi_\Omega\right) + \\
& \quad \cos\left(\left(\omega_k^+ - \omega_{k'}^-\right)t + \Phi_R\left(\omega_k^+\right) - \Phi_R\left(\omega_{k'}^-\right) + (k-k')\frac{\pi}{2} + (k+k')\Phi_\Omega\right)\Bigg]\Bigg].
\end{aligned}
$$

Using $\omega_k^{\pm} = \omega \pm k\Omega$, the reflected intensity reads

$$
\begin{aligned}
I_R = E_0^2 \Big[& J_0^2(m)\mathcal{R}(\omega)\frac{1}{2}\left[\cos\left(2\omega t + 2\Phi_R(\omega)\right) + 1\right] \\
& + \sum_{k,k'=1}^{\infty} J_k(m)J_{k'}(m)\sqrt{\mathcal{R}(\omega+k\Omega)}\sqrt{\mathcal{R}(\omega+k'\Omega)} \\
& \frac{1}{2}\Big[\cos\Big(\left(2\omega + (k+k')\,\Omega\right)t + \Phi_R(\omega+k\Omega) + \Phi_R(\omega+k'\Omega) + (k+k')\frac{\pi}{2} + (k+k')\,\Phi_\Omega\Big) + \\
& \cos\Big(+(k-k')\,\Omega t + \Phi_R(\omega+k\Omega) - \Phi_R(\omega+k'\Omega) + (k-k')\frac{\pi}{2} + (k-k')\,\Phi_\Omega\Big)\Big] \\
& + \sum_{k,k'=1}^{\infty} J_k(m)J_{k'}(m)\sqrt{\mathcal{R}(\omega-k\Omega)}\sqrt{\mathcal{R}(\omega-k'\Omega)} \\
& \frac{1}{2}\Big[\cos\Big(\left(2\omega - (k+k')\,\Omega\right)t + \Phi_R(\omega-k\Omega) + \Phi_R(\omega-k'\Omega) + (k+k')\frac{\pi}{2} - (k+k')\,\Phi_\Omega\Big) + \\
& \cos\Big(-(k-k')\,\Omega t + \Phi_R(\omega-k\Omega) - \Phi_R(\omega-k'\Omega) + (k-k')\frac{\pi}{2} - (k-k')\,\Phi_\Omega\Big)\Big] \\
& + 2\sum_{k=1}^{\infty} J_0(m)J_k(m)\sqrt{\mathcal{R}(\omega)}\sqrt{\mathcal{R}(\omega+k\Omega)} \\
& \frac{1}{2}\Big[\cos\Big(\left(2\omega + k\Omega\right)t + \Phi_R(\omega) + \Phi_R(\omega+k\Omega) + k\left(\frac{\pi}{2} + \Phi_\Omega\right)\Big) + \\
& \cos\Big(\left(-k\Omega\right)t + \Phi_R(\omega) - \Phi_R(\omega+k\Omega) - k\left(\frac{\pi}{2} + \Phi_\Omega\right)\Big)\Big] \\
& + 2\sum_{k=1}^{\infty} J_0(m)J_k(m)\sqrt{\mathcal{R}(\omega)}\sqrt{\mathcal{R}(\omega-k\Omega)} \\
& \frac{1}{2}\Big[\cos\Big(\left(2\omega - k\Omega\right)t + \Phi_R(\omega) + \Phi_R(\omega-k\Omega) + k\left(\frac{\pi}{2} - \Phi_\Omega\right)\Big) + \\
& \cos\Big(\left(+k\Omega\right)t + \Phi_R(\omega) - \Phi_R(\omega-k\Omega) - k\left(\frac{\pi}{2} - \Phi_\Omega\right)\Big)\Big] \\
& + 2\sum_{k,k'=1}^{\infty} J_k(m)J_{k'}(m)\sqrt{\mathcal{R}(\omega+k\Omega)}\sqrt{\mathcal{R}(\omega-k'\Omega)} \\
& \frac{1}{2}\Big[\cos\Big(\left(2\omega + (k-k')\,\Omega\right)t + \Phi_R(\omega+k\Omega) + \Phi_R(\omega-k'\Omega) + (k+k')\frac{\pi}{2} + (k-k')\,\Phi_\Omega\Big) + \\
& \cos\Big(\left((k+k')\,\Omega\right)t + \Phi_R(\omega+k\Omega) - \Phi_R(\omega-k'\Omega) + (k-k')\frac{\pi}{2} + (k+k')\,\Phi_\Omega\Big)\Big]\Big] . \qquad (297)
\end{aligned}
$$

A fraction $\Gamma(1-\Gamma)$ (Γ transmitivity of the beam splitter) of the intensity of the reflected field is directed through a photodiode (with a conversion factor κ) by a beam splitter. The photodiode is not fast enough to detect the high frequencies $(\omega, \omega \pm k\Omega)$ of the reflected intensity I_R. Indeed if τ is the integration time of the photodiode, for an intensity $i(t) = \cos(\omega t + \phi)$, what will actually be measured is

$$
I_d(t) = \frac{1}{\tau}\int_t^{t+\tau} i(t')dt' = \frac{1}{\tau}\int_t^{t+\tau} \cos(\omega t' + \phi) = \frac{1}{\omega\tau}\left[\sin(\omega t' + \phi)\right]_t^{t+\tau}
$$

$$
I_d(t) = \frac{2}{\omega\tau}\cos(\frac{\omega\tau}{2})\sin(\omega t + \phi + \frac{\omega\tau}{2})
$$

If the photodiode integration time τ is large wrt $1/\omega$ the detected intensity is zero. Thus the reflected intensity seen by the photodiode will give the following photo current

$$
\begin{aligned}
i_{R,d} = \Gamma(1-\Gamma)\kappa\frac{1}{2}E_0^2[\, & J_0^2(m)\mathcal{R}(\omega) \\
& + \sum_{k,k'=1}^{\infty} J_k(m)J_{k'}(m)\sqrt{\mathcal{R}(\omega+k\Omega)}\sqrt{\mathcal{R}(\omega+k'\Omega)} \\
& \cos\left(+(k-k')\,\Omega t + \Phi_R(\omega+k\Omega) - \Phi_R(\omega+k'\Omega) + (k-k')\,\frac{\pi}{2} + (k-k')\,\Phi_\Omega\right) \\
& + \sum_{k,k'=1}^{\infty} J_k(m)J_{k'}(m)\sqrt{\mathcal{R}(\omega-k\Omega)}\sqrt{\mathcal{R}(\omega-k'\Omega)} \\
& \cos\left(-(k-k')\,\Omega t + \Phi_R(\omega-k\Omega) - \Phi_R(\omega-k'\Omega) + (k-k')\,\frac{\pi}{2} - (k-k')\,\Phi_\Omega\right) \\
& + 2\sum_{k=1}^{\infty} J_0(m)J_k(m)\sqrt{\mathcal{R}(\omega)}\sqrt{\mathcal{R}(\omega+k\Omega)} \\
& \cos\left(-k\Omega t + \Phi_R(\omega) - \Phi_R(\omega+k\Omega) - k\left(\frac{\pi}{2}+\Phi_\Omega\right)\right) \\
& + 2\sum_{k=1}^{\infty} J_0(m)J_k(m)\sqrt{\mathcal{R}(\omega)}\sqrt{\mathcal{R}(\omega-k\Omega)} \\
& \cos\left(+k\Omega t + \Phi_R(\omega) - \Phi_R(\omega-k\Omega) - k\left(\frac{\pi}{2}-\Phi_\Omega\right)\right) \\
& + 2\sum_{k,k'=1}^{\infty} J_k(m)J_{k'}(m)\sqrt{\mathcal{R}(\omega+k\Omega)}\sqrt{\mathcal{R}(\omega-k'\Omega)} \\
& \cos\left((k+k')\,\Omega t + \Phi_R(\omega+k\Omega) - \Phi_R(\omega-k'\Omega) + (k-k')\,\frac{\pi}{2} + (k+k')\,\Phi_\Omega\right)\,].
\end{aligned}
$$

After amplification (gain G_d), the photodiode signal is mixed with the oscillator at frequency Ω. Mixing is equivalent to multiplying the amplified photo-current by $V_0\cos(\Omega t + \Phi_{\Omega_M})$. After the mixer,

one gets the following voltage:

$$
\begin{aligned}
V_{R,d} = \frac{1}{2}\chi G_d R_0 \Gamma(\Gamma-1)\kappa E_0^2 \cos\left(\Omega t + \Phi_{\Omega_M}\right)\Big[\, & J_0^2(m)\mathcal{R}\left(\omega\right) \\
& + \sum_{k,k'=1}^{\infty} J_k(m) J_{k'}(m)\sqrt{\mathcal{R}\left(\omega+k\Omega\right)}\sqrt{\mathcal{R}\left(\omega+k'\Omega\right)} \\
\cos\Big(+\left(k-k'\right)\Omega t + & \Phi_R\left(\omega+k\Omega\right) - \Phi_R\left(\omega+k'\Omega\right) + \left(k-k'\right)\frac{\pi}{2} + \left(k-k'\right)\Phi_\Omega\Big) \\
& + \sum_{k,k'=1}^{\infty} J_k(m) J_{k'}(m)\sqrt{\mathcal{R}\left(\omega-k\Omega\right)}\sqrt{\mathcal{R}\left(\omega-k'\Omega\right)} \\
\cos\Big(-\left(k-k'\right)\Omega t + & \Phi_R\left(\omega-k\Omega\right) - \Phi_R\left(\omega-k'\Omega\right) + \left(k-k'\right)\frac{\pi}{2} - \left(k-k'\right)\Phi_\Omega\Big) \\
& + 2\sum_{k=1}^{\infty} J_0(m) J_k(m)\sqrt{\mathcal{R}\left(\omega\right)}\sqrt{\mathcal{R}\left(\omega+k\Omega\right)} \\
\cos\Big(-k\Omega t + & \Phi_R\left(\omega\right) - \Phi_R\left(\omega+k\Omega\right) - k\left(\frac{\pi}{2} + \Phi_\Omega\right)\Big) \\
& + 2\sum_{k=1}^{\infty} J_0(m) J_k(m)\sqrt{\mathcal{R}\left(\omega\right)}\sqrt{\mathcal{R}\left(\omega-k\Omega\right)} \\
\cos\Big(+k\Omega t + & \Phi_R\left(\omega\right) - \Phi_R\left(\omega-k\Omega\right) - k\left(\frac{\pi}{2} - \Phi_\Omega\right)\Big) \\
& + 2\sum_{k,k'=1}^{\infty} J_k(m) J_{k'}(m)\sqrt{\mathcal{R}\left(\omega+k\Omega\right)}\sqrt{\mathcal{R}\left(\omega-k'\Omega\right)} \\
\cos\Big(\left(k+k'\right)\Omega t + & \Phi_R\left(\omega+k\Omega\right) - \Phi_R\left(\omega-k'\Omega\right) + \left(k-k'\right)\frac{\pi}{2} + \left(k+k'\right)\Phi_\Omega\Big)\,\Big].
\end{aligned}
$$

Leading to

$$V_{R,d} = \frac{1}{2}\chi G_d R_0 \Gamma(\Gamma-1)\kappa E_0^2 \left[J_0^2(m)\mathcal{R}(\omega)\cos(\Omega t + \Phi_{\Omega_M}) \right.$$
$$+\frac{1}{2}\sum_{k,k'=1}^{\infty} J_k(m)J_{k'}(m)\sqrt{\mathcal{R}(\omega+k\Omega)}\sqrt{\mathcal{R}(\omega+k'\Omega)}$$
$$\left[\cos\left((+(k-k')+1)\,\Omega t + \Phi_R(\omega+k\Omega) - \Phi_R(\omega+k'\Omega) + (k-k')\frac{\pi}{2} + (k-k')\,\Phi_\Omega + \Phi_{\Omega_M}\right) + \right.$$
$$\left. \cos\left((+(k-k')-1)\,\Omega t + \Phi_R(\omega+k\Omega) - \Phi_R(\omega+k'\Omega) + (k-k')\frac{\pi}{2} + (k-k')\,\Phi_\Omega - \Phi_{\Omega_M}\right) \right]$$
$$+\frac{1}{2}\sum_{k,k'=1}^{\infty} J_k(m)J_{k'}(m)\sqrt{\mathcal{R}(\omega-k\Omega)}\sqrt{\mathcal{R}(\omega-k'\Omega)}$$
$$\left[\cos\left((-(k-k')+1)\,\Omega t + \Phi_R(\omega-k\Omega) - \Phi_R(\omega-k'\Omega) + (k-k')\frac{\pi}{2} - (k-k')\,\Phi_\Omega + \Phi_{\Omega_M}\right) + \right.$$
$$\left. \cos\left((-(k-k')-1)\,\Omega t + \Phi_R(\omega-k\Omega) - \Phi_R(\omega-k'\Omega) + (k-k')\frac{\pi}{2} - (k-k')\,\Phi_\Omega - \Phi_{\Omega_M}\right) \right]$$
$$+\sum_{k=1}^{\infty} J_0(m)J_k(m)\sqrt{\mathcal{R}(\omega)}\sqrt{\mathcal{R}(\omega+k\Omega)}$$
$$\left[\cos\left((-k+1)\,\Omega t + \Phi_R(\omega) - \Phi_R(\omega+k\Omega) - k\left(\frac{\pi}{2}+\Phi_\Omega\right) + \Phi_{\Omega_M}\right) + \right.$$
$$\left. \cos\left((-k-1)\,\Omega t + \Phi_R(\omega) - \Phi_R(\omega+k\Omega) - k\left(\frac{\pi}{2}+\Phi_\Omega\right) - \Phi_{\Omega_M}\right) \right]$$
$$+\sum_{k=1}^{\infty} J_0(m)J_k(m)\sqrt{\mathcal{R}(\omega)}\sqrt{\mathcal{R}(\omega-k\Omega)}$$
$$\left[\cos\left((+k+1)\,\Omega t + \Phi_R(\omega) - \Phi_R(\omega-k\Omega) - k\left(\frac{\pi}{2}-\Phi_\Omega\right) + \Phi_{\Omega_M}\right) + \right.$$
$$\left. \cos\left((+k-1)\,\Omega t + \Phi_R(\omega) - \Phi_R(\omega-k\Omega) - k\left(\frac{\pi}{2}-\Phi_\Omega\right) - \Phi_{\Omega_M}\right) \right]$$
$$+\sum_{k,k'=1}^{\infty} J_k(m)J_{k'}(m)\sqrt{\mathcal{R}(\omega+k\Omega)}\sqrt{\mathcal{R}(\omega-k'\Omega)}$$
$$\cos\left(((k+k'+1)\,\Omega)\,t + \Phi_R(\omega+k\Omega) - \Phi_R(\omega-k'\Omega) + (k-k')\frac{\pi}{2} + (k+k')\,\Phi_\Omega + \Phi_{\Omega_M}\right) +$$
$$\left. \cos\left(((k+k'-1)\,\Omega)\,t + \Phi_R(\omega+k\Omega) - \Phi_R(\omega-k'\Omega) + (k-k')\frac{\pi}{2} + (k+k')\,\Phi_\Omega - \Phi_{\Omega_M}\right) \right].$$

This signal is sent to a low pass filter, cutting all frequencies above Ω, therefore

$$
\begin{aligned}
V_{R,d}^{DC} = \frac{1}{2}\chi G_d R_0 \Gamma(\Gamma-1)\kappa E_0^2 \, [\\
\frac{1}{2}\sum_{k=1}^{\infty} J_k(m) J_{k+1}(m) \sqrt{\mathcal{R}(\omega+k\Omega)}\sqrt{\mathcal{R}(\omega+(k+1)\Omega)} \\
\cos\left(\Phi_R(\omega+k\Omega) - \Phi_R(\omega+(k+1)\Omega) - \frac{\pi}{2} - \Phi_\Omega + \Phi_{\Omega_M}\right) \\
+\frac{1}{2}\sum_{k}^{\infty} J_k(m) J_{k-1}(m) \sqrt{\mathcal{R}(\omega+k\Omega)}\sqrt{\mathcal{R}(\omega+(k-1)\Omega)} \\
\cos\left(\Phi_R(\omega+k\Omega) - \Phi_R(\omega+(k-1)\Omega) + \frac{\pi}{2} + \Phi_\Omega - \Phi_{\Omega_M}\right) \\
+\frac{1}{2}\sum_{k=1}^{\infty} J_k(m) J_{k-1}(m) \sqrt{\mathcal{R}(\omega-k\Omega)}\sqrt{\mathcal{R}(\omega-(k-1)\Omega)} \\
\cos\left(\Phi_R(\omega-k\Omega) - \Phi_R(\omega-(k-1)\Omega) + \frac{\pi}{2} - \Phi_\Omega + \Phi_{\Omega_M}\right) \\
+\frac{1}{2}\sum_{k=1}^{\infty} J_k(m) J_{k+1}(m) \sqrt{\mathcal{R}(\omega-k\Omega)}\sqrt{\mathcal{R}(\omega-(k+1)\Omega)} \\
\cos\left(\Phi_R(\omega-k\Omega) - \Phi_R(\omega-(k+1)\Omega) - \frac{\pi}{2} + \Phi_\Omega - \Phi_{\Omega_M}\right) \\
+J_0(m) J_1(m) \sqrt{\mathcal{R}(\omega)}\sqrt{\mathcal{R}(\omega+\Omega)} \\
\cos\left(\Phi_R(\omega) - \Phi_R(\omega+\Omega) - \frac{\pi}{2} - \Phi_\Omega + \Phi_{\Omega_M}\right) + \\
+J_0(m) J_1(m) \sqrt{\mathcal{R}(\omega)}\sqrt{\mathcal{R}(\omega-\Omega)} \\
\cos\left(\Phi_R(\omega) - \Phi_R(\omega-\Omega) - \frac{\pi}{2} + \Phi_\Omega - \Phi_{\Omega_M}\right)] .
\end{aligned}
\tag{298}
$$

And at first order in the modulation amplitude

$$
\begin{aligned}
V_{R,d}^{DC} \simeq \frac{1}{2}\chi G_d R_0 \Gamma(\Gamma-1)\kappa E_0^2 \, [\\
\frac{1}{2} J_0(m) J_1(m) \sqrt{\mathcal{R}(\omega)}\sqrt{\mathcal{R}(\omega+\Omega)} \cos\left(\Phi_R(\omega) - \Phi_R(\omega+\Omega) - \frac{\pi}{2} - \Phi_\Omega + \Phi_{\Omega_M}\right) + \\
J_0(m) J_1(m) \sqrt{\mathcal{R}(\omega)}\sqrt{\mathcal{R}(\omega+\Omega)} \cos\left(\Phi_R(\omega) - \Phi_R(\omega+\Omega) - \frac{\pi}{2} - \Phi_\Omega + \Phi_{\Omega_M}\right) + \\
\frac{1}{2} J_0(m) J_1(m) \sqrt{\mathcal{R}(\omega)}\sqrt{\mathcal{R}(\omega-\Omega)} \cos\left(\Phi_R(\omega) - \Phi_R(\omega-\Omega) - \frac{\pi}{2} + \Phi_\Omega - \Phi_{\Omega_M}\right) + \\
J_0(m) J_1(m) \sqrt{\mathcal{R}(\omega)}\sqrt{\mathcal{R}(\omega-\Omega)} \cos\left(\Phi_R(\omega) - \Phi_R(\omega-\Omega) - \frac{\pi}{2} + \Phi_\Omega - \Phi_{\Omega_M}\right)] ,
\end{aligned}
$$

$$
\begin{aligned}
V_{R,d}^{DC} \simeq \frac{3}{4}\kappa\eta E_0^2 J_0(m) J_1(m) \\
[\sqrt{\mathcal{R}(\omega)}\sqrt{\mathcal{R}(\omega+\Omega)} \sin\left(\Phi_R(\omega) - \Phi_R(\omega+\Omega) - (\Phi_\Omega - \Phi_{\Omega_M})\right) + \\
\sqrt{\mathcal{R}(\omega)}\sqrt{\mathcal{R}(\omega-\Omega)} \sin\left(\Phi_R(\omega) - \Phi_R(\omega-\Omega) + (\Phi_\Omega - \Phi_{\Omega_M})\right)]
\end{aligned}
\tag{299}
$$

This voltage will be used as the discriminator signal for the Servo system mastering the laser frequency.

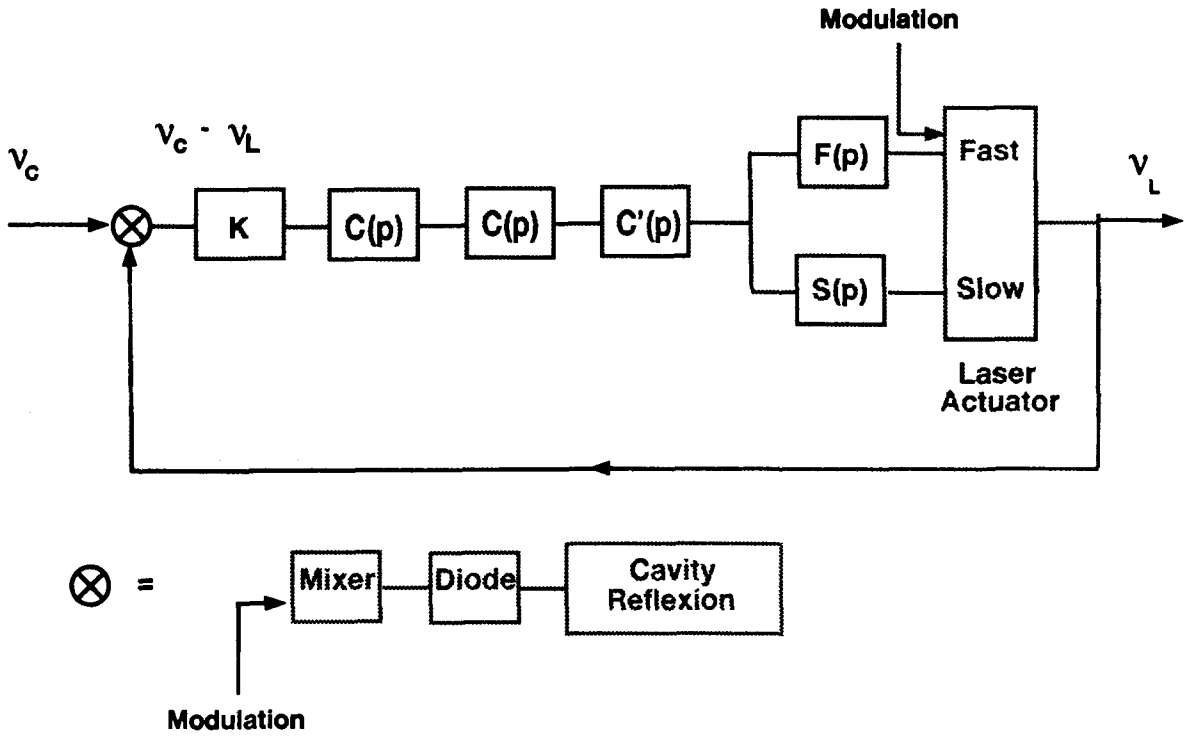

Figure 57: ***Principle of the PVLAS servo*** *The Discriminator* $\otimes$ *is followed by a pure Gain* K*, three Integral Proportional Correctors* C, C, C' *and an integrator for the Fast* F *and Slow* S *control of the Laser.*

G.4 Principle of the PVLAS Feedback Loop

We plan to use a servo inspired by the one used by the PVLAS experiment [15]. A description of this servo follows.

As explained in section 8.8, the error signal (discriminator), proportional to the difference between the laser frequency ν_L and the cavity resonant frequency ν_c, is given by the modulated laser light reflected from the cavity, measured by a photo diode and sent through a mixer for demodulation. As depicted on Fig. 57 and Fig. 60, for the PVLAS experiment Servo, this error signal is first amplified, K, and then integrated by three integral proportional correctors $C(p), C(p)$, and $C'(p)$. There is two different branch $F(p)$ and $S(p)$ that command the two different inputs (fast and Slow) of the Laser actuator (See section 8.5). The feedback loop is thus realized by the system cavity, diode and mixer.

In this section, the various elements used to build the discriminator signal are first presented, then the servo is detailed in order to demonstrate the stability of the feedback control.

G.4.1 Elements to produce the Discriminator Signal

Frequency response of the discriminator The cavity being a central part of the discriminator, one has to study its frequency response. One can show [15] that the cavity is a first order system, with cut-off requency given by

$$\nu_{cut} = \frac{\Delta\nu_{ax}}{2}$$

Photodiode Voltage

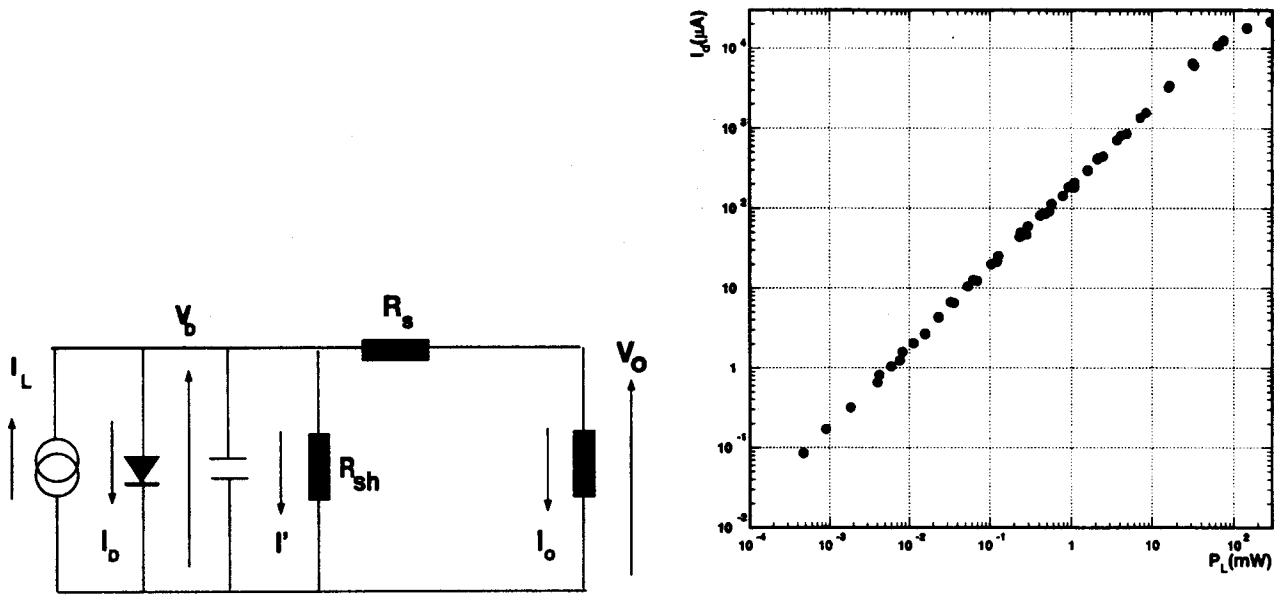

Figure 58: ***Photodiode equivalent circuit.S1123 Hamamatsu PIN photodiode response function***

- **Photodiode characteristics**

  We use a S1123 Hamamatsu PIN photodiode (2.2mm x 2.8 mm), whose equivalent circuit is represented on figure 58. I_L is the current generated by the incident light and is proportional to the amount of incident light. There is a junction capacity C_j. The diode has a voltage V_D and a current I_D (photodiode reverse saturation current I_S).

$$I_D = I_S \left(e^{\frac{eV_D}{kT}} - 1 \right) \tag{300}$$

  There is a shunt resistance R_{sh} with current I' and a serie resistance R_s. The output is done on a load resistance R_{load} and is defined by the voltage V_O and the current I_O, given by :

$$I_O = I_L - I' - I_D = I_L - I' - I_S \left(e^{\frac{eV_D}{kT}} - 1 \right) \tag{301}$$

  The open circuit voltage is the voltage when the output current is zero $I_O = 0$, thus

$$V_{OC} = V_D = \frac{kT}{e} \log \left(\frac{I_L - I'}{I_S} + 1 \right)$$

  The short circuit current is the output current when the load resistance is zero $R_{load} = 0$ and the output voltage is also zero $V_O = 0$, thus

$$I_{sc} = I_L - I_S \left(e^{\frac{eR_s I_{sc}}{kT}} - 1 \right) - \frac{R_s I_{sc}}{R_{sh}} \simeq I_L$$

  since R_s is several Ω and R_{sh} is 10^7 to 10^{11}. When used with a reverse voltage, the photodiode has a shorter response time. This response time is defined by the time needed to go from 10 % to 90 % of the maximum peak current, and is given by

$$t_r = 2.2 C_t R_{load}$$

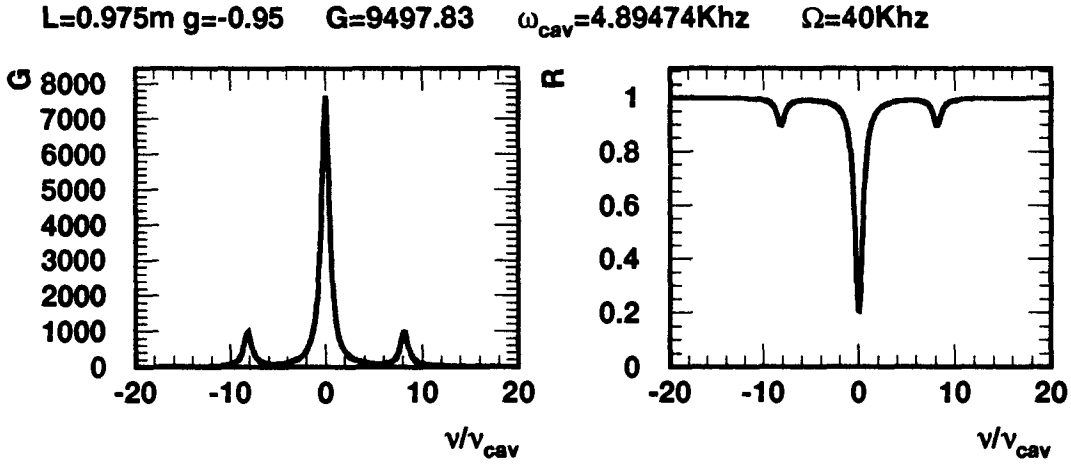

Figure 59: ***Gain and Reflectivity with modulation*** *at 40 kHz for a 97.5 cm cavity with g=-0.95 and a cavity width of 5kHz*

where C_t is called the terminal capacity, including the junction capacity and the package capacity. Applying a reverse voltage results in a larger depletion zone, and thus in a smaller junction capacity. With a $20V$ reverse voltage, the terminal capacity is $C_t = 10pF$. At the same voltage, the dark current is $0.2nA$ and increases with the reverse voltage. The S1123 PIN has a short circuit current of 6.2 μA for 100 lx[2], e.g 12.4μA/(mW/cm^2).

The light reflected by the cavity is directed to the photodiode using a beam splitter. generating a Photodiode current i_{Ph}, the voltage at the 1 kΩ resistance (R_{Ph}) is thus $V_{Ph} = R_{Ph} i_{Ph}$.

- **Photodiode output**
  When searching a resonance of the cavity, a triangle voltage (typically 10 Vpp at a few Hz) and the modulation (a few mV at a few hundred kHz) are applied to the fast control of the Laser resulting in a frequency change of a few MHz (typically 30 MHz). This is not sufficient to cover the Free spectral range (typically 150 MHz for a 1 m cavity), so one also have to use the slow control of the Laser. On expect to see on the R_{Ph} resistance a voltage similar to figure 59.

V_L Derivator and first order passive high pass filter The photodiode current separates through resistance R_L and self L :

$$i_{Ph} = i_1 + i_2 \quad ; V_L = R_L i_1; \quad V_L = L\frac{di_2}{dt} = iL\omega i_2.$$

Therefore

$$\frac{V_{Ph}}{R_{Ph}} = \frac{V_L}{R_L} + \frac{V_L}{iL\omega} \; ; \; V_L = V_{Ph}\frac{1}{R_{Ph}}\frac{1}{\frac{1}{R_L} + \frac{1}{iL\omega}};$$

i.e

$$\frac{V_L}{V_{Ph}} = \frac{R_L}{R_{Ph}}\frac{i\omega\frac{L}{R_L}}{1 + i\omega\frac{L}{R_L}}.$$

[2] 200 lx = 1 mW/cm^2

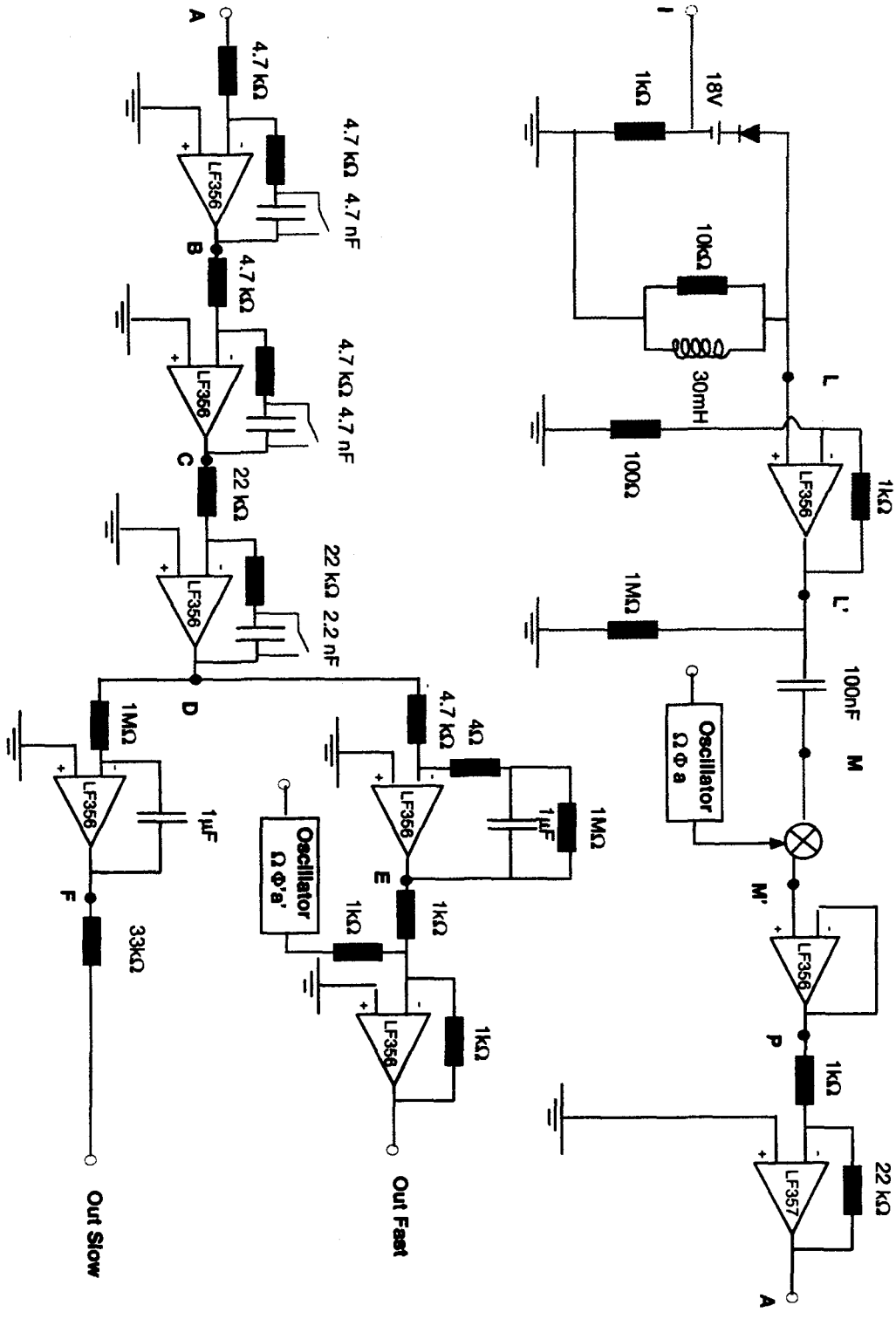

Figure 60: ***Electronic of the Servo***

This is thus a derivator in cascade with a first order high pass filter with gain

$$G = \frac{R_L}{R_{Ph}} = 10 \ (20dB)$$

and cut off frequency

$$w_c = \frac{R_L}{L} = 333kHz \quad and \quad \nu_c = 53kHz.$$

When the frequency $\omega \ll \omega_c$, the amplitude is equivalent to $+6dB/Oct$ with a 90° phase, whereas for $\omega \gg \omega_c$, the amplitude is $0dB/Oct$ and the phase is 0° (See Fig. 61-a).

The goal of this filter is to eliminate the DC level from the diode signal.

V_L' First amplification stage Once the DC level from the diode signal has been removed, the signal is amplified, at the input of the first ampli we have :

$$V_- \simeq V_+ = V_L = R_1 i \ ; \ V_{L'} = (R_1 + R_2)i = (R_1 + R_2)\frac{V_L}{R_1}$$

$$\frac{V_{L'}}{V_L} = \frac{(R_1 + R_2)}{R_1}.$$

This is a pure gain

$$G = \frac{(R_1 + R_2)}{R_1} = \frac{100\Omega + 1k\Omega}{100\Omega} = 11 \ (1.04dB).$$

Mixer Input The signal is then sent to one of the two input channels of the double balanced mixer. If Z_M is the mixer impedance, than

$$V_{L'} = (\frac{1}{iC\omega} + Z_M)i \ ; \ i = \frac{V_{L'}}{\frac{1}{iC\omega} + Z_M}$$

moreover,

$$V_M = Z_M i = V_{L'}\frac{Z_M}{\frac{1}{iC\omega} + Z_M}.$$

Thus

$$V_M = V_{L'}\frac{1}{\frac{1}{i\omega C Z_M} + 1} = \frac{i\omega C Z_M}{1 + i\omega C Z_M}.$$

If the mixer input impedance is purely resistive, than this is a passive high pass filter with cut off frequency given by:

$$\omega_c = \frac{1}{R_M C}$$

(See Fig. 61-a).

Mixer We use the ZP-10514 Mixer from Mini-circuit. This circuit (See fig. 62) allows a maximum of $7dbm$ ($500mV$) for the the LO (local Oscillator) input and $1dbm$ ($25mV$) for the RF input.

G.4.2 Elements of the Servo

Operational Amplifiers The PVLAS servo uses two types of Operational Amplifier from National semiconductor : a wide band LF356 and a wide band decompensated LF357. They both requires ± 18 V supply voltage.

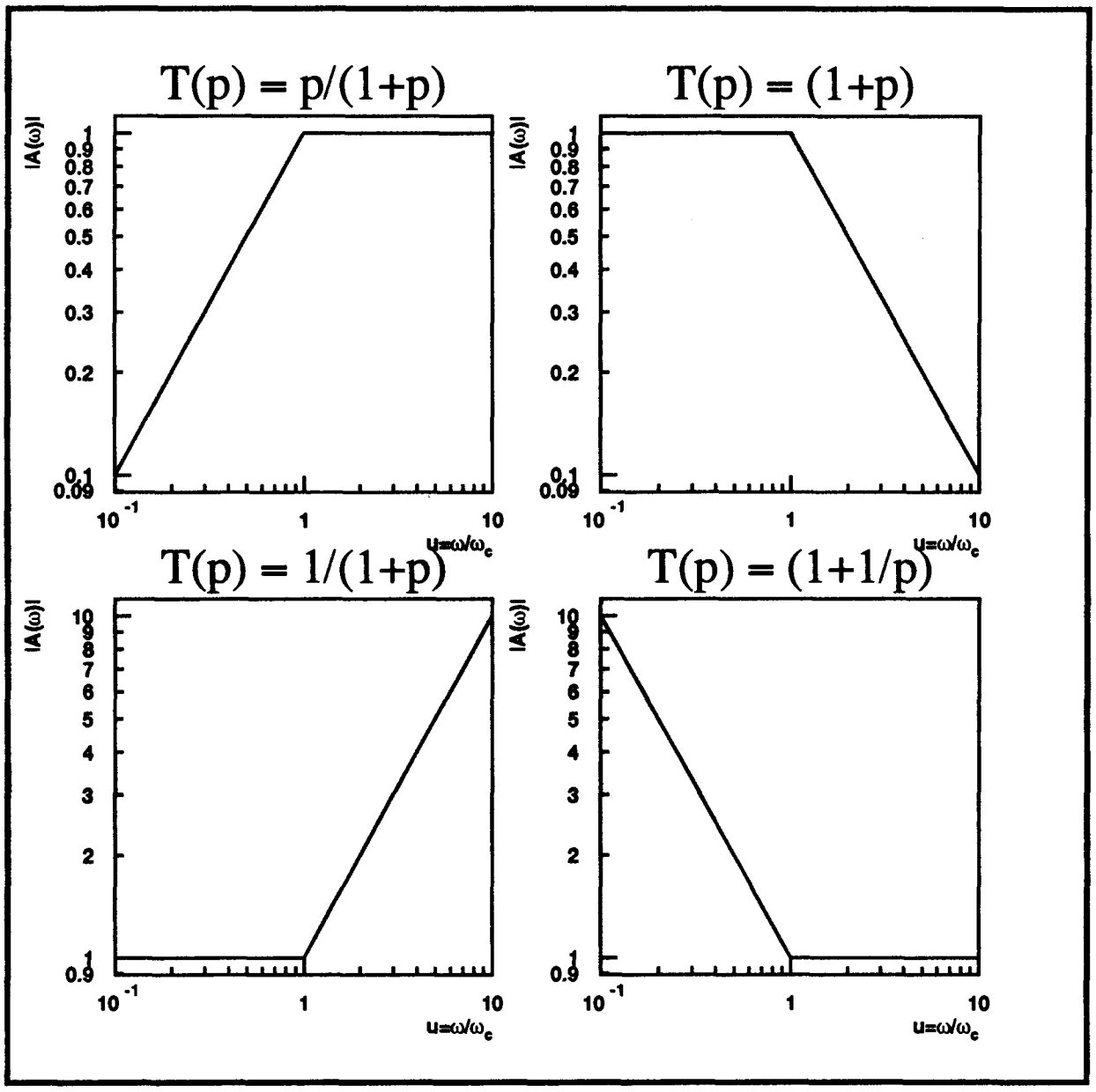

Figure 61: ***Various Filters** used in error signal builder and Servo: a) Self V_L ($\omega_c = 53kHz$) and Mixer input $V_M/V_{L'}$(ω_c =??kHz) ; b) Fast derivative part($\omega_c = 40kHz$) ; c) Fast integration part($\omega_c = 0.16Hz$) ; d) 3 integration levels $AB(\omega_c = 7.2kHz)$,$BC(\omega_c = 7.2kHz)$,$CD(\omega_c = 3.2kHz)$)*

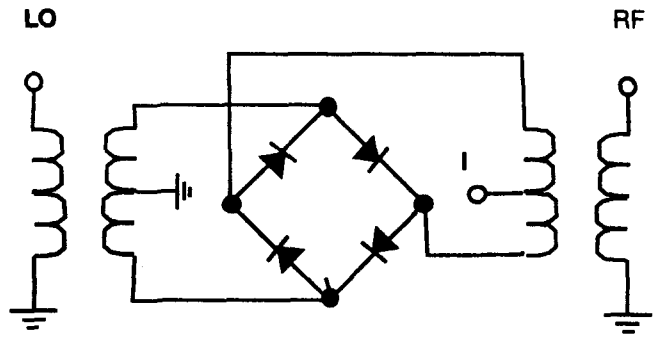

Figure 62: ***Double balanced Mixer.*** *The Signal from the photodiode is applied to the RF input, whereas the demodulation is applied to the LO input.*

K **: Active amplification and inversion** V_A After M' the first amplifier is only a "follower". We than have an inversion with amplification:

$$V_P = R_3 i \quad ; \quad V_A = -R_4 i$$

$$V_A = -V_P \frac{R_4}{R_3}.$$

The gain is thus

$$G = \frac{R_4}{R_3} = \frac{22k\Omega}{1k\Omega} = 22 \ (26.85dB)$$

and the phase is $\phi_A = -180^o$.

$C(p), C(p), C'(p)$ **Three Integral Proportional Correctors** V_B,V_C,V_D Between A and B, B and C and C and D we have, three gain -1 when the Capacity switch is off. When the capacity is on, the following relations hold:

$$V_{out} = -\left[R_C{}^j + \frac{1}{i\omega C_j}\right] i \ ; \ V_{in} = R_j i$$

Thus

$$V_{out} = -V_{in} \frac{R_C^j}{R_j} \left[1 + \frac{1}{i\omega R_C^j C_j}\right]$$

The resistances are selected so that $R^j = R_C^j$, resulting in an unit Gain $G = 1 \ (0dB)$. So after an inversion $\phi = -180^o$, we have an integration, with cut off frequency

$$\omega_c = \frac{1}{R_C^j C_j}.$$

When the frequency $\omega \ll \omega_c$, the amplitude is equivalent to $-6dB/Oct$ with a -90^o phase, whereas for $\omega \gg \omega_c$, the amplitude is $0dB$ and the phase is 0^o (See Fig. 61-d). For B and C level the cut off frequency is

$$\omega_c = \frac{1}{4.7k\Omega 4.7nF} = 45kHz; \ \ and \ \nu_c = 7.2kHz,$$

whereas for C level

$$\omega_c = \frac{1}{22k\Omega 2.2nF} = 20.6kHz; \ \ and \ \nu_c = 3.2kHz.$$

ν	[0,0.16 Hz]	[0.16Hz,3.2 kHz]	[3.2 kHz, 7.2 kHz]	[7.2kHz,40 kHz]	[40kHz,∞]
A_{PA}	0dB/Oct	0dB/Oct	0dB/Oct	0dB/Oct	0dB/Oct
A_{AB}	-6dB/Oct	-6dB/Oct	-6dB/Oct	0dB/Oct	0dB/Oct
A_{BC}	-6dB/Oct	-6dB/Oct	-6dB/Oct	0dB/Oct	0dB/Oct
A_{CD}	-6dB/Oct	-6dB/Oct	0dB/Oct	0dB/Oct	0dB/Oct
A^1_{DE}	0dB/Oct	-6dB/Oct	-6dB/Oct	-6dB/Oct	-6dB/Oct
A^2_{DE}	0dB/Oct	0dB/Oct	0dB/Oct	0dB/Oct	+6dB/Oct
A^{Fast}_{Servo}	-18dB/Oct	-24dB/Oct	-18dB/Oct	-6dB/oct	0dB/Oct

Table 76: ***Amplitude for the various part of the Fast Servo at the Output of the Mixer***

$F(p)$ Integration level for the Fast Output

$$V_D = Ri;\ V_E = -(R' + Z)i;\ Z = \frac{R_C}{1 + iR_CC\omega}$$

$$V_E = -V_D\frac{R' + \frac{R_C}{1+iR_CC\omega}}{R}$$

$$V_E = -V_D\frac{R_C + R'}{R}\frac{1}{1 + iR_CC\omega}\left[1 + i\frac{R'R_C}{R' + R_C}C\omega\right].$$

This is thus a Gain

$$G = \frac{R_C + R'}{R} = \frac{1M\Omega + 4\Omega}{4.7k\Omega} = 46dB$$

and a low pass filter, with cut off frequency

$$\omega_c = \frac{1}{R_CC} = \frac{1}{1M\Omega 1\mu F} = 1Hz;\ \nu_c = 0.16Hz,$$

for which, when the frequency $\omega \ll \omega_c$, the amplitude is equivalent to $0dB$ with a 0° phase, whereas for $\omega \gg \omega_c$, the amplitude is $-6dB/Oct$ and the phase is $-90°$(See Fig. 61-c). This low pass filter is followed by a derivator, with cut off frequency

$$\omega_c = \frac{1}{\frac{R'R_C}{R'+R_C}C} = 250kHz;\ \nu_c = 40kHz.$$

When the frequency $\omega \ll \omega_c$, the amplitude is equivalent to $0dB$ with a 0° phase, whereas for $\omega \gg \omega_c$, the amplitude is $+6dB/Oct$ and the phase is $+90°$(See Fig. 61-c). The Bode plot for the fast Servo is represented on figure 63, whereas the Nyquist plots are given in figure 64

$S(p)$ Integration level for the Slow Output

$$V_D = Ri \ and\ V_F = -\frac{i}{iC\omega}$$

$$\frac{V_F}{V_D} = -\frac{1}{iRC\omega}$$

This is a pure integrator with unit gain and cut off frequency

$$\omega_c = RC = 1M\Omega 1\mu F = 1Hz \ and\ \nu_c = 0.16Hz$$

The amplitude is $-6dB/oct$ and the phase is $-90°$. Bode and Nyquist Plots for the Slow output are given in figures 65 and 66.

ν	[0,0.16 Hz]	[0.16Hz,3.2 kHz]	[3.2 kHz, 7.2 kHz]	[7.2kHz,40 kHz]	[40kHz,∞]
ϕ_{PA}	-180°	-180°	-180°	-180°	-180°
ϕ^0_{AB}	-180°	-180°	-180°	-180°	-180°
ϕ^1_{AB}	-90°	-90°	-90°	0°	0°
ϕ^0_{BC}	-180°	-180°	-180°	-180°	-180°
ϕ^1_{BC}	-90°	-90°	-90°	0°	0°
ϕ^0_{CD}	-180°	-180°	-180°	-180°	-180°
ϕ^1_{CD}	-90°	-90°	0°	0°	0°
ϕ^0_{DE}	-180°	-180°	-180°	-180°	-180°
ϕ^1_{DE}	0°	-90°	-90°	-90°	-90°
ϕ^2_{DE}	0°	0°	0°	0°	+90°
ϕ^{Fast}_{Servo}	-90°	-180°	-90°	+90°	-180°

Table 77: ***Phase for the various part of the Fast Servo at the Output of the Mixer***

A_{PA}	26.85dB
A_{AB}	0dB
A_{BC}	0dB
A_{CD}	0dB
A_{DE}	46dB
G^{Fast}_{Servo}	72.85dB

A_{PA}	26.85dB
A_{AB}	0dB
A_{BC}	0dB
A_{CD}	0dB
A_{DF}	0dB
G^{Slow}_{Servo}	26.85dB

Table 78: ***Amplitude Gain for the various part of the Fast and Slow Servo at the Output of the Mixer***

ν	[0,3.2 kHz]	[3.2 kHz, 7.2 kHz]	[7.2kHz,∞]
A_{PA}	0dB/Oct	0dB/Oct	0dB/Oct
A_{AB}	-6dB/Oct	-6dB/Oct	0dB/Oct
A_{BC}	-6dB/Oct	-6dB/Oct	0dB/Oct
A_{CD}	-6dB/Oct	0dB/Oct	0dB/Oct
A_{DF}	-6dB/Oct	-6dB/Oct	-6dB/Oct
A^{Slow}_{Servo}	-24dB/Oct	-18dB/Oct	-6dB/Oct

Table 79: ***Amplitude for the various part of the Slow Servo at the Output of the Mixer***

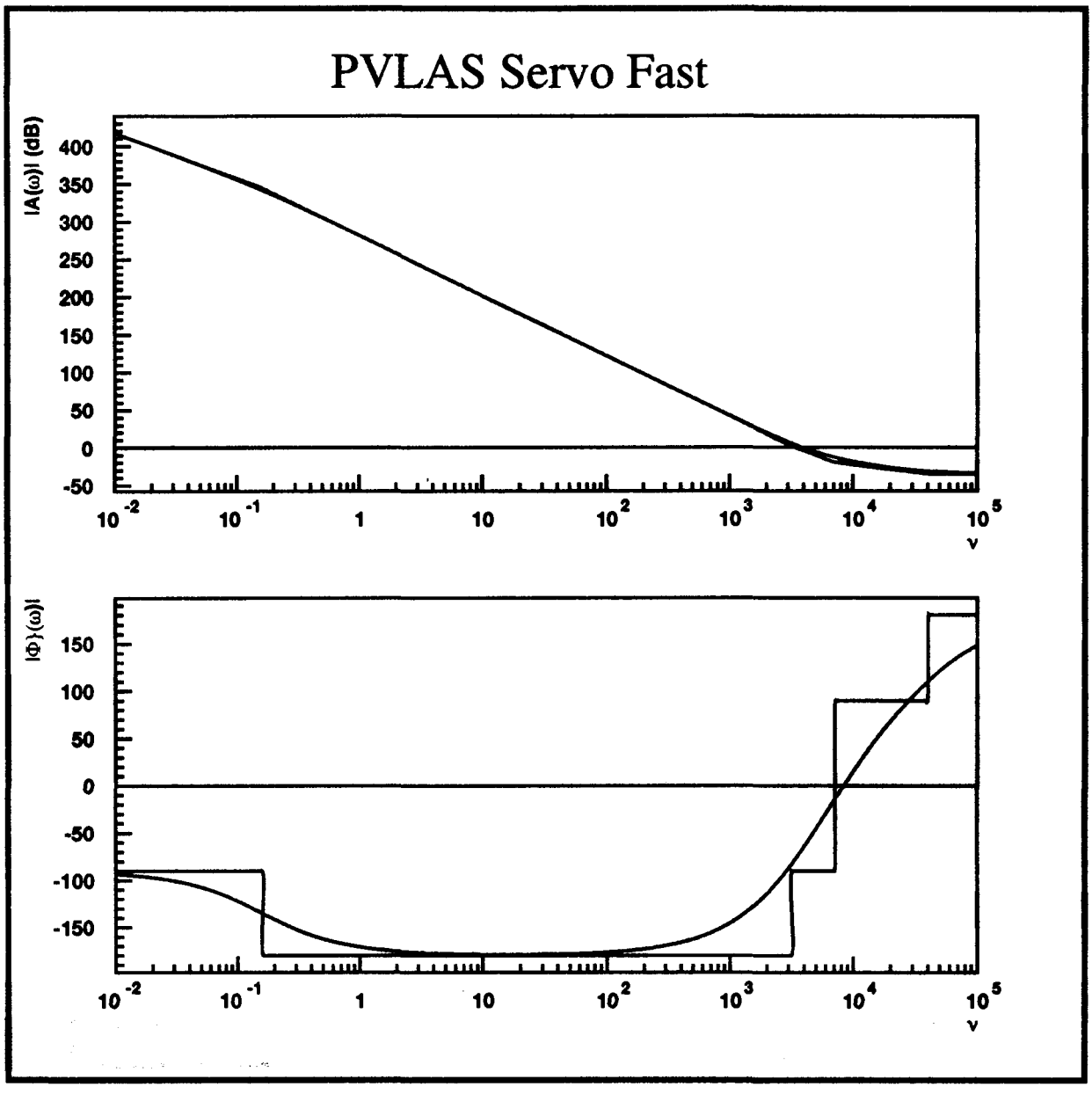

Figure 63: ***Bode plot for the Fast output of the Servo*** *(Starting at the Mixer output and ending at the adder input of the fast output)*

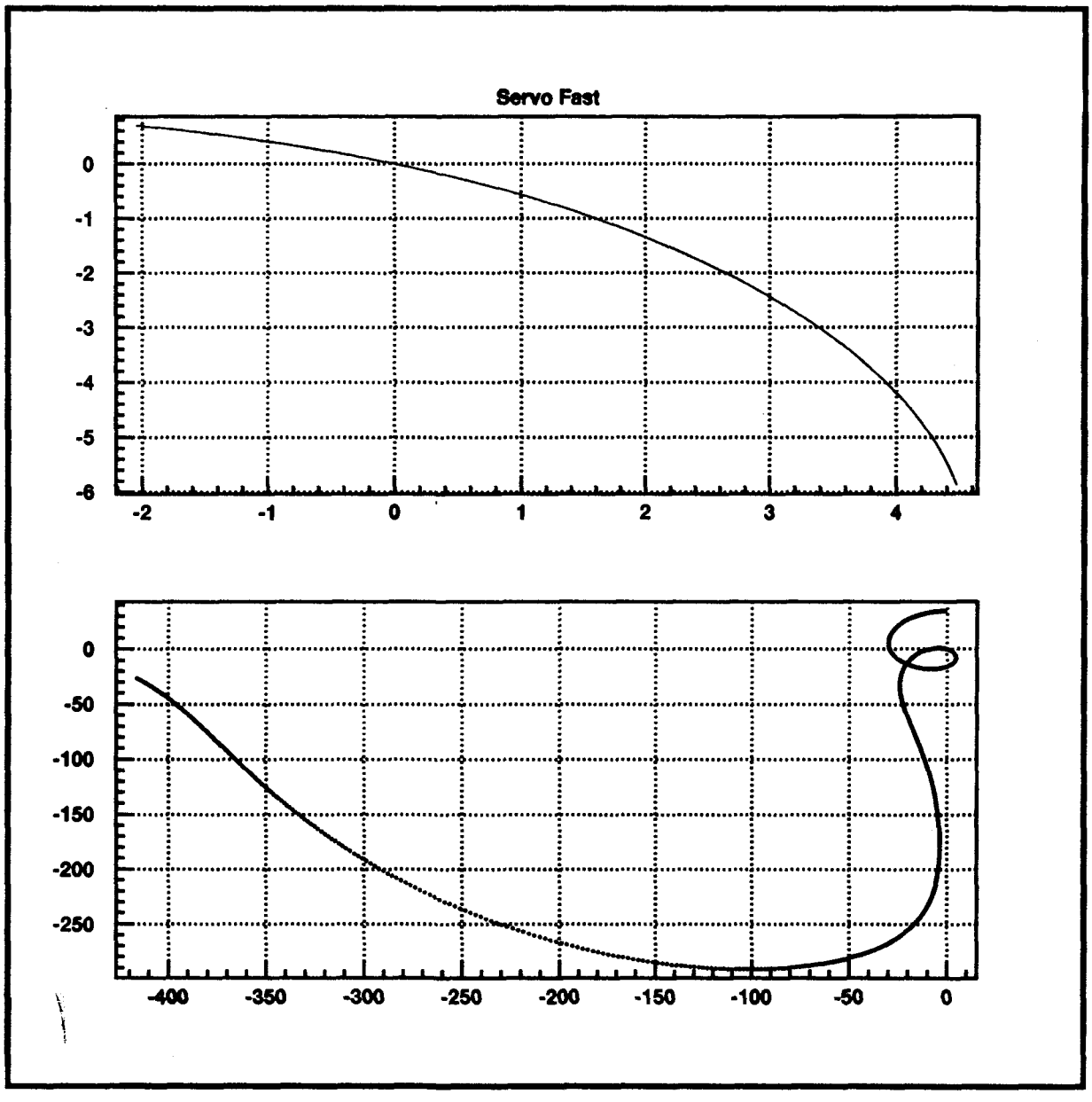

Figure 64: ***Nyquist plot (dB) for the Fast output of the Servo*** *(Starting at the Mixer output and ending at the adder input of the fast output)*

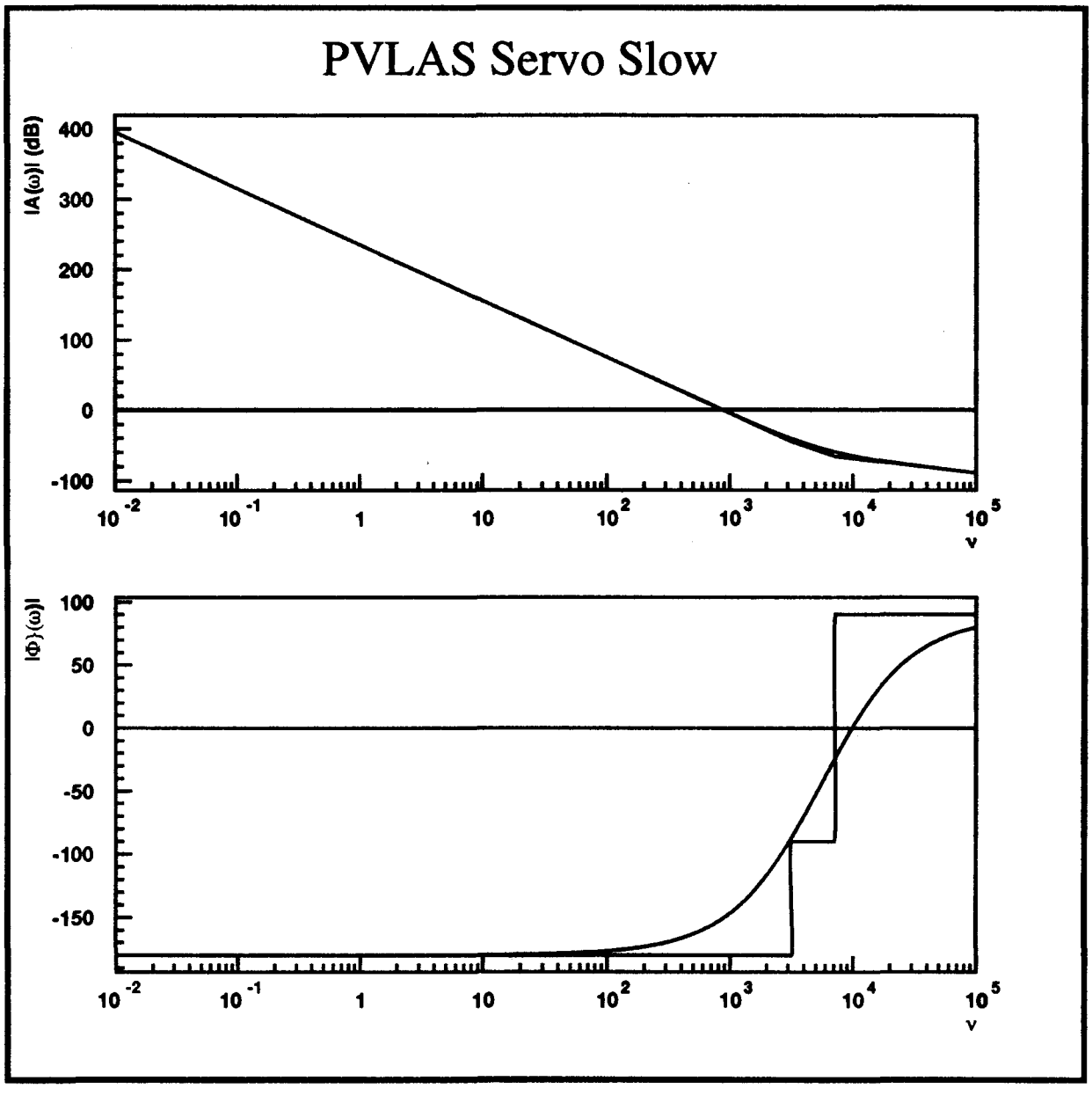

Figure 65: ***Bode plot for the Slow output of the Servo*** *(Starting at the Mixer output)*

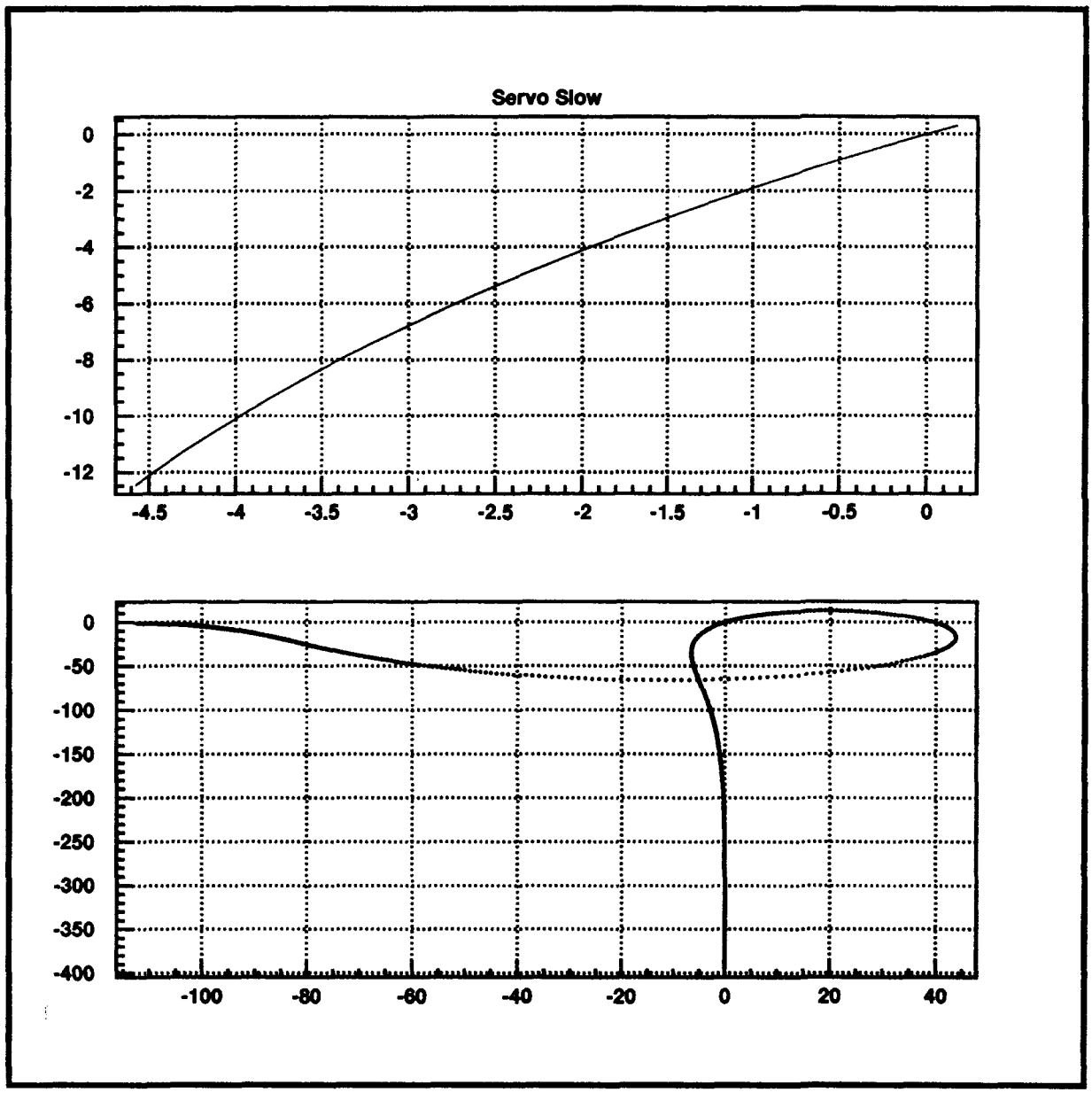

Figure 66: ***Nyquist plot (dB) for the Slow output of the Servo*** *(Starting at the Mixer output)*

ν	[0,3.2 kHz]	[3.2 kHz, 7.2 kHz]	[7.2kHz,∞]
ϕ_{PA}	-180°	-180°	-180°
ϕ^0_{AB}	-180°	-180°	-180°
ϕ^1_{AB}	-90°	-90°	0°
ϕ^0_{BC}	-180°	-180°	-180°
ϕ^1_{BC}	-90°	-90°	0°
ϕ^0_{CD}	-180°	-180°	-180°
ϕ^1_{CD}	-90°	0°	0°
ϕ^0_{DF}	-180°	-180°	-180°
ϕ^1_{DF}	-90°	-90°	-90°
ϕ^{Slow}_{Servo}	-180°	-90°	+90°

Table 80: ***Phase for the various part of the Slow Servo at the Output of the Mixer***

Actuator of the Laser LightWave 126-1064-300 As explained in section 8.5, the Laser actuator is realized for :

- **Slow Frequency control**
  By applying a voltage to a thermoelectric cooler under the laser crystal, this allows for a tuning range of tens of GHz with a relatively slow time constant (1 to 10 s). The input impedance is 10 kΩ and the maximum design-case voltage is $\pm$ **10 V**. Between mode hops, the tuning coefficient is **+5.0 GHz/V**, and averaged to include mode hops effect, this coefficient is **+1.6 GHz/V**.

- **Fast Frequency control.**
  By applying a voltage to a piezoelectric bonded onto the crystal,this allows to vary the frequency by tens of MHz at rates up to **30 kHz**. The tuning coefficient is **+3.2 MHz/V at 10 V DC**, and **+3.1 MHz/V at 10 Vpp AC at 5kHz**. The piezo can operates at frequencies greater than 30 kHz, but the tuning coefficient can vary substantially above 30 kHz.

G.4.3 Stability of the feedback Control

The stability of the system can be studied by looking at the total gain when the feedback loop is open G_{OL}:

$$G^F_{OL}(\omega) = \frac{d\epsilon}{d\nu}(\omega) G^F_{servo}(\omega) A_F(\omega) \;\; ; G^S_{OL}(\omega) = \frac{d\epsilon}{d\nu}(\omega) G^S_{servo}(\omega) A_S(\omega), \tag{302}$$

where $\frac{d\epsilon}{d\nu}$ is the slope of the error signal, the gain of the servo is given by

$$G^F_{servo}(\omega) = KC(\omega)C(\omega)C'(\omega)F(\omega) \;\; ; G^S_{servo}(\omega) = KC(\omega)C(\omega)C'(\omega)S(\omega), \tag{303}$$

and A_F and A_S are the fast and slow actuator of the Laser. The system will be stable if the open loop gain $G^F_{OL}(\omega)$ reaches $0dB$ at a frequency where the phase is $\phi(\omega) < -180°$.

The response of the closed loop feedback to a step function $e(t) = \nu_c u(t)$ being given by

$$\lim_{t\to\infty} \nu_c - \nu_L = \frac{1}{1 + |G_{OL}(0)|},$$

one wants to work with the highest possible static gain $|G_{OL}(0)|$ that will keep the system stable.

H Magnet Specifications

The chicane will consist of four type C dipole magnets whose specifications [44] are listed in table 81 and whose dimensions are summarized on figure 67.

The magnetic circuit of the proposed magnets is made of very soft iron. The iron is rolled. A Magnet is composed of two blocks. The 8 iron blocks will come from the same casting. The amount of Carbon will be less than 0.06%. The magnetic permeability [45] is given by figure 68.

The coils are made hollow conductor (Copper), with resistivity less than $1.7\,10^{-8}\ \Omega/m$ and insulated with glass fiber. The proposed power supply is a high stability current regulated power supply. The four magnets will be fed in serie. The power supply specifications are listed in table 82. The power supply is locally controlled and can be remotely controlled.

Each dipole will dissipate $24\,V$ x $365\,A\ =\ 8.76kW$. The Cebaf water pressure (100 $psi \simeq 0.69$ Mpa) and flow (30 $gallons/min$) is adequate for the proposed magnet (0.6 Mpa and 13 $l/s \simeq 3.5$ $gallon/min$) requirement. We expect an increase in temperature of 17 F.

The SIGMAPHI commercial proposal is

1. 4 C type dipole magnets : 637 kF
2. 1 current regulated Power Supply with its 120 m cable : 221 kF

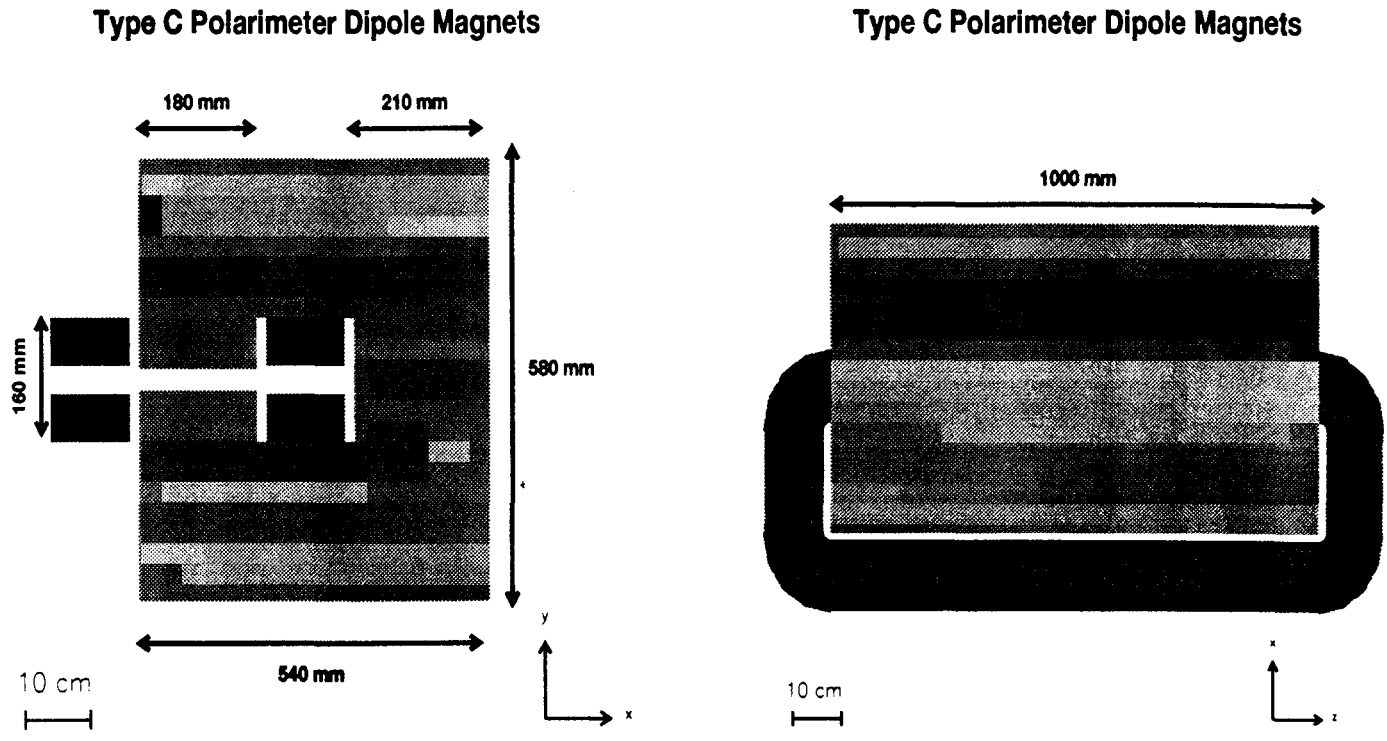

Figure 67: ***Dimensions for a C type Dipole Magnet. Entrefer 25.4 mm***

Main Trajectory Radius (m)	17.79
Deviation angle (o)	3.2
Entrance face inclination angle (o)	0
Exit face inclination angle (o)	3.2
Rectangular pole shape	yes
Air gap length (mm)	25.4
Pole width excluding the desaturating profile (mm)	150
Pole width including the desaturating profile (mm)	180
Maximum magnetic induction (T)	1.5
Pole length (mm)	1000
Effective length dispersion between dipoles(%)	≤ 0.1
Maximum fault of parallelism of the air gap(mm)	$\pm$ 0.02
Homogeneous radial width(mm)	40
Fault of homogeneity in this width(%)	$\pm$ 0.01
Maximum current intensity(A)	365
Maximum voltage drop per dipole(V)	24
Water flow rate per dipole(l/min)	13
Water pressure drop (Mpa)	0.6
Approximate Mass (kg)	2400

Table 81: ***Dipole magnet specifications***

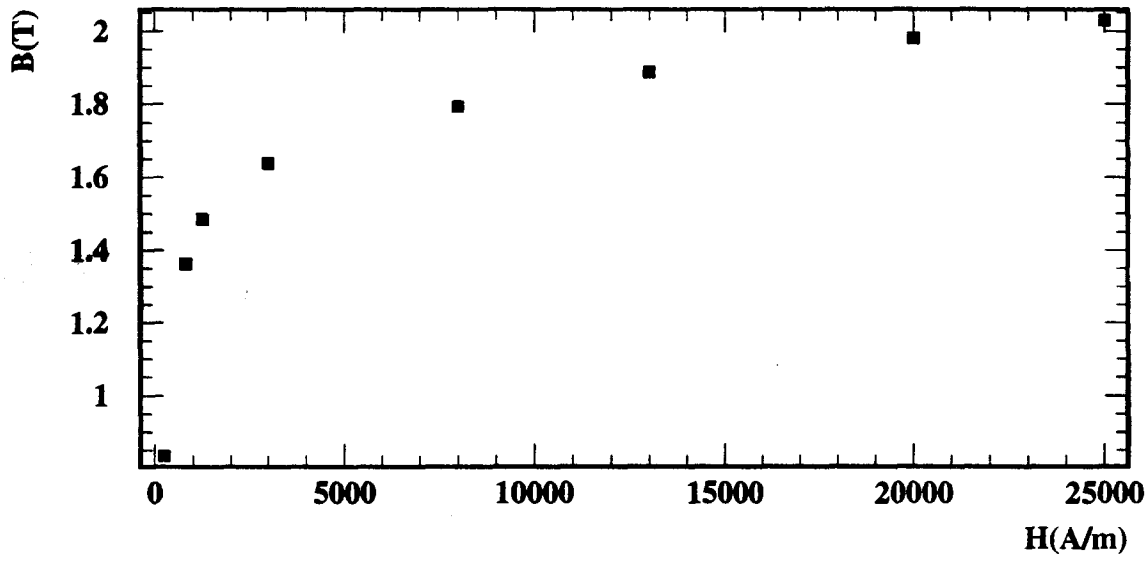

Figure 68: ***Magnetic permeability of the proposed magnetic circuit, as measured by SIGMAPHI***

Output Voltage	0 to 115 V
Output Current	4 to 375 A
Current intensity adjustment by	10 turns potentiometer
Current reading by	3.5 digit DVM
Voltage reading by	3.5 digit DVM
Current stability at maximum current for a $\pm 10\%$ line variation	$2\,10^{-4}$

Table 82: ***Dipole magnet Power Supply specifications***

I Consideration on the light collection for $PbWO_4$ crystal

We recall that for light falling on a boundary between two homogeneous media, the laws of reflection and refraction led to :

- The angle of reflection θ_r wrt the direction normal to the boundary is related to the incident angle θ_i by

$$\theta_r = \pi - \theta_i. \tag{304}$$

- The angle of the transmitted light θ_t from the incident medium, with index n_1 to the transmission medium with index n_2 is

$$n_1 \sin\theta_i = n_2 \sin\theta_t. \tag{305}$$

- The reflectivity $\mathcal{R}$ (resp. transmitivity $\mathcal{T}$), defined as the ratio of the incident and reflected (resp. transmitted) intensity are

$$\mathcal{R}_\perp = \frac{\tan^2(\theta_i - \theta_t)}{\tan^2(\theta_i + \theta_t)}, \quad \mathcal{T}_\perp = 1 - \mathcal{R}_\perp; \tag{306}$$

$$\mathcal{R}_\parallel = \frac{\sin^2(\theta_i - \theta_t)}{\sin^2(\theta_i + \theta_t)}, \quad \mathcal{T}_\parallel = 1 - \mathcal{R}_\parallel. \tag{307}$$

At normal incidence, this becomes

$$\mathcal{R} = \left(\frac{(n-1)}{(n+1)}\right)^2, \quad \mathcal{T} = 1 - \mathcal{R}, \tag{308}$$

where $n = \frac{n_2}{n_1}$. For $PbWO_4$, the refractive index is $n_2 \simeq 2.2$, thus the reflectivity between air and the crystal is $\mathcal{R} \simeq 14\%$.

References

[1] P. Souder et al., " Parity violation in elastic scattering from p", E-91-004. E. Beise et al., " Parity violation in elastic scattering from p and ^{4}He", E-91-010.

[2] C. Perdrisat et al., "Measurement of electric form factor of the proton by recoil polarization", PR-93-027.

[3] R. Lourie et al., " Investigation of the $N \rightarrow \Delta$ transition via polarization observable in Hall A", E-91-011

[4] G. Gates, Z. Meziani et al., "Measurement of the neutron spin structure function at low Q^2", PR-94-010.

[5] C. Glashausser et al., " Measurement of recoil polarization in $^{16}O(\vec{e}, e', \vec{p})$ reaction with 4 GeV electrons", E-89-033.
V. Burkert et al., " Measurement of electron asymmetry in $p(\vec{e}, e', p)\pi^0$ and $p(\vec{e}, e', \pi^+)n$ in the mass region $P_{33}(1232)$ for $Q^2 \leq 2GeV^2$", E-89-042.
P. Ulmer et al., " Polarization transfer in the reaction $^4He(\vec{e}, e', \vec{p})^3H$ in the quasi-elastic region", E-98-049.
J.J. Kelly et al., " The $p(\vec{e}, e', \vec{N})\pi$ reaction with HARP", E93-013.

[6] A. Denner, S. Dittmaier, Nucl. Phys. B407 (1993) 43

[7] "Compton Polarimeter at SLAC SPEAR", *(NIM 165 (1979) 177)*.
" Compton Polarimeter at DESY Doris", *(Phys. Lett. 135B (1984) 498)*.

[8] Hermes Collaboration, "Propsal to DESY for a Longitudinal Electron Polarimeter" (1995).
D.P. Barber, et al. NIM A329 (1993) 79.

[9] G. Shapiro, et al. SLAC-PUB-6261 (1993).

[10] C. Prescott, SLAC internal report, SLAC TN 73 1.

[11] S. Kerhoas, SACLAY internal report, (1994).

[12] B. Norum, T. Welch, " An intense polarized photon source at CEBAF hall B", CEBAF, LOI 93-012.

[13] C. Bradaschia et al., " The VIRGO project", NIM A289 (1990) 519.

[14] A. Abramovici et al., " LIGO, the Laser Interferometer Gravitational-Wave Observatory", Science 256 (1992) 325.

[15] Guido Zavattini et al, Rev. Sci. Inst. 66 (1995) 2785.
P. Pace, Tesi di Laurea in Fisica (1993-94), Trieste University, Unplubished.
G. Ruoso, Tesi di Dottorato in Fisica (1993-94), Padova University, Unplubished.

[16] " PRECISION MEASUREMENTS OF THE SLC SPECTROMETER MAGNETS" M.E. Levi (LBL, Berkeley), J. Nash (SLAC), S. Watson (UC, Santa Cruz), SLAC-PUB-4654, Mar 1989. 40pp. NIM A281 (1989) 265-276.

[17] G. Alexeev, et al, NIM 364 (1995) 307.

[18] J.P. Merlo et al., CMS TN/94-262 (1994).

[19] R. Chipaux et al., Symposium on Scintillator and Phosphor Materials, San Francisco (1994).

[20] S. Inaba, KEK Preprint 94-105.

[21] P.W. Milonni, J.H. Eberly, "LASERS", Willey interscience, N.Y. , p. 470 and p 502.

[22] M. Born, and E. Wolf, "Principles of Optics", Pergamon Press, (1975).

[23] "Lasers", A. Siegman, University Science Book, Mill Valley, California (1986), p. 413, p.627.

[24] Micro-controle Catalogue (1994) p. 7.16.

[25] J.M. Makowsky, Private communication

[26] LightWave 126-1064-300, Users Manual, (1995).

[27] R. W. P. Drever et al, Appl. Phys. B31 (1983) 97.

[28] N. M. Sampas, Thesis, Colorado University (1990) unpublished.

[29] T. Day, Thesis, Stanford University (1990) unpublished.

[30] M. E. Couprie, et al., "Proc. Int. Symp. of Optical Interference Coating", Grenoble (1994).

[31] M. E. Couprie, et al., Applied Optics 30 (1991) 344.

[32] R. Ent, et al. "Laser backscattering facility at CEBAF".

[33] S. Huard, "Polarisation de la lumière", Masson, 1994.

[34] H. Amiel, Optilas, Offre de Prix N°16.2700/Fast

[35] R. D. Elia, Slac Report SLAC-429, April 1994.

[36] V. Bargman, L. Michel, V. Telegdi, Phys. Rev. Lett. 10 (1959) 435.

[37] R. Hagedorn, " Relativistic Kinematic, (1964) Benjamin Inc. NY.

[38] A. Saha, Private Communication.

[39] J. P. Chen, Private Communication.

[40] L. Cardman, Private Communication.

[41] A. Hofmann, CERN 90-03 (1990) 115.

[42] Y.S. Tsai, Rev. Mod. Phys. 46 (1974) 815.

[43] S.M. Seltzer and M.J. Berger, NIM B12 (1985) 95. Prentice-Hall Edition.

[44] M. Juillard, DAPNIA/SEA, Private Communication.

[45] J. Miscopein, SIGMAPHI proposal for the 4 type C dipole, Private Communication.